Biomolecular Materials

2024 Principal Investigators' Meeting

July 30-August 1, 2023

Program and Abstracts

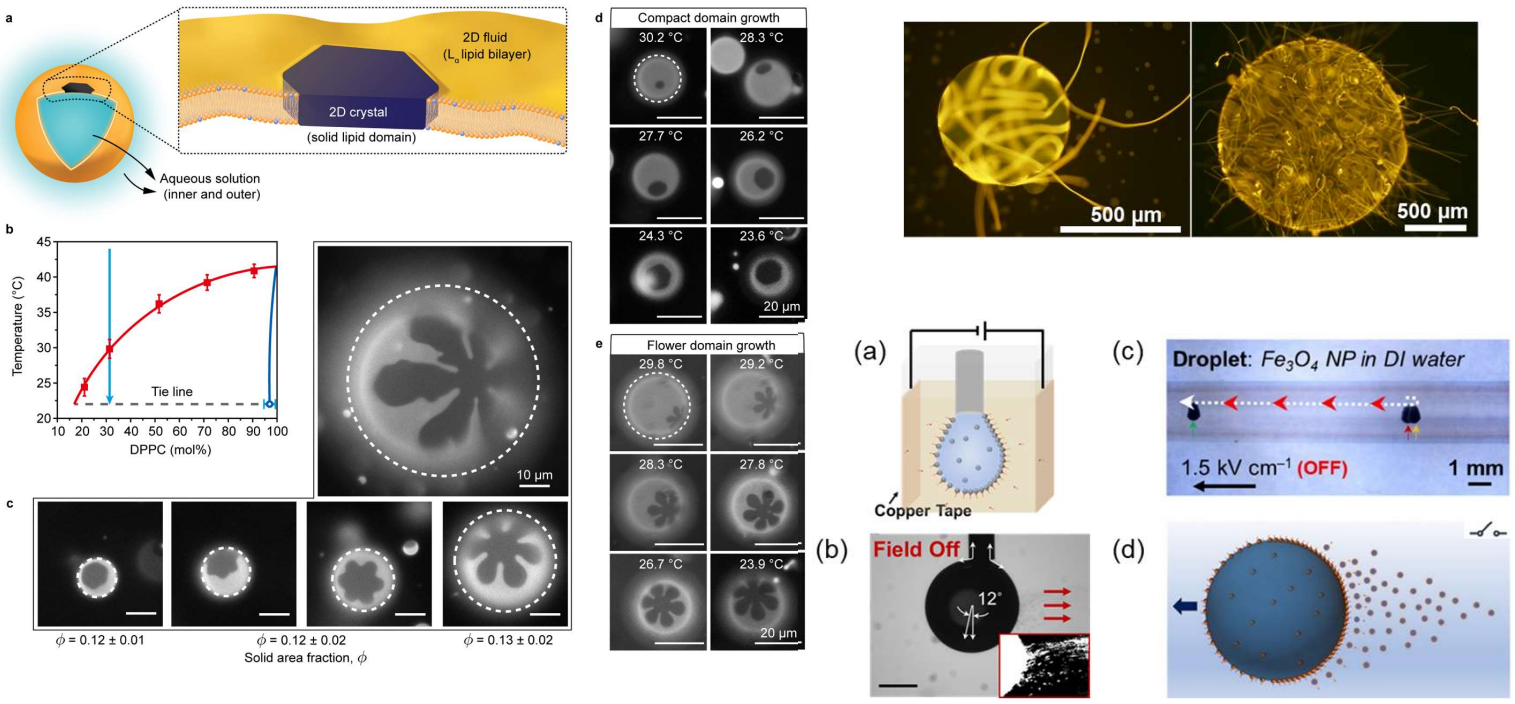

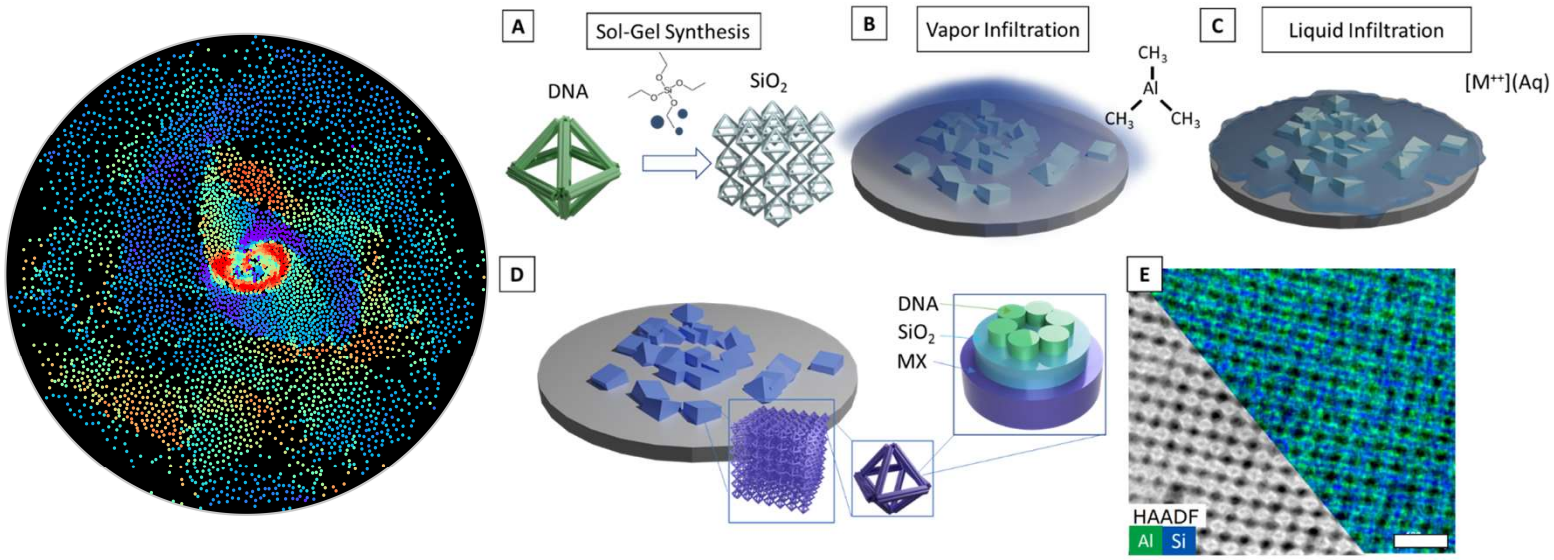

U.S. DEPARTMENT OF ENERGY | Office of Science

Office of Basic Energy Sciences
Materials Sciences and Engineering Division

On the Cover

Clockwise from top left-

Exploiting bending stress to impart a vesicle size-dependence that controls the morphology of single 2D crystals nucleated and grown in phospholipid membranes. Shapes with more extended features grow on larger vesicles to relax the combined elastic cost in the fluid and solid membranae phases. Early development of the final shape results from vesicle size dependent tension evolution during cooling into the two-phase region. “Flower-shaped 2D crystals grown in curved fluid vesicle membranes” H. Wan, W. Xin, G. Jeon, G. Grason, and M. M. Santore*. *Nat. Commune.* 15, Article number: 3442 (2024) .

Building synthetic mimics of dendritic cells. Under some conditions droplets that are heavily loaded with appendages that get closer to dendritic cell like morphology. Todd Emrick, UMass-Amherst.

Self-Propulsion by Directed Explosive Emulsification. (a) Schematic of a pendant drop (PD) containing negatively charged nanoparticles, surrounded by an immiscible oil phase with cationic surfactant, under a DC electric field; (b) Optical image of the PD after the field is turned off; (c) Self-propulsion of the aqueous droplet resulting from the asymmetric explosive emulsification; (d) Schematics of the asymmetric packing of the NPSs at the surface of aqueous droplet undergoing explosive emulsification after the field is turned off. X. Wu, H. Xue, G. Bordia, Z. Fink, P.Y. Kim, R. Streubel, J. Han, B.A. Helms, P.D. Ashby, A.K. Omar, T.P. Russell, *Adv. Mater.* 2310435 (2024).

Three-dimensional Nanoscale Inorganic Frameworks through DNA-programmable Assembly and Templating. Inorganic template of 3D DNA nano-framework: first into silica (A), then templating is achieved via vapor- (B) or liquid- (C) infiltration by metal salt solutions penetrating the framework. (D) The formed structure is silica coated with metal/metal oxide (MX) on a 3D DNA scaffold. (E) Electron microscopy image of silica (blue) coated with alumina (purple). The scale bar is 100 nm. A. Michelson et al. and Oleg Gang. Three-dimensional nanoscale metal, metal oxide, and semiconductor frameworks through DNA-programmable assembly and templating. *Sci. Adv*. 10, eadl0604 (2024).

Reversal of a global polar state in active colloidal fluid. Experimental snapshot of a Quincke roller suspension during a vortex reversal induced by a temporal modulation of activity. Groups of particles with identical colors represent spontaneous flocks moving in the same direction. The formation of subsequent global states is not random upon termination of the activity due to the presence of dynamic ensemble memory imprinting the dynamic state of the system. Alex Snezhko, Argonne National Laboratory.

Foreword

This volume comprises the scientific content of the presentations made at the 2024 Biomolecular Materials Principal Investigators' Meeting, sponsored by the Materials Sciences and Engineering (MSE) division in the Office of Basic Energy Sciences (BES) of the U.S. Department of Energy (DOE). The meeting's focus is on the fundamental science supported by the Biomolecular Material Core Research Area (CRA). The meeting took place July 30-August 1, 2024, in Rockville, MD as an in-person event with virtual option.

This is one of the series of Principal Investigators' Meetings organized regularly by BES. The purpose of the meeting is to bring together all the Principal Investigators with currently active projects including new projects in the Biomolecular Materials program for the multiple purposes of raising awareness among PIs of the overall program content and of each other's research, encouraging exchange of ideas, promoting collaboration, and stimulating innovation. The meeting also provides an opportunity for the Program Managers and MSE/BES management to get a comprehensive overview of the program on a periodic basis, which provides opportunities to identify program needs and potential new research directions.

Biomolecular Materials (BMM) program supports fundamental materials science research for discovery, design and synthesis of functional materials and complex structures based on principles and concepts of biology to create materials and multiscale systems that exhibit well-coordinated resiliency, functionality and information content approaching that of biological materials but capable of functioning under harsher, non-biological environments. New synthetic approaches, unconventional assembly pathways, and development of predictive models and AI/ML for data-driven science are sought to accelerate discovery/design of materials with transformative potential on carbon dioxide removal, advanced manufacturing, and energy transfer and storage technologies.

This was the first BMM PI Meeting since the untimely passing of Mike Markowitz who served as the Program Manager for the BMM program from 2009 to 2022. Mike has had a tremendous impact on the shaping of the BMM program and related soft matter and active matter fields. He is greatly missed for his surprisingly dry sense of humor and his deep technical and programmatic knowledge. I would like to specially thank Anna Balazs and Suri Vaikuntanathan for organizing and leading the Special Session in Honor of Mike Markowitz and all those who shared their stories.

Finally, I would like to thank the meeting attendees for their active participation and for sharing their ideas and new research results, which will bring fresh insights into the continued development of this field. Sincere thanks also go to Teresa Crockett of BES/MSE and Stephanie Fox and her colleagues at the Oak Ridge Institute of Science and Education (ORISE) for their excellent work providing all the logistical support for the meeting.

J. Aura Gimm
Program Manager, Biomolecular Materials
Materials Sciences and Engineering Division
Office of Basic Energy Sciences
U.S. Department of Energy

Table of Contents

Agenda

Tuesday, July 30, 2024

8:00-8:50 AM	**Breakfast and presentation /poster set-up.** (Give copies of presentations to Teresa Crockett prior to Wednesday afternoon)
8:50-9:00 AM	**Opening remarks** **Aura Gimm**, Program Manager, Biomolecular Materials **Todd Emrick** and **Akif Tezcan** Meeting Co-Chairs
Session 1	**Programmed Assembly and Dynamics of Biomacromolecular Materials** Session Chair: **Darrin Pochan**, University of Delaware
9:00-9:20 AM	**Gabriela Schlau-Cohen**, Massachusetts Institute of Technology (MIT). *Synthesizing Functionality in Excitonic Systems Using DNA Origami*
9:20-9:30 AM	Discussion
9:30-9:50 AM	**Oleg Gang**, Columbia University. *Controlling Lattice Organization, Assembly Pathways, and Defects in Self-assembled DNA-based Nanomaterials*
9:50-10:00 AM	Discussion
10:00-10:20 AM	**Jong Hyun Choi**, Purdue University. *Design Principles of Biomolecular Materials*
10:20-10:30 AM	Discussion
10:30-10:50 AM	**Break**
10:50-11:10 AM	**Akif Tezcan**, University of California San Diego *Protein Self-assembly by Rational Chemical Design*
11:10-11:20 AM	Discussion
11:20-11:40 AM	**Samuel Stupp**, Northwestern University. *Superstructures and Dynamics in Functional Supramolecular Assemblies*
11:40-11:50 AM	Discussion
11:50-12:10 PM	**Zvonimir Dogic**, University of California, Santa Barbara. *Microtubule-based Three-dimensional Active Matter*
12:10-12:20 PM	Discussion
12:30-1:30 PM	**Working Lunch with continued discussion and updates on DOE-BES and the Biomolecular Materials program**
1:30 3:00 PM	Poster Session 1 (last names A-H) and Discussion
Session 2	**Active and Adaptive Materials and Assemblies – Part 1** Session Chair: **Todd Emrick**, University of Massachusetts Amherst
3:00-3:20 PM	**Paul Nealey**, Argonne National Laboratory. *Precision Synthesis and Assembly of Ionic and Liquid Crystalline Polymers*
3:20-3:30 PM	Discussion

3:30-3:50 PM	**Joanna Aizenberg**, Harvard University. *Opto-chemomechanical Energy Transduction in Biomimetic Ensembles of Reconfigurable Microparticles of Liquid Crystal Elastomers*
3:50-4:00 PM	Discussion
4:00–4:20 PM	**Break**
4:20-4:40 PM	**Lara Estroff**, Cornell University. *Early Formation Stages and Pathway Complexity in Functional Bio-hybrid Nanomaterials*
4:40-4:50 PM	Discussion
4:50-5:10 PM	**Monica Olvera de la Cruz**, Northwestern University. *Electrostatic Driven Self-assembly Design of Functional Nanostructures*
5:10-5:20 PM	Discussion
5:30-7:00 PM	Poster Session 1, continued
7:00-8:30 PM	**Working dinner with discussion of new opportunities for cross-disciplinary collaboration and DOE user facilities**

Wednesday, July 31, 2024

8:00-8:55 AM	**Breakfast and presentation /poster set-up.** (Give copies of presentations to Teresa Crockett prior to Wednesday afternoon)
9:00-9:20 AM	**Aura Gimm**, Program Manager for Biomolecular Materials BES/BMM Updates.
9:20-9:30 AM	Discussion
Session 3	**New Projects – New Directions** Session Chair: **Kathleen Stebe**, University of Pennsylvania
9:30-9:45 AM	**Guillaume Duclos**, Brandeis University. *Hierarchical Assembly of Biomimetic Active Matter Driven by Non-equilibrium Actin Turnover*
9:45-9:50 AM	Discussion
9:50-10:05 AM	**Jason Green**, University of Massachusetts Boston. *Data-driven Learning of Dissipation from Microscopy of Chemically Active Materials*
10:05-10:10 AM	Discussion
10:10-10:25 AM	**Jacob Monroe,** University of Arkansas. *Physically Motivated Linking of Resolutions in Multiscale Models to Predict Thermal and Charge Transport in Self-Assembling Soft Materials*
10:25-10:30 AM	Discussion
10:30-10:45 AM	**(Virtual) Ahmad Omar**, University of California Berkeley. *Transport Mechanisms in Active and Biomolecular Materials*
10:45-10:50 AM	Discussion
10:50-11:05 AM	**William Shih**, Harvard University. *Principles of Self-navigation for Cell-sized Gliders*
11:05-11:10 AM	Discussion

11:10-11:30 AM	**Break**
Session 4	**Active and Adaptive Materials and Assemblies – Part 2** Session Chair: **Michael Solomon**, University of Michigan
11:30-11:50 AM	**Alexey Snezhko**, Argonne National Laboratory. *Dynamics of Active Self-Assembled Materials*
11:50-12:00 PM	Discussion
12:00-12:20 PM	**Qian Chen,** University of Illinois and **Erik Luijten,** Northwestern University. *Understanding and Informed Manipulation of Functional Dynamics on the Nanoscale through Integrated Experiments and Computation*
12:20-12:30 PM	Discussion
12:30-1:30 PM	**Working Lunch with discussions on potential new programmatic directions**
1:30-3:00 PM	Poster Session 2 (last names K-Y)
Session 5	**Active and Adaptive Materials and Assemblies – Part 3** Session Chair: **Michael Hagen**, Brandeis University
3:00-3:20 PM	**Anna Balazs,** University of Pittsburgh. *Growth in Heterogeneous, Evolving Macromolecular Networks: toward Functional, Biomimetic Materials*
3:20-3:30 PM	Discussion
3:30-3:50 PM	**John Brady,** California Institute of Technology, **Daphne Klotsa**, University of North Carolina at Chapel Hill, and **David Pine**, New York University. *Activity-enhanced Self-assembly of Colloidal-based Materials*
3:50-4:00 PM	Discussion
4:00-4:20 PM	**Break**
4:20-4:40 PM	**Thomas P. Russell**, Lawrence Berkeley National Laboratory. *Adaptive Interfacial Assemblies Towards Structuring Liquids*
4:40-4:50 PM	Discussion
4:50-5:50 PM	**Special Session in Honor of Dr. Michael Markowitz** Co-Chairs: **Anna Balazs**, and **Suriyanarayanan Vaikuntanathan**
5:50-7:00 PM	Poster Session 2, continued
7:00-8:30 PM	**Working dinner with discussion of inter-project opportunities**

Thursday, August 1, 2024

8:00-8:50 AM	**Breakfast** (Give copies of presentations to ORISE staff)
Session 6	**Active and Adaptive Materials and Assemblies – Part 4** Session Chair: **Akif Tezcan**, University of California at San Diego
9:00-9:20 AM	**Suriyanarayanan Vaikuntanathan**, University of Chicago. *Using AI and Non-equilibrium Statistical Mechanics to Design Adaptive Force-generating Bio-inspired Materials*
9:20-9:30 AM	Discussion
9:30-9:50 AM	**Nicholas Abbott**, Cornell University. *Bio-inspired Active Transport and Energy Transduction Using Liquid Crystals Beyond Equilibrium*
9:50-10:00 AM	Discussion
10:00-10:20 AM	**Break**
10:20-10:40 AM	**Rebecca Schulman**, Johns Hopkins University and **Elisa Franco**, University of California, Los Angeles. *Programmable Dynamic Self-Assembly of DNA Nanostructures*
10:40-10:50 AM	Discussion
10:50-11:05 AM	**Sidney Nagel**, University of Chicago. *Path dependence of memory formation in jammed packings*
11:05-11:20 AM	**Andrea Liu**, University of Pennsylvania. *Robustness of bio-mimetic material design to thermal noise*
11:20-11:30 AM	Discussion
11:30-12:00 PM	**Concluding Remarks and Discussion** **Todd Emrick** and **Akif Tezcan** Meeting Co-Chairs **Aura Gimm**, Program Manager, Biomolecular Materials
12:00 PM	**Adjourn**

Poster Session

Poster Session 1

Tuesday, August July 30, 2024

Last Name	First Name	Institution(s)	Poster Title
Hartley	Scott	Miami University, Oxford	Chemically Fueled Dissipative Assembly of Complex Molecular Architectures
Emrick	Todd	University of Massachusetts Amherst	Bio-inspired Materials Designs: Reactive, Functional Droplets, Mesoscale Structures, and Smart Interfaces
Osmanovic	Dino	University of California, Los Angeles	Generating Forces in Confinement via Polymerization
Chaikin	Paul	New York University	Self-Assembly and Self-Replication of Novel Materials from Particles with Specific Recognition
Guan	Zhibin	University of California Irvine	Electrically Fueled Dissipative Liquid-Liquid Phase Separation for Active Coacervates
Chen	Chun-Long	Pacific Northwest National Laboratory, University of Washington, University of Puerto Rico	Bio-inspired Durable Storage of CO2
Dishari	Shudipto	University of Nebraska-Lincoln	Biological Ion Channel-Inspired Ionomers with sub-nm sized Gated Ion Channels for High Ion Conductivity and Selectivity
Grover	Piyush	University of Nebraska-Lincoln	A framework for exploring and controlling non-equilibrium coherent states in active fluids based on global phase space geometry
Bathe	Mark	Massachusetts Institute of Technology	Synthesizing functionality in excitonic systems using DNA origami

Poster Session 2

Wednesday, August 1, 2024

Last Name	First Name	Institution(s)	Poster Title
Mallapragada	Surya	AMES National Laboratory	Bioinspired Metamaterials
Santore	Maria	University of Massachusetts, Amherst	Bending Controlled 2D Crystal Morphology, Domain Interactions, Patterning, and Impact on Vesicle Shapes
Sacanna	Stefano	New York University, University of Massachusetts Lowell	Energy-Efficient Self-Organization and Swarm Behavior in Active Matter
Solomon	Michael	University of Michigan	Biomimetic Strategies for Field-Driven Defect Annealing in Microparticle Crystals
Tezcan	Akif	University of California, San Diego	Rational Design of Protein Weaves and Isopeptide Bonds
Williard	Adam	Massachusetts Institute of Technology	Synthesizing Functionality in Excitonic Systems using DNA Origami
Ye	Tao	University of California, Merced Duke University Emory University	Steering the Pathways of Hierarchical Self-Assembly at Solid Surfaces
Pochan	Darrin	University of Delaware University of Pennsylvania	Biomolecules for non-biological things: Peptide 'Bundlemer' design for model colloidal particle creation and hierarchical solution assembly
Snezhko	Alexey	Argonne National Laboratory	Dynamics of Active Self-Assembled Materials
Ashby	Paul	Molecular Foundry Lawrence Berkeley National Laboratory UC Berkeley University of Massachusetts Amherst	A Closer Look at Structured Liquids
De Yoreo	Jim	Pacific Northwest National Laboratory University of Washington, Seattle Lawrence Livermore National Laboratory University of California, Merced	Design, synthesis, and assembly of biomimetic materials with novel functionalities – Precise Control over the Assembly and Transformation of Artificial Peptoid Membranes

Last Name	First Name	Institution(s)	Poster Title
De Yoreo	Jim	Pacific Northwest National Laboratory University of Washington, Seattle Lawrence Livermore National Laboratory	Design, synthesis, and assembly of biomimetic materials with novel functionalities – Two-dimensional Silk on van der Waals Substrates
Noy	Aleksandr	Lawrence Livermore National Laboratory Pacific Northwest National Laboratory University of Washington	Design, synthesis, and assembly of biomimetic materials with novel functionalities – Water, Solute, and Ion Transport in De Novo Protein Pores and Biomimetic Boron Nitrite Nanotube Porins
Noy	Aleksandr	Lawrence Livermore National Laboratory	Design, synthesis, and assembly of biomimetic materials with novel functionalities – Neuromorphic Ionic Computing in Droplet Interface Synapses
Silberstein	Meredith	Cornell University Sibley School of Mechanical and Aerospace Engineering	Bio-inspired Polymer Membranes for Resilience of Electrochemical Energy Devices
Strano	Michael	Massachusetts Institute of Technology	Materials Exhibiting Biomimetic Carbon Fixation and Self Repair: Methanotrophic Materials I
Kim	Jimin	Massachusetts Institute of Technology	Materials Exhibiting Biomimetic Carbon Fixation and Self Repair: Methanotrophic Materials II
Stebe	Kate	University of Pennsylvania	Far-from-equilibrium topological defects on active colloids in nematic liquid crystals (NLCs) or bio-inspired materials
Saven	Jeffrey	University of Pennsylvania University of Delaware	Computationally designed coiled coil ‘bundlemers’ as model colloidal nanoparticles for solution and materials design
Kumar	Manish	The University of Texas at Austin	Transport and Molecular Discrimination in Biomimetic Artificial Water Channels for Lanthanide Separations

Laboratory Abstracts

Computationally Driven Design and Synthesis for Electron Transfer Materials based on Nonnatural Polymers

Marcel D. **Baer,** Pacific Northwest National Laboratory

Keywords: nonnatural polymer, reduction potential, computational design

Research Scope

This project focuses on the computational design of biomimetic polymer units that integrate adjustable redox centers and structural elements, such as helices, to facilitate assembly into robust materials.

Using nature's blueprint, which employs ancient small protein modules, we aim to regulate electron transfer processes crucial for energy production and storage. These modules drive coupled oxidation and reduction reactions through redox centers, with their reduction potential and spatial arrangement controlled by the local environment, enabling precise electron flow control. However, replicating nature's intricate design in energy technologies involves overcoming the challenge of harsh non-biological conditions. By elucidating the structural requirements for incorporating these redox centers into synthetic biomimetic polymers, we aim to develop robust, functional materials to enhance the creation of advanced materials for energy applications.

The objectives include predicting the minimal sequence for binding redox-active iron-sulfur clusters (FeS), elucidating the conformational stability of non-natural polymers, and developing biomimetic units for the higher length-scale organization. These designed units can enable materials that mimic nature's spatial control of electron transfer, offering complex functionality in non-biological conditions.

Recent Progress

To test the hypothesis that *redox cofactors stabilized and tuned locally by the residues of synthetic, sequence-defined polymers—without relying on secondary structure elements—exhibit the same range of redox properties as natural redox cofactors stabilized by proteins or synthetic alpha peptides*, it is essential to improve our predictive capabilities for local structure, secondary structure elements, and the reduction potential of FeS clusters based on ligating residues and the local environment. We have made significant strides in developing atomistic interaction potentials that efficiently incorporate new chemical functionalities and enable accurate exploration of conformational space while considering solvent-specific polarization effects. We identified several stable helical backbone conformations for peptoids that increase the potential design space. Additionally, we benchmarked the prediction of reduction potentials for materials containing multiple iron centers, which pose challenges for quantum mechanical methods. We developed a model revealing a linear relationship between charge magnitude and ionization potential for [2Fe-

2S] and [4Fe-4S] clusters, significantly advancing our understanding of their electronic properties and redox behavior.

Development of a solvent-specific systematic and extensible force field for peptoids (STEPs-SOL). Peptoids (N-substituted glycines) are a class of biomimetic polymers gaining significant attention due to their accessible synthesis and enhanced enzymatic and thermal stability compared to natural polypeptides. While these polymers hold promise for creating robust functional materials through hierarchical approaches, they pose challenges for computational structure prediction in materials design. We have developed a solvent-specific, systematic, and extensible force field for peptoids, termed STEPs-SOL. Building on our previously developed STEPs force field,[1] designed for a systematic and expandable description of peptoids, we present the STEPs-SOL force field parameterization. This advancement significantly enhances the simulation of biomimetic polymers by incorporating solvent effects to improve accuracy, particularly in describing cis/trans equilibria. The general workflow, depicted in **Figure 1**, involves optimizing partial charges by considering all relevant backbone and sidechain conformations. This addresses computational challenges from non-bonded energies influenced by electrostatic and Lennard-Jones interactions, thus broadening the applicability of the STEPs force field across various solvents, including acetonitrile, chloroform, methanol, and water. Using meta-dynamics for conformational sampling, we evaluated equilibrium cis/trans ratios to capture the impact of solvent-specific polarization on peptoid architecture and structural dynamics. These findings contribute significantly to biomolecular materials research, offering crucial insights that can drive further advancements in material science and biomimetic polymer design.

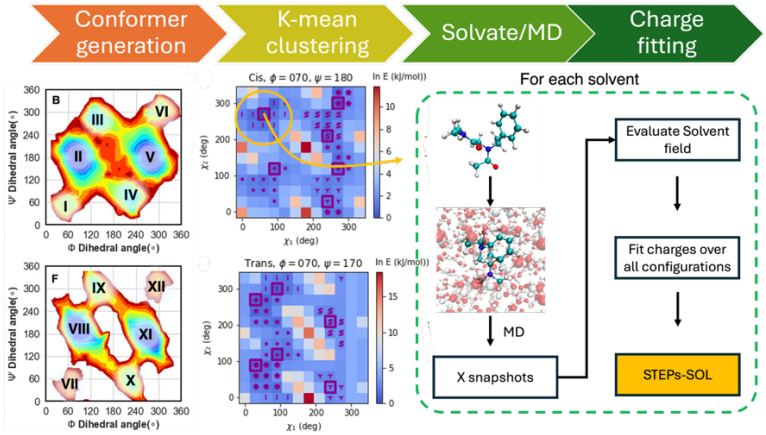

Figure 1. Workflow for Peptoid Conformational Analysis and Charge Fitting. Peptoid conformations are generated using the STEPs force field based on initial 12 backbone state defined conformational space, represented in a Ramachandran-like plot. The conformations undergo energy evaluation and K-means clustering based on rotatable side chain dihedrals with representative low-energy conformations selected from each cluster. Subsequently, the conformations are solvated and simulated, with partial charges fitted using the ipolq scheme in Ambertools. This workflow integrates molecular dynamics and density functional theory calculations to optimize peptoid design and accurately represent major conformations.

We identified several potential stable helical backbone conformations. We identified several potential stable helical backbone conformations based on our previously calculated peptoid backbone library. In this library, we precompute the available conformational space, considering all combinations for up to 7 monomers using the minima (I-XII) as shown in **Figure 1.** Helical structures were identified for capped peptoid 15-mer. **Figure 2** shows the three lowest energy helical structures, including their pitch and residues per turn, and highlights the position of the side chains that can be optimized using a new PyRosetta protocol by probing the stability through point mutations. Understanding how non-natural sequence-defined polymers fold into different helical structures is crucial for predicting their physical and chemical properties. This knowledge enables precise control over their structural configuration, providing insights into designing and optimizing new biomimetic materials with tailored properties.

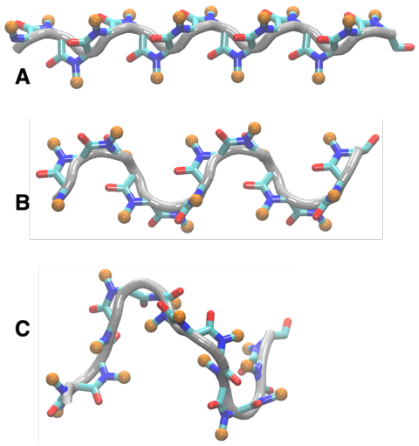

Figure 2. Low energy helical structures for peptoid 15-mer; backbone shown in licorice and sidechain position are highlighted in orange. A) the experimentally and theoretically proposed most stable helical structure[2] with a pitch of 6.6 Å and three residues per turn (ccc), B) helix with a pitch of 10.7 Å and five residues per turn (ccccc), and C) helix with a pitch of 12.3 and 8 residues per turn (ctcctc).

We developed a qualitative model that can predict the changes in the reduction potential for Fe_2S_2 and Fe_4S_4 clusters due to a single-charged residue. Testing 50 DFT functionals identified B3LYP as the most reliable for single iron complexes across low-lying spin states. For multi-iron systems, broken-symmetry DFT accurately described spin states and reduction potentials, validated against Fe_2S_2 complexes like Ferredoxin and Rieske (see **Figure 3**). Our computational and theoretical assessment of electrostatic interactions across the full dielectric range from gas to liquid water replicated experimental observations for biologically derived materials. Introducing a point charge at various positions on the van der Waals surface revealed pronounced anisotropy effects near bridging sulfides compared to ligating thiolates, with a linear relationship between charge magnitude and ionization potential (see **Figure 3**). The observed

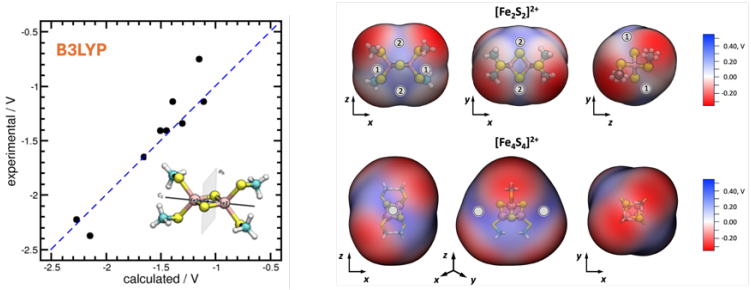

Figure 3. Left: computed versus experimental reduction potentials for F2S2 containing small sysnthetic molecules show good performance of BS-DFT. Right: Response of vertical electron affinity EVEA, ∂EVEA/∂q, to the field of a point charge at different locations around the $[2Fe\text{-}2S](SCH_3)_4^{2-}$ (top panels) and $[4Fe\text{-}4S](SCH_3)_4^{2-}$ complexes. Different views for each cluster are shown. Positive (blue) values correspond to a shift toward more positive values, the converse for negative (red) values. The positions that affect the VEA the most are highlighted as grey circles.

ionization potentials varied with Fe coupling constants, indicating overall tuning of reduction potentials through electrostatic interactions. These findings are crucial for understanding the electronic properties and redox behavior of [4Fe-4S] clusters, essential for developing design principles for materials that mimic nature's use of FeS clusters for electron transfer.

Future Plans

Using the methodological advancements discussed above, as well as the developed framework to predict the structure and reduction potential for short sequences bound to FeS clusters, we will test our hypotheses by exploring the conformational space of sequence-defined polymer chains and their capacity to bind FeS clusters (1) and investigate the stability and properties of secondary structure elements (2).

(1) Unlike in proteins, where the most common ligating residue is cysteine, we will screen tens of sulfur-containing side chains and their combinations. Initial combinations are chosen to span the relevant reduction potential space using our XTB^3-based framework. The ionization potential will be screened at the XTB level for stable conformations, and the reduction potential will be calculated using a Marcus theory approach to include solvation and dynamic effects. The systematic variation of sequence, ligand, and the predicted reduction potential allows testing the hypothesis that *FeS-clusters can be stabilized and tuned locally by the residues of synthetic sequence-defined polymers without relying on secondary structure elements having the same range of redox properties as natural redox cofactors stabilized by proteins or within synthetic alpha peptides.*

(2) To understand the stability and properties of secondary structure elements, we will study the helical peptoid sequences and triazine-based polymers known to form secondary structure elements. Qualitative effects on the electronic properties of these secondary structure elements will be studied using quantum mechanical methods. We will utilize the already-developed force field by systematically modifying side chain chemistry (charged, hydrophobic, steric). This approach will allow us to test the hypothesis that *secondary structure elements' stability and electronic properties can be tuned through side chain chemistry and linker choice, enabling the design of features that either block or enhance electron transfer.*

References

1. B. S. Harris, K. K. Bejagam, and M. D. Baer, Development of a Systematic and Extensible Force Field for Peptoids (STEPs), J. Phys. Chem. B, 2023, 127, 29, 6573–6584, doi:10.1021/acs.jpcb.3c01424
2. Armand, P.; Kirshenbaum, K.; Goldsmith, R. A.; Farr-Jones, S.; Barron, A. E.; Truong, K. T.; Dill, K. A.; Mierke, D. F.; Cohen, F. E.; Zuckermann, R. N.; Bradley, E. K., NMR determination of the major solution conformation of a peptoid pentamer with chiral side chains. *Proc Natl Acad Sci U S A* **1998,** *95* (8), 4309-14.

3. Bannwarth, C.; Ehlert, S.; Grimme, S., GFN2-xTB—An Accurate and Broadly Parametrized Self-Consistent Tight-Binding Quantum Chemical Method with Multipole Electrostatics and Density-Dependent Dispersion Contributions. J. Chem. Theo. Comp. **15** (3), 1652-1671 (2019).

Publications

1. B. S. Harris, K. K. Bejagam, and M. D. Baer, *Development of a Systematic and Extensible Force Field for Peptoids (STEPs)*, J. Phys. Chem. B, **2023**, 127, 29, 6573–6584, doi:10.1021/acs.jpcb.3c01424

Bio-inspired Durable Storage of CO_2

Principal Investigator: Chun-Long **Chen**, Pacific Norwest National Laboratory (PNNL) and University of Washington (UW)
Co-Principal Investigators: Jim De Yoreo (PNNL/UW), Chris Mundy (PNNL/UW), Kevin Rosso (PNNL), Wendy Shaw (PNNL), Jinhui Tao (PNNL), Praveen Thallapally (PNNL), Marvin Bayro (University of Puerto Rico)

Keywords: Peptoids, CO_2 mineralization, crystal nucleation and growth, phase transformation

Research Scope: The purpose of this project is to develop bio-inspired peptoid-based materials that enable removal and durable storage of atmospheric CO_2. Motivated by the urgency of reducing CO_2 levels in the atmosphere, our vision is to (1) discover and exploit the physical and chemical principles underlying accelerated CO_2 mineralization by peptoids and (2) use those principles to develop rules for designing robust and scalable organic additives that convert CO_2 into useful metal carbonate materials.

Recent Progress

A molecular view of peptoid-induced acceleration of calcite growth (*PNAS 2024, in review*). Previously we discovered that amphiphilic peptoids were able to accelerate the calcite step speeds by more than an order of magnitude at only nanomolar concentrations[1]. However, the lack of systematic experimental or computational insights into either the structural relationship between these growth accelerants and the steps to modify step edge structure and dynamics, interfacial hydration structure and energetics, or the barriers to desolvation and/or to deprotonation of the solute ions, leaves the mechanisms by which they impact step rates at the crystal surface largely unknown. To evaluate the roles of peptoid sequences, supersaturation and the stoichiometry of ions on accelerating the incorporation of growth units into the crystal steps and achieve the molecular level mechanistic understanding, herein, we designed a series of peptoids through systematic variations of the sequence that exhibited the greatest level of acceleration in our previous study[1].We systematically investigated the acceleration in step growth rate of calcite crystals using *in-situ* atomic force microscopy (AFM), varying peptoid sequences and

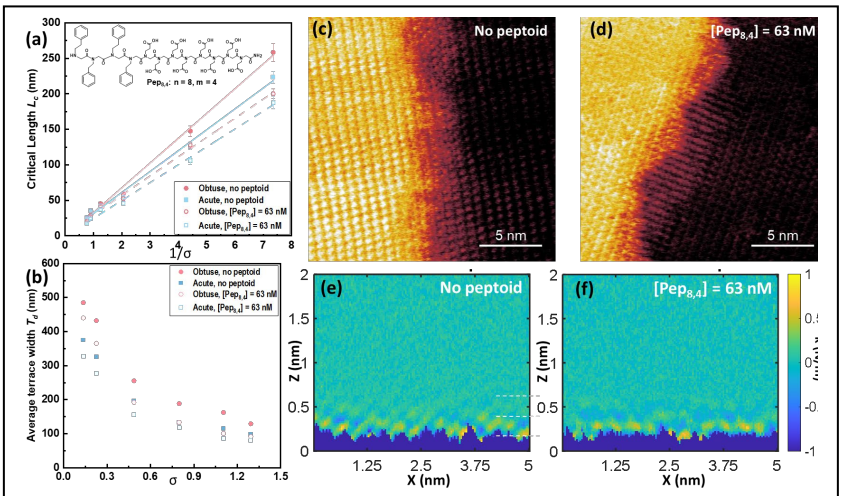

Figure 1. Mechanistic studies shown that the most potent peptoid promoters can facilitate HCO_3^- deprotonation, Ca^{2+} desolvation, and disruption of the calcite surface hydration structure, thus promoting calcite crystal growth. (a) Dependence of critical length of calcite steps on inverse supersaturation (1/σ), (b) dependence of average terrace width on supersaturation (σ), (c) and (d) *In situ* high resolution AFM image of the calcite step structure in a supersaturated solution (σ=0.226), (e) 3D AFM slices from force gradient maps normal to calcite surface with the hydration layers labeled with white dashes, in the absence and presence of $Pep_{8,4}$ (63.1 nM).

concentrations, $CaCO_3$ supersaturations, and the ratio of Ca^{2+}/ HCO_3^-. Mechanistic studies (Figure 1) using NMR, three-dimensional fast force mapping (3D AFM), and isothermal titration calorimetry (ITC) were conducted to reveal the interactions of peptoids with Ca^{2+} and HCO_3^- ions in solution, as well as the effect of peptoids on solvation and energetics of calcite crystal surface. Our results indicate the multiple roles of peptoid in facilitating HCO_3^- deprotonation, Ca^{2+} desolvation, and the disruption of interfacial hydration layers of the calcite surface, which collectively contribute to the peptoid-accelerated calcite growth. These results provide a molecular view of peptoid-induced acceleration of calcite growth, as well as essential principles of designing biomimetic organic additives that promoting CO_2 sequestration *via* $CaCO_3$ mineralization.

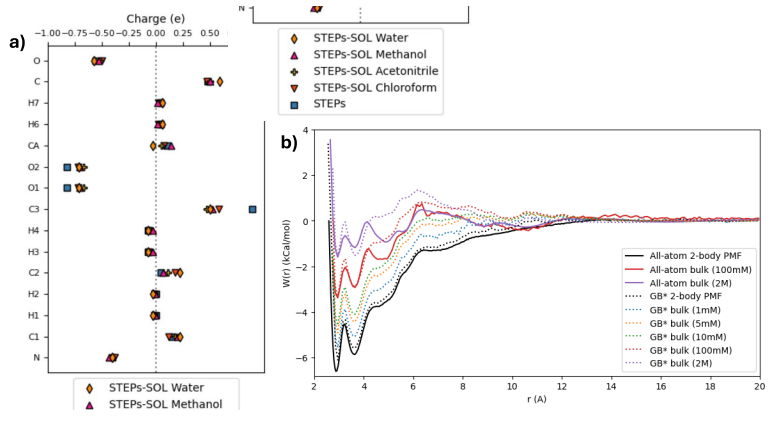

Figure 2. a) Peptoid monomer charges in STEPs force field (blue squares) and compared to STEPs-SOL force field in water (orange diamonds), methanol (pink upward-pointing triangles), acetonitrile (yellow '+' signs), and chloroform (red downward-pointing triangles). b) Energy as a function of distance between ions in simulation with Ca^{2+} and CO_3^{2-} in a box of water. All atom simulations with explicit water (solid lines). Simulations run with our reduced model, GB* (dotted lines).

Computational understanding of peptoid-promoted $CaCO_3$ nucleation. We have previously developed tools for modeling the initial stages of nucleation under bulk homogenous conditions.[2] The additional complexity of considering how a designed peptoids can alter the initial stages of $CaCO_3$ nucleation requires the extension and development of theory and molecular simulation tools. In this project, we developed peptoid force fields (FFs) with enhanced accuracy in liquid phase simulation. Specifically, we used the IPolQ method to extend the previously developed the STEPs[3] FF for peptoid parameterization, and tested the higher accuracy of these FFs in four solvents – water, acetonitrile, chloroform, and methanol that differ in dielectric constants. This extension captures polarization effects of the solvents on peptoid charges, which is especially important for peptoids with charged side chains. An example of the adjustment in charges is shown in Figure 2a). We also developed an efficient simulation framework to study the effects of peptoid sequence on the initial stages of $CaCO_3$ nucleation, which enables us to create an efficient model for simulating dilute solutions of $CaCO_3$ (e.g. ~1-10 mM) that can be extended to describe interactions with peptoids. Our previously developed tools[2] necessitated the construction of a reduced model for ion—ion interactions *via* the potential of mean force (PMF) between all ion pairs to capture the physics of short range interactions, and a continuum model for long range interactions. To consider additional complexity in the model to capture both peptoids and ion clustering, herein we utilized and extended the Generalized Born (GB) to GB* where the "*" denotes corrections to GB to account for the molecular details of the short-ranged interactions afforded by molecular simulation. We corrected for this difference by adding an external potential

that represents the difference between the Generalized Born and the all-atom PMF. Once this correction was implemented, we achieved perfect agreement with the all-atom PMF (Figure 2b). The GB* reduced model achieves perfect agreement with the all-atom model in the dilute limit that is corrected to fit the infinite dilution potential of mean force of all ion pairs. Moreover, the GB* performed well even at high concentrations demonstrating the efficacy to capture the collective effects of solutions both efficiently and accurately. Using this reduced model allows us to easily probe the dominant physics of interactions at $CaCO_3$ supersaturation concentrations and below, saving over five orders of magnitude in computational time and resources while keeping the simulation in a lower order of time complexity. Future work will be to incorporate both newly extended tools into simulation to probe $CaCO_3$ dynamics in the presence of peptoids.

Understanding interactions of peptoids with $CaCO_3$ surfaces using solid-state NMR. To understand mechanisms of peptoid-promoted $CaCO_3$ formation, a peptoid with alternating hydrophobic and carboxylic acid side chains was bound to ACC. With the hypothesis that the tighter the peptoid binds to a surface, the less motion it will have, we characterized this binding with solid state NMR to assess the dynamics of the surface bound peptoid, specifically looking at the backbone carbonyls, on the timescale of 10^{-3} to 10^{-5} seconds.[4] Three different labeled peptoids were synthesized by having the: 1) last two C-terminal, 2) middle two or 3) first two N-terminal backbone carbonyls ^{13}C labeled. These ^{13}C labeled peptoids were incubated with pre-formed amorphous calcium carbonate (ACC) to produce the peptoid bound ACC sample for solid-state NMR. A peptoid shoulder is present for the C-terminal labeled peptoid in preliminary cross polarization magic angle spinning (CP-MAS) experiments, whereas only a weak shoulder is detectable for the N-terminal labeled peptoid and no shoulder is detectable for the spectra with the peptoid labeled at the middle two backbone carbonyls. Since cross-polarization efficiency is expected to decrease as a function of increased mobility, we conclude from these NMR results that the C-terminus is highly rigid on the ACC surface, whereas the N-terminus is only interacting moderately, and the middle region of the peptoid has nearly no interaction with the surface. Similar approaches were used to investigate these three ^{13}C labeled peptoids for their interactions with aragonite. Again, there appears to be a distinct peptoid shoulder present for the C-terminus labeled sample, whereas no detectable peptoid shoulder is present for the N-terminus or middle-labeled samples, further confirming the most important role of C-terminus for interacting with $CaCO_3$.

Peptoid-based crystalline nanomaterials as carbonic anhydrase (CA) mimics for promoted hydration and sequestration of CO_2 (Figure 3**).** CA mimics have recently received significant attention due to their promising applications in the enhanced hydration and sequestration of CO_2. Despite significant advances have been made in design and synthesis of CA mimics using sequence-defined macromolecules, this area is underexplored with limited success. Herein, we report the assembly of peptoids into crystalline nanomaterials with controlled microenvironment of active sites as CA mimics through the coordination of imidazolyl with Zn and the variation of peptoid side chains. These synthesized Zn-containing crystalline nanomaterials exhibited effectively mimetic function with natural CA for catalytic *p*-nitrophenyl acetate (*p*-NPA). We demonstrated that the tuning of morphology, crystallinity, surface and ligand chemistries of

peptoid assemblies are crucial for catalytic hydrolysis of *p*-NPA. Among them, **Pep12-Zn^{2+}** nanotubes exhibited the catalytic efficiency comparable to those of bovine carbonic anhydrase, a natural enzyme often used to evaluate CA mimetics. Molecular dynamics (MD) simulations revealed the critical roles of peptoid-Zn^{2+} binding energy and of the local microenvironment of active sites on the catalytic performance of these peptoid-based biomimetic catalysts. Moreover, they could remarkably promote the hydration and sequestration of CO_2 while retaining high thermal and chemical stability. NMR results (Figure 3b-e) further confirmed the catalytic nature of these CA mimics and the accelerated CO_2 hydration and CO_2 mineralization through a unique formation pathway. This work offers essential guidance for the future design of high-performance CA-mimics for applications in carbon capture and sequestration.

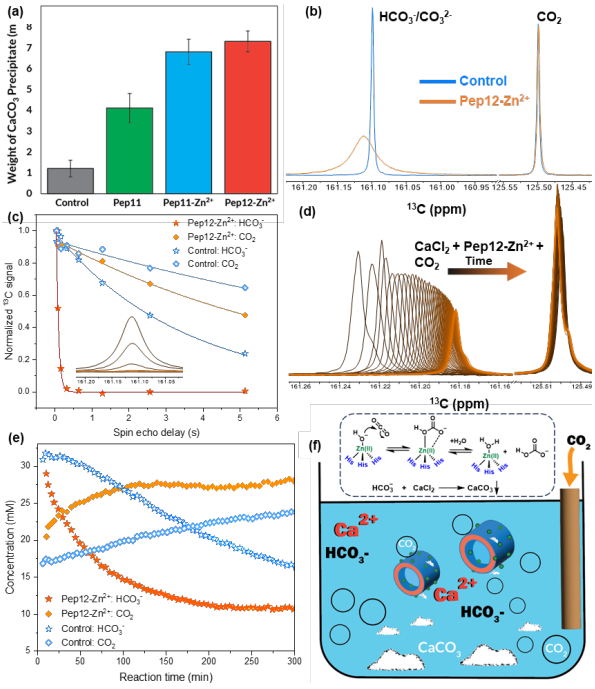

Figure 3. Assembled peptoid crystalline nanomaterials as CA mimics to promote CO_2 hydration and sequestration. (a) Weights of $CaCO_3$ precipitates induced by CA mimics. (b) ^{13}C NMR spectra showing **Pep12-Zn^{2+}** promote CO_2 hydration and conversion. (c) Normalized ^{13}C NMR signal showing that **Pep12-Zn^{2+}** dynamically interact with both CO_2 and HCO_3^- to promote CO_3^{2-} formation. (d) In-situ ^{13}C NMR monitoring of CO_2 sequestration to $CaCO_3$. (e) Evolution of concentrations of HCO_3^- and CO_2 during CO_2 sequestration with and without **Pep12-Zn^{2+}** nanotubes. (f) Proposed mechanism showing the CA-mimic promoted CO_2 hydration and sequestration.

Future Plans

Our future plans center on continuing to design and synthesize peptoid sequences and crystalline materials for promoting the nucleation and crystal growth of carbonate crystals. To better understand how peptoids function at the solid-liquid interfaces of carbonate crystals for accelerated crystal nucleation and/or growth, we will continue using solid-state NMR along with 3D AFM techniques to investigate how peptoid sequences, assembly structures and surface chemistries impact the interfacial solution structure to promote carbonate crystal nucleation and phase transformation.

References

1. Chen, C. L.; Qi, J. H.; Tao, J. H.; Zuckermann, R. N.; DeYoreo, J. J. Tuning calcite morphology and growth acceleration by a rational design of highly stable protein-mimetics. Sci. Rep. **2014**, 4, 6266; Chen, C. L.; Qi, J. H.; Zuckermann, R. N.; DeYoreo, J. J. Engineered biomimetic polymers as tunable agents for controlling CaCO3 mineralization. J. Am. Chem. Soc. **2011**, 133 (14), 5214-5217.

2. Henzler, K.; Fetisov Evgenii, O.; Galib, M.; Baer Marcel, D.; Legg Benjamin, A.; Borca, C.; Xto Jacinta, M.; Pin, S.; Fulton John, L.; Schenter Gregory, K.; et al. Supersaturated calcium carbonate solutions are classical. Sci. Adv. **2018**, 4 (1), eaao6283.

3. Harris, B. S.; Bejagam, K. K.; Baer, M. D. Development of a Systematic and Extensible Force Field for Peptoids (STEPs). J. Phys. Chem. B **2023**, 127 (29), 6573-6584.

4. Shaw, W. J.; Ferris, K. Structure, orientation, and dynamics of the C-terminal hexapeptide of LRAP determined using solid-state NMR. J Phys Chem B **2008**, 112 (51), 16975-16981.

Publications since 2023 PI meeting.

1. M. Zhang, Y. Chen, C. Wu, R. Zheng, Y. Xiao, E. G. Saccuzzo, T. K. H. Trinh, E. A. Q. Mondarte, E. Nakouzi, B. Rad, B. A. Legg, W. J. Shaw, J. Tao, J.J. De Yoreo, C.-L. Chen, *A Molecular View of Peptoid-Induced Acceleration of Calcite Growth*, **Proc. Natl. Acad. Sci. USA**, in review (2024).

2. L. Shao, D. Hu, S.-L. Zheng, T. K. H. Trihn, W. Zhou, H. Wang, Y. Zong, C. Li, C.-L. Chen, *Hierarchical Self-Assembly of Multidimensional Functional Materials from Sequence-Defined Peptoids,* ***Angew. Chem. Int. Ed.*** 63, e202403263 (2024).

3. A. Y. Heble, C.-L. Chen, *Access to Advanced Functional Materials through Postmodification of Biomimetic Assemblies via Click Chemistry*, ***Biomacromolecules*** 25, 3, 1391–1407 (2024).

Bioinspired Metamaterials

Surya **Mallapragada**, Andrew Hillier, Marit Nilsen-Hamilton, Tanya Prozorov, Alex Travesset, David Vaknin, and Wenjie Wang, Ames National Laboratory

Affiliation: Division of Materials Science and Engineering, Ames Laboratory, Ames, IA 50011

Keywords: metamaterials, DNA origami, metallization, self-assembly

Research Scope

The Bioinspired Metamaterials FWP at the Ames National Laboratory focuses on developing fundamental bioinspired approaches for creating self-assembled mesoscale two- and three-dimensional (2D and 3D) structures that can serve as optical metamaterials. We are developing bioinspired, bottom-up synthesis approaches using DNA origami templates for further metallization to create nanoresonators that are functionalized to enable their assembly into 2D and 3D mesoscale organization and alignment. Our interdisciplinary collaborative approach integrates experiment and theory and aligns with DOE's priorities laid out in the Synthesis Science workshop report for the synthesis of complex nanostructures and multi-scale assemblies. It also addresses the *DOE's Grand Challenge,* to orchestrate atomic and electronic constituents to control material properties.

Recent Progress

We have focused on fabricating conductive resonant meta-atoms, using DNA origami templates, optimizing and improving their structure and morphology, enhancing the quality of their optical resonance behaviors, developing characterization tools that allow detailed measurement of the optical scattering profiles of individual metallic nano-objects, and pursuing strategies to create ordered, two-dimensional surface patterns of origami-templated resonant meta-atoms. We have also focused on efforts, using gold nanoparticles as model nanostructures to develop 3D assembly approaches of these nanoparticles using polymer functionalization. Synthesis and fabrication approaches have been complemented by development and use of synchrotron X-ray scattering and transmission electron microscopy to characterize meta-atoms and their assemblies. The experiments have been closely coupled with theoretical efforts for optical properties and predicting self-assemblies of nanostructures.

Design and Characterization of Individual Meta-atoms: We have created ~100 nm sized DNA origami templates of various shapes for further metallization to create meta-atoms that mimic split-ring nanoresonators (SRR). The triangle-shapes, because of their symmetry, have an in-plane-isotropic electric dipole resonance as their lowest Mie mode and are thus not interesting as functional meta-atoms. However, this triangular origami modified by introducing a gap or by omitting a complete side of the triangle can produce resonant meta-atoms that implement the very important SRR motif, for both electric and magnetic dipole resonances. Initially using a silver photochemical seeding process followed by electroless deposition of gold, allowed reproducible formation of large numbers of similarly-shaped, surface-bound conductive meta-atoms using DNA origami [1]. We used High Angle Annular Dark Field Scanning Transmission Electron Microscopy (HAADF-S/TEM) imaging to follow metallization of DNA origami triangles utilizing

a two-step approach: (1) formation of Pd clusters (seeds) at the surface of DNA origami triangles, and (2) forming Au particles at the surface of seeded DNA triangles, with Pd clusters acting as nucleation points. **Fig. 1** shows the metallized uniform nanostructures. We have developed disorder models for DNA-templated metallized meta-atoms to predict the degree of disorder that the meta-atom structures can tolerate to still exhibit desired optical properties.

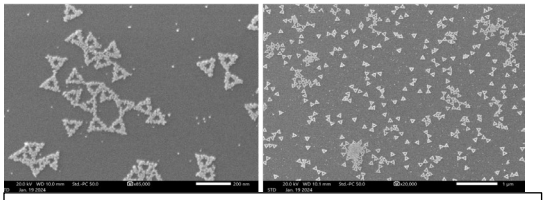

Fig. 1 Enhanced metallization using palladium seeding (left) and gold ELD (right)

Since the optical properties of metamaterials are derived from the collective response of the assembly of meta-atom units, it is crucial to understand the construction and scattering behavior of individual meta-atoms. Nanoscale optical characterization of the meta-atoms and their assemblies are being conducted using optically-coupled atomic force microscopy (AFM) imaging in the form of nano-FTIR and scattering-near field scanning optical microscopy (s-SNOM). The nano-FTIR (or s-SNOM) is able to essentially measure the dipole Greens function scanning over the surface of the nanostructure, the imaginary part of which represents the local density of states for the electromagnetic field in the vicinity of the resonant scatterers (for s-SNOM, the amplitude ratio and phase of the measured optical signal correlates with the real and imaginary components of the material's refractive index). We have performed proof-of-concept measurements of s-SNOM on our DNA origami samples in unmodified and metallized forms. **Fig. 2** shows AFM and s-SNOM phase images of both bare and Pd-coated DNA origami triangles. AFM height images of the DNA reflects heights of ~1 nm for the bare DNA (Fig.2A) and ~12 nm for the Pd-coated sample (Fig.2C). s-SNOM images taken with a 632 nm laser source shows no contrast for the bare DNA (Fig.2B) but a strong signal in the phase data for the Pd-coated sample (Fig.2D), indicating the presence of a strong optical resonance from the metal coating.

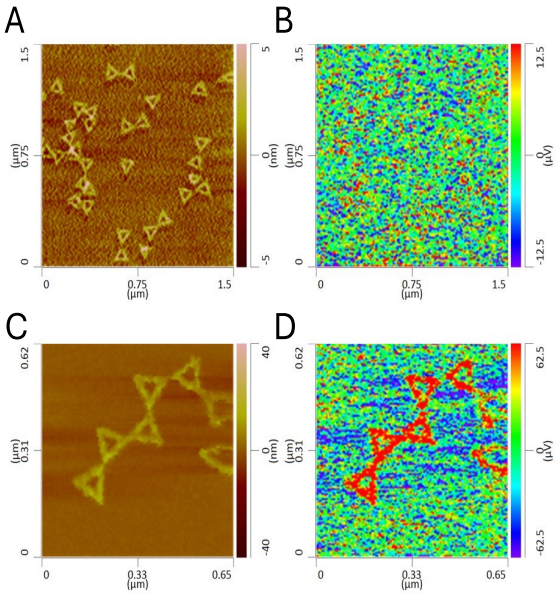

Fig. 2. AFM and s-SNOM images of DNA origami. (A) AFM height and (B) s-SNOM phase images of uncoated DNA origami triangles. (C) AFM and (D) s-SNOM phase images of Pd-coated DNA origami triangles. Samples are mounted on n-Si and imaged in tapping mode using HeNe (λ=632 nm) laser excitation.

Controlling Self-Assembly of Nanoparticles and Nanostructures: Preliminary efforts were pursued to create organized two-dimensional patterns of resonant meta-atoms. A patterning strategy based upon NanoSphere Lithography was used to create two-dimensional patterned surfaces with specific binding sites for DNA origami. DNA origami was selectively adhered to the hydrophilic sites using ion-pairing interactions to create a hexagonally-packed monolayer of origami, to be further metallized to create an organized, two-dimensional pattern of meta-atom resonators. For a bottom-up approach to assembly, we have

used DNA-hybridization as inspiration, but designed assembly strategies based on synthetic polymers such as poly(ethylene glycol) (PEG) and poly(acrylic acid) (PAA), interacting with each other through hydrogen bonding or with external stimuli in solution to drive the assembly of metallic nanostructures. The use of synthetic polymers expands the range of chemistries, and also allows for robust self-assembled structures that are stable when removed from solution. For these studies, carried out in parallel with the development of the meta-atoms as described above, metal nanostructures, mimicking metalized DNA origami, offer an exceptional platform to investigate particle interactions and assembly in aqueous (and solvent) environments under mild conditions. We have used gold nanoparticles as model nanostructures to develop methods for 2D and 3D self-assembly by functionalizing with polymers.

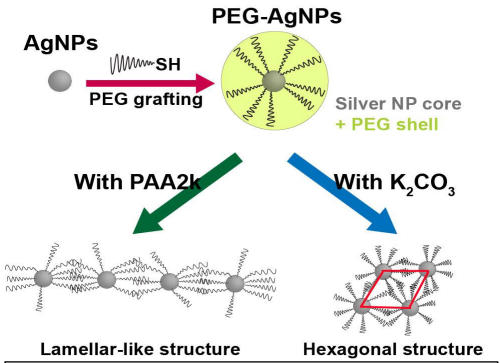

Fig. 3 Lamellar and hexagonal assemblies of PEG-grafted AgNPs

We have used interpolymer complexation to create robust nanoparticle superlattices that can be tuned by changing temperature and/or pH. Our unique approach involved attaching PEG chains to both gold (AuNPs) and silver nanoparticles (AgNPs), subsequently cross-linking them with PAA chains, culminating in the successful fabrication of densely packed 2D and 3D superstructures (**Fig. 3**)[2]. Our findings indicate that less efficient grafting onto AgNPs can instigate directional bonding.

We investigated functionalizing the nanostructures with water-soluble polymers that terminate with charged end groups in aqueous solutions. This innovative approach offers salt-free control over assembly behavior, achieved through precise adjustments in pH and temperature. Our strategy involved grafting AuNPs with PEG terminated with CH_3 (charge-neutral), COOH (negatively charged), or NH_2 groups (positively charged). In our investigations, we discovered intriguing differences among these terminations. Notably, our ability to fine-tune the charge density on the surface of AuNPs enables precise control over aggregation and solubility [3]. We have shown that we can create nanoparticle superlattices with negative thermal expansion (NTE) coefficients by grafting temperature-responsive polymers such as poly(N-isopropylacrylamide) to the gold nanostructures [4]. We also showed that two distinct complex two-dimensional binary superlattices were self-assembled by co-crystallizing gold nanoparticles (AuNPs) of two distinct sizes, allowing for greater control over the packing density [5].

Switching from the charge-neutral PEG ligand terminal[6] methyl, to negatively and positively charged terminals, allows us to assemble ordered assemblies via regulating the strength of the Coulombic interactions. Based on synchrotron small-angle x-ray scattering data, we show that oppositely charged AuNPs with carboxyl and amine terminals can act as super-ions and form various 3D binary ionic superlattices in suspension. We have shown that we can create pH-

controlled superstructures with different lattice arrangements (**Fig. 4).** Through systematically adjusting pH levels and mixing ratios, we achieved unique checkerboard square lattices, a departure from the ubiquitous hexagonal patterns observed with neutral PEG-AuNPs [7].

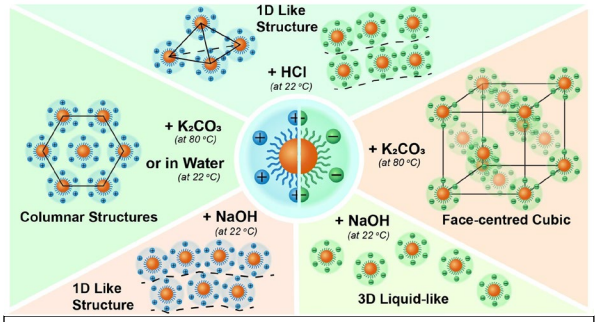

Fig. 4 Tuning self-assembly of AuNP grafted with charged polymers by varying temperature and electrolytes

We have derived theoretical approaches to pack cubic nanocrystals as well as mixtures of cubic and spherical nanocrystals [8]. The model allows for prediction of packing density without any fitting parameters. We have been able to extend the Orbifold Topological Model (OTM) to account for the role of ligands beyond spherical nanocrystals and its generalization to arbitrary nanocrystal shapes. We have expanded methods to compute free energies and internal energies for nanoparticle systems in molecular dynamics to achieve high precision [9]. We demonstrated the assembly of a new type of chiral superlattice in a collaborative study, where the chirality is induced by the substrate [10]. The simplicity and versatility of substrate-supported chiral superlattices facilitate the formation of meta-structured coatings with unusual optical, mechanical and electronic characteristics.

Future Plans

We have been able to create uniform conductive meta-atom structures using metallized DNA origami templates and functionally characterize these individual meta-atoms to show that they exhibit both electric and magnetic resonances as seen with split ring resonators. We have conducted initial studies to assemble them on surfaces and have also developed approaches for the assembly of model nanostructures in aqueous solutions through synthetic polymer functionalization, mimicking DNA hybridization approaches to create meso-scale assemblies. Our future work will now build on this progress, to focus on creating hierarchically self-assembled 2D and 3D mesoscale structures of meta-atoms and functionally characterize these 2D and 3D assemblies to demonstrate the existence of the desired resonances characteristic of functional metamaterials, and gain insights into structure-function relationships of these materials. A thorough understanding of the complex interplay involving different interactions for hierarchical assembly that we will gain through this work will represent a fundamental advance towards our ability to form robust and highly stable 2D and 3D meta-atom superstructures, but also have broader impact on other systems.

Publications (10 most relevant)

1. M.M. Islam, M.M. Hossen, J.Adjasoo, P. E. Palo, L. Bendickson, N.E. Kallmyer, N.F. Reuel, M. Nilsen-Hamilton, T. Koschny, A.C. Hillier, *Direct Measurement of Optical Resonance Modes in Gold Meta-Atoms Fabricated by Metallization of Triangle- and V-Shaped DNA Origami Templates*, Journal of Physical Chemistry C*,* **127,** 50, 24291–24302 (2023).
2. H.J. Kim, W. Wang, W. Bu, S.K. Mallapragada, and D. Vaknin, *Lamellar and Hexagonal Assemblies of PEG-Grafted Silver Nanoparticles: Implications for Plasmonics and Photonics*, ACS Appl. Nanomaterials, **5**, 17556-64 (2022). https://doi.org/10.1021/acsanm.2c03042
3. H.J. Kim, B.P, Nayak, H.H. Zhang, B.M. Ocko, A. Travesset, D.Vaknin, S.K. Mallapragada and W.J. Wang, *Two-Dimensional Assembly of Gold Nanoparticles Grafted with Charged-end-group Polymers.* J Colloid Interfacial Sci., **650**, 1941-8 (2023) doi: 10.1016/j.jcis.2023.07.095.
4. B.P. Nayak, H.J. Kim, S. Nayak, W. Wang, W. Bu, S.K. Mallapragada, and D. Vaknin, *Assembling PNIPAM-Capped Gold Nanoparticles in Aqueous Solutions*, ACS Macro Letters*,* **12,** 1659-1664 (2023). https://doi.org/10.1021/acsmacrolett.3c00617
5. H.J. Kim, W. Wang, H. Zhang, G. Freychet, B.M. Ocko, A. Travesset, S.K. Mallapragada, D. Vaknin, *Binary Superlattices of Gold Nanoparticles in Two Dimensions*, J. Phys. Chem. Lett., **13** (15), 3424-3430 (2022). https://doi.org/10.1021/acs.jpclett.2c00625
6. E. Macias, and A. Travesset, *Hydrogen Bond Network Disruption by Hydration Layers in Water Solutions with Salt and Hydrogen Bonding Polymers (PEO)*, J. Phys. Chem.B., **127**, 6778-6794 (2023). https://doi.org/10.1021/acs.jpcb.3c02505
7. B.P. Nayak, H. Zhang, W. Bu, B.M. Ocko, A. Travesset, D. Vaknin, S.K. Mallapragada, and W. Wang, *Ionic-Like Superlattices by Charged Nanoparticles: A Step Toward Photonics Applications*, ACS Applied Nano Materials*,* **7,** 3, 3220–3228 (2024). https://doi.org/10.1021/acsanm.3c05566
8. J. Hallstrom, I. Cherniukh, X. Zha, M.V. Kovalenko, and A. Travesset, *Ligand Effects in Assembly of Cubic and Spherical Nanocrystals: Applications to Packing of Perovskite Nanocubes*, ACS Nano**, 17**, 7219-7228 (2023).
9. A. Upah, A. Thomas, J. Hallstrom, and A. Travesset, *High-Precision Calculation of Nanoparticle (Nanocrystal) Potentials of Mean Force and Internal Energies*, Journal of Chemical Theory and Computation*,* **20**, 4, 1559–1567 (2023). https://doi.org/10.1021/acs.jctc.3c00749
10. S. Zhou, J. Li, J. Lu, H. Liu, J.Y. Kim, A. Kim, L. Yao, C. Liu, C. Qian, Z. Hood, X. Lin, W. Chen, T.E. Gage, I. Arslan, A. Travesset, K. Sun, N.A. Kotov, and Q. Chen, *Chiral Assemblies of Pinwheel Superlattices on Substrates*, Nature*,* **612**, 259–265 (2022).

Precision synthesis and assembly of ionic and liquid crystalline polymers

Paul **Nealey***, Juan J de Pablo*, Matthew Tirrell*, and Jie Xu[+]

Materials Science Division*, and Nanoscience and Technology[+], Argonne National Laboratory, Lemont, Illinois 60439, USA

Keywords: precision synthesis, self-assembly, hetero-charged polymers, molecular simulation, nanostructured polyelectrolytes, mixed conductors

Research Scope

This project advances the discovery of new principles towards a fundamental understanding of the chemistry, physics, and materials science of charged nanostructured and functional polymer and soft matter systems, both at equilibrium and far from equilibrium. Our approach relies on the synthesis of polymers with precise composition and sequence, as well as the processing these new materials through controlled molecular self- and directed self-assembly. Molecular self-assembly, with basic tenets derived from biology, is arguably the most promising strategy for imparting structure and function to materials at the molecular, meso-, and macro-scale and for developing functional soft and biomolecular materials; information encoded into the building blocks introduces specific and controllable intra- and intermolecular interactions to drive assembly with hierarchical structure. Because the assembly, structure, and dynamics of functional polymer and soft matter systems are complicated, a unifying concept and defining strength of our overall project is the combination of experiment, autonomous laboratories, theory, computation, and data driven approaches to accelerate materials discovery and design. Our effort and progress reported below is organized along three interrelated thrusts: Thrust 1: Fundamental Investigation of Water Absorption and Ion Transport Mechanisms in Homopolymer and Block Copolymer Electrolytes, Thrust 2: High-Throughput Robotic Experimentation and Computation for Designing Mixed Conducting Polymers, and Thrust 3: Hybrid Coacervation, Surface Interactions and Their Modification with Polyampholytes. Fundamental materials and principles discovered in his project will impact a wide array of energy technologies, ranging from fuel cells, electrolyzers, and desalination, to energy storage, energy-efficient devices, neuromorphic computing, and electrochemical sensors, to antifouling coatings for separation membranes.

Recent Progress

Thrust 1: Fundamental Investigation of Water Absorption and Ion Transport Mechanisms in Homopolymer and Block Copolymer Electrolytes:

Understanding the interplay between polymer, water, and ion's structure and dynamics is crucial to overcoming the current limitations of anionic exchange membranes (AEMs) for energy applications at scale. We employed a multidisciplinary approach combining controlled polymer synthesis, precise water and ion transport properties characterization in nanometer-sized films, and multi-scale computational simulations. With this approach, we can characterize water structure and dynamics at a molecular level of detail, over time and length scales that range from molecular vibrations and rotations to macroscopic polyelectrolyte performance.

Water Dynamics, Water Structure, and Ion Transport in AEMs. Ion transport is crucial for the functionality of polyelectrolyte materials in energy storage, with water playing a pivotal role in facilitating this process. A widely held view of ion and water dynamics in such materials holds

that, beyond a threshold concentration, water assumes a bulk-like behavior that enables what is referred to as "fast" ion transport. In this work, we attribute the enhanced ionic conduction in polymers under high humidity to structural and topological changes in the network of ions and hydration water. Our findings challenge the conventional view that fast ion transport depends on the presence of free, bulk-like water and fully dissociated ions. Instead, we find that the faster ion transport mechanism occurs when the reorientation of water molecules in the second solvation shell is fast, allowing a robust hydrogen bond network to form. This mechanism is supported by ultra-fast two-dimensional infrared (2D IR) spectroscopy, which measures rapid water reorientation dynamics, and molecular dynamics (MD) simulations, which correlate the fast transport regime with changes in water structure and dynamics. MD simulations further show that the robustness of a percolating network of hydrated ions characterized by a large proportion of water in the second hydration shell allows for fast water and ions dynamics. Our results serve to establish that, the combination of spectroscopic and computational techniques provides a powerful tool for characterization of dynamics in these types of materials.

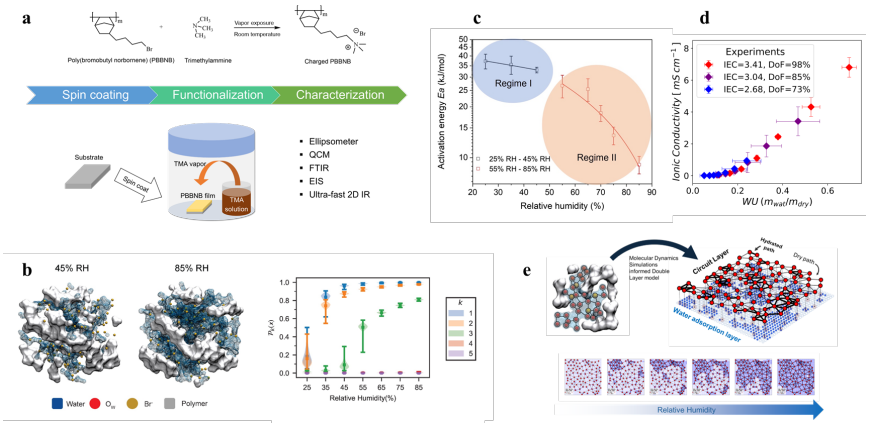

Figure 1. (A) Experimental Workflow. (B) Characteristic configurations of the polymer at low and high relative humidity (RH) and network percolation analysis. (C) Ionic transport activation energy as a function of RH measured experimentally. (D) Universal curve of ionic conductivity vs water uptake for polymers of different IEC. (E) Description of the Coupled Layer Model showing characteristic snapshots of the simulation at increased RH.

Ionic conduction and water uptake in polymers with different ionic exchange capacity (IEC). To test the validity of our conclusion, we extended the previous analysis to polymers with different IECs, which measure the charge concentration in the polymer matrix. Informed by the percolation analysis over MD simulations, we developed a minimal simulation model of the membrane that couples the thermodynamics of water adsorption to the conductivity of random resistor networks at low computational cost (fig 1(e)). Both experiments and simulations confirmed that fast conduction begins when water forms a percolated network facilitated by favorable interactions between water molecules connecting ion hydration shells. Furthermore, we found that to ultimately be the reason for the universal relationship between ionic conductivity and water content shown in fig. 1 (d). The curves collapse because all networks percolate at the same water content, but water only binds to water already adsorbed around the ions (there is no free water). That leads to lower water content and lower conductivity in polymers with lower IEC.

Thrust 2: High-Throughput Robotic Experimentation and Computation for Designing Mixed Conducting Polymers:

Redox Gating for Colossal Carrier Modulation and Unique Phase Control. Redox gating is a novel technique distinct from traditional electrolyte gating, employing reversible redox functionalities combined with ionic electrolyte components to achieve efficient charge transport and electronic

phase control [1]. This method enables substantial sheet carrier density modulation exceeding 10^{16} cm^{-2}, maintained over thousands of cycles within a sub-volt regime for functional oxide thin films. Unlike conventional electrolyte gating, redox gating injects many carriers without causing ionic defects or intercalated species. The study specifically demonstrated the control of the electronic phase transition in VO_2 using redox gating, highlighting the influence of metal-containing poly(ionic liquids) (PILs) on semiconducting metal oxides and materials with strongly correlated electron behaviors (Figure 2). These findings confirm the low-voltage properties and high efficiency of the redox-active polymer electrolyte, underscoring its potential for future applications in advanced electronic devices. Redox gating decouples electrical and structural phase transitions, supporting isostructural metal-insulator transitions and enhancing device endurance. This method is applicable across various materials, regardless of crystallinity or carrier type, offering significant improvements in the efficiency and power consumption of microelectronic devices. Consequently, redox gating could lead to the development of smaller, more energy-efficient semiconductors and quantum devices. This work is a new application of our developing expertise in ionic polymers.

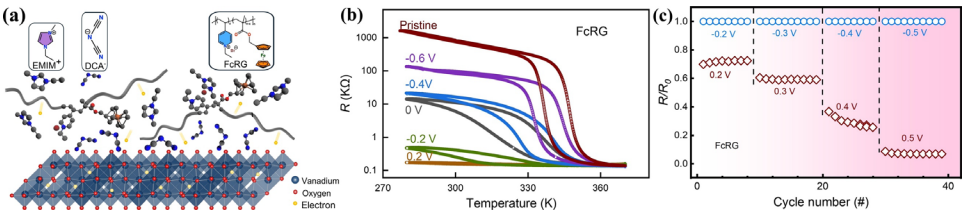

Figure 2. Redox Gating and Electric Field Control of VO_2 Films. (a) Schematic illustration of redox gating, where yellow balls represent electrons generated in the electrolyte and injected into VO_2, enabling carrier manipulation and electric field control of the electronic state. (b) Suppression of the temperature-driven metal-insulator transition in VO_2 films using FcRG electrolytes. (c) Normalized resistance measurements during gate voltage cycling, demonstrating the controllable modulation of the electronic state.

Thrust 3: Hybrid Coacervation, Surface Interactions and Their Modification with Polyampholytes:

Stretching of Immersed Polyelectrolyte Brushes in Shear Flow. Polymer brushes are vital in various applications, including antifouling, corrosion protection, and stimuli-responsive materials, but their behavior under shear flow is not understood. Our study examines the structural response of poly(styrene sulfonate) (PSS) brushes to shear flow using *in situ* X-ray reflectivity across various environments, including isopropanol (IPA), water, and aqueous solutions with different cations (Cs^+, Ba^{2+}, La^{3+},

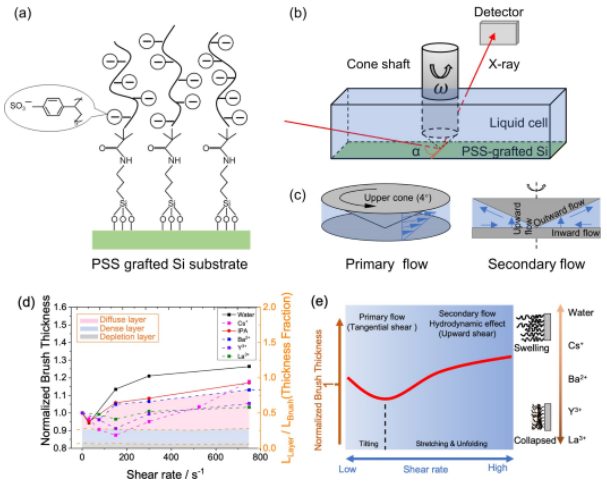

Figure 3. Characterization and Shear-Induced Deformation of PSS Brushes. (a) Chemical structure of PSS brushes attached to a silicon substrate. (b) Schematic of the beam path during X-ray reflectivity measurement. (c) Diagram of the primary and secondary flow within the cone-plate geometry. (d) Normalized brush thickness variation with increasing shear rates for PSS brushes in various solvents (IPA, water, and cation solutions: Cs^+, Ba^{2+}, La^{3+}, and Y^{3+}). The colored map illustrates the thickness fractions of the depletion layer and dense layer, and their shear-induced changes. (e) Schematic illustration of the structural response of PSS brushes in cation solutions under shear flow, depicting the deformation and rearrangement of the brushes.

Y^{3+}) [6]. We designed a custom apparatus that applies tangential and upward shear forces to the PSS brushes, revealing that low shear rates cause brush contraction due to chain tilting, while higher shear rates induce brush expansion by stretching the chains (Figure 3). The initial brush configuration, influenced by the solvent and cations, significantly impacts their response, with stronger salt bridge networks providing greater resistance to stretching. Analysis of electron density profiles highlights the critical role of the diffuse layer in brush structural evolution. Our findings show that PSS stretches more in water and Cs^+ solutions compared to IPA and trivalent cation solutions, offering valuable insights into polymer brush behavior. This understanding is crucial for applications and sets the stage for further exploration of factors such as chain length, counterions, and ion size to develop a comprehensive theory of polymer brush stretching behaviors.

New XPCS Method to Explore Non-equilibrium Dynamics in Soft Materials. This research enhances X-ray Photon Correlation Spectroscopy (XPCS) for studying the dynamics of soft, structured materials [10]. Our new method avoids data averaging and extracts a microscopic transport coefficient, $J(t)$, directly from XPCS intensity correlations, linking small-scale behaviors to large-scale properties. For example, in a polymer-particle gel system under mechanical perturbation, $J(t)$ mirrored dissipation dynamics in an underdamped Brownian oscillator dominated by elastic force (Figure 4 (a)). The method also identified avalanche dynamics, marked by a sudden increase in $J(t)$, indicating rapid particle rearrangement and stress release. Another example is a charged particle suspension undergoing shear band transitions during creep, where three distinct bands formed: a slow-flowing band, a fast-flowing band, and a static band (Figure 4 (b)). Our approach uncovered detailed dynamics, including particle merging, band transitions, and internal structure breakdowns, revealing complex phenomena e.g., jamming and reflow. Imminent synchrotron facility upgrades will further expand XPCS capabilities, enabling the study of local dynamics and broadening applications in advanced manufacturing, natural phenomena, and beyond.

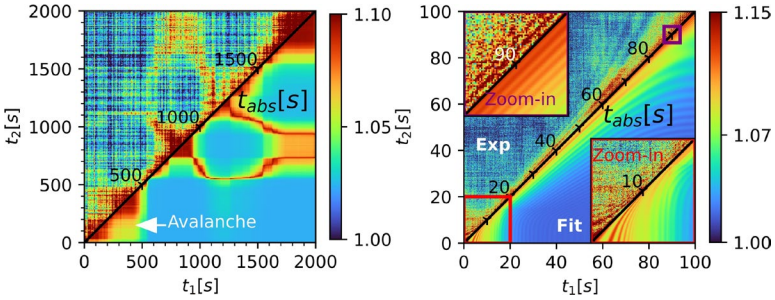

Figure 4. Transport coefficient approach applied to a gel system under mechanical perturbation (a) and a charged particle suspension undergoing shear band transitions during a creep test (b). Experimental XPCS data are in the upper left; fitting results are in the lower right.

Future Plans

We will build on past accomplishments and deepen our understanding of precision synthesis and molecular self-assembly of neutral and charged polymers with controlled architectures and soft materials in three interconnected topic areas described above. The synergisms and multiple cross-cutting themes between the three thrusts will provide exciting opportunities for intra-project cross fertilization and advances that will lead to discovery and innovation in synthesis, characterization, and modeling.

Publications

1. L. Zhang, C. Liu, H. Cao, A. J. Erwin, D. D. Fong, A. Bhattacharya, L. Yu, L. Stan, C. Zou, M. V. Tirrell, H. Zhou, W. Chen, *Redox Gating for Colossal Carrier Modulation and Unique Phase Control*, Adv. Mater. **36**, 2308871 (2024).
2. G. A. Vásquez-Montoya, T. Emeršič, N. Atzin, A. Tavera-Vázquez, A. Mozaffari, R. Zhang, O. Guzmán, A. Snezhko, P. F. Nealey, J. J. de Pablo, *Control of liquid crystals combining surface acoustic waves, nematic flows, and microfluidic confinement*, Soft Matter **20**, 397–406 (2024).
3. X. Tang, N. Atzin, A. Mozaffari, S. Das, N. L. Abbott, J. J. de Pablo, *Generation and Propagation of Flexoelectricity-Induced Solitons in Nematic Liquid Crystals*, ACS Nano **18**, 10768–10775 (2024).
4. R. J. Sánchez-Leija, J. A. Mysona, J. J. de Pablo, P. F. Nealey, *Phase Behavior and Conformational Asymmetry near the Comb-to-Bottlebrush Transition in Linear-Brush Block Copolymers*, Macromolecules **57**, 2019–2029 (2024).
5. J. A. Mysona, P. F. Nealey, J. J. de Pablo, *Machine Learning Models and Dimensionality Reduction for Prediction of Polymer Properties*, Macromolecules **57**, 1988–1997 (2024).
6. Y. Qiao, Q. He, H.-H. Huang, D. Mastropietro, Z. Jiang, H. Zhou, Y. Liu, M. V. Tirrell, W. Chen, *Stretching of immersed polyelectrolyte brushes in shear flow*, Nanoscale **15**, 19282–19291 (2023).
7. N. Atzin, A. Mozaffari, X. Tang, S. Das, N. L. Abbott, J. J. de Pablo, *Minimal Model of Solitons in Nematic Liquid Crystals*, Phys. Rev. Lett. **131**, 188101 (2023).
8. Y. N. Fang, A. M. Rumyantsev, A. E. Neitzel, H. Liang, W. T. Heller, P. F. Nealey, M. V. Tirrell, J. J. de Pablo, *Scattering Evidence of Positional Charge Correlations in Polyelectrolyte Complexes*, Proc. Natl. Acad. Sci. **120**, e2302151120 (2023).
9. K. C. Stevens, M. V. Tirrell, *Structure and properties of bottlebrush polyelectrolyte complexes*, *J. Polym. Sci.* in press (2024).
10. H. He, H. Liang, M. Chu, Z. Jiang, J. J. de Pablo, M. V. Tirrell, S. Narayanan, W. Chen, *Transport Coefficient Approach for Characterizing Non-equilibrium Dynamics in Soft Matter*, Proc. Natl. Acad. Sci. in press (2024).

Design, Synthesis, and Assembly of Biomimetic Materials with Novel Functionality

Aleksandr **Noy**, Anthony van Burren (LLNL), David Baker (U. of Washington), James J. **De Yoreo**, Chun-Long Chen, Marcel Baer (PNNL)

Keywords: artificial membrane assemblies, biomimetic membrane channels, *de novo* designed proteins, designed sequence polymers, membrane transport

Research Scope

The long-term vision of this project is to develop synthetic self-assembling systems that emulate the hierarchical nature of biology and carry out complex functions based on a predictive understanding of assembly and function. Specifically, we seek to create fully synthetic self-assembling biomimetic structures that mimic the environment, versatility, and functionality of cell membranes based on physico-chemical principles underlying (1) co-assembly of biomimetic membrane matrices, artificial membrane channels, and de novo designed protein nanopores into artificial membrane assemblies, (2) the structuring of water and ions near membrane surfaces and pores, and (3) fast and selective transport through the pores. Our proposed research seeks to achieve rational design of fully synthetic multicomponent membranes based on an understanding of (1) controls on co-assembly and ordering, (2) transport mechanisms through the synthetic protein nanopores and (3) the relationship between protein pore design and ion-selectivity. Our approach integrates synthesis of novel biomimetic materials and nanopores, in situ characterization of interfacial structure, interactions, and assembly, molecular simulations of structure, assembly and transport, and measurements of ion and water transport through nanopores. These advances will build a foundation for designing biomimetic functional materials where the transport and selectivity can be tuned for applications in energy systems.

Recent Progress.

Boron nitride nanotube porins (*Sci. Adv., 2024, in revision*). We developed a new type of synthetic membrane nanopore based on a BN nanotube scaffold. These *BN nanotube porins* (BNNTPs) were synthesized by cutting long BN nanotubes and solubilizing them in lipids. BNNTPs spontaneously insert into the lipid membranes (Fig. 1a) and form stable pores with defined ionic conductance (Fig. 1b). A combination of ion conductance measurements with the reversal potential ion selectivity measurements indicated

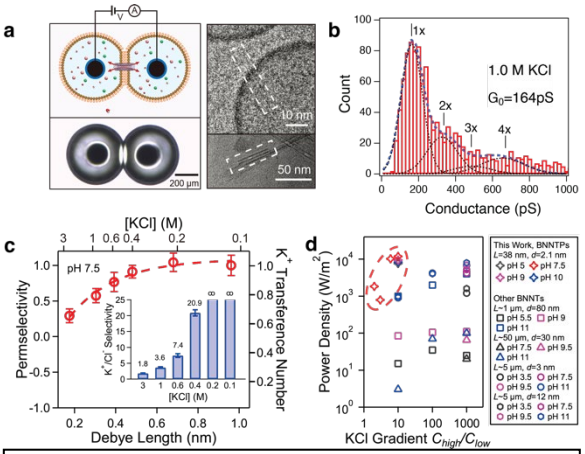

Figure 1. Boron nitride nanotube porins. a. Schematic of droplet interface bilayer measurement (*left*) and EM images of (*top*) BBNTP inserted into lipid vesicle shell and (*bottom*) HR-TEM of a single BNNTP. **b.** Histogram of ionic conductance values of BNNTPs. **c.** BNNT permselectivity values at different KCl concentrations. **d.** Osmotic power density for a single BNNT pore compared to literature values. *Li, el.al. (2024).*

that BNNTPs carry a permanent negative charge on the walls, attributed to OH^- chemisorption on BN walls. This charge is responsible for strong cation selectivity of these pores (Fig. 1c). We have also demonstrated that BNNTPs are highly efficient osmotic gradient power converters with power density reaching to over 10kW/m^2, exceeding literature values for osmotic power harvesting channels.

Water and ion transport in de novo designed protein pores. (***Submitted***) The Baker group has used parametric design to generate de novo designed protein pores that allow exquisite control over the size and precise channel functionality for incorporation into synthetic membranes (Fig. 2). We have synthesized, and characterized a series of 8, 10, and 12-stranded transmembrane β-barrel protein channels (Fig 2a), which form asymmetric barrel structures. We determined water permeabilities of these pores and showed that they increase with the pore size and also correlate with the literature values for the biological pores of similar size (Fig. 2b). In contrast, the water permeability of the 8-stranded barrel protein (TMB8), which contains only a single-file water chain does not correlate to that of aquaporins, but rather to that of gramicidin A (Fig. 2b). Unlike the aquaporin pore, the TMB8 pore is lined up with polar groups that suppress the conditions necessary for fast single-file water transport, demonstrating how control over pore size and chemistry can control transport properties. We also determined ion conductance of individual de novo pores and demonstrated that, while TMB8 is too small to enable ion transport, TMB10 and TMB12 show ion conductance that increases with the pore size. MD simulations quantified the potential energy profile for ion transport through these pores and determined their molecular size cutoff, which correlate with the experiments, further clarifying structure-function relations in this system.

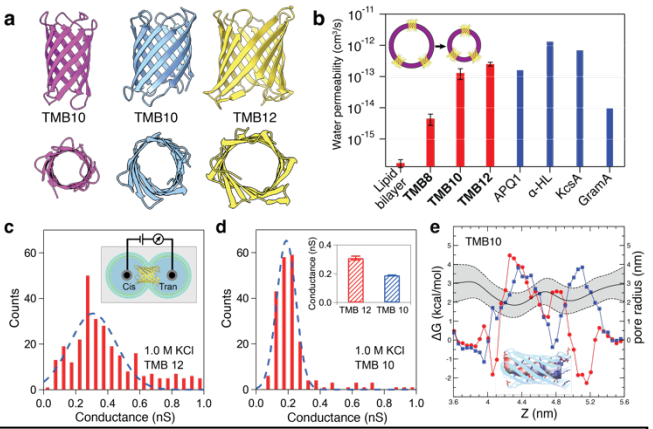

Figure 2. **Transport in de novo designed protein pores**. **a**. Structure of 8,10, and 12-strand de novo designed transmembrane β-barrel proteins. **b**. Water permeability of de novo proteins (red) compared to the literature permeability values of biological pores (blue). **c,d**. Histograms of ion conductance of de novo pores. **e**. Calculated potential energy profile through TMB10 pore. (*Li, Baer, Baker, De Yoreo, Noy, et.al., subm. 2024*)

Two-dimensional silk (*Sci. Adv., 2024 in revision*). We have also discovered a 2D crystalline phase of silk that assembles epitaxially on van der Waals substrates, including graphene and MoS_2 (Fig. 3). Silk is a natural protein-based material that has been used by humankind for over 5,000 years. Silk fibroin (SF) has been exploited in recent decades for its ability to self-assemble into a range of fiber-based architectures that exhibit exceptional mechanical, optical, and electronic properties, as well as excellent biocompatibility and biodegradability. Yet, a number of potential SF bio-electronic applications has been limited by challenges associated with the poor order of films of SF fibers deposited from bulk solution, and the mismatch between the soft SF proteins

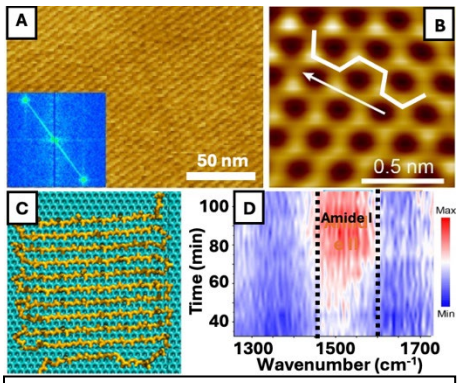

Figure 3. Silk forms a highly ordered 2D epitaxial film on graphene. (A) AFM image of 2D silk on graphene. (B) Underlying carbon lattice showing armchair direction along which silk lamellae are aligned. (C) Molecular dynamics simulations showing predicted structure of lamellae. (D) Synchrotron-based nano-FTIR showing the development of b-sheet crystalline structure recorded through the evolution of the amide I adsorption band. *Shi et.al. 2024*

and the hard, planar substrates. Our discovery now provides a simple means for creating *highly ordered silk films directly interfaced with electronic materials*. Moreover, using *in situ* AFM, synchrotron-based nano-FTIR, and molecular dynamics, we found that the structure is formed through surface-directed assembly and folding of the SF molecules, with a final architecture comprised of fully ordered monolayers of β-sheet lamellae (Fig. 3C). Moreover, we showed that assembly proceeds along two distinct pathways: direct epitaxial growth at low SF concentrations and a two-step process passing through a transient disordered phase at high concentration. These findings provide a mechanistic understanding of assembly for this canonical biomaterial that can enable efficient approaches to designing and fabricating highly oriented silk-based bio-electronics.

Dynamics of peptoid self-assembly into 2D membranes (*ACS Nano, 2024*). Peptoids, which readily assemble into highly ordered, chemically robust, self-repairing 2D solids that comprise hydrophobic cores and functionalizable hydrophilic surfaces, are versatile membrane matrices. We investigated the effect of peptoid sequence on the mechanism and kinetics of 2D assembly on mica surfaces using *in situ* AFM and time-resolved X-ray scattering using three distinct, but systematically varied, peptoid amphiphilic sequences. The results (Fig. 4) show that assembly starts with deposition of aggregates that spread to establish 2D islands, which then grow by attachment of peptoids—either monomers or unresolvable small oligomers—following well known laws of crystal step advancement. Extraction of the key thermodynamic and kinetic parameters from the dependence of growth rate on peptoid concentration reveals striking differences between the sequences. The one with the lowest stability in the bulk exhibits the highest stability when grown on the surface. In fact, once a growth unit attaches to the island edge there is almost no probability of detaching. Furthermore, the conjugation of a hydrophobic tail to the hydrophilic block to enhance hydrophobic interactions greatly reduced the stability but enhances the growth kinetics by three-fold. These assembly outcomes show conjugated that,

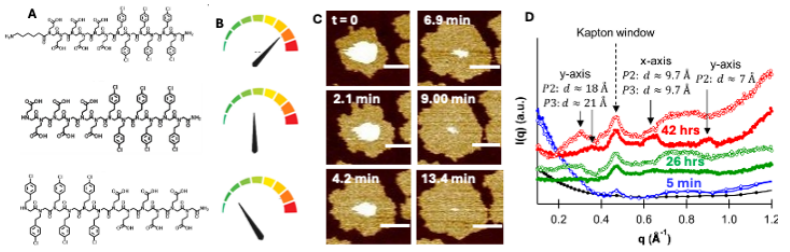

Figure 4. Slight changes in peptoid sequence led to dramatic changes in the thermodynamic stability and 2D assembly kinetics. (**A**) Sequences used in this study. (**B**) Relative assembly speed. (**C**) AFM images showing formation of 2D film by adsorption and spreading. Scale bar: 150nm. (**D**) XRD at three time-steps during assembly. Closed symbols: P2. Open symbols: P3. Black curve is for 1:1 acetonitrile:water. Data has been offset for clarity. *Yadav et.al. 2024*

while the π–π interactions between adjacent hydrophobic blocks play a major role in peptoid assembly, sequence details, particularly the location of charged groups, as well as interaction with the underlying substrate can significantly alter the thermodynamic stability and assembly kinetics.

Pore-forming peptoids for antibacterial activity (*ACS Nano, in revision, 2024*). We have recently designed a new family of low molecular weight peptoid antibiotics that form membrane-disrupting assemblies that exhibit excellent broad-spectrum activity and high selectivity toward a panel of Gram-positive and Gram-negative bacterial strains, including vancomycin-resistant *E. faecalis* (VREF), methicillin-resistant *S. aureus* (MRSA), methicillin-resistant *S. epidermidis* (MRSE), *E. coli*, *P. aeruginosa*, and *K. pneumoniae*. Mechanistic studies using TEM, bacterial membrane depolarization and lysis, and time-kill kinetics assays along with MD simulations reveal that these peptoids kill bacteria through the formation of artificial channels in the cell membranes. Tuning peptoid sidechain chemistry and structure enabled us to further increase the efficacy of antimicrobial activity.

Rare earth ion transport in biomimetic carbon nanotube membrane pores with defined electronic properties. (***2024****, in preparation*). Artificial membrane channel platform allows exploration of transport phenomena that are inaccessible with traditional membrane systems. We explored the impact of channel wall electronic properties on the transport efficiency of rare earth ions in carbon nanotube pores. To probe REE transport efficiency, we used a vesicle-based permeability assay that exploited REE-dependent fluorescence of Calceine Blue dye. Crucially, we have used two kinds of CNTP channels, semiconducting (6,5) CNTPs and metallic (7,4) CNTPs. As both channels had nearly identical diameter, yet different wall electronic properties, these experiments allowed us to isolate the impact of the interactions of the ion with the channel walls (Fig. 5). We have observed that for most REE ions semiconducting nanotubes showed statistically significant higher rate of transport than the metallic nanotubes. The curious exception was the Dy^{3+} ion, where the selectivity trend was inconclusive. Ongoing work is exploring the atomistic origins of this selectivity.

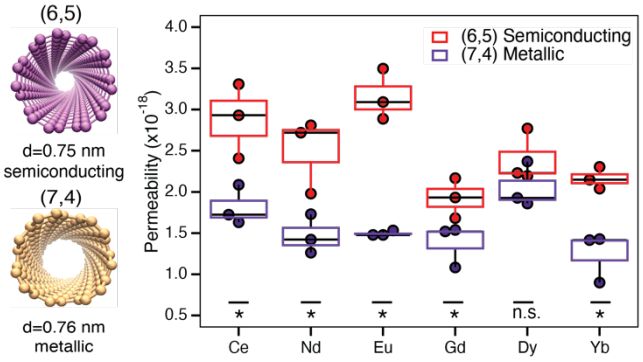

Fig. 5. Rare earth ion transport in chiral carbon nanotube porins. Box plots of single channel permeability for different REE ions for metallic (7,4) and semiconducting (6,5) carbon nanotube porins of *identical* inner diameter. Semiconducting CNTPs show higher transport efficiency for most REE ions. *Abdullah, Li, Noy, et. al. 2024*

Future Plans

Our future research will be focused on assembling synthetic pores and *de novo* designed proteins into lipid, peptoid and block copolymer membrane matrices, determining the efficiency of

molecular transport in these assemblies, establishing the structure-function relationships, as well as refining the pore designs to target applications in energy-related systems.

10 selected project publications (since 2023 PI meeting).

1. Y. Li, B.S. Harris, Z. Li, C. Shi, J. Abdullah, S. Majumder, S. Berhanu, A. Vorobieva, S.K. Myers, J. Hettige, M.D. Baer, J.J. De Yoreo, D. Baker, A. Noy, *Water, solute, and ion transport in de novo designed membrane protein channels*, submitted (**2024**).
2. Z. Li, A. T. Hall, Y. Wang, Y. Li, F. I. Allen, J. Cumings, A. Noy*, Ion transport and ultra-efficient osmotic power generation in boron nitride nanotube porins,* **Science Adv.**, in revision (**2024**).
3. C. Shi, M. Zorman, X. Zhao, M. B. Salmeron, J. Pfaendtner, X-Y. Liu, S. Zhang, J. J. De Yoreo, *Two-dimensional silk*, **Science Adv.**, in revision (**2024**).
4. T. Jian, M. Wang, J. Hettige, Y. Li, L. Wang, R. Gao, W. Yang, R. Zheng, S. Zhong, M.D. Baer, A.Noy, J.J. De Yoreo, J. Cai, C-L. Chen, *Self-assembling and pore-forming peptoids as novel antimicrobial biomaterials*, **ACS Nano**, in revision (**2024**).
5. R. Zheng, M. Zhao, J. S. Du, T. R. Sudarshan, Y. Zhou, A. K. Paravastu, J. J. De Yoreo, A. L. Ferguson, C.-L. Chen, *Assembly of short amphiphilic peptoids into nanohelices with controllable supramolecular chirality*, **Nature Comm**., **15**, 3264, (**2024**).
6. L. Shao, D. Hu, S.-L. Zheng, T. K. H. Trinh, W. Zhou, H. Wang, Y. Zong, C. Li and C.-L. Chen, *Hierarchical Self-Assembly of Multidimensional Functional Materials from Sequence-Defined Peptoids*, **Angew. Chem., Int. Ed**., **63**, e202403263, (**2024**).
7. Y. Song, X. Cai, M. Wang, D. Du, Y. Lin and C.-L. Chen *Assembly of highly efficient aqueous light-harvesting system from sequence-defined peptoids for cytosolic microRNA detection*. **Nano Res.** *17* (2), 788-796, (**2024**).
8. S. Zhang, W. Zhou, B.S. Harris, R. Zheng, P. Mu, W. Yang, J. Chen, M. Monahan, A. Noy, M. Baer, C.-L. Chen; J.J. De Yoreo, *Hierarchical assembly of peptoids on MoS_2*, **Mater. Today Phys.**, DOI: 10.1016/j.mtphys.2024.101406, (**2024**).
9. S. Yadav Schmid, X. Ma, J. A. Hammons, S. T. Mergelsberg, B. S. Harris, T. Ferron, W. Yang, W. Zhou, R. Zheng, S. Zhang, B. A. Legg, A. Van Buuren, M. D. Baer, C.-L. Chen, J. Tao, J. J. De Yoreo, *Influence of Peptoid Sequence on the Mechanisms and Kinetics of 2D Assembly*. **ACS Nano**, **18** , 3497-3508 (**2024**).
10. S. Zhao, A. J. Gillen, Y. Li, A. Noy, *Sonochemical synthesis and ion transport properties of surfactant stabilized carbon nanotube porins,* **J. Phys. Chem. Lett., 14**, 9372-9376 (**2023**). Front Cover.

Adaptive Interfacial Assemblies Towards Structuring Liquids

Ahmad Omar, Materials Science Department, University of California Berkeley
Paul Ashby, Molecular Foundry, Lawrence Berkeley National Laboratory
Brett Helms, Molecular Foundry, Lawrence Berkeley National Laboratory
Alex Zettl, (retired) Physics Department, University of California Berkeley
Thomas P. **Russell,** Materials Sciences Division, Lawrence Berkeley National Laboratory and Polymer Science and Engineering Department, University of Massachusetts-Amherst
Keywords: Structured liquids, evolutionary structures, active matter, Droplet Interface Bilayers

Research Scope

This FWP advances a new concept in materials based on the interfacial formation, assembly and jamming of nanoparticle surfactants (NPSs). By learning how to manipulate the interfacial packing of the NPSs using external triggers, a new class of materials will emerge that synergistically combines the desirable characteristics of fluids with the structural stability of a solid, i.e., a structured liquid. We are developing theoretical models to understand the interfacial packing of the NPSs and its role on spontaneous emulsification, and the developments of a thermodynamic understanding of three phase emulsion systems driven by the interfacial assembly of NPSs. Experimentally, we are using the chemistries of the ligands anchored to generate structured liquids where the dissipative chemical reactions are used to control the interfacial energy that make and break the assemblies in a well-defined time that depends on the reaction rates of the components in the liquid phases. *In situ* scanning probe microscopies are being used to quantify the packing densities and dynamics of the NPS assemblies, relating these to interfacial tension. By encapsulating active matter within the structured liquids, the shapes of structured liquid domains are found to evolve in time, providing an ideal platform to mimic living systems. By controlling the aerial destines of NPSs on the surface of liquid droplets we have been able to prescribe the extent to which two droplets will coalesce, limiting the formation of channels connecting the droplets to tens of nanometers, opening pathways to generate all-liquid ion and electron based devices, Prior to channel formation, the droplet interface bilayer formed when the droplets are initially joined, provides a robust platform to theoretically and experimentally probe pore nucleation and growth with unprecedented detail. Fundamental experimental and theoretical challenges are faced in each of these areas to tailor NPS chemistries, their assembly and dynamics, and the translation of events occurring on the nanoscopic level to controlled macroscopic assemblies.

Recent Progress

Shape evolving structured liquid driven by active magnetic rollers (Omar, Ashby, Helms, Russell): Migration, division, and reconfiguration—behaviors inherent to living systems—are driven by active processes. Developing synthetic mimics remains a challenge due to the difficulty in deforming membranes from within the confined liquids. Lipid bilayers comprising the membranes that bound natural systems are locally deformed by active species, e.g., microtubules, but the non-equilibrium shapes relax when active species motions cease, and the shape changes lack immediate control. We have been pursuing a fully synthetic system, driven by active particles encapsulated by a reconfigurable nanoparticle surfactant membrane that reproduces the shape fluctuations of living cells, yet the shape changes can be preserved. Surfactant concentration can be used to tune the interfacial tension over three orders of magnitude, making on-demand shape evolution possible. Directional migration, division, and reconfiguration across multiple scales are possible, leading to a new class of biomimetic, reconfigurable, and responsive materials, paving the way to autonomous synthetic machines. The motion of active matter is the basic form of locomotion in biology, a vital ingredient in many functions of cells, and an essential design challenge in nanorobotics. We integrated active matter into structured liquids to harness its motions to perform work on liquid interfaces (**Figure 1**). The structured liquids, produced by interfacial jamming of NPSs are reconfigurable and therefore provide an ideal platform for generating active energy-consuming systems.

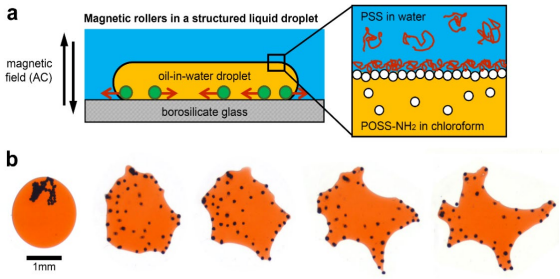

Fig. 1. (a) Schematics of the experiment. (b) Time-lapsed images of the deformation of a structured liquid droplet.

Prescribing and sustaining the lifetime of interfacial films used to transiently structure liquids. (Ashby, Russell, Helms): Structured liquids stabilized by interfacial assemblies enable compartmentalization of reactive species and spatial control over chemical systems. To prescribe a lifetime for structured liquids requires that the assemblies, initially confined to the interface, eventually revert to molecularly dissolved species over time. In **Figure 2**, we show, that poly(acrylic acid) in water fueled with carbodiimide segregates to and forms assemblies of aggregates at an interface with oil, solidifying the interface. When the fuel is consumed, the assembly dissipates to re-form soluble polymer chains, destroying any out-of-equilibrium structure imparted to the liquid. We exploit this phenomenon for controlled coalescence and demonstrate that liquid compartment lifetimes are readily extended by re-fueling the system. Using interfacial rheology, we identify crossover points in the interfacial storage and loss moduli at times commensurate with the amount of fuel, evidencing transitions of the assemblies between solid-like and liquid-like that cause compartmentalized liquids to burst. These solid-like fueled interfacial assemblies demonstrate reduced permeability to dye, showing the potential of this system to be used for timed release or temporally-controlled molecular transfers across liquid interfaces. This work opens a pathway to time- and shape-programmable chemical systems.

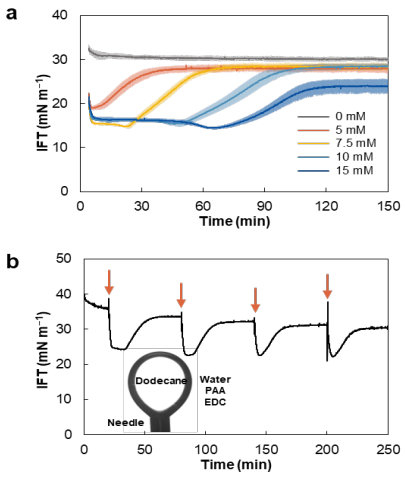

Fig. 2. a. *IFT* over time for a toluene–water/PAA interface with different concentrations of fuel added. **b** *IFT* over time for a dodecane–water/PAA interface with EDC added at 20, 80, 140, and 200 minutes (indicated with arrows). Inset shows an image of an inverted pendant drop.

Responsive-Hydrogel Aquabots: (Shum (HKU), Zettl, Russell): Marine organisms, in response to internal or external stimuli, can change shape to adapt to a complex and ever-changing environment. Such responsive adaptability requires the integration of sensors and actuators without compromising the mechanical flexibility necessary to realize rapid deformation. We integrated stimuli-responsive hydrogels into aquabots, nanoparticle-polyelectrolyte stabilized all-aqueous robots recently developed in our laboratories, to generate adaptive, multiple stimuli-responsive soft robots incorporating a shrink-on-demand function. By combining aqueous phase-separation-induced photopolymerization and all-aqueous 3D printing hierarchical compartmentalized tubular and multicellular structures of printed aquabots were functionalized by a responsive hydrogel membrane during the aqueous phase separation. The functionalized aquabots respond to a range of stimuli and pass through spaces much smaller than their original sizes by an on-demand, reversible shrinkage that can be further enhanced by

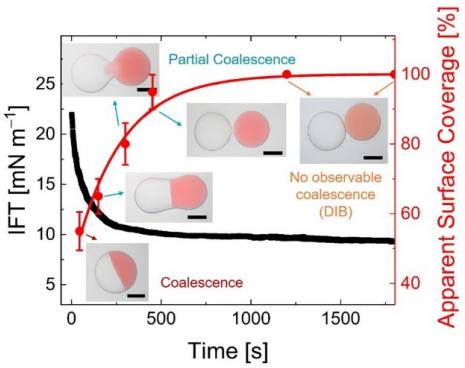

Fig. 3. The interfacial tension (IFT) between the SiO_2 NPs aqueous dispersion and silicone oil with POSS-NH_2 and its apparent surface coverage evolves over time. Insets illustrate different coalescence behaviors: full coalescence, partial coalescence, and no observable coalescence forming a droplet interface bilayer (DIB). The right droplet contains Rhodamine 6G (0.1 μM) while the left droplet does not. Scale bar: 500 μm.

the higher water content in the compartmentalized structures. Adaptive, shrink-on-demand aquabots are produced by functionalizing their walls with complex hydrogel membranes that are responsive to temperature, light, and magnetic fields.

Controllable Droplet Coalescence (Omar, Ashby, Helms, Russell): Arrested coalescence occurs in structured liquid droplets when nanoparticle-surfactants (NPSs) absorbed at the interface become crowded, inhibiting both the relaxation of the droplet shape and further coalescence. Although this phenomenon has been reported and investigated in the context of liquid marbles or Pickering emulsions, detailed investigation on NP-decorated droplets is still lacking. By controlling the surface coverage fraction of the NPs we realized well-defined pore dimensions between the droplets, even down to the nano-scale.

We immersed aqueous droplets (5 μL) containing carboxylated 13-nm-diameter silica NPs (SiO_2-COOH) in a solution of amine-modified polyhedral oligomeric silsesquioxane (POSS-NH_2) in silicone oil. The POSS-NH_2, acting as a surfactant, assembles at the interface and electrostatically interacts with the SiO_2 NPs, anchoring a well-defined number of POSS-NH_2 molecules to the NPs, forming NPSs that are irreversibly absorbed at the oil/water interface. Over time, the NPSs gradually absorb to the interface, lowering the interfacial tension (IFT) until it becomes fully covered. Using the pendant drop tensiometer, the plot of IFT over time was recorded (black line in **Figure 3**), which is consistent with the surface coverage trend (red dots in Fig. X). The neck size between the connected droplets undergoing partial coalescence decreases with assembly time. We have initiated a cooperative electric measurement experiment with Oak Ridge National Laboratory, and the high conductivity results support the possibility of nanopore formation.

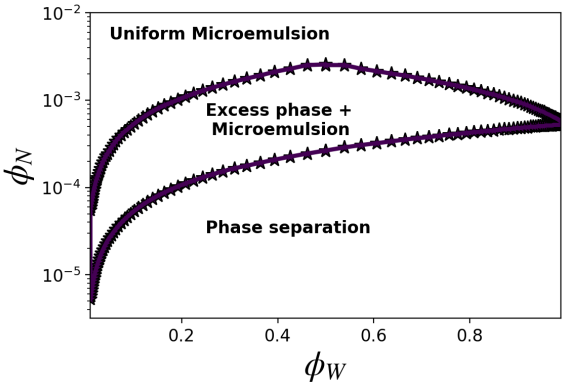

Fig. 4. Phase Diagram of a microemulsion system as a function of volume fraction of surfactant particles (y-axis) and volume fraction of the water component (x-axis). The lower boundary differentiates the phase separated regime (bulk oil + bulk water coexistence) from the 2-phase emulsification failure regime. The upper boundary delineates the transition from the two phase coexistence and the uniform emulsion.

Microemulsions (Ashby, Helms, Russell, Omar): We develop a general thermodynamic theory applicable to a wide variety of non-ionic 3 component surfactant systems that predicts the phase behavior of microemulsions. We nanoparticle surfactants that gain amphiphilic character as they assemble at the water-oil interface. A preliminary phase diagram is shown in **Figure 4**. The two controllable experimental parameters, the volume fraction of surfactant and the volume fraction of the water component control the phase behavior of the system. The phase separation regime denotes coexistence between a bulk water and bulk oil phase with surfactant on the interface and in solution. Upon increasing the volume fraction of surfactant, the interfacial tension between the two bulk fluids decreases. At some critical volume fraction, the interfacial energy vanishes. This results in the production of an emulsion phase which coexists with a bulk excess fluid of the minority component. The 2-phase region is stable over a larger range of surfactant and water volume fraction at smaller values of the intrinsic curvature. Upon further increasing the volume fraction of surfactant, one finds that the excess phase will decompose

into a uniform emulsion. The single phase or 2-phase region may intersect with a droplet-droplet phase separation region arising from droplet-droplet attractive interactions.

In addition to studying the bulk phase behavior of particle stabilized interfaces we also studied the microscopic curvature properties of a model nanoparticle surfactant system. A fluid-fluid interface has a well characterized fluctuation spectrum characterized by two energy scales, the interfacial tension and the bending rigidity. The Interfacial tension penalizes large length scale fluctuations while the bending rigidity penalizes lower wavelength fluctuations. We studied the phase behavior of quasi-2D assemblies of patchy particles as a function of prescribed curvatures. We find that patchy particles with varying valency can display a wide variety of phases, as a function of the curvature. **Figure 5** illustrates the assembly and summarizes our preliminary results.

Future Plans

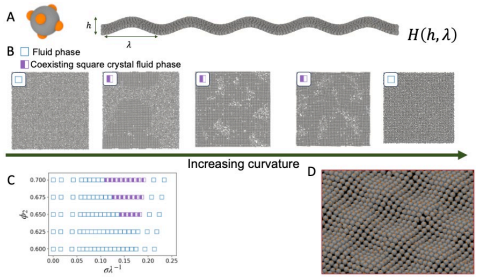

Fig. 5 Quasi-2D patchy particle assemby on curved surface. A. Schwmatic of interfacial assembly. B. Increasing survature at fixed particle density. C. Phase diagram as a function of surface density and wavelength. D. Snapshot of the particle assembly in the square crystal.

- We plan to further study emulsification to extract microscopic indicators on phase behavior, e.g., local density distributions and orientational order parameters.
- We have developed a liquid TEM cell to probe the assembly of the NPSs at liquid/liquid interfaces, to obtain time dependent images of the NPSs to characterize, in real space, the dynamics of the assembled NPSs.
- We will continue studies on dissipative interfacial processes to generate chemically responsive interfacial assemblies. Turning membranes by reaction diffusion control.
- We will continue our experimental studies on the controlled coalescence and robust droplet interface bilayers from NPS ladened droplets. We plan to use classical theories of domain coalescence to determine the length and timescales of this process.
- We plan to study how shape evolves from initial non-equilibrium 3D printed shapes and how, using localized external triggers, to direct the location and extent of shape change.

Publications (10 of 22)

1. Fink Z; Wu X; Kim P Y; McGlasson A; Abdelsamie M; Emrick T; Sutter-Fella C M; Ashby P D; Helms B A; Russell T P. Mixed Nanosphere Assemblies at a Liquid–Liquid Interface, *Small* **2023**: 2308560. https://doi.org/10.1002/smll.202308560.
2. Ghaffarkhah A; Hashemi S A; Ahmadijokani F; Goodarzi M; Riazi H; Mhatre S E; Zaremba O; Rojas O J; Soroush M; Russell T P; Wuttke S; Kamkar M; Arjmand M. Functional Janus structured liquids and aerogels, *Nat. Commun.* **2023**, 14 (1): 7811. https://doi.org/10.1038/s41467-023-43319-7.
3. Popple D; Shekhirev M; Dai C; Kim P; Wang K X; Ashby P; Helms B A; Gogotsi Y; Russell T P; Zettl A. All-Liquid Reconfigurable Electronics Using Jammed MXene Interfaces, *Adv. Mater.* **2023**, 35 (13): 2208148. https://doi.org/10.1002/adma.202208148.
4. Seong H-G; Fink Z; Chen Z; Emrick T; Russell T P. Bottlebrush Polymers at Liquid Interfaces: Assembly Dynamics, Mechanical Properties, and All-Liquid Printed Constructs, *ACS Nano* **2023**, 17 (15): 14731-14741. https://doi.org/10.1021/acsnano.3c02684.
5. Wu X; Bordia G; Streubel R; Hasnain J; Pedroso C C S; Cohen B E; Rad B; Ashby P; Omar A K; Geissler P L; Wang D; Xue H; Wang J; Russell T P. Ballistic Ejection of Microdroplets from Overpacked Interfacial Assemblies, *Adv. Funct. Mater.* **2023**, 33 (20): 2213844. https://doi.org/10.1002/adfm.202213844.
6. Xie G; Zhu S; Kim P Y; Jiang S; Yi Q; Li P; Chu Z; Helms B A; Russell T P. Relaxing Wrinkles in Jammed Interfacial Assemblies, *Angew. Chem., Int. Ed. Engl.* **2023**, 62 (36): e202307713. https://doi.org/10.1002/anie.202307713.
7. Fink Z; Kim P Y; Han J; Wu X; Popple D; Zhu S; Xue H; Zettl A; Ashby P D; Helms B A; Russell T P. Repairable and Reconfigurable Structured Liquid Circuits, *Adv. Funct. Mater.* **2024**. https://doi.org/10.1002/adfm.202402708.
8. Gleeson S E; Fink Z; Ashby P D; Russell T P; Helms B A. Transient structuring of liquids using dissipative interfacial assemblies, *Matter* **2024**. https://doi.org/10.1016/j.matt.2023.12.025.
9. Wu X; Xue H; Bordia G; Fink Z; Kim P Y; Streubel R; Han J; Helms B A; Ashby P D; Omar A K; Russell T P. Self-Propulsion by Directed Explosive Emulsification, *Adv. Mater.* **2024**, 36 (19): e2310435. https://doi.org/10.1002/adma.202310435.
10. Wu X; Xue H; Fink Z; Helms B A; Ashby P D; Omar A K; Russell T P. Oversaturating Liquid Interfaces with Nanoparticle-Surfactants, *Angew. Chem., Int. Ed. Engl.* **2024**, 63 (24): e202403790. https://doi.org/10.1002/anie.202403790.

Dynamics of Active Self-Assembled Materials

PI: Alexey **Snezhko**. Co-Investigators: Andrey Sokolov, Andreas Glatz

Keywords: active matter, out-of-equilibrium self-assembly

Research Scope

Self-assembly, a natural tendency of simple building blocks to organize into complex architectures, is a unique opportunity for materials science. Materials that can spontaneously organize into hierarchical structures with unique and complex properties are currently exhibited only by living systems. In-depth understanding of out-of-equilibrium collective dynamics and self-assembly paves the way for the discovery of tailored self-assembled materials and structures that can adapt to new conditions, self-heal, and regulate physical properties. Understanding and control of self-assembled out-of-equilibrium (*active*) materials pose a significant challenge as they are intrinsically complex, with often hierarchical organization occurring on many nested length and time scales.

The program is focused on the fundamental aspects of out-of-equilibrium dynamics and self-organization of bio-inspired materials. It synergistically integrates experiment and simulations, and tackles the fundamental issues at the forefront of contemporary materials science. The main research directions focus on the design of novel active materials that can arise from a fundamental understanding of dynamic self-assembly and organization in colloids far from equilibrium. We explore highly complementary model systems: self-propelled colloids driven by external fields, and active liquid crystals. The difference between the two is in the way the injected energy is utilized: driven colloids transform it into a mechanical particle motion, while in active liquid crystals it is used for reorientations of a local nematic order. The challenges are: understanding fundamental principles leading to a collective behavior and dynamic self-organization from the interactions between unitary building blocks, and designing new active materials with tunable structural and transport characteristics at the microscale.

Recent Progress

In the past two years the program has been exploring the role chirality plays in dynamics of active colloids. We investigate how chiral behavior of active units contributes and enriches the dynamic self-organization of out-of-equilibrium ensembles. One of the directions has been targeting the behavior of active fluids with memory realized by the use of temporal activity modulations when the system has a partial "memory" of its previous state either at a particle or ensemble level ("collective memory"). Another major direction of the research investigates pattern formation and topological defects dynamics in recently discovered active liquid crystals powered by acoustic waves.

During the past two years our program yielded discoveries of spontaneous activity shockwaves [1], a hidden order and polar state reversal in active roller fluids [2]; reported hyperuniform active

chiral fluids with tunable internal structure [3], demonstrated guided self-assembly of active colloids with temporal modulation of the activity [4]; discovered novel arrested-motility states in populations of shape-anisotropic active Janus particles [5]; investigated the emergence of multi-vortical states and globally correlated vortex lattices in active magnetic liquids [6,7]; developed a fully synthetic active liquid crystal energized by an acoustic field.

Spontaneous shockwaves in pulse-stimulated flocks of active rollers. Temporal activity modulations, realized by modulated external electric fields, represent an effective tool to expand the variety of accessible dynamic states in active ensembles [2, 4].The suspending media also plays a significant role in active ensembles dynamics. In the case of Quincke rollers, the observed complex dynamics of rolling colloids is always accompanied by electrohydrodynamic (EHD) flows induced by the electric field powering the system. We discovered the emergence of spontaneous shockwaves (see Figure 1) that became accessible under temporal activity modulations in crowds of colloidal Quincke rollers with the increased strength of the EHD flows. In response to the increased media conductivity, the EHD flows are no longer negligible and promote intermittent rollers densifications in the system at the uncorrelated gas state. The particle shockwaves continuously emerge and dissipate on the background of spontaneous density variations in the transition region between the gas and vortex states. The shockwaves originate in regions where rollers develop velocity correlations and spontaneously start to move collectively significantly faster than the average particle speed in the ensemble. Multiple shock-waves continuously arise and vanish in the system. The speed of the shockwave is about 40% higher than the peak particle velocity! By combining experiments and computational modeling we demonstrate that the shock waves originate from the transient vortex cores due to vortex meandering instability and occur when the active rollers' translational and rotational decoherence times (controlled by the activity modulations) become comparable. The findings highlight the importance of the interplay between transient system memory, manipulated by a pulsed field, and EHD flows in accessing unconventional dynamic phases that are not accessible under a continuous energy input.

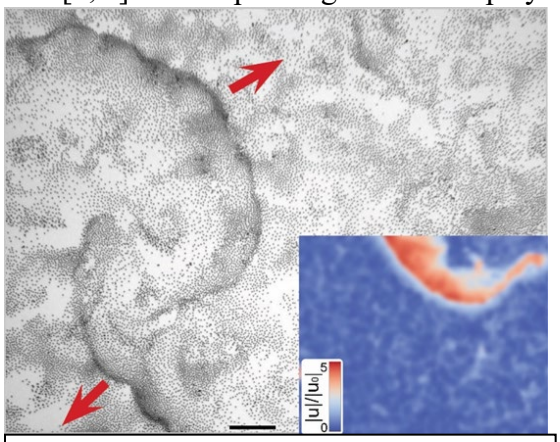

Figure 1. Spontaneous activity shockwaves in populations of Quincke rollers under temporal activity modulations. The red arrows indicate the propagation directions of two major particle waves. Insert: particle velocity map of a propagating shockwave. Red region indicates rollers in the wave front moving coherently at velocities several times of the average particle velocity. The scale bar is 100μm.

Active fluids with memory: shape anisotropy inverses the behavior of active chiral fluids. In geometrically confined systems, the formation of globally correlated polar states proceeds through the formation of a macroscopic steadily rotating vortex, which spontaneously selects a clockwise or counterclockwise global chiral state. Once the global state is formed, it is often robust and stable. However, subsequent control of such polar states remains elusive. We previously discovered that a global vortex formed by colloidal Quincke rollers exhibits dynamic state memory giving rise to a controllable polar state reversal of the globally correlated state [2]. The robustness of the chiral state reversal long after the termination of the activity suggests the development of certain particle positional arrangements (hidden order) in the ensemble "imprinting" the dynamic state of the system and preserving it long after the activity is removed! We revealed that hydrodynamic long-range interactions between the active particles are responsible for the emergence of locally asymmetric particle distributions while electrostatic interactions facilitate a mechanism by which the particle distributions become relevant in the process of a vortex formation. In the case of shape anisotropic rollers we reveal that an introduction of a slight degree of shape anisotropy into an ensemble of dielectric Quincke rollers turns it into a chiral active fluid comprised of rollers of arbitrary handedness. The chiral rollers dynamically self-assemble into multiple self-organized freestanding vortices with spontaneously selected sense of rotation. We demonstrate that upon reactivation of the system after a complete cessation of activity beyond all relevant timescales the vortices simultaneously restore their previous chiral states in striking contrast to the chiral state reversal demonstrated by spherical particles, see Fig.2. The analysis of the local asymmetries imprinted by the hydrodynamic interactions in the particle positional order within the vortices reveals that the shape-anisotropy reverses the sign of the effective tangential force parameter in each vortex, resulting in the suppression of the reversals and the restoration of chiral states of all vortices in the multi-vortical state in consecutive periods of activity. The results provide insights into the emergence of complex collective behavior in chiral colloidal fluids

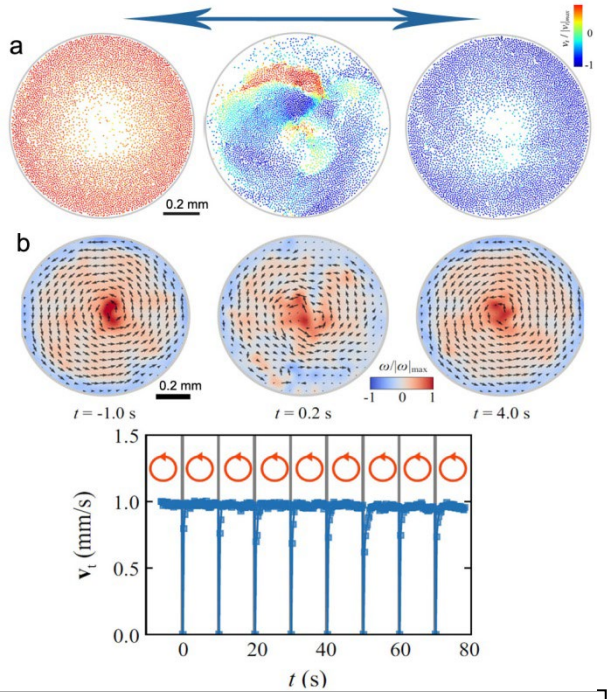

Figure 2. Control of emergent polar state in ensembles of active rollers. (a) a vortex reversal induced by a temporal modulation of the activity in suspension of spherical Quincke rollers. Color encodes tangential velocities of the particles. The system robustly switches between clockwise (blue) and counter-clockwise (red) states. Transitions between the polar states proceed through a chaotic flocking regime. (b) Restoration of self-organized polar states by a temporal activity modulation in ensemble of shape anisotropic rollers forming a chiral active fluid.

governed by a delicate interplay between the shape anisotropy, chiral motion, and temporal activity modulations.

Acoustically powered active liquid crystals. Active liquid crystals represent a rapidly expanding class of non-equilibrium systems that combine mechanical properties of liquid crystals with motility introduced on a microscopic level. We recently realized a novel fully synthetic active nematic system-acoustically energized active liquid crystal - free from biological agents or supplementary motile components, and with the activity level controlled externally in a wide range by the amplitude of the acoustic field. We experimentally demonstrate the conversion of the acoustic energy into local extensile stresses of the liquid crystalline media (lyotropic chromonic liquid crystals), resulting in the emergence of undulation instability with the characteristic wavelengths governed by the amplitude of the acoustic field, see Fig. 3. As the activity increases, the system transitions into a turbulent-like state characterized by a chaotic generation, motion, and annihilation of topological defects. We reveal the spontaneous formation of the unconventional free-standing persistent hydrodynamic vortices at high activity levels not previously observed in biologically-based active nematic systems. The results provide a foundation for the design of externally energized fully synthetic active nematic fluids with stable material properties and tunable topological defects dynamics.

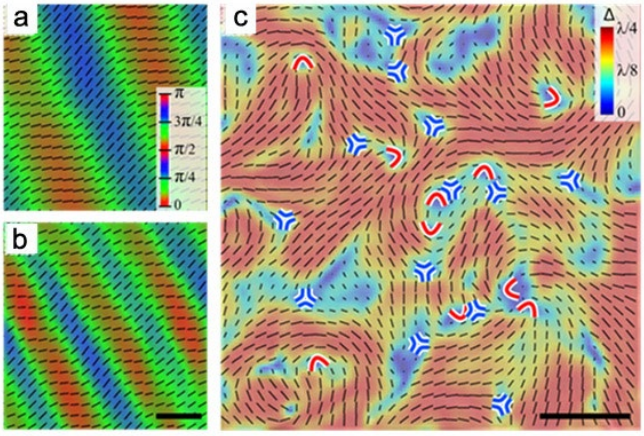

Figure 3. Acoustically powered liquid crystal. (a)-(b) the emergence of undulations of the director field in acoustic field with characteristic wavelength dependent on the amplitude of the field. The background color visualizes the angle between the local director field and the x-axis. (c) An experimental snapshot of fully developed turbulent-like state manifested by continuously reconfiguring director (black lines) and generation and annihilation of topological defects shown by red (+1/2) and blue (-1/2) symbols. Scale bar: 30 μm.

Future Plans

We plan to continue focusing our research on new approaches to discovery, synthesis and characterization of active (out-of-equilibrium) colloidal materials. In the next few years, we plan to explore a broad class of self-assembled active materials stemming from advances of our program. We will explore and investigate a nontrivial interplay between chiral motion, shape, confinement and temporal activity modulations in the generation of a hidden order, dynamic state memory, and control of the system behavior. We plan to systematically investigate the emergence of collective behavior in active chiral fluids realized by rollers and spinners with spontaneous selection of chiral states and those with prescribed handedness. We plan to continue investigating, experimentally and computationally, long-lived emergent multi-vortical states in active magnetic roller fluids energized by an alternating magnetic field and subjected to spatially periodic

confinement. We will continue to advance the fundamental understanding of the recently discovered active liquid crystals powered by acoustic waves focusing on dynamic self-organized patterns, spontaneous flows, and topological defect transport.

References

1. B. Zhang, A. Glatz, I. Aranson, A. Snezhko, *Spontaneous shock waves in pulse-stimulated flocks of Quincke rollers*, Nature communications **14**, 7050 (2023).
2. B. Zhang, H. Yuan, A. Sokolov, M. Olvera de la Cruz, A. Snezhko, *Polar state reversal in active fluids*, Nature Physics **18**, 154 (2022).
3. B. Zhang, A. Snezhko, *Hyperuniform Active Chiral Fluids with Tunable Internal Structure*, Physical Review Letters **128**, 218002 (2022).
4. B. Zhang, A. Snezhko, A. Sokolov, *Guiding self-assembly of active colloids by temporal modulation of activity*, Physical Review Letters **128**, 018004 (2022).
5. J. Katuri, R. Poehnl, A. Sokolov, W. Uspal, A. Snezhko, *Arrested-motility states in populations of shape-anisotropic active Janus particles*, Science Advances **8**, eabo3604 (2022).
6. K. Han, A. Sokolov, A. Glatz, A. Snezhko, Manipulation of self-organized multi-vortical states in active magnetic roller suspensions, Journal of Magnetism and Magnetic Materials **589**, 171625 (2024).
7. K. Han, A. Glatz, A. Snezhko, *Globally correlated states and control of vortex lattices in active roller fluids*, Physical Review Research **5**, 023040 (2023).

Publications (10 most relevant out of 15)

1. K. Han, A. Glatz, A. Snezhko, *Globally correlated states and control of vortex lattices in active roller fluids*, Physical Review Research **5**, 023040 (2023).
2. B. Zhang, H. Yuan, A. Sokolov, M. Olvera de la Cruz, A. Snezhko, *Polar state reversal in active fluids*, Nature Physics **18**, 154 (2022).
3. B. Zhang, A. Snezhko, *Hyperuniform Active Chiral Fluids with Tunable Internal Structure*, Physical Review Letters **128**, 218002 (2022).
4. B. Zhang, A. Glatz, I. Aranson, A. Snezhko, *Spontaneous shock waves in pulse-stimulated flocks of Quincke rollers*, Nature communications **14**, 7050 (2023).
5. G. Vásquez-Montoya, T. Emeršič, N. Atzin, A. Tavera-Vázquez, A. Mozaffari, . R. Zhang, O. Guzmán, A. Snezhko, P. Nealey, J. J de Pablo, *Control of liquid crystals combining surface acoustic waves, nematic flows, and microfluidic confinement*, Soft Matter **20**, 397-406 (2024).
6. K. Han, A. Sokolov, A. Glatz, A. Snezhko, *Manipulation of self-organized multi-vortical states in active magnetic roller suspensions*, Journal of Magnetism and Magnetic Materials **589**, 171625 (2024).
7. B. Zhang, A. Snezhko, A. Sokolov, *Guiding self-assembly of active colloids by temporal modulation of activity*, Physical Review Letters **128**, 018004 (2022).

8. J. Katuri, A. Snezhko, A. Sokolov, *Motility of acoustically powered micro-swimmers in a liquid crystalline environment*, Soft Matter **18**, 8641-8646 (2022).
9. G. Kokot, H.A. Faizi, G.E. Pradillo, A. Snezhko, P.M. Vlahovska, *Spontaneous self-propulsion and non-equilibrium shape fluctuations of a droplet enclosing active particles*, Communications Physics **5**, 91 (2022).
10. J. Katuri, R. Poehnl, A. Sokolov, W. Uspal, A. Snezhko, *Arrested-motility states in populations of shape-anisotropic active Janus particles*, Science Advances **8**, eabo3604 (2022).

University Abstracts

Bioinspired Active Transport and Energy Transduction using Liquid Crystals Beyond Equilibrium

Nicholas L. **Abbott** (Cornell University) and Juan J. de Pablo (University of Chicago)

Keywords: Non-equilibrium, bioinspired, hierarchical, liquid crystals, solitons

Research Scope

Biological systems function out of equilibrium, with structure and dynamics that arise from dissipative processes involving the interplay of advective and diffusive transport. The complex dynamic behaviors found in biology often reflect highly non-linear phenomena that lead to surprisingly localized responses to delocalized fields. These principles offer inspiration for new designs of soft materials that harvest and transduce non-localized sources of energy. In this project, we are exploring an emerging class of dynamic, cooperative phenomena that have been observed in liquid crystals (LCs) – solitary waves, or "solitons", as the basis of new designs of active soft matter for achieving rapid and directed transport processes and new modes of energy transduction. These localized responses have analogies to many other physical and biological phenomena, and have only recently been shown to occur in LCs [1]. In LCs, solitons consist of waves of localized orientational perturbations that can travel at high speed and over long distances. Through closely coupled simulations and experiments, this project is addressing open questions regarding the mechanisms by which solitons form in LCs and subsequently interact with fluid interfaces, with the long-term goal of creating fundamentally new ways to transduce soliton energy into new states of matter.

A particular focus of our efforts over the past year has revolved around investigations of the remarkably complex behaviors of solitons at interfaces, including solid and fluid interfaces (interfaces between LC domains as well as LC-isotropic phases), which hint at fundamentally new ways to transduce soliton energy into new states of matter. We have been addressing key questions regarding the interactions of solitons at boundaries between LC domains with distinct orientations, building on our discovery that solitons can reflect, refract, split and annihilate at these boundaries. We have also been exploring how the orientational anchoring of films of LCs (e.g., LCs with homeotropic orientations), including with pre-engineered strains, impacts the generation and propagation of solitons. At the interfaces between LCs and isotropic liquids, we have been testing the hypothesis that soliton energies can be harnessed to trigger the "budding" of new phases in a manner similar to biological processes. The need to incorporate a coupling between hydrodynamic effects and structure to describe such interfacial processes is providing exciting challenges for theoretical and computational advances. Overall, this effort is creating designs of active soft matter with new modes of energy transduction, opening up the possibility of new approaches to active transport with applications, for example, to nanoscale separations and assembly processes. The relevant physics arise at the mesoscale but can propagate at high speeds over macroscopic scales, and thus an integrated program of theory, simulation, and experiment is needed to interpret the

results of our research and to design hierarchical materials systems with engineered behaviors. Below we summarize progress towards these goals over the past year.

Recent Progress

One thrust of our research has revolved around investigations of collisions between LC solitons and interfaces to isotropic fluids, and the discovery that the interactions can generate a range of interfacial hydrodynamic phenomena. Specifically, we have discovered that single solitons can either generate single droplets or, alternatively, form jets of LC that subsequently break-up into organized assemblies of droplets (Figure 1). We have also shown that the influence of key parameters, such as electric field strength, LC film thickness and LC-oil interfacial tension, map onto a universal state diagram that characterizes the transduction of soliton flexoelectric energy into droplet interfacial energy. Overall, these results reveal that solitons in LCs can be used to focus the energy of non-localized electric fields to generate a new class of non-linear electrohydrodynamic effects at fluid interfaces, including jetting and emulsification.

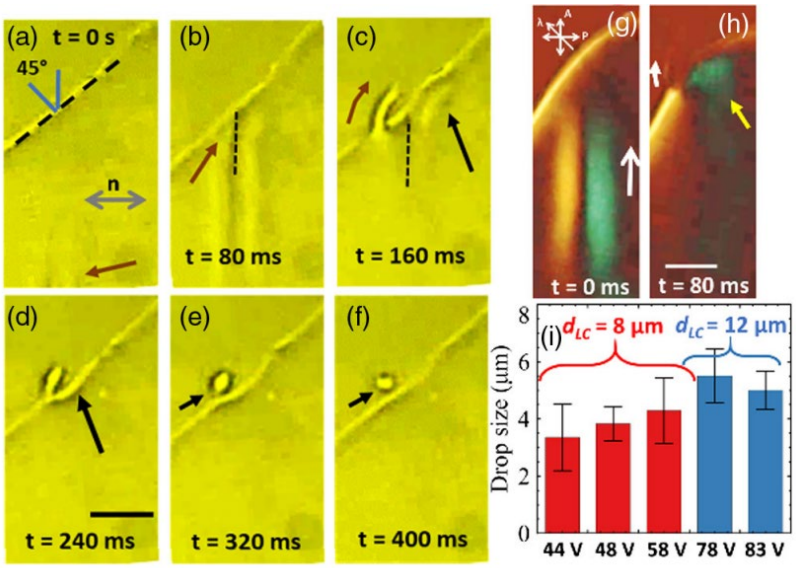

Figure 1: (a)–(f) Bright-field images showing the nematic CCN47–squalane interface following the collision of a single soliton with the interface. The brown arrows in (a) and (b) indicate the incident soliton traveling at an angle 45° with respect to the interface. The dashed line in (a) indicates the CCN-47–squalane interface. The dashed line in (b) and (c) indicates the centerline of the soliton. The left wing of the soliton collides first with the interface and forms a jet indicated by the brown curved arrow in (c). The droplet generated by the soliton collision is indicated by arrows in (e) and (f). Scale bar 15 µm. The black arrows in (c) and (d) point to LC director perturbations in the LC that are generated by the right wing of the soliton. (g),(h) Cross-polar images showing the director perturbations in the LC near the interface after a collision with a soliton. The white arrows in (g) and (h) indicate the propagating soliton and the LC jet, respectively. The yellow arrow in (h) shows the director perturbations created by the right wing of the soliton. Scale bar 15 µm. Image contrast in (a)–(h) has been enhanced for visualization. (i) Sizes of LC drop generated for two different LC film thicknesses. The red and blue bars correspond to 8-µm- and 12-µm-thick LC films.

We have also further developed our minimal model for soliton generation and propagation in a nematic LC using a Landau-de Gennes free energy functional for the tensorial order parameter Q. The relaxational dynamics of Q are expressed in terms of a Ginzburg-Landau equation [2]. The free energy includes a flexoelectric contribution, which is necessary to generate the soliton structure. In the presence of an externally applied electric field, flexoelectricity arises due to the interplay of nematic distortion and polarization [3]. Over the past year, the model has been used to construct a state diagram as a

function of the strength of the applied field and its frequency (Figure 2). Several regimes are predicted in simulations, including a uniform state, a stripe state, a chaotic state, and a soliton state, which occurs only over a narrow range of voltage strength. Good agreement is obtained between the results of the simulations and our own experimental observations, serving to establish the validity of the model. The findings from this study contribute to foundational knowledge for the development of systems that facilitate the controlled production of solitons.

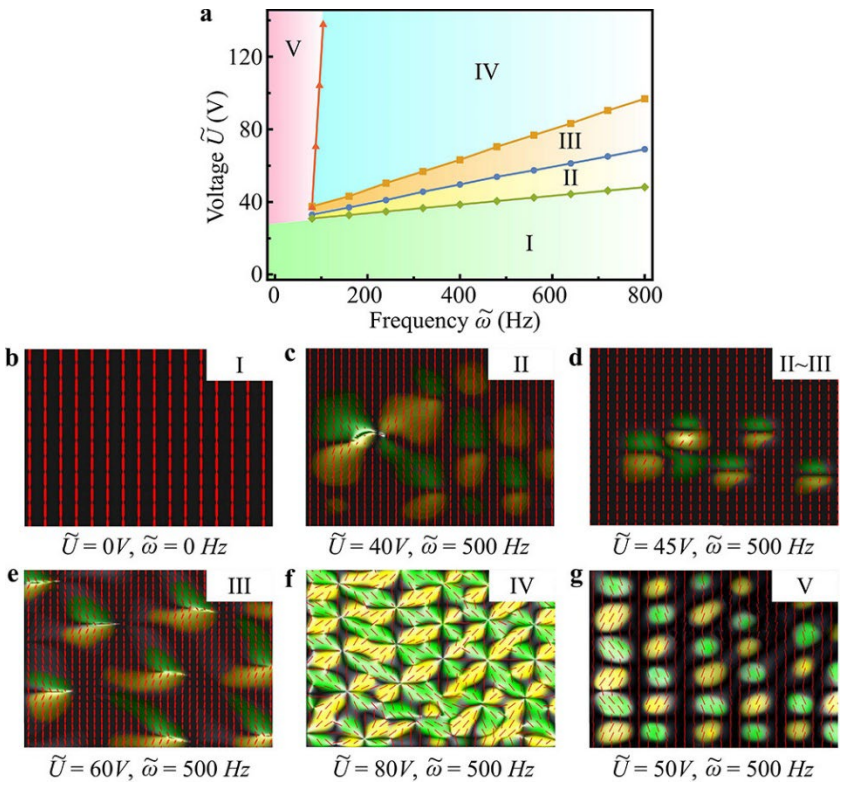

Finally, we have also explored the influence of surface interactions on the generation and propagation of solitons. In particular, we have designed hybrid cells using self-assembled monolayers (SAMs) of alkanethiols on gold surfaces, combining one surface that promotes planar anchoring of the LC and a second surface than promotes homeotropic anchoring. As shown in Figure 3a, this set of boundary conditions results in continuous bend distortions of the LC in the xz-plane which, under a specific set of field strength and frequency, can sustain the propagation of solitons. However, unlike solitons propagating in samples confined between surfaces promoting planar anchoring, we observe a voltage/frequency-dependent soliton trajectory (Figure 3). The coexistence of two distinct propagation axes, at fixed frequency and voltage, is unique to LC films bounded by at least one homeotropic surface and such behavior has not been observed previously. Concurrently with these experimental observations, we also have further developed our soliton model, as well as acquired high-speed imaging of propagating solitons, in order to gain insights into the mechanisms leading to oblique trajectories, which we attribute to the asymmetry in the far-field director created by the presence of bend distortions.

Figure 2: (a) Phase diagram depicting the morphology of a nematic liquid crystal system as influenced by the voltage and frequency under an AC field. Panels (b) to (g) trace the system's transition from a uniform state: (b) illustrates the initial uniform state; (c) shows the emergence of a periodic pattern as voltage increases; (d) captures bullets forming from the butterfly structure; (e) presents a state enriched with bullets; (f) describes the chaotic regime encountered at elevated voltages; and (g) delineates the R-state observed at low frequencies.

Future Plans

A key unresolved issue to be addressed in future research is identification of the microscopic factors that control the behaviors of solitons at interfaces, including reflection and destruction at liquid-LC interfaces, and reflection, refraction, generation, splitting and destruction of solitons at boundaries between patterned LC domains. One of our central hypotheses, which we are testing in ongoing experiments and simulations, is that out-of-plane director tilt within a soliton (i.e., phase of the soliton), at the instant it reaches the interface between distinct LC domains, selects for the observed behavior. Our ongoing experimental efforts include the use of high-speed imaging to map director orientations, which fluctuate with the applied electric field, prior to impact. We also aim to exploit the use of LC far-field director distortions (in particular bend) to control the trajectory of solitons. For example, by controlling the presence of bend in the LC, we can influence the in-plane direction of soliton trajectories and thus design complex propagation pathways. This can be engineered by patterning gold films with different SAMs using microcontact printing. An unresolved goal related to simulations is the inclusion of hydrodynamic interactions, which we predict are particularly important in governing the dynamics of solitons at fluid interfaces (both LC-LC and LC-isotropic oil).

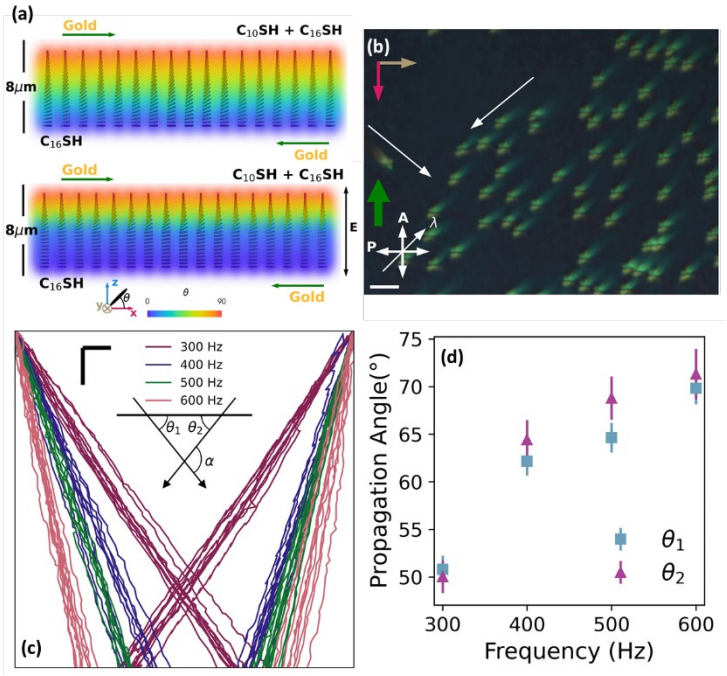

Figure 3: (a) Simulated director field of a hybrid cell, assembled using one gold film with a $C_{16}SH$ SAM, promoting planar anchoring, and one gold film decorated with a mixed SAM of C_{10}- and $C_{16}SH$, promoting homeotropic anchoring, without (top) or with (bottom) an electric field applied along the z-axis . Green arrows indicate the direction of gold deposition. (b) Propagating solitons in a hybrid cell. The green arrow indicates the direction of gold deposition on the planar surface, and the white arrows highlight the two oblique axes of propagation of solitons. (c) Trajectories of individual solitons going along two separate oblique axes. Increasing the electric field frequency yields a monotonic increase of both angles θ_1 and θ_2. (b) Propagation angles, θ_1 and θ_2, plotted against the electric field frequency. Scale bars: 50μm

References

1. X. Li, R. L. Xiao, S. Paladugu, S. V. Shiyanovskii, and O. D. Lavrentovich, *Three-Dimensional Solitary Waves with Electrically Tunable Direction of Propagation in Nematics*, Nat. Commun. **10,** 1 (2019).

2.A. L. Alexe-Ionescu, *Flexoelectric Polarization and Second Order Elasticity for Nematic*

Liquid Crystals, Phys. Lett. A **180**, 456 (1993).

3. A. N. Beris and B. J. Edwards, *Thermodynamics of Flowing Systems : With Internal Microstructure*, 683 (1994).

Publications

1. X. Tang, N. Atzin, A. Mozaffari, S. Das, N. L. Abbott, and J. J. de Pablo, *Generation and Propagation of Flexoelectricity-Induced Solitons in Nematic Liquid Crystals*, ACS Nano **18**, 10768 (2024).

2. S. Das, N. Atzin, X. Tang, A. Mozaffari, J.J. de Pablo, and N.L. Abbott, *Jetting and Droplet Formation Driven by Interfacial Electrohydrodynamic Effects Mediated by Solitons in Liquid Crystals,* Physical Review Letters **131**, 098101 (2023).

3. N. Atzin, A. Mozaffari, X. Tang, S. Das, N. L. Abbott, and J. J. de Pablo, *Minimal Model of Solitons in Nematic Liquid Crystals*, Physical Review Letters **131**, 188101 (2023).

4. S. Das, S. Roh, N. Atzin, A. Mozaffari, X. Tang, J. J. De Pablo, and N. L. Abbott, *Programming Solitons in Liquid Crystals Using Surface Chemistry*, Langmuir **38**, 3575 (2022).

*5. V. Palacio-Betancur, J. C. Armas-Pérez, J. P. Hernández-Ortiz, and J. J. de Pablo, Curvature and confinement effects on chiral liquid crystal morphologies, Soft Matter **19**, 6066 (2023).*

6. S. Norouzi, R. Zhang, J. G. Munguia-Fernández, L. de Pablo, Y. Zhou, N. Taheri-Qazvini, H. Shapiro, S. Morin, J. A. Martinez-Gonzalez, M. Sadati, and J. J. de Pablo, *Director Distortion and Phase Modulation in Deformable Nematic and Smectic Liquid Crystal Spheroids*, Langmuir **38**, 15272 (2022).

7. K. He, Y. Zhou, H. Ramezani-Dakhel, J. J. De Pablo, A. Fernandez-Nieves, and T. Lopez-Leon, *From Nematic Shells to Nematic Droplets: Energetics and Defect Transitions*, Soft Matter **18**, 1395 (2022).

8. Y. Yang, V. Palacio-Betancur, X. Wang, J. J. De Pablo, and N. L. Abbott, *Strongly Chiral Liquid Crystals in Nanoemulsions*, Small **18**, 2105835 (2022).

9. A. de la Cotte, N. Atzin, X. Tang, J. J. de Pablo, and N. L. Abbott, *Fréedericksz Transition and Soliton Formation in Thin Films of Nematic Liquid Crystals with Hybrid Boundary Conditions*, in preparation (2024).

Rational design of liquid crystalline elastomers with programmable multi-step deformability for ambidirectional actuators and as photoresponsive walkers

Joanna **Aizenberg**, Harvard University, Anna Balazs, University of Pittsburgh

Keywords: liquid crystal elastomers, ambidirectional motion, soft actuator, light responsive walker.

Research Scope

Ambidirectionality, i.e the ability of structural elements to move beyond a reference state in two opposite directions, is ubiquitous in nature. However, conventional soft materials are typically limited to a single, unidirectional deformation, unless complex, multimaterial constructs are used. Through comprehensive theoretical and experimental studies, we exploit the combination of mesogen self-assembly, polymer chain elasticity, and polymerization-induced stress to design a class of side-chain end-on liquid crystalline elastomers that exhibit two ordered mesophases – chevron smectic C and smectic A. Inducing this two-step phase transition leads to an unusual inversion of the strain field in microstructures, resulting in opposite deformation modes (e.g., consecutive shrinkage/expansion or right-handed/left-handed tilting and twisting) and high frequency nonmonotonic oscillations. This ambidirectional movement is scalable and can be used to generate unprecedented Gaussian curvature transformations at the macroscale. Our findings expand the range of achievable deformations for shape-changing polymers, providing a chemical strategy complementary to, but fundamentally distinct from current mechanics-centered designs for soft machines, opening doors to multimodal, single-material actuators.

In parallel, we demonstrate the potential of complex deformations in soft actuators toward bioinspired motility by designing a multimodal soft robot based in photoresponsive side-on LCEs. This design takes advantage of the nonreciprocal motions derived from the evolution of an isomerization wavefront in photoresponsive side-on LCE pillars upon UV irradiation. Using our finite element simulation framework, we can predict the response of the device as a function of its dimensions and the parameters of the incident UV light used to control it. We expect that by varying the stimulus on this walking robot we can induce a range of behaviors, including forward and backward translation and rotation, allowing it to fully explore a two-dimensional environment.

Recent Progress

Compared to side-chain side-on and main-chain LCEs, end-on LCEs have higher rotational freedom of mesogens relative to polymer chain (Fig.1A). By rationally designing molecular modifications in end-on LCEs which synergize intermesogenic, mesogen-polymer, and polymer-polymer interactions, we have created a class of elastomers which exhibit rich phase behaviors and corresponding deformations yet to be observed in any single-material soft-matter system. Further, we elucidate the mechanism of such phase behavior and suggest a generalizable strategy for realizing higher ordered LC phases in LCEs. Unlike previous strategies to realize complex

deformations in soft matter, including inhomogeneous stimuli fields or multicomponent structural composites[1-3], the ability of end-on LCEs to invert direction of the strain field during the sequential phase transitions makes it possible to achieve previously unseen *multi-step ambidirectional deformations in chemically homogeneous micro- and macroscopic* end-on LCE-based soft actuators.

By taking advantage of magnetic fields to encode a desired mesogenic orientation before polymerization (Fig.1B)[1], we readily achieve a variety of reversible non-monotonic deformations, such as sequential contraction-expansion (Fig.2A), in response to monotonic temperature increase. Furthermore, this system is tunable to enable distinct oscillatory ambidirectional movements under different temperature ranges, including high-frequency oscillations in response to light (Fig.2B). Any desired sequence of monotonic or non-monotonic microstructure oscillations can be programed by 'reading' a prescribed temperature sequence, enabling remote control of microstructure movements.

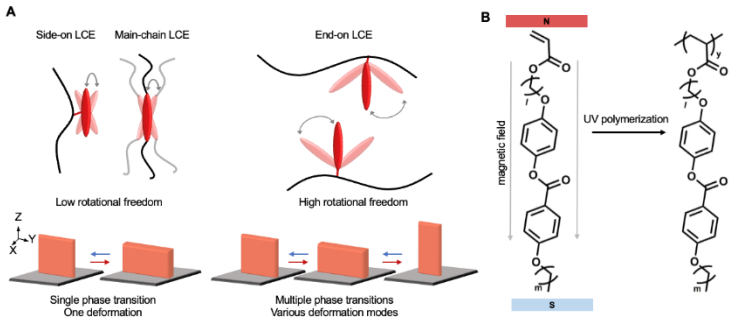

Fig. 4: A) Depiction of enhanced rotational freedom in end-on LCEs compared to side-on and main-chain counterparts. B) Photopolymerization of proposed family of end-on mesogens pre-aligned in magnetic field.

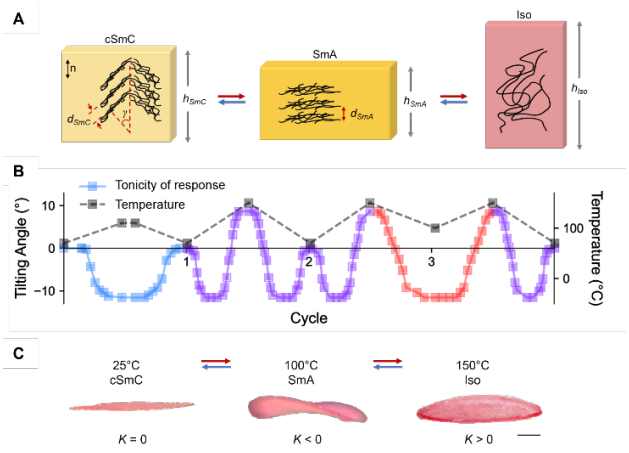

Fig. 5: A) Schematic of polymer chain configuration during cSmC-SmA-Iso phase transitions enabling consecutive opposite deformations. B) Programmed variations in temperature (dashed grey lines) define tonicity of the mechanical response of the same end-on LCE microplate (solid lines). Blue, red, and purple curves illustrate monotonically decreasing, increasing and non-monotonic responses, respectively. C) Deformation of a radially aligned end-on LCE disk upon heating. Scale bar, 2 mm.

Further, we develop macroscopic LCE disks (1 cm diameter) which sequentially switch Gaussian curvature (K) to show that these ambidirectional deformations can be extended across length scales (Fig.2C). Using magnetic alignment to molecularly encode a radial pattern within the disk, we achieve a zero-negative-positive Gaussian curvature transformation upon heating. Dynamic Gaussian curvature formation plays a critical role in motion in nature, such as nastic motion in plants and motility in marine life. Synthetic actuators that change Gaussian curvature have been developed to replicate the capabilities seen in nature; however, their design is generally based on multi-material constructs and architected materials. Realizing single-material

systems with ambidirectional Gaussian curvatures widens the application space for use as biomimetic soft actuators.

We note that the family of end-on LCEs described here represents just one example within a wide range of LCEs where the synergy between mesogen-polymer, mesogen-mesogen, and polymer-polymer interactions plays an important role to introduce complex phase behaviors elicited by a chemically homogeneous soft material in response to a single stimulus. We believe that the approach described here serves as an adaptable and general solution for existing soft actuator systems to address needs for ophisticated motion from the micro- to macroscale and complement current mechanics-centered designs aimed at achieving soft machines.

While developing strategies to realize novel deformations in LCE systems, we simultaneously develop photoresponsive LCE walker using computational techniques to predict locomotive behaviors. The proposed design comprises a square body, connected to four legs arranged in a diamond pattern, as shown in Fig. 3. The legs and body serve as analogs to previous work analyzing photosensitive LCE flexible sheets[4] and bending pillars[5]. For ease of design and fabrication, we assume that the device is molded in a single piece, with a uniform programmed orientation of the nematic director throughout the body and legs, oriented in the plane of the body and orthogonal to the long axis of the legs.

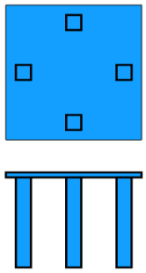

Fig. 3: Bottom and side view of LCE robot

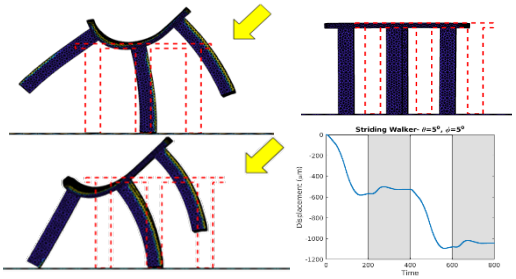

Fig. 4: Striding motion. Under UV exposure, the body curls inward and the legs tip away from the light.

Using finite element simulations, we can predict that for a low polar angle of incident light, the legs will bend away from the light source. With the feet planted on the surface, this will push the body of the walker towards the light. By cycling the light source on and off, the walker can be made to ‘shuffle” towards the light in this fashion.

When subjected to light at a higher polar angle (here 45°, as seen in Fig. 4) the light causes the back of the walker to curl inward, lifting two legs off the surface. The walker is now unstably balanced on the two remaining legs, and the induced bending tips it away from the light, onto one of the lifted legs. Repeating this over multiple cycles causes the robot to walk away from the light source.

Future Plans

Through the introduction of photoresponsive moieties in multiphase end-on LCEs, we can produce light-driven architectures capable of evolving into complex bimorphs of actuated and non-actuated material which, in combination with magnetic alignment to encode mesogenic orientation, result in structures capable of complex non-reciprocal motions in multiple directions upon application of a static light source.[5] Furthermore, taking advantage of photochemical actuation, we can produce materials which undergo separate sequences of phase transition between actuation versus recovery. This material system can then be incorporated into our photoresponsive walker design to produce even more complex locomotion and functionality without the need for multimaterial constructs or spatially varying stimuli.

Furthermore, after establishing the potential of the walking LCE robot to exhibit a range of useful modes of locomotion, we can optimize the parameters of the device to achieve these modes more effectively while maintaining its diverse capabilities. While exploring the design space using simulation and theory, we will simultaneously work on constructing and testing these LCE devices in the lab to demonstrate their effectiveness.

References

1. S. Li, M. Aizenberg, M.M. Lerch, and J. Aizenberg, *Programming Deformations of 3D Microstructures: Opportunities Enabled by Magnetic Alignment of Liquid Crystalline Elastomers*, Acc. Mater. Res. **4**, 12, 1008–1019 (2023).
2. S. Li, B. Deng, A. Grinthal, A. Schneider-Yamamura, J. Kang, R. S. Martens, C. T. Zhang, J. Li, S. Yu, K. Bertoldi, and J. Aizenberg, *Liquid-induced topological transformations of cellular microstructure,* Nature **592**, 386–391 (2021).
3. Y. Yao, J. T. Waters, A. V. Shneidman, J. Cui, X. Wang, N. K. Mandsberg, S. Li, A. C. Balazs, and J. Aizenberg, *Multiresponsive polymeric microstructures with encoded predetermined and self-regulated deformability,* Proc. Natl. Acad. Sci. U.S.A. **115**, 201811823 (2018).
4. J. T. Waters, and A.C. Balazs, *Achieving controllable and reversible snap-through in pre-strained strips of liquid crystalline elastomers*, Soft Matter **20**, 3256-3270 (2024).
5. S. Li, M. M. Lerch, J. T. Waters, B. Deng, R. S. Martens, Y. Yao, D. Y. Kim, K. Bertoldi, A. Grinthal, A. C. Balazs, and J. Aizenberg, *Self-regulated non-reciprocal motions in single-material microstructure,* Nature **605**, 76–83 (2022).

Publications

1. T. B. H. Schroeder, J. Aizenberg, *Patterned crystal growth and heat wave generation in hydrogels*, Nat. Commun. **13**(1), 259 (2022).

2. S. Kolle, O. Ahanotu, A. Meeks, S. Stafslien, M. Kreder, L. Vanderwal, L. Cohen, G. Waltz, C. S. Lim, D. Slocum, E. M.Greene, K. Hunsucker, G. Swain, D. Wendt, S. L. M. Teo, J. Aizenberg, *On the mechanism of marine fouling-prevention performance of oil-containing silicone elastomers*, Sci. Rep. **12** (1), 11799 (2022).

3. A. B. Tesler, S. Kolle, L. H. Prado, I. Thievessen, D. Böhringer, M. Backholm, B. Karunakaran, H. A. Nurmi, M. Latikka, L. Fischer, S. Stafslien, Z. M. Cenev, J. V. I. Timonen, M. Bruns, A. Mazare, U. Lohbauer, S. Virtanen, B. Fabry, P. Schmuki, R. H. A. Ras, J. Aizenberg, W. H. Goldmann *Long-term stability of aerophilic metallic surfaces underwater,* Nat. Mater., **22** (12), 1548 (2023).

4. X. Zhou, Y. Zheng, H. Zhang, L. Yang, Y. Cui, B. P. Krishnan, S. Dong, M. Aizenberg, A. Zeng, Y. Hu, J. Aizenberg, J. Cui, J. *Reversibly growing crosslinked polymers with programmable sizes and properties*, Nat. Commun. **14**, 3302 (2023).

5. S. Li, M. Aizenberg, M. M. Lerch, J. Aizenberg, *Programming Deformations of 3D Microstructures: Opportunities Enabled by Magnetic Alignment of Liquid Crystalline Elastomers,* Acc. Mater. Res. B, 12, 1008-1019 (2023).

6. J. T. Waters, A. C. Balazs *Achieving controllable and reversible snap-through in pre-strained strips of liquid crystalline elastomers,* Soft Matter, **20** (15) (2024).

7. Y. Yao, A. M. Wilborn, B. Lemaire, F. Trigka, S. Li, F. Stricker, A. Grinthal, M. Zhernenkov, G. Freychet, P. Wasik, R. Bennet, T. C. Cheung, B. Kozinsky, M. M. Lerch, X. Wang, J.; Aizenberg *Rational design of liquid crystalline elastomers with programmable multi-step deformability for ambidirectional actuators*, in review at Science

8. X. Xiong, X. Zhou, H. Zhang, M. Aizenberg, Y. Yao, Y Hu, J. Aizenberg, J. Cui *Controlled macroscopic shape evolution of self-growing polymeric materials*, in review at Adv. Mater.

9. S. Wang, S. Li, W. Zhao, Y. Zhou, L. Wang, J. Aizenberg, P. Zhu, P. *Programming hierarchical anisotropy in microactuators for multimodal actuation*, in revision at Lab on a Chip

Growth in heterogeneous, evolving macromolecular networks: toward functional, biomimetic materials

PI: Anna C. **Balazs** (Univ. of Pittsburgh); Co-PI: Krzysztof Matyjaszewski (Carnegie Mellon University); Co-Investigator: Tomasz Kowalewski (Carnegie Mellon University)

Keywords: Macromolecular networks; Controlled radical polymerization; Orthogonal chemistry

Research Scope

Structurally Tailored and Engineered Macromolecular (STEM) gels are transformable materials with latently active functionalities previously developed in this program [1]. In this project, we explore the use of latently active materials as heterogeneous platforms for well-defined synthesis. Additionally, we investigate the formation of hyperbranched polymers using inibramers, a unique building block, and how that may inform material design. STEM gels [2] and other networks with static crosslinking, however, eventually face the obstacle of embrittlement, brought on by the increase in strain associated with adding matter. This necessitated the development of a material capable of anisotropic growth in its primary scaffold. We studied a new class of *expandable* materials that can continue to increase in mass without mechanical failure by incorporating a latently active expandable functionality into the primary network chains.

Recent Progress

Crosslinked PEG scaffolds for solid phase synthesis

Inspired by well-defined solid-phase peptide synthesis, we utilized ChemMatrix (CM), a crosslinked, functionalized PEG-based scaffold decorated with various photocatalysts (PCs) for different applications. First, the CM resin was functionalized with an iridium complex (Figure 1A) for applications in photocatalytic dehalogenation [3]. The resins were recycled up to four times before the complex leeched from the scaffold due to the relatively weak coordination interaction holding the complex to the network. Alternatively, CM was *covalently* functionalized with an eosin Y derivative (Figure 1B). This resin could be effectively recycled five times with no discernible loss in efficiency. Polymers synthesized using CM-EY were well controlled throughout each cycle. The usage of a heterogeneous PC also significantly simplified the purification with no unwanted staining of the final product with the PC as homogenous reactions tend to do.

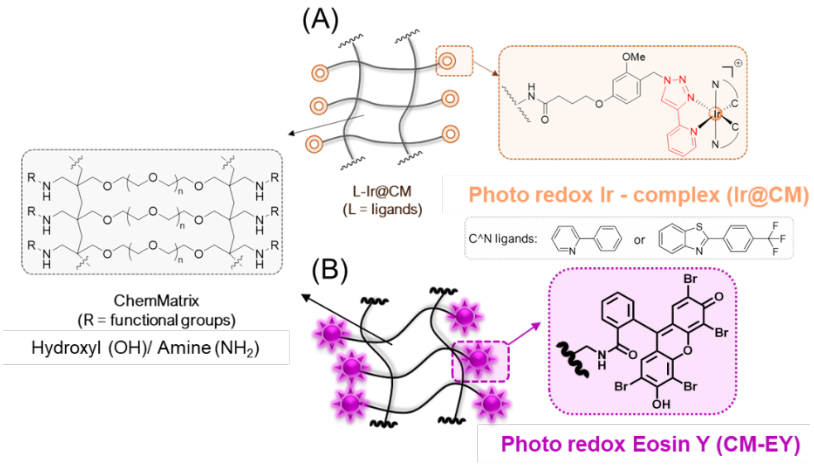

Figure 6. Schematic representation of the heterogenous photoactive catalysts (PCs) – (A) Ir@CM and (B) CM-EY

Understanding hyperbranched polymer formation with inibramers

Since the development of inibramers, monomers capable of initiating branching upon incorporation into a polymer chain, there has been questions regarding the uniformity and topology of the hyperbranched macromolecule that is produced. Using dissipative particle dynamics (DPD), we simulated growth of hyperbranched polymers with different reactivity ratios, solvent concentration, and inibramer concentrations. We probed dispersity, polymerization kinetics, radius of gyration, and branching distribution as a result of manipulating these variables. Additionally, the utilization of DPD allowed us to observe the topology of inidividual macromolecules, which shed light on the branching efficiency and uniformity in the structure. (see below). The high dispersities reported experimentally originated from the asymmetric inibramer-inibramer versus inibramer-monomer reactivities. The asymmetric reactivity ratios also result in a more disordered branch structure, due to faster incorporation of inibramers, leading to a higher number of branching (Figure 2).

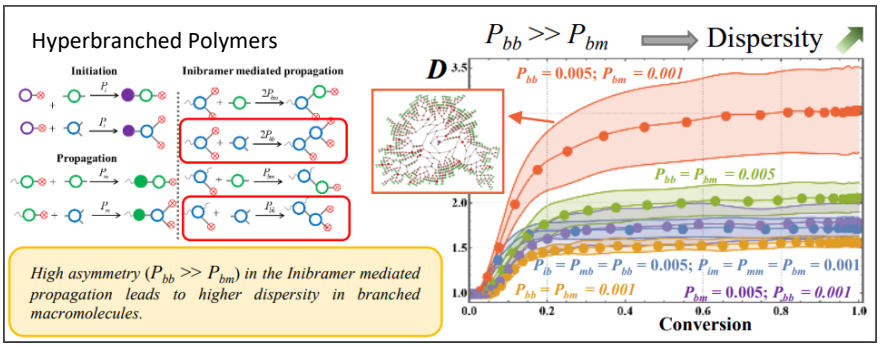

Figure 7. Dispersities of hyperbranched polymers synthesized with inibramers is dictated by the reactivity ratios between inibramers and monomers, as elucidated by DPD simulations.

Expandable polymer networks

This project aims to develop materials capable of expanding without embrittlement. This is enabled by reversibly deactivated functionalities, such as trithiocarbonates (TTC) in RAFT polymerization. With the incorporation of one TTC unit in each network chain, the material should be able to assimilate new mass without adding strain to the existing structure. When expanded with only monomer, the crosslinking density is diluted, resulting in a softer material with increased mesh size. However, by controlling the crosslinker ratio added to the network during growth, the crosslinking density can be kept constant, or even increased to yield materials with different properties from a single parent network. Additionally, since TTCs are photolabile, growth of the material can be patterned with photomasks, making them highly appealing in additive manufacturing. A schematic of the synthesis of such network is shown in Figure 3.

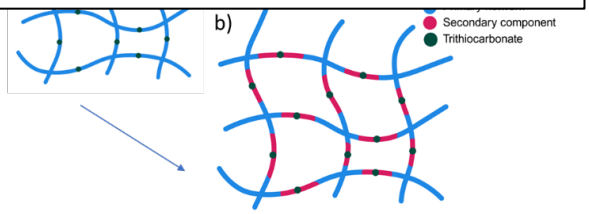

Figure 3. Schematic representation of growth of expandable networks.

Modeling growth of polymer networks using inibramers

Hyperbranched polymers (HBPs) offer distinguishing, advantageous, properties that arise from their distinctive densely packed topology. The synthesis of hyperbranched structures was facilitated by the development of inibramers, which stands for "initiator," "monomer," and "branching junction creator". Inibramers are a branching initiator that is activated only after incorporation into a polymer chain. There remain, however, challenges in determining and charactering the structures of the synthesized HBPs.

We used dissipative particle dynamics (DPD) to probe the effects of inibramer concentration, solvent concentration, and inibramer reactivity on the kinetics, molecular weight, and dispersity of HBPs [4]. In particular, we carried out simulations of branched macromolecules prepared with inibramers *via*

ATRP (See Figure 2, left panel for the ATRP modeling scheme). By varying parameters, e.g., number/concentration of inibramers, number of solvent molecules, and the probability of reactions between inibramer-monomer and inibramer-inibramer, we obtained deeper insights into the effect these parameters have on the polymerization kinetics, molecular weight distribution, spatial structures (characterized by the radius of gyration, branching distribution and the network topology) of the grown branched macromolecules (See Figure 2, right panel).

For example, we conducted simulation scenarios where the reaction rate of inibramer-inibramer (B-B) and the inibramer-monomer (B-M) mediated propagations were varied. In the symmetric scenario, we maintained the same reaction probabilities for reaction rates for the B-B and B-M processes. In the asymmetric case, B-M and B-B the reactions rates were set to different values. Our simulations clearly revealed that higher dispersity (*D*) of the macromolecules were attained due to asymmetry in the reaction rate kinetics. The reason for such high dispersity in macromolecules is primarily due to the faster kinetics of the reaction mediated between the inibramers (inibramer-inibramer reaction). Having an asymmetric reaction rate with higher inibramer-monomer propagation helps the branches of inibramers grow homogeneously without branching, and thus the *D* stays low.

For the symmetric cases, the plots clearly show that higher reaction rates lead to faster branching and lead to higher *D*. Since the inibramer-monomer mediated reaction value is the same for the symmetric case, the frequency of branching is less and helps stabilize the disperse nature of the macromolecule and does not lead to very high *D* values as achieved in the asymmetric case with high inibramer-inibramer mediated propagation (see Figure 2).

We found that for a given choice of our reaction probabilities, increasing the concentration of the inibramers led to faster polymerization of the branched macromolecules. The increase in solvent concentration provides a stabilizing effect in terms of slowing down the effect of branching kinetics. We further demonstrated that systems with lower number of inibramers shows randomly branched polymers while increasing the number of inibramer leads to a dendrimer-like structure with defects (see Figure 2 dendrogram (Inset)). Overall, these studies provide insight into factors affecting the salient features of hyperbranched polymers. Further, these insight could help in synthesizing HBPS to achieve micron-scale growth from a surface. Since these HBPs are valuable in various applications, the results provide guidelines for synthesizing hyperbranched polymers that meet the specific requirements for different technologies.

Biomimetic growth in polymer gels

By modeling gels growing in confined environments, we uncovered a biomimetic feedback mechanism between the evolving gel and confining walls that enables significant control over the properties of the grown gel [5]. Our new model describes the monomer adsorption, polymerization and cross-linking involved in forming new networks and the resultant morphology and mechanical behavior of the grown gel. Confined between two hard walls, a thin, flat “parent” gel undergoes buckling; removal of the walls returns the gel to the flat structure (Figure 4). Polymerization and cross-linking in the confined parent generates the next stage of growth, forming a random copolymer network (RCN). When the walls are removed, the RCN remains in the buckled state, simultaneously “locking in” these patterns and increasing the Young's modulus by two orders of magnitude. Confinement of thicker gels between harder or softer 3D walls leads to controllable mechanical heterogeneities, where the Young's modulus between specific domains can differ by three orders of magnitude. These systems effectively replicate the

feedback between mechanics and morphology in biological growth, where mechanical forces guide the structure formation throughout stages of growth. The findings provide new guidelines for shaping "growing materials" and introducing new approaches to matching form and function in synthetic systems. This study will help provide guidelines and corroborate the experimental synthesis of expandable polymer networks (discussed earlier).

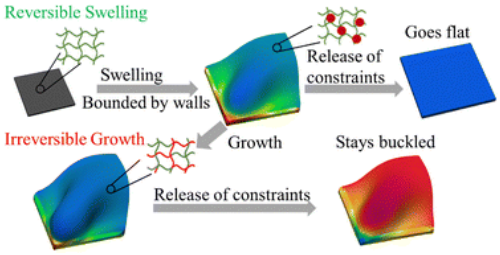

Figure 8 Modeling growth and shape change in polymer gels. As-prepared gel (top panel) undergoes reversible shape changes (swelling) upon bound (release) of constraints while a grown gel (bottom panel) when subjected to constraints and release stays buckled leading to irreversible growth and form.

Future Plans

Inibramers present a unique opportunity for surface-initiated growth. Typically, growing polymer chains via radical polymerization will eventually undergo diradical termination, resulting in only nano-scale growth. With inibramers, however, dormant chain ends (R-Br) will continue to be replenished as they are incorporated. This could be a method to achieve micron-scale growth from a surface. With expandable networks as a platform, morphogenetic behavior of polymer networks can be verified experimentally. Expandable networks are also a good candidate for hard-soft interfaces, since the trithiocarbonate units are able to rearrange, which may alleviate some of the strain that occurs in such materials.

References

1. J. Cuthbert, A. C. Balazs, T. Kowalewski and K. Matyjaszewski, *STEM Gels by Controlled Radical Polymerization*, Trends in Chemistry **2**, 341-353, (2020).
2. S. DiLuzio, T. U. Connell, V. Mdluli, J. F. Kowalewski and S. Bernhard, *Understanding Ir(III) Photocatalyst Structure–Activity Relationships: A Highly Parallelized Study of Light-Driven Metal Reduction Processes*, Journal of the American Chemical Society **144**, 1431-1444, (2022).
3. J. Cuthbert, T. Zhang, S. Biswas, M. Olszewski, S. Shanmugam, T. Fu, E. Gottlieb, T. Kowalewski, A. C. Balazs and K. Matyjaszewski, *Structurally Tailored and Engineered Macromolecular (STEM) Gels as Soft Elastomers and Hard/Soft Interfaces*, Macromolecules **51**, 9184-9191, (2018).
4. S. Biswas, V. V. Yashin, and A. C. Balazs, *Biomimetic Growth in Polymer Gels,* Materials Horizons, **11**, 163-172, (2023).
5. Santidan Biswasa, Ya Liua, Victor Yashin, Ting-Chih Lin, Kriti Kapil, Tomasz Kowalewski, Krzysztof Matyjaszewski, Anna C. Balazs, *Modeling Hyperbranched Polymer Formation via ATRP Using Dissipative Particle Dynamics,* submitted, Polymer.

8 publications with acknowledged DoE support during the last 2 years

1. K. Matyjaszewski, *Current Status and Outlook for ATRP*, European Polymer Journal, **211**, 113001, (2024).
2. K. Matyjaszewski, *Future Directions for Atom Transfer Radical Polymerizations*, Chemistry of Materials, **36**, 1775-1778, (2024).

3. S. Biswas, V. V. Yashin, and A. C. Balazs, *Biomimetic Growth in Polymer Gels,* Materials Horizons, **11**, 163-172, (2023).
4. J. Jeong, S. Y. An, X. Hu, Y. Zhao, R. Yin, G. Szczepaniak, H. Murata, S. R. Das, and K. Matyjaszewski, *Biomass RNA for the Controlled Synthesis of Degradable Networks by Radical Polymerization*, ACS Nano, **17**, 21912-21922, (2023).
5. M. Yasir and K. Matyjaszewski, *Highly Swollen ROMP-based gels*, European Polymer Journal, **196**, 112295, (2023)
6. P. Polanowski, J. K. Jeszka and K. Matyjaszewski, *Crosslinking and Gelation of Polymer Brushes and Free Polymer Chains in a Confined Space during Controlled Radical Polymerization─A Computer Simulation Study*, Macromolecules **56**, 2608-2618, (2023).
7. J. Lyu, Y. Li, Z. Li, P. Polanowski, J. K. Jeszka, K. Matyjaszewski and W. Wang, *Modelling Development in Radical (Co)Polymerization of Multivinyl Monomers*, Angewandte Chemie International Edition **62**, e202212235, (2023).
8. Santidan Biswasa, Ya Liua, Victor Yashin, Ting-Chih Lin, Kriti Kapil, Tomasz Kowalewski, Krzysztof Matyjaszewski, Anna C. Balazs, *Modeling Hyperbranched Polymer Formation via ATRP Using Dissipative Particle Dynamics,* submitted, Polymer.

Using Modeling to Determine Effects of Feedback on Soft Active Matter

Anna C. **Balazs**, Department of Chemical Engineering, University of Pittsburgh, Pittsburgh, PA, 15261

Keywords: chemo-mechanical transduction, feedback loop, oscillations, biomimetic communication

Research Scope

Using computational modeling [1-11], we are designing autonomously functioning materials that integrate biomimetic energy transduction to fuel physical actions and bio-inspired feedback loops to regulate these actions. In particular, such materials have the capability to: **1)** Generate and store energy; **2)** Transport energy to specific locations; **3)** Utilize the energy to undergo self-propelled motion, shape changes; and **4)** Harness feedback loops to seamlessly regulate the entire enterprise.

The outstanding challenge in these studies is to design materials systems that can accomplish **Tasks 1-4** in a smoothly integrated manner with just a low input of energy and display life-like autonomy. Ideally, such materials will spontaneously trigger energy utilization when needed, encompass a mechanism to store and supply energy for future events, and adapt to a range of different stimuli. Ultimately, this material will act autonomously, so that one energy input can trigger a cascade of dynamic events, with each previous step inherently informing the next. In this way, only one instruction set is needed to spontaneously drive the system through a multi-stage process *via* a single initial input. Finally, these materials will be self-regulating to maintain successful operating conditions and their functionality. We aim to address the challenge by designing materials that utilize a small input of chemical energy to controllably and spontaneously perform multiple, coordinated tasks.

Recent Progress

A. Flexible Sheets undergoing chemo-mechanical interactions

1. ***Autonomous shape-changing of flexible sheets in solution*** In nature, the energy released from enzymatic reactions "fuels" a range of mechanical processes, from metabolic events to large-scale motion. Inspired by this mode of biological chemo-mechanical transduction, we used theory and computational modeling to design two-dimensional sheets coated with enzymes that generate chemical energy, which drives the sheets to spontaneously morph into three-dimensional structures and perform mechanical work in fluids.

The reactants and products of the catalytic (enzymatic) reactions can occupy different volumes, producing local density differences, which generate a force that causes the fluid to flow. The latter mechanism is referred to as "solutal buoyancy" and produces an effect throughout the bulk of the fluid. For flexible sheets, the chemically generated flows affect not only the motion of the object, but also the object's ultimate shape. (**Fig. 1, left**) [12]. The coupling of chemo-mechanical transduction and shape changing of elastic 2D sheets can empower fluidic devices to carry out an entirely new repertoire of useful tasks, and ultimately enable new types of chemically driven

Fig. 1 Journal covers from our recent publications.

microscale to mesoscale machines. The latter functionalities can lead to the creation of portable, chemical devices and the discovery of new modes of dynamic self-assembly.

2. Sheets Regulated by a Promotor-Inhibitor Feedback Loop Using our models, we captured the effect of chemical feedback loops on the dynamic behavior of the flexible, mobile sheets (**Fig. 1, right**) [6]. We focused on the inhibitor-promoter feedback loop, which is a vital component in regulatory pathways that control functionality in living systems. In this loop, the production of chemical *A* at one site promotes the production of chemical *B* at another site, but *B* inhibits the production of *A*. The convective rolls of fluid generated above the catalytic patches (red and blue regions right figure), by solutal buoyancy can circulate inward or outward, depending on the values β_i, the solutal expansion coefficient. Within the regime displaying chemical oscillations, the dynamic fluid-structure interactions morph the shape of the sheet to periodically "fly", "crawl", or "swim" along the bottom of the confining chamber, revealing an intimate coupling between form and function in this system. The oscillations in the sheet's motion in turn affect the chemical oscillations in the solution. In the regime with non-oscillatory chemistry, the induced flow still morphs the shape of the sheet, but now the fluid simply translates the sheet along the chamber. The findings reveal the potential for enzymatic reactions in the body to generate hydrodynamic behavior that modifies the shape of neighboring soft tissue, which in turn modifies both the fluid dynamics and the enzymatic reaction. The findings indicate that this non-linear dynamic behavior can be playing a critical role in the functioning of regulatory pathways in living systems.

B. Arrays of flexible, biomimetic microposts

1. ***Stationary patterns: fingerprints, and mandala patterns*** We developed computational models [9] to show that even the stationary states produced by the chemically generated flows lead to an unexpected richness of stable designs, from Mandela figures (**Fig. 2**) to kaleidoscopic images (**Fig. 3**). The arrays also produced unique "fingerprints" that characterize the system, reflecting the type of enzymes used, placement of the enzyme-coated posts, height of the chamber, and bending modulus of the elastic posts. This behavior enables microfluidic devices to be spontaneously reconfigured for specific applications without construction of new chambers and the fabrication of standalone sensors that operate without extraneous power sources.

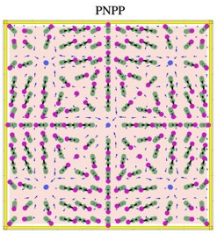

Fig. 2. Self-organization of posts into Mandala pattern.

2. *Dynamic patterns*: *self-oscillations*, *non-reciprocal interactions, and communication* The rich, collective dynamics exhibited by biological cilia has prompted researchers to probe cooperative behavior in synthetic analogues, i.e., arrays of closely spaced, stimuli-responsive gel posts that are tethered to the surface of a fluid-filled chamber. There has, however, been little attention paid to cilia-like arrays in the opposite limit, where the tethered posts lie relatively far apart and do not rely on mutual contact, or external fields for their actuation. Such studies are key to designing biomimetic synthetic systems that can spontaneously transmit long-range signals to distant components and thereby achieve greater control over the entire system.

Using theory and simulation, we designed a system of flexible microposts in solution that convert non-oscillartory chemical input into self-organized oscillatory motion, which enabled the posts to spontaneously propagate a chemical signal over long distances (i.e., larger than the characteristic length in the system) (*work in progress, unpublished*). Here, the oscillations arise due to the chemo-mechanical triggered in the system and the fluid-structure interactions in the fluid. The fluid provides the medium by which these interactions and "instructions" are transmitted over significant distances.

We first focused on one passive and one centrally located active post in the fluid-filled chamber. If the active post is located far from both the wall and passive post, the reaction at the active post generated relatively symmetric flow that kept the post up-right. The fluid-structure interaction with the surrounding walls and the passive post, however, cause the passive post to oscillate. In this manner, a non-oscillatory source can direct oscillations of posts.

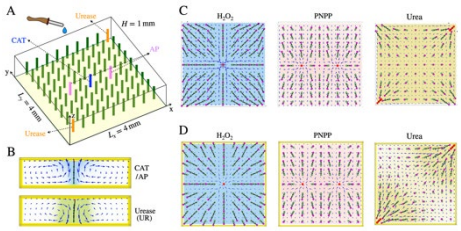

Fig. 3 | The different types of enzymes and the selectively of the enzymatic reactions allows us to produce kaleidoscopic patterns, where one geometrically complex geometry can morph into another with the sequentially addition of the appropriate reactants, as shown in C and D.

The observed non-reciprical oscillations are due to fluid-structure interactions that bend the tips of posts in the closed chamber. The specific conformation of this bent post and its dynamic behavior depends on its placement in the array and its bending stiffness, enabling the posts to exhibit a range of dynamic motion. Moreover, the generated non-reciprocal movement can be propagated among multiple posts in an array and hence, the system can permit extensive directional flow and broader propagation of "instructions" within in microfluidic chambers. The oscillation frequency due to the non-reciprocal interactions can be modified by introducing additional passive posts, which can drive the synchronization of multiple posts in the array (see **Fig. 4**), revealing the significant cooperative activity in the chamber.

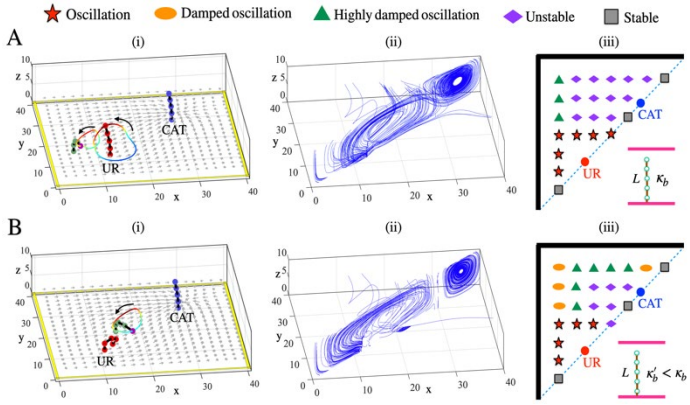

Fig. 4 Oscillation of passive post (colored in green with tip (colored in magenta) trajectory in presence of two active posts (one CAT-coated post and one UR-coated) and corresponding streamlines, as well as the state diagram showing different modes of motion of the passive post, for the two values of the bending stiffness. State diagram obtained by placing passive post in one location, doing the calculation, and then placing the post in another position to redo calculation.

We also examined systems that involved two active posts, which were coated with distinct catalysts, urease (UR) and catalase (CAT). The oscillatory behavior occurred on just the UR-coated post even though the two posts were placed at symmetric positions along the diagonal line that cuts through the box and both exhibited the same bending stiffness. Here, the combination of the local inward and outward flows led to a specifically oriented motion, which flowed toward UR at the top and away from UR at the bottom. This flow pattern yielded an oriented vortex about the UR-coated post. By taking into account the flow patterns for the two indivdual pumps and the relative placement of the pumps, the flow can be combined to enhance, suppress, or reverse the fluid motion in the chamber.

The system in **Fig. 4** encompasses a UR-CAT pair and a single passive post (in green). The panels in the figure show: (i) the position of a passive post with the corresponding trajectories of the post tips, (ii) the streamlines in the diagonal plane, and (iii) the state diagram that summarizes

different modes of motion of the passive post in the presence of the active ones. We consider only the half of the domain due to the symmetry of the system.

For the cases in **Fig. 4A**, the bending stiffness for all the posts was set to $\kappa_b = 0.17\ p\text{Nmm}^2$ Of the two active posts, only the UR-coated post exhibits oscillatory behavior at the specific separation distances depicted in **Fig. 4A(i).** The phase map (**Fig. 4A(iii)**) reveals that the flow pattern generated by the two active posts enables passive posts closest to the UR-coated one (shown by stars) to sense and respond to the oscillatory behavior enforced by this active post.

Figure 4B shows the behavior for the more flexible posts, which have $\kappa_b = 0.057\ p\text{Nmm}^2$. Relative to **Fig. 4A**, the decrease in the bending stiffness for **Fig. 4B** affects the behavior of posts near the walls in the upper half plane. The posts at the unstable points in **Fig. 4A** show highly damped behavior in the corresponding locations in **Fig. 4B**. Similarly, posts with the highly damped behavior in **Fig. 4A** show damped dynamics in **Fig. 4B** for the same locations.

The calculated phase maps (**Fig. 4**) allow the designer to select the appropriate parameters (placement in the array, bending stiffness) and thereby access a particular dynamic state and desired functionality. The coupling of the different flows generated at the pumps (outward and inward) provides a distinct means of controlling the global circulation of the fluid, transporting a chemical message along a particular path and producing the desired mechanical response of the tethered posts. For a given array containing a specified number, location, and type of active and passive posts, the system can still be reconfigured by specifying which of the appropriate reactants are to be added and the sequence in which they are added. Once all the reagents have been consumed, the chamber can be reinvigorated by adding new reactants, and thus, the system can be used multiple times.

Notably, the phase maps for arrays containing both active and passive posts reveal a wealth of dynamic behavior, where each mode of chemically triggered motion can serve a distinct purpose and the entire array can offer a range of utility. The system only requires low energy input to drive autonomous materials, including in soft robots.

Future Plans

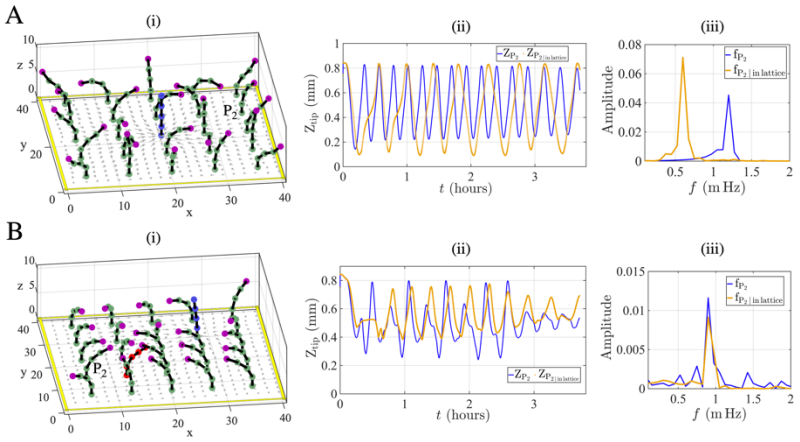

We will determine the additional dynamic motions of the posts with the introduction of cascade reactions, where the product of one reaction is the reactant for the next. The latter behavior will allow the transmittance of chemical signals and messages over a larger distance in the chamber, allowing posts at one position to remotely control the behavior of distant ones.

We will also examine the behavior of multiple posts' systems shown above. **Figure 5A** shows the behavior of the array containing one active post, the CAT-coated post in the center (in blue) and **Fig. 5B** shows a multi-post array with a UR-CAT pair. Here, the presence of the

additional passive posts led all posts to operate at the same frequency (**Fig. 5B**). With this wealth of dynamic behavior, each mode of motion can serve different purposes and offer a range of utility. Ultimately, these self-oscillating systems can facilitate the development of autonomously moving robots in solution, the directed transport of specific chemicals in the chamber.

References (Papers acknowledging DOE support for last two years)

1. Manna, R.K., Gentile, K., Shklyaev, O.E., Sen, A., and Balazs, A.C., "Self-generated Convective Flows Enhance the Rates of Chemical Reactions" *Langmuir* 38(4) (2022) 1432-1439. doi: 10.1021/acs.langmuir.1c02593
2. Laskar, A., Manna, R.K., Shklyaev, O.E., and Balazs, A.C., "Computer Modeling Reveals Modalities to Actuate Mutable, Active Matter" *Nature Communications* 13 (2022) 2689 (4 pages). doi: 10.1038/s41467-022-30445-x
3. Manna, R.K., Laskar, A., Shklyaev, O.E., and Balazs, A.C., "Harnessing the Power of Chemically Active Sheets in Solution" *Nature Reviews Physics* 4 (2022) 125-137.
4. Manna, R.K. Shklyaev, O.E., Stone, H.A., and Balazs, A.C., "Solutal-buoyancy driven intertwining and rotation of patterned elastic sheets" *PNAS Nexus*, 1 (2022) 1–12 https://doi.org/10.1093/pnasnexus/pgac072
5. Zhang, Jianhua, et al. "Light-powered, fuel-free oscillation, migration, and reversible manipulation of multiple cargo types by micromotor swarms." *ACS nano* 17.1 (2022): 251-262.
6. Manna, R.K., Shklyaev, O.E., and Balazs, A.C., "Chemically Driven Multimodal Locomotion of Active, Flexible Sheets", *Langmuir* 39 (2023), 39, 780–789
7. A Laskar, JE Kauffman, BM Tansi, A Sen, AC Balazs Autonomous Photothermally-driven Fluid Pumping and Particle Transport and Assembly. Out-of-equilibrium Soft Matter: Active Fluids. 2023 Mar 24;17:296.
8. Shklyaev, Oleg E., Abhrajit Laskar, and Anna C. Balazs. "Engineering confined fluids to autonomously assemble hierarchical 3D structures." *PNAS nexus* 2.7 (2023): pgad232.
9. Moradi M, Shklyaev OE, Balazs AC. Integrating chemistry, fluid flow, and mechanics to drive spontaneous formation of three-dimensional (3D) patterns in anchored microstructures. Proceedings of the National Academy of Sciences of the United States of America. 2024 Mar 3;121(11).
10. Jiaqi Song, Oleg E. Shklyaev, Aditya Sapre, Anna C. Balazs, Ayusman Sen. "Self-propelling macroscale sheets powered by enzyme pumps." *Angewandte Chemie* 136.6 (2024): e202311556.
11. Jiaqi Song, Jianhua Zhang, Jinwei Lin, Oleg E. Shklyaev, Shanid Shresha, Aditya Sapre, Anna C. Balazs, and Ayusman Sen "Programming Fluid Motion Using Multi-Enzyme Micropump Systems: Design of a Vectorial Flow-Based Sensor , *ACS Applied Materials & Interfaces, in revision*
12. Manna, Raj Kumar, et al. "Chemically controlled shape-morphing of elastic sheets." *Materials Horizons* 7.9 (2020): 2314-2327. (*published earlier than 2022, but still noted here as a reference*).

Self-Assembly and Self-Replication of Novel Materials from Particles with Specific Recognition

Paul M. **Chaikin** and David Pine, Dept. of Physics, New York University
Ruoji Sha and Marcus Weck, Dept. of Chemistry, New York University

1. Pine –Keywords : DNA-coated Colloids, TIRM, Electrophoresis

Characterization of DNA Brushes on Colloids using TIRM and Electrophoresis

DNA-coated colloids (DNACCs) offer unprecedented control over colloidal self-assembly, with the ability to dynamically assemble and disassemble new structures ranging from new 3-dimensional crystal structures to chains, colloidal micelles, and sheets. Here, we report experiments focused on developing a detailed understanding of DNA-mediated interactions between DNACCs, developing and using total internal reflection microscopy (TIRM), video particle tracking, and electrophoresis to measure the interaction potential between DNA-coated surfaces as a function of temperature near the melting temperature.

We build a predictive model to understand how microscopic material design affects macroscopic melting. A careful account of the polymer brush, especially of entropic costs due to loss of degrees of freedom upon binding, is central for quantitative description. Here, we avoid loosely defined variables and fitting and rely on a mean-field description to account for the detailed geometry of our brushes, based on an extension of the Milner-Witten-Cates theory. Our theory identifies a subtle competition between DNA binding and steric repulsion and accurately predicts adhesion and melting at a molecular level. The theory provides a quantitative, consistent description of the experimental measurements and thus provides a predictive approach for guiding material design with DNA nanotechnology and, by extension, to a diversity of colloidal and biological systems.

During our research, we uncovered a fundamental limit to the spatial resolution with which TIRM can measure colloidal interactions, a limit that had not been appreciated in its 35 years of use (and misuse). We developed an analytical description of the resolution limit, which comes from the quantum mechanical nature of photon counting statistics in the measurement of light intensity.

We also study DNA-coated colloids diffusing near surfaces coated with complementary strands for various coating designs. We find colloids rapidly switch between 2 modes: they hop (with long and fast steps) and crawl (with short and slow steps). Both modes occur at all temperatures around the melting point. The particles become increasingly subdiffusive as temperature decreases, consistent with subsequent velocity steps becoming increasingly anti-correlated, corresponding to switchbacks in the trajectories. Overall, crawling (or hopping) phases are more predominant at low (or high) temperatures; crawling is also more efficient at low temperatures than hopping to cover large distances. We rationalize this behavior within a simple model: at lower temperatures, the number of bound strands increases, and detachment of all bonds is unlikely; hence, hopping is prevented, and crawling is favored. We thus reveal the mechanism behind a common design rule relying on increased strand density for long-range self-assembly: dense strands on surfaces are required to enable crawling, possibly facilitating particle rearrangements.

We also have made extensive measurements of the electrophoretic mobility of DNACCs as a function of salt concentration. When the Debye screening length is comparable to the brush length, the electrophoretic mobility is strongly suppressed. Treating the brush as a porous medium that impedes electroosmotic flow provides a quantitative description of the data. These measurements provide detailed information about the microscopics of grafted polymer brushes on colloids.

2. Weck – Keywords: Dielectrophoresis, DNA Coated colloids, Colloidal machines

A second strategy of combining DNACCs and an external field to direct and control assembly is the use of a dielectrophoretic (DEP) field. Our strategy to introduce complexity and anisotropy to a colloidal particle is via surface functionalization. In particular, we are incorporating metal coatings onto the surface of patchy DNACCs. Gold nanoparticles, in particular, present high stability, variable optical properties, and tunable surface functionalization and can be synthesized in a straight fashion. During the past funding period, we have developed a bottom-up technique for the sequential seeded growth synthesis of customized colloidal non-linear particles with three lobes, the selective coating of individual lobes with gold, and the use of DEP to manipulate and direct the assembly of these particles. The tailored customization of each compartment can be tuned by incorporating a layer of gold nanoparticles on site-specific lobes (Figure 1), thereby changing the physicochemical properties of the lobe, their interaction with an electric field, and ultimately their directionality during assembly.

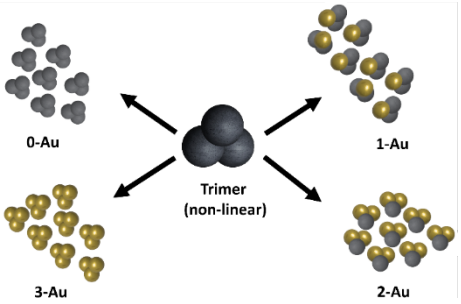

Figure 1 Schematic representation of the site-specific gold-customization of trimer particles investigated in this study. Grey lobes represent the bare lobes, Gold lobes represent the site-specific gold coating (for varying lobes) of each trimer particle.

We explored the assembly of symmetrical lobe protrusions with different metallodielectric characteristics in deionized water ($\mathcal{E}$ = 78.5) and aqueous potassium chloride (0.15mM, $\mathcal{E}$ = 40). An electrolyte with a significantly lower dielectric constant, like potassium chloride, causes a decrease in the distance between particle surfaces due to electrostatic interactions. Our study elucidates the DEP assemblies of colloidal trimers by varying the frequency of the electric field and the permittivity of the surrounding medium.

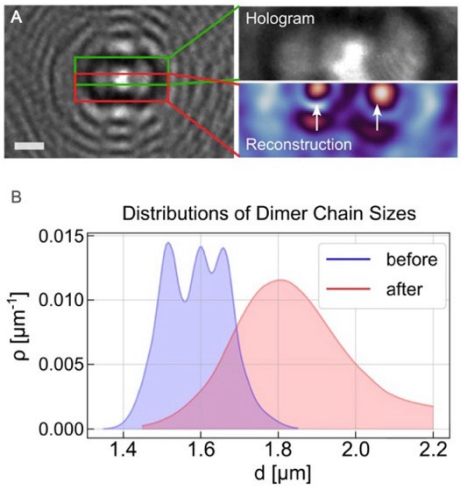

Figure 2. Holographic Analysis of Dimer Chain Superstructures and Swollen Chain Superstructures. A) Left, holographic image of a swollen crosslinked dimer chain. Right, cropped hologram from the image on the left along with an intensity pattern reconstructed using Rayleigh-Sommerfeld backpropagation to bring features into focus. The arrows denote the centers of monomers. B) Distribution of dimer chain sizes in μm before swelling in PBS (blue) and after swelling with THF (red). A) Scale bar 1 μm.

Muscle-like Colloidal Actuators

We also expanded the use of DNACCs towards colloidal machines. We reported the synthesis and holographic imaging analysis of colloidal artificial muscle analogs through the assembly of shape-shifting responsive and non-responsive colloidal subunits. Our building blocks are assembled utilizing cooperative depletion and DNA interactions resulting in the selective formation of linear

chained structures of various lengths. The muscle-like actuation was explored through cycling experiments and total holographic characterization (Figure 2).

Our binary system of alternating DNA linked subunits retains integrity when swollen, swells reversibly, and changes in rigidity between states, achieving the synthesis of a colloidal-based artificial muscle that does not degrade. This chain assembly can be incorporated into systems for biomedical applications, medical instrumentation, and engineering applications in soft robotics.

3. Sha -Keywords: DNA Reconfiguration, Electrical and Light-driven Stimuli

We explored the manipulation of DNA through external stimuli like electricity and light. Leveraging electricity-induced changes to the oxidation state of metal ions or disulfide bonds and light-induced changes to pH (via photoacids and photobases), we aim to precisely control DNA nanoconstruct self-assembly, self-replication, engineered DNA crystals and DNA conductivity.

Metal-mediated DNA (mmDNA) strand displacement by pH change. Previously, we found that the silver(I) ion (Ag^+) has a changing preference for pyrimidine:pyrimidine DNA base pairs across the pH spectrum. As a proof-of-principle, we have modified the DNA tensegrity triangle to include a single stranded DNA tail, in which a change in environmental pH allows for isothermal binding to different complementary strands through the matching metal-mediated toehold. We altered DNA crystal color to match configuration states with fluorescence dyes attached to complementary strands (Fig. 3a). We successfully reduced silver ion (Ag^+) incorporated between C:C base pairs in the DNA tensegrity triangle and solved the molecular structure by x-ray crystallography (Fig. 3b). This tool will enable isothermal association and dissociation of DNA tiles by cyclic redox of metal ions using mmDNA strands as the sticky ends. We simplified the process for the robust ligated DNA crystals. Instead of complicated, time consuming ligation by DNA ligase or psoralen/^{CNV}K, we used UV light to crosslink two thymines flanking the nick position in the sticky ends of the self-assembled DNA crystals. Thymine dimerization has been shown to be reversible, which may yield a tool for self-replication.

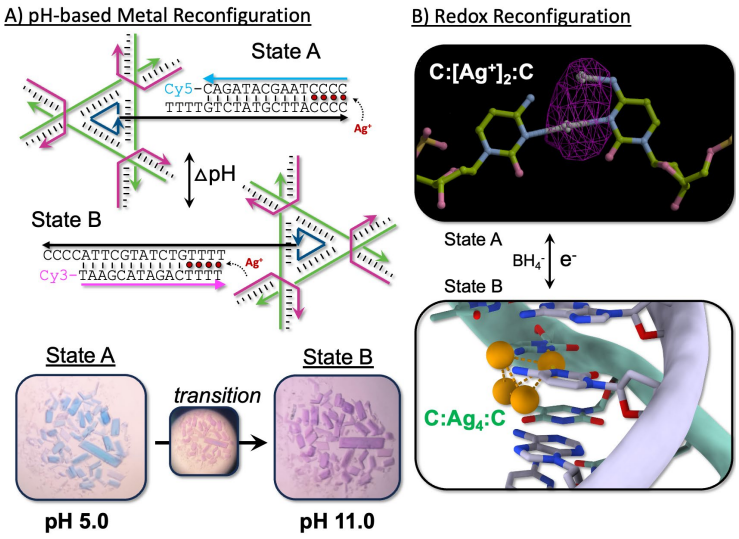

Figure 3. A) Metal-mediated strand displacement in a self-assembled crystal attained by pH change between two states. B) Reduction of the C:Ag^+:C base pair yields fluorescent 4-atom nanoclusters within DNA crystals.

Future Plans

1. We will replace the vertical sticky ends of the DNA rafts by mmDNA strands in our previous DNA origami self-replication experiments, and the replication cycles will be operated isothermally by changing the oxidation states of metal ion. **2.** We will combine isothermal association and dissociation of mmDNA in the redox cycling of metal ions together with the selective binding of mmDNA in different pH conditions regulated by certain wavelength light by adding photoacids and photobases to explore the selection and competition abilities in our previous DNA origami self-replication experiments. **3.** We will incorporate thio-modified DNA bases such as 2-thio-dT, 6-thio-dG to flank the nick position in the sticky ends of DNA crystals and use redox reaction to control the formation of disulfide bonds to make reversible robust DNA crystals.

4. Chaikin - Keywords: Self-replication, Cooperativity, Complexity, Heat cycles and Ligation

We have previously demonstrated self-replication, exponential growth and selection/competition in systems using temperature and light cycles and avoiding the use of enzymes a in a prebiotic environment. To speed up processing and address larger more complex structures where production inhibition may play a role, we have introduced ligation to our toolbox.

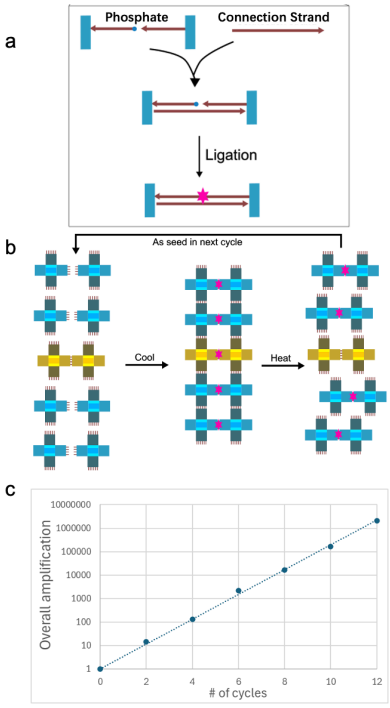

Artificial Self-Replication of DNA Crosstiles Using T4 Ligase: Our self-replication scheme uses DNA crosstiles with vertical DNA sticky ends to bind monomers to parents/seeds on cooling, and horizontal sticky ends to join the templated tiles to make an offspring, Fig. 1. The offspring is made permanent, previously by covalently binding the hybridized horizontal sticky ends using UV light, and presently by using a connection strand and a ligase. In previous experiments using ^{CNV}K and UV we made "litters" of offspring by building a ladder. The same works with the ligase fixing, Fig. 4.

Figure 4. Litters replication a) T4 Ligation of horizontal strands. b) 1D ladder for litter replication. c) Overall amplification from serial self-replication. ~2,000,000-fold amplification is achieved after 12 self-replication cycles.

Cooperativity and Cycling and Production Inhibition. In many processes, including self-replication the products are bound more tightly than the initial components, e.g. the binding energy of monomers to seed is less than the binding of the seed and its offspring approximately by the number n of the n-mer created. This can limit the size and complexity of self-replicated species. However, in a simple model where each segment has the same entropy and enthalpy contribution the melting temperature is:

$$T_{mn} \approx \frac{n\Delta H^0_{DNA}}{nR+n\Delta S^0_{DNA}+n\Delta S_p+R\ln\left(\frac{CAp}{2}\right)} = \frac{\Delta H^0_{DNA}}{R+\Delta S^0_{DNA}+\Delta S_p+\left(\frac{R}{n}\right)\ln\left(\frac{CAp}{2}\right)}$$

Here cooperativity comes from only having to pay the price of translational entropy, ln(CAp), only once. Tmn saturates to a finite value as n $\rightarrow\infty$. Further, unlike an isothermal process, a cyclic process avoids much of the production inhibition problem by assuring that the components can separate for at least the high temperature part of the cycle.

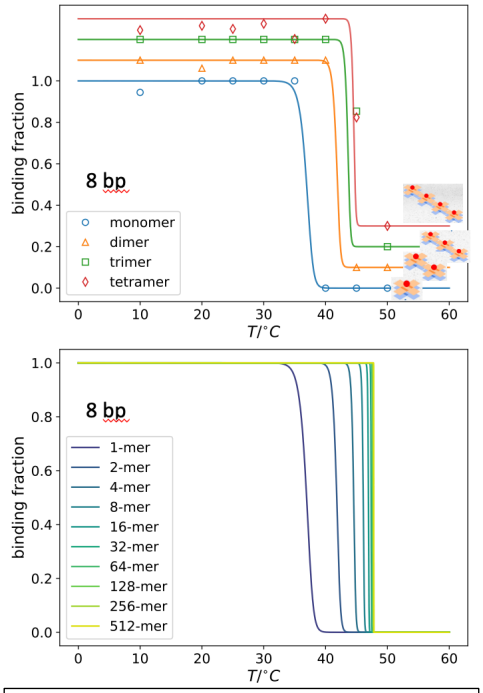

Figure 5. Bottom) Fig. Predicted melting curves for n-mer linear tiles on their complementary n-mer tiles. Top) compared with their melting curves from gels run at different temperatures.

10 Publications from DOE DE-SC0007991 2023-2024

Barrat, Jean-Louis, Emanuela Del Gado, Stefan U. Egelhaaf, Xiaoming Mao, Marjolein Dijkstra, David J. Pine, Sanat K. Kumar et al. "Soft matter roadmap." *Journal of Physics: Materials* 7, no. 1 (2023): 012501.

Jo, In-Seong, Joon Suk Oh, Matthieu Soula, Manhee Lee, David J. Pine, Etienne Ducrot, and Gi-Ra Yi. "DNA-Coated Microspheres with Base Mismatches for Stepwise Programmed Assembly." *Chemistry of Materials* 36, no. 8 (2024): 3820-3828.

Jackson, Nicolle S., Samira Munkaila, Lasya Damaraju, and Marcus Weck. "Progress in the Synthesis of Colloidal Machines." *Accounts of Materials Research* 5, no. 3 (2024): 249-258.

Huang, Qiuyan, Jiyeon Kim, Kun Wang, Simon Vecchioni, Yoel P. Ohayon, Nadrian C. Seeman, Nataša Jonoska, and Ruojie Sha. "Environmentally controlled oscillator with triplex guided displacement of DNA duplexes." *Nano Letters* 23, no. 16 (2023): 7593-7598.

Lu, Brandon, Simon Vecchioni, Yoel P. Ohayon, Karol Woloszyn, Tiffany Markus, Chengde Mao, Nadrian C. Seeman, James W. Canary, and Ruojie Sha. "Highly Symmetric, Self-Assembling 3D DNA Crystals with Cubic and Trigonal Lattices." *Small* 19, no. 3 (2023): 2205830.

Lu, Brandon, Karol Woloszyn, Yoel P. Ohayon, Bena Yang, Cuizheng Zhang, Chengde Mao, Nadrian C. Seeman, Simon Vecchioni, and Ruojie Sha. "Programmable 3D hexagonal geometry of DNA tensegrity triangles." *Angewandte Chemie International Edition* 62, no. 6 (2023): e202213451.

Wang, Tianqi, Tanxi Bai, Zhenyu Tan, Yoel P. Ohayon, Ruojie Sha, Simon Vecchioni, Nadrian C. Seeman, and Bryan Wei. "Mesojunction-based design paradigm of structural DNA nanotechnology." *Journal of the American Chemical Society* 145, no. 4 (2023): 2455-2460.

Zhou, Feng, Heng Ni, Guolong Zhu, Lev Bershadsky, Ruojie Sha, Nadrian C. Seeman, and Paul M. Chaikin. "Toward three-dimensional DNA industrial nanorobots." *Science Robotics* 8, no. 85 (2023): eadf1274.

Wang, Kun, Qiuyan Huang, Mohammed Ragab Elshaer, Brian Knorr, Paul Chaikin , and Guolong Zhu. "Tri-state logic computation by activating DNA origami chains." *Nanoscale* 16, (2024): 11991-11998.

Modin, Alvin, Matan Yah Ben Zion, and Paul M. Chaikin. "Hydrodynamic spin-orbit coupling in asynchronous optically driven micro-rotors." *Nature Communications* 14, no. 1 (2023): 4114.

Design Principles of Biomolecular Metamaterials

Jong Hyun **Choi**, School of Mechanical Engineering, Purdue University

Keywords: DNA nanotechnology, mechanical metamaterials, mechanics, mechanical design, free energy landscape

Program Scope

Architected mechanical metamaterials are designed by strategically arranging cellular building blocks to achieve auxetic behaviors and tunable responses, which may be exploited for shape morphing, adaptive devices, and energy absorption mechanisms.[1,2] The benefits from such designs are yet to be leveraged at the nanoscale. DNA self-assembly may be an ideal approach to bridge the gap in lengthscale and develop architected nanomaterials, given the excellent programmability and structural predictability. This research aims to demonstrate nanoscale auxetic metastructures from DNA and develop general design principles. We have used the DNA origami method to construct several architected DNA assemblies and studied their nanomechanics and auxetic deformations. During this reporting period, we have focused on (1) demonstration of nanoscale auxetics with tunability and geometric frustration with programmed buckling, (2) elucidation of structural properties and free energy landscapes, and (3) development of 3D deployable metastructures that can store and release elastic energy. Our work also develops theoretical and computational basis for designing architected DNA nanomaterials.

Recent Progress

1. Auxetic nanostructures with tunable deformation behaviors

Architected metamaterials respond to external loading with their mechanically coupled, periodic cellular structures deforming in unison. The unit cell design thus determines auxetic deformation patterns and the relevant negative Poisson's ratio (NPR) is prefixed.[3] A design that allows tunable deformation behaviors, if possible, would allow for programmable auxetics and open new opportunities. To address this challenge, we have introduced a new design of auxetic nanostructures with tunability using DNA origami. This metastructure can deform in different directions in response to external forces. As shown in Fig. 1, our DNA origami design consists of three 4-point nanostars with identical sizes and internal angles of $\pi/4$ which can slide against each other in two distinct directions. External loading in horizontal directions leads to sliding actions along the edges of neighboring stars as shown in Fig. 1a. This results in a compression of the structure both horizontally and vertically with a Poisson's ratio of $\nu = -0.4$. On the other hand, a new configuration will emerge if the neighboring edges slide both vertically and horizontally due to a different loading (Fig. 1b). Here, the structure will rotate for an angle of $\pi/8$, which will lead to $\nu = -1$. To demonstrate such a tunability, we performed molecular dynamics (MD) simulations using oxDNA platform[4] and experimentally constructed the DNA nanostars and characterized them using AFM. The coarse-grained MD modeling helped us design sliding mechanisms and

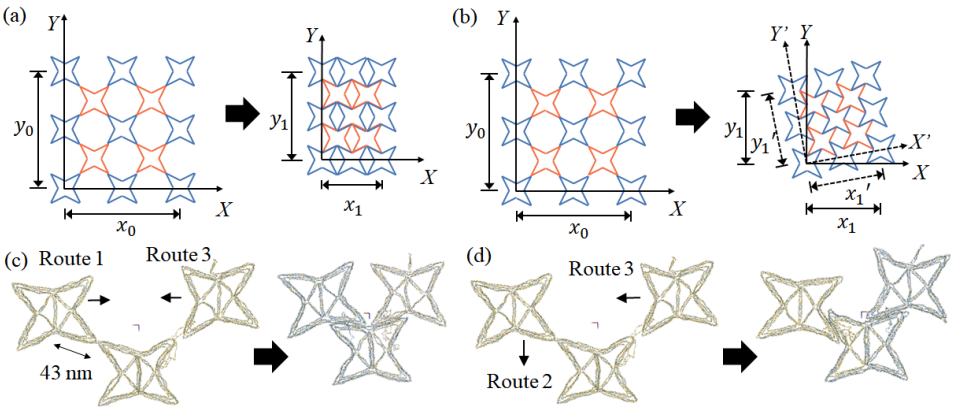

Figure 1. Auxetic DNA nanostars with tunability. (a) Horizontal sliding of the periodic cellular structure leads to an overall contraction with a negative Poisson's ratio. (b) Sliding vertically and horizontally results in an auxetic rotation with $\nu = -1$. (c)-(d) Coarse-grained MD simulations of reversible and programmable sliding mechanisms corresponding to (a) and (b).

revealed the structural integrity. We successfully confirmed the origami sliding in experiment with the two distinct NPR values. Of considerable utility is that our DNA design and sliding mechanisms enable tunability and reversibility.

2. Mechanical frustration and free energy profiles

We have introduced a new approach of designing metastructures using mechanical frustration. Geometric frustration occurs when neighboring building blocks in a lattice cannot interact cooperatively due to geometric constraints, thus resulting in a 'frustration'. This concept was originally developed in magnetism, where electronic spin energies cannot be minimized (e.g., antiferromagnetic) as described by the Ising model.[5,6] We drew an analogy between magnetic and mechanical frustrations by replacing electronic spin with mechanical strain. As a model system, we designed a Kagome-like, six-cell hexagonal lattice (Fig. 2a) made of 28-nm-long edges. This

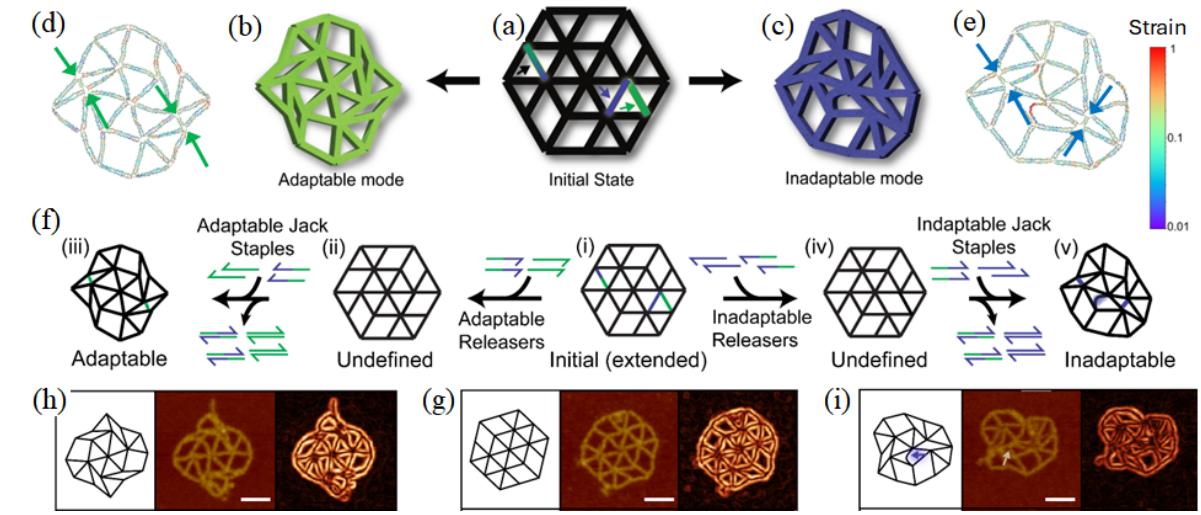

Figure 2. Mechanical frustration. (a) DNA origami design which can be deformed into (b) adaptable or (c) inadaptable structures upon external forces on blue/green and green edges or blue/green and blue edges, respectively. (d)-(e) MD simulated (normalized) mechanical strains. Green and blue arrows indicate loading. (f) Scheme for chemical loading (via 2-step DNA reactions) for switching between the two modes. Schematics, AFM scans, and contrast images of (g) initial, (h) adaptable, and (i) inadaptable structures. Scale bar: 50 nm.

design allowed us to demonstrate both frustrated and non-frustrated states in a single lattice by engineering reconfigurable 'jack' edges shown in blue and green. This metastructure can switch between adaptable and inadaptable modes in response to external loading (Fig. 2b-c). The two modes are identical except for one loading spot. The adaptable structure can distribute mechanical strain evenly (Fig. 2d). In the inadaptable mode, however, the strain is localized in an edge, i.e., buckling (shown in red in Fig. 2e).

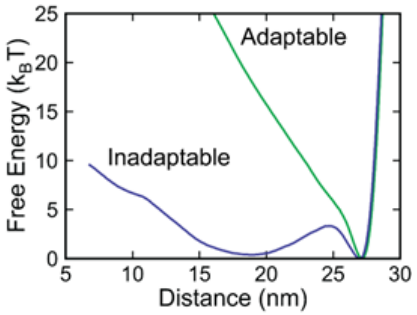

Figure 3. Free energy profiles of adaptable and inadaptable structures.

Figure 2f shows our experimental scheme using chemical loading methods. Starting from the initial state with all the edges extended (Fig. 2g), we used two-step DNA reactions to first remove the staples for adjustable jack edges via toehold-mediated strand displacement (undefined states) and then add another set of staples, forming either adaptable or inadaptable structures. AFM imaging confirms a buckled edge (indicated by arrows in Fig. 2i) with end-to-end distance of ~18 nm in the inadaptable mode. In contrast, all the edges are extended in the adaptable structure (Fig. 2h). Our experiment demonstrated programmable reversibility between the initial, adaptable, and inadaptable states.

We also computed free energy landscapes of the two modes as a function of end-to-end distance (where buckling occurs) using umbrella sampling, as shown in Fig. 3. The adaptable mode shows a single free-energy minimum at ~28 nm, implying that the structure will be most stable when all the edges are fully extended. In contrast, the inadaptable state displays a doublet: a broad minimum at ~18 nm besides the 28-nm minimum. This observation provides several insights. Free energy calculations accurately predict experiments. The dual minima suggest a snap buckling between two distinct states (no intermediates). Lastly, free energy landscape can be a framework for designing mechanically frustrated metastructures.

3. 3D deployable metastructures

Deployable structures are a class of metamaterials with a finite size that can maintain its symmetry during contraction and expansion. In nature, viruses show such remarkable structural properties. For example, a cowpea chlorotic mottle virus (CCMV) deploys its icosahedral configuration upon pH change, and this is a critical step for injecting its genetic molecules. Inspired by such dynamic nanomachinery, we have introduced a 3D deployable nanostructure that can switch between octahedron and cuboctahedron as illustrated in Fig. 4. Here, a cuboctahedron (with 6 squares and 8 equilateral triangles) may transform into an octahedron if all six squares collapse. Likewise, a cuboctahedron will emerge from an octahedron if the squares open up, which increases the volume by a factor of 5 and the surface area by a factor of $1+\sqrt{3}$. During the transformation

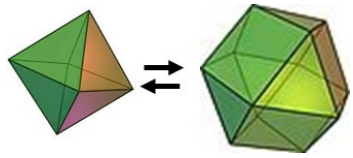

Figure 4. A Jitterbug transformer design that switches between octahedron and cuboctahedron.

process, the triangles do not change but are subject to a translation-rotation along the symmetry axis. This design is termed a Jitterbug transformer.[7]

We constructed this deployable metastructure using wireframe DNA origami that is composed of 28-nm-long edges with a 6-helix-bundle cross-section. There are several key design strategies. First, we built stiff triangles (as they do not reconfigure) while the squares have some flexibility for opening and closing. This was achieved by differing unpaired nucleotides at the vertices. Several adjustable jack edges were also engineered for opening and closing of the squares. This design requires nucleotides more than a single scaffold (e.g., M13mp18) offers. Thus, we used two orthogonal scaffolds for this structure. Lastly, this structure was designed such that it can transform from the compressed to expanded conformations spontaneously, but not the other way around. That is, the octahedron is the high free-energy conformation while the cuboctahedron is more stable. MD calculations helped us develop this deployment scheme by storing elastic energy at the joints of the octahedron using jack edges. When the jacks were removed, the elastic energy was released and the structure spontaneously transitioned from octahedron to cuboctahedron. We also estimated the forces needed to pack the elastic energy into the metastructure. Our AFM and TEM imaging confirmed this design and 3D structural deployment.

Future Plans

This project highlights the synergy between architected metastructures and DNA nanotechnology towards a previously unexplored class of nanoscale metamaterials. In the next year, we will develop mechanisms that can route strain from external loading. This ability may be exploited to develop methods of storing and releasing mechanical strain within metastructures on demand. Such capabilities will open new possibilities. We will also explore 3D deployment with environmental adaptability. We aim to develop mechanisms for reconfiguring conformations in response to environmental changes like pH change or irradiation conditions. Lastly, we will investigate the details of reconfiguration dynamics. We plan to use fluorescence resonance energy transfer or FRET to probe structural dynamics. Our effort will establish general design strategies for architected metastructures and auxetic nanomachinery based on both mechanics and energetics.

References

1. K. E. Evans and A. Alderson, *Auxetic Materials: Functional Materials and Structures from Lateral Thinking*, Advanced Materials **12**, 617-628 (2000).
2. K. Bertoldi, V. Vitelli, J. Christensen, and M. van Hecke, *Flexible Mechanical Metamaterials*, Nature Reviews Materials **2**, 17066 (2017).
3. J. Bauer, L. R. Meza, T. A. Schaedler, R. Schwaiger, X. Zheng, and L. Valdevit, *Nanolattices: An Emerging Class of Mechanical Metamaterials*, Advanced Materials **29**, 1701850 (2017).
4. F. Romano, D. Chakraborty, J. P. K. Doye, T. E. Ouldridge, and A. A. Louis, *Coarse-grained Simulations of DNA Overstretching*, Journal of Chemical Physics **138**, 085101 (2013).

5. K. Kano and S. Naya, *Antiferromagnetism. The Kagomé Ising Net*, Progress of Theoretical Physics **10**, 158-172 (1953).
6. A. S. Meeussen, E. C. Oğuz, Y. Shokef, and M. van Hecke, *Topological Defects Produce Exotic Mechanics in Complex Metamaterials*, Nature Physics **16**, 307-311 (2020).
7. H. F. Verheyen, *The Complete Set of Jitterbug Transformers and the Analysis of Their Motion*, Computers and Mathematics with Applications **17**, 203-250 (1989).

Publications (BES supported, last two years)

1. A. Swett, S. Seo, R. Li, M. Eder, A. S. Madhvacharyula, Y. Du, F. C. Simmel, and J. H. Choi, *Deployable DNA Nanostructures Resembling Jitterbug Transformers*, (2024). In preparation
2. S. Madhvacharyula, R. Li, A. A. Swett, Y. Du, F. C. Simmel, and J. H. Choi, *Realizing Mechanical Frustration at the Nanoscale Using DNA Origami*, bioRxiv (2024). DOI: 10.1101/2024.06.26.600849
3. J. Yang, P. Zhan, X. Jing, M. Škugor, C. Benitez-Martin, J. Rouillon, J. Andreásson, J. H. Choi, P. Wang, and N. Liu, *Light-responsive DNA Ribbons for Membrane Pore Formation and Molecular Transport*, (2024). Under review
4. Y. Du, R. Li, A. S. Madhvacharyula, A. A. Swett, and J. H. Choi, *DNA Nanostar Structures with Tunable Auxetic Properties*, Molecular Systems Design & Engineering, **9**, 765-774 (2024).
5. Shrivastava, Y. Du, H.K. Adepu, R. Li, A. S. Madhvacharyula, A. A. Swett, and J. H. Choi, *Motility of Synthetic Cells from Engineered Lipids*, ACS Synthetic Biology **12**, 2789-2801 (2023).
6. R. Li, A. S. Madhvacharyula, Y. Du, H. K. Adepu, and J. H. Choi, *Mechanics of Dynamic and Deformable DNA Nanostructures*, Chemical Science **14**, 8018-8046 (2023).

Energy-Efficient Self-Organization and Swarm Behavior in Active Matter

Paul Chaikin , Dept. of Physics, New York University
Jerome **Delhommelle**, Dept. of Chemistry, University of Massachusetts Lowell
Stefano **Sacanna**, Mark Tuckerman, Dept. of Chemistry, New York University

Keywords: active matter; nonequilibrium assembly; entropy production; colloidal synthesis; nonequilibrium simulations

Research Scope

Living systems have the unique ability to form hierarchical assemblies in which individual constituents can perform tasks cooperatively and emergently. Harnessing such properties is a long-standing challenge for the rational design of dynamic materials that can respond to their environment, communicate with one another, and undergo a rapid, reversible assembly. Recent developments in the design of smart and active colloidal building blocks have led to tremendous breakthroughs, such as the onset of synthetic photoactivated active assemblies. In this project, we combine experiments, theory, and computations to identify novel couplings between elemental active building blocks, elucidate diffusiophoretic cluster growth, shed light on how to program inverse assembly and assembly in active matter and determine local entropy production and extractable work in active matter.

Recent Progress

Diffusio-phoresis and Diffusio-osmosis

The field of active synthetic matter has produced a wealth of exciting behavior from self-driven motile particles to flocking to motility induced phase separation. There is no shortage of diverse experimental results from similar systems, but therein lies a key problem – what determines the overall motile behavior for a given situation? We provide a means to simplify phoretic chemotaxis by quantitatively breaking down the motion of a particle within a chemical gradient to phoretic and osmotic components. Through this, a clear picture emerges that lays the foundation to describe phoretic chemotaxis quantitatively and generally near surfaces. With this knowledge in hand, we expect old systems can be understood and new behaviors discovered that have implications from advanced materials to biology. Micro-scale objects responding to chemical gradients by migrating towards or away from a preferred species is a simple yet constitutive mechanism by which transport occurs in biological organisms. We demonstrate how a chemical gradient can locally select particles through the two competing effects. We present the first quantitative measurements separating the effects of phoresis and osmosis acting on individual taxing particles. Through this, we are able to develop a more accurate picture of particle transport at the single particle level.

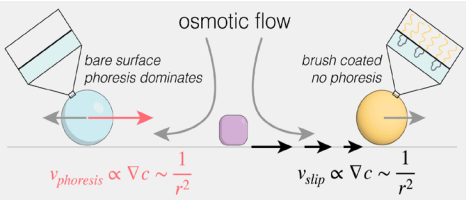

Fig. 1. Summary of chemotaxic behavior. Photocatalytic particles (purple cube) generate a chemical gradient that bare particles (blue) migrate towards, whereas brush coated particles (yellow) migrate away due to osmotic effects.

We consider a system of colloidal α- iron oxide (hematite) in a basic solution containing hydrogen peroxide that, upon blue light illumination, catalyzes the degradation of H_2O_2 into water and O_2. Using continuity and flux conservation of the generated chemical species, the chemical concentration goes as $c(r) \propto 1/r$, where r is the distance from the center of the catalyst. According to the hydrodynamic theory of chemophoresis, the velocity v(r) of a spherical colloid in a varying concentration gradient c(r) goes as $v(r) \propto \nabla c(r)$ which implies that velocity scales as $v(r) \propto \nabla(1/r) \propto 1/r^2$. In basic solution, bare poly(3-(trimethoxysilyl) propylmethacrylate) (TPM), sulfate-initiated poly(styrene) (PS) or silica (SiO_2) colloids, tax up the chemical gradient concentrating near the catalyst and clustering around it to form a hexagonal lattice due to excluded volume effects. If the experiments are performed near a substrate such as glass that is also attracted to higher concentrations of product, a lateral osmotic slip velocity arises at the surface directed away from the catalyst that also scales as $v_{slip}(r) \propto 1/r^2$. This creates an advective flow that depends on the specific geometry of the system purely due to interaction of the chemical species generated with the substrate.

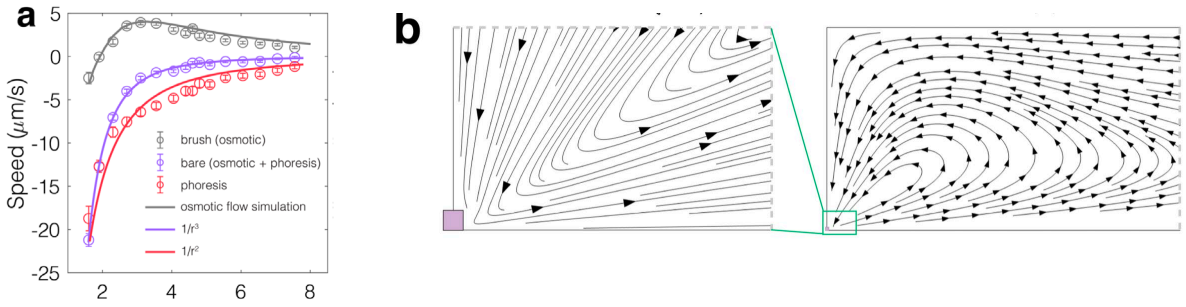

Fig. 2. Individual taxis. (a) Single particle speeds measured from center-center distance between a spatially fixed catalyst and brush coated particles (gray circles) or bare particles (purple circles). The purely phoretic contribution (red circles) is acquired by subtracting the gray points from the purple; the gray line is a result from finite element simulations shown in (b); the purple line is a best fit to $1/r^3$ and the red line is a best fit to $1/r^2$. **(b)** Flow lines from finite-element simulations of our system with a defined slip velocity at the lower boundary of $v = \alpha/r^2$ and no-slip conditions on all other surfaces; the solid line in (a) is found by taking the velocity at the height of the catalyst particle (1 μm); α is determined empirically through a best match of the experimental data.

As the schematic in Fig. 1a suggests, if one is able to "turn off" phoresis, a nearby particle will follow this developed advective flow away from the catalyst. We are able to experimentally observe this with polymer brush coated particles that effectively remove the phoretic effect. A mixture of the bare TPM and silica show that the catalyst collects the silica and bare TPM at nearly the same ratio as the background concentration as one would expect for a randomly distributed particle mixture. In contrast, when brush coated TPM and silica are mixed, the catalyst selects the silica particles almost exclusively, while the brush coated TPM are repelled by osmotic flow.

Stimulus-controlled assembly, information encoding, and transport in heterogeneously active systems

We focus here on developing strategies for the design of microscopic machines and reconfigurable materials from active building blocks. Active matter exhibits unique properties that arise from its inherent nonequilibrium nature, thereby providing access to a wealth of assembly pathways beyond the conventional equilibrium routes and to the fine-tuning of the material properties. The microscopic machines so obtained may then serve a wide range of purposes, from the encoding of information in soft memory cells to the transport of colloidal cargo.

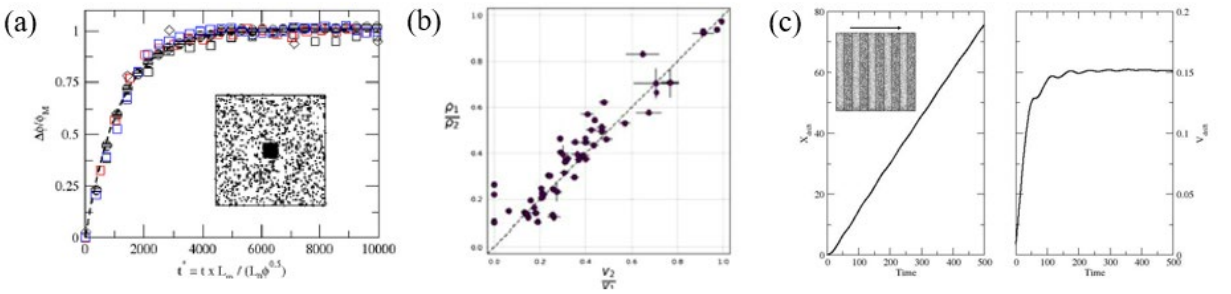

Fig. 3: (**a**) and **(b)**. Static stimulus patterns: scaling relations for imprinting of a densely populated square. The density in the square for different (square dimensions, persistence length) sets falls onto the same plot if plotted against the scaled time. This results from the $v \propto 1/\rho$ relation measured experimentally in (b) for the microswimmers. **(c)** Dynamic stimulus patterns: Transport along *x* of the ABP population (left) and steady-state drift velocity (right). (Inset) Snapshot of ABPs subjected to a moving alternating dark and bright stripes.

Leveraging the ability of active matter to exhibit dynamics-dependent density distributions, we start by developing protocols to achieve the smart templated assembly. To this end, we program spatially-varying stimulus patterns to control locally the level of activity for the self-propelled particles, thereby enabling the formation of sparsely populated regions in domains of high activity (inverse-templated assembly) and of densely populated regions in domains of low activity (templated assembly). We perform simulations on systems of active Brownian particles to explore the parameter space and identify scaling relations that quantify the interplay between the persistence length L_p and the spatial resolution used for the programmed stimulus pattern. These findings are validated by our experiments that demonstrate how spatial light patterns allow for the encoding of information in soft matter in Fig. 3(a). We add that coating the particles with UV-sensitive cross-linkers would also enable fixing the designed material permanently for removal and external use. We then design protocols applicable to the propagation of encoded information in active matter and to colloidal transport. To this end, we apply dynamic stimulus patterns that vary both *spatially* and *temporally*. For instance, subjecting a system of photoactivated microswimmers to a dynamic light pattern, composed of alternating dark and bright stripes moving at constant speed along an axis, imparts a drift velocity to the active particles along this axis in Fig. 3(b). Using simulations and experiments, we analyze the transport mechanisms for active and passive particles, as well as for systems composed of particles with different types of activity and exhibiting non-reciprocal interactions.

Light-Triggered Inflation of Microdroplets.

The domain of driven systems, particularly those involving droplets and fuel, encompasses a vast array of microbiological functions. Despite numerous advancements, fully synthetic systems performing diverse tasks within a uniform bulk at the micrometer scale remain scarce. Here, we focus on a novel design for solid-in-oil composite microdroplets. These microdroplets are meticulously engineered to nucleate an internal phase, inflate, and ultimately burst, all powered by a consistent and uniform energy input. By adjusting the background input, we demonstrate control over volumetric change and burst timing. Upon releasing their inner contents, these inflated droplets transiently attract colloidal particles to the release point. Moreover, the system is capable of performing multiple inflation-burst cycles. This conceptual design of internally powered microdroplets is anticipated to spark further research into autonomous systems with intricate communication abilities and to inspire the development of advanced, responsive materials.

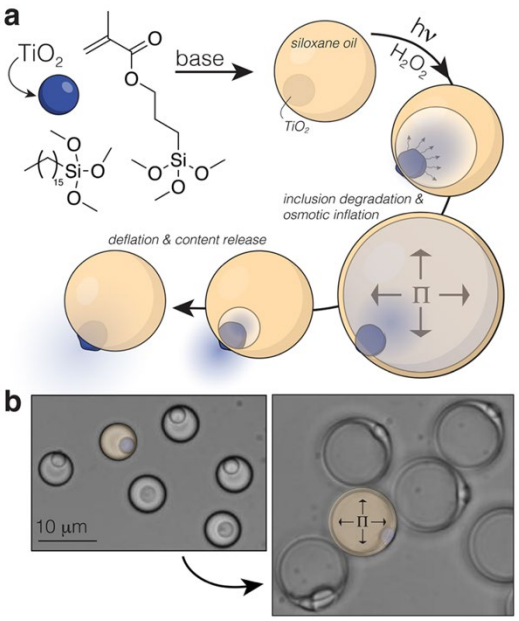

Fig. 4: (**a**) TiO_2 colloids are used as seeds for heterogeneous nucleation and growth of siloxane oil droplets. The TiO2 inclusion begins to degrade upon introduction of fuel (H_2O_2) and blue light, which in turn creates an osmotic pressure that initiates the inflation process until a failure occurs and the inner contents are released to the local surroundings; (**b**) optical images of droplets before and during inflation.

Our first generation of responsive solid-in-oil composite droplets was created by encapsulating specially treated TiO2 colloids within TPM oil droplets (see Fig.4(a)). Under blue/UV illumination, the TiO2 colloids degrade, producing degradation products that are trapped in the oil phase. This generates an osmotic pressure that draws water into the droplets, causing them to inflate (see Fig.4(b)). We demonstrated that both the rate of inflation and the final volume of the droplets can be precisely controlled by adjusting the light intensity and the concentration of the fuel.

Future plans

Having quantitatively investigated two non-equilibrium and non-reciprocal forces, phoresis and osmosis, we want to play one against the other in making both static and dynamic structures and devices. We have also begun the study of how static and dynamic light patterns can organize and activate colloidal structures and flows. Another objective will be the determination of the local entropy production during stimulus-guided navigation and coordination processes in active matter. Finally, we will unveil innovative frameworks to synthesize active particles that exhibit communication and morphogenesis.

Publications 2022-2024

1. S. Ro, B. Guo, A. Shih, T. V. Phan, R. H. Austin, D. Levine, P. M. Chaikin, S. Martiniani, *Model-free measurement of local entropy production and extractable work in active matter,*Phys. Rev. Lett. **129**, 220601 (2022).
2. I. Essafri, B. Ghosh, C. Desgranges, J. Delhommelle, *Designing, synthesizing, and modeling active fluids,* Phys. Fluids **34**, 071301 (2022).
3. A. Ghosh, J. Radhakrishnan, P. M. Chaikin, D. Levine, G. Shankar, *Coupled dynamical phase transitions in driven disk packings*, Phys. Rev. Lett. **129**, 188002 (2022).
4. M. Y. B. Zion, A. Modin, P. M. Chaikin, *Hydrodynamic spin-orbit coupling in asynchronous optically driven micro-rotors*, Nat. Commun. **14**, 4114 (2023).
5. C. Desgranges, M. Ferrari, P. M. Chaikin, S. Sacanna, M. E. Tuckerman, J. Delhommelle, *Microswimmers under the spotlight: interplay between agents with different levels of activity*, Soft Matter **19**, 7334 (2023).
6. N. Naleem, C. R. Abreu, K. Warmuz, M. Tong, S. Kirmizialtin, M. E. Tuckerman, *An exploration of machine learning models for the determination of reaction coordinates associated with conformational transitions*, J. Chem. Phys. **159**, 034102 (2023).
7. F. Zhou, H. Ni, G. Zhu, L. Bershadsky, R. Sha, N. C. Seeman, P. M. Chaikin, *Toward three-dimensional DNA industrial nanorobots*, Science Robotics **8**, eadf1274 (2023).
8. S. Wilken, A. Z. Guo, D. Levine, P. M. Chaikin, *Dynamical approach to the jamming problem*, Phys. Rev. Lett. **131**, 238202 (2023).
9. A. W. Hauser, Q. Zhou, P. M. Chaikin, S. Sacanna, *Light-triggered inflation of microdroplets*. Chem. Mater. **36**, 3970 (2024).
10. A. V. Hardikar, A. W. Hauser, T. M. Hopkins, S. Sacanna, P. M. Chaikin, *Osmotic and phoretic competition explain chemotaxic assembly and sorting*, PNAS, out for review (2024)

Porin-Inspired Ionomers with sub-nm Gated Ion Channels for High Ion Conductivity and Selectivity

Shudipto Konika **Dishari**, University of Nebraska-Lincoln

Keywords: ion conduction, ionomers, porin, biological ion channel, gating

Program Scope

The physiological functions of natural living systems heavily rely on biological ion channels, and their dysfunction can lead to diseases. These channels result from the intricate self-assembly of various proteins, activated by different stimuli, and are responsible for the selective and controlled passage of water, ions, or small molecules. Similarly, ionomers used in energy conversion and storage devices play a crucial role in ion transport across membrane separators and catalyst binder layers. This DOE Career project adopts a nature-mimicking approach to establish fundamental design principles for ionomers inspired by biological ion channels. The goal here is to understand the proton conduction mechanism by strategically designing macrocyclic calix[4]arene-containing ionomers, which are closely relevant to proton exchange membrane fuel cells (PEMFCs). The project leverages the sub-nm sized macrocyclic pores which can facilitate very fast ion transport (beneficial to address the sluggish ORR kinetics of PEMFC electrodes), and act like ionic diodes under the influence of electrochemical fields, beneficial for selective transport/separation.

Recent Progress

In the early years of this project, we worked extensively to demonstrate the feasibility of designing representative proton-conducting ionomers using macrocyclic calix[4]arenes as either backbone repeat units or pendants.[1,2,3] Our findings showed that calix-containing polymeric ionomers with sulfonic acid functional groups exhibit significantly higher proton conductivity compared to Nafion, the current state-of-the-art ionomer. In addition, we showed that the non-macrocyclic variants of these ionomers displayed several orders of magnitude lower proton conductivity than macrocyclic counterparts.[1] We also observed faster-than-bulk water transport within calix-containing ionomer films.[2]

Now that we have demonstrated the proof-of-concept, we are delving deep into calix[4]arene derivatives to identify the chemical and structural features that are more responsible for creating efficient proton transporting systems. Specifically, we are examining the side chain structure and the charged states of the upper and lower rims of monomeric calix[4]arene. In the lab, we synthesized several variations of monomeric derivatives of calix[4]arene. We recently studied three variations (Figure 1a): one has -SO_3H at the upper rim and -OH at the lower rim (**SC**). The 2nd one has -SO_3H at both upper and lower rims (**DISC**). The 3rd one has -SO_3H at the upper rim and quaternary ammonium chloride (-$N(CH_3)_3^+$) at the lower rim (**QSC**). Despite being monomeric, all these variants significantly improved the proton conductivity of thin films (Figure

1b). We mixed Nafion and any of these monomeric calix variants in solution and spun sub-µm thick composite films. At a low calix content (Nafion-to calix ratio of 1: 0.5), a ~150 nm thick annealed Nafion-SC (1: 0.5) film showed a proton conductivity of 16 mS/cm, which was 5 times higher than pure Nafion film (3.69 mS/cm) at ~82-85% RH (Figure 1b). At low %RH (20-45%RH), Nafion-calix composite films exhibited proton conductivity an order of magnitude higher than Nafion films, for example, at 25% RH, Nafion: 8.6×10^{-5} mS/cm *vs.* Nafion-SC: 8.1×10^{-4} mS/cm in 150 nm thick films (Figure 1b). Similar improvements in proton conductivity over Nafion were achieved using Nafion-DISC and Nafion-QSC films at both low and high %RHs (Figure 1b). While this requires further understanding, the consistent improvement in proton conductivity, regardless of the charged state of calix, suggested a major role of the macrocyclic cavities in improving thin-film proton conductivity.

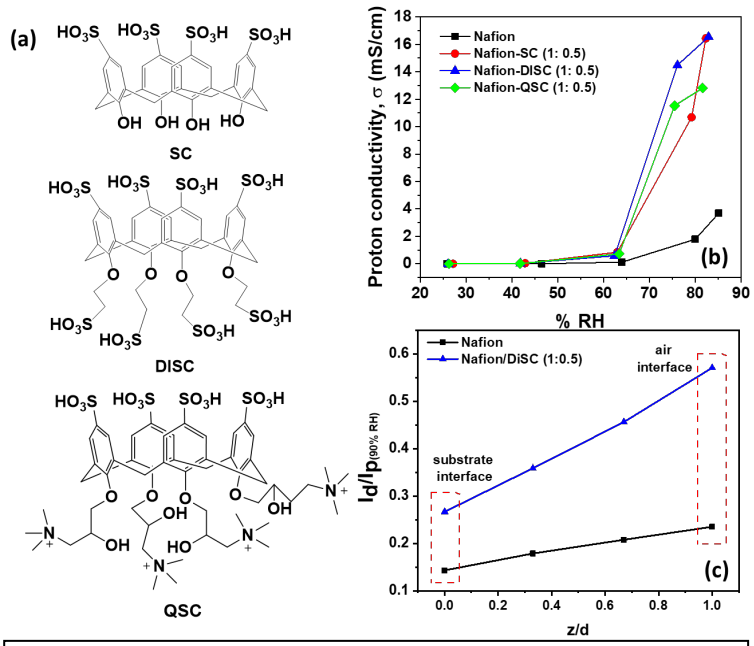

Figure 1. (a) Chemical structure of monomeric calix[4]arene derivatives: SC, DISC, QSC. (b) Proton conductivities of ~150 nm thick Nafion and Nafion-calix composite films where calix monomers were randomly distributed. (c) Proton conduction (I_d/I_p) profile of ~150 nm thick Nafion and Nafion-DISC composite films at 90% RH. An increase in I_d/I_p a certain location indicates an increase in proton transport in that location or depth within the ionomer film. The term z/d indicates the thickness normalized distance from substrate interface, where z/d of 0 and 1 represents substrate and air interface, respectively. All the films were annealed.

In an earlier work, we located self-assembled features made of calix-based oligomeric ionomers using confocal laser scanning microscopy (CLSM) and showed that in a composite film, ion conduction is more favorable at places where macrocycles are located. Unlike oligomers, monomeric calix-based ionomers did not form well-defined features visible under atomic force microscopy (AFM). However, scanning across photoacid (HPTS) stained Nafion and Nafion-DISC films, we observed an increase in the deprotonation ratio of HPTS (I_d/I_p) at all depths within the Nafion-DISC film compared to the Nafion film. This proved that DISC improved the proton conduction throughout the film, including at the substrate interface (Figure 1b). This is a notable achievement since the state-of-the-art ionomer Nafion is known for negligible proton transport next to substrate interface, leading to ion transport limitation and slower kinetics of ORR. The birefringence changed from negative for pure Nafion film to positive for Nafion-calix composite films, suggesting that the presence of calix significantly altered the molecular organization and orientation of Nafion in the films, thereby minimizing ion transport resistance next to substrate and across the ionomer films.

So far, we have studied the performance of calix monomers randomly distributed within Nafion-calix composite films. Next, we leveraged self-assembly to localize calix ionomers (DISC here) adjacent to the substrate before depositing the Nafion layer on top. As shown in the Nyquist plots (Figure 2), the DISC-localized Nafion film exhibited a semicircle diameter similar to that of the Nafion-DISC random films, while both samples displayed smaller semicircle diameters than the pure Nafion film. This indicated lower ion transport resistance in both Nafion-DISC and DISC-localized Nafion films compared to the pure Nafion film. These results suggest that a thin layer of calix next to the substrate may achieve the same ion transport benefits as randomly distributed calix, effectively addressing ion transport limitations. This is logical, as the primary contributor to thin-film ion transport limitations is the substrate interface, where Nafion chains orient parallel to the substrate and experience pinning with their side chains.[4,5] By selectively placing the calix molecules next to the substrate, we were able to modify this pinning and improve the proton conductivity of the entire Nafion film.

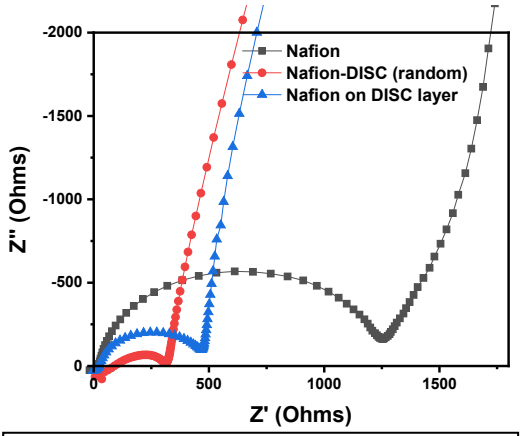

Figure 2. Nyquist plots of pure Nafion film (black line), Nafion-DISC composite film where DISC was randomly distributed within Nafion matrix (red line) and DISC-localized Nafion film (blue line). The diameter of the semicircles represents the resistance of the films to ion transport.

Finally, we investigated how these calix monomers influenced directionality in ion transport within Nafion-calix mixed membranes by performing I-V measurements (Figure 3). As expected, Nafion showed no difference in ionic current when measured under forward and reverse biasing. However, some varieties of calix-based monomeric ionomers acted like voltage-biased ionic diodes, though not all. The results suggested that the magnitude of ionic current depends on the orientation of the charged rims of the calix units relative to the direction of electron flow. Flipping a single calix unit with respect to the electron flow direction can result in different forward and reverse bias currents and varying rectification ratios. In a random setup, like Nafion-calix, where there is no control over the orientation of calix units with respect to the applied voltage, the experimentally observed rectification ratio could be a cumulative effect of how all the calix units are oriented and how they collectively influence the current.

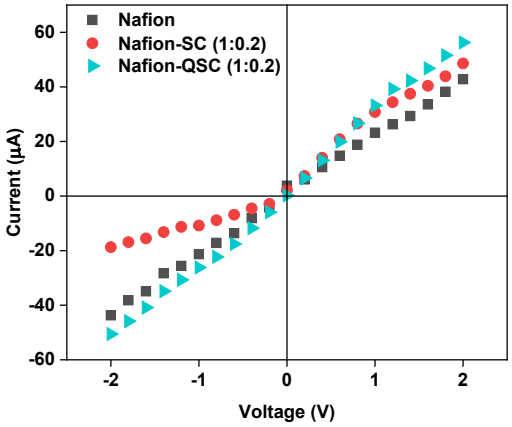

Figure 3. I-V curves of pure Nafion, Nafion-SC and Nafion-QSC composite membranes. The I-V data were recorded using 0.1 M KCl in DI water.

Future Plans

Based on the work done so far, the asymmetry in charge distribution and mass distribution of calix-based ionomers with respect to the substrate yielded thought-provoking results. This necessitates further studies to understand the effects of localization versus randomization of calix with varied chemical structures (monomer *vs* .oligomer vs polymer, type of charge, charge asymmetry, charge on backbone *vs*. side chain, calix on backbone *vs.* as pendant). With additional funding from DOE-BES, these investigations could significantly enhance our understanding of the proton conduction mechanism within calix-based ionomers, a promising class of ionomers for energy conversion and storage devices, in the coming years.

References

1. Chatterjee, S.; Zamani, E.; Farzin, S.; Evazzade, I.; Obewhere, O. A.; Johnson, T.; Alexandrov, V.; Dishari, S. K. Molecular-Level Control Over Ionic Conduction and Ionic Current Direction by Designing Macrocycle-Based Ionomers. *JACS Au* **2022**, *2*, 1144–1159. https://doi.org/10.1021/jacsau.2c00143.
2. Chatterjee, S.; Obewhere, O. A.; Zamani, E.; Keloth, R.; Farzin, S.; Morton, M. D.; Sarella, A.; Dishari, S. K. Advancing Ionomer Design to Boost Interfacial and Thin-Film Proton Conductivity via Styrene-Calix[4]Arene-Based Ionomers. *Cell Rep. Phys. Sci.* **2023**, *4*, 1–39. https://doi.org/10.1016/j.xcrp.2023.101282.
3. Dishari, S. K. Ionomers with Macrocyclic Moieties for Ion Conductivity and Permselectivity, 2021.
4. Obewhere, O. A.; Dishari, S. K. Engineering Ionomer-Substrate Interface to Improve Thin-Film Proton Conductivity in Proton Exchange Membrane Fuel Cells. *ACS Appl. Polym. Mater.* **2024**, *6*, 4535–4546. https://doi.org/10.1021/acsapm.3c03218.
5. Dishari, S. K.; Hickner, M. A. Antiplasticization and Water Uptake of Nafion® Thin Films. *ACS Macro Lett.* **2012**, *1*, 291–295.

Publications Supported by BES (2021-2024)

1. Chatterjee, S.; Obewhere, O. A.; Zamani, E.; Keloth, R.; Farzin, S.; Morton, M. D.; Sarella, A.; Dishari, S. K. *Advancing Ionomer Design to Boost Interfacial and Thin-Film Proton Conductivity via a Styrene-Calix[4]arene-based Ionomers*. Cell Rep. Phys. Sci. **4**, 1-20 (2023).
2. Chatterjee, S.; Zamani, E.; Farzin, S.; Evazzade, I.; Obewhere, O. A.; Johnson, T. J.; Alexandrov, V.; Dishari, S. K. *Molecular-Level Control over Ionic Conduction and Ionic Current Direction by Designing Macrocycle-based Ionomers*. JACS Au **2**, 1144-1159 (2022).
3. Dishari, S. K. Ionomers with Macrocyclic Moieties for Ion conductivity and Permselectivity (2021) (Patent, PCT/US21/70432).
4. Obewhere, O.A.; Acurio Cerda, K.; Sutradhar, S.; Dike, M.; Keloth, R.; Dishari, S. K. *"Unravel-Engineer-Design"- A 3-pronged Approach for Ionomers at Interfaces to Address Challenges of Proton Exchange Membrane Fuel Cells*, submitted to Chem. Commun. as an invited Feature Article (2024).

5. Obewhere, O.A.; Dishari, S. K. *Engineering Ionomer-Substrate Interface to Improve Thin-Film Proton Conductivity in Proton Exchange Membrane Fuel Cells*, ACS Appl. Polym. Mater. **6**, 4535-4546 (2024).
6. Farzin, S.; Acurio Cerda, K.; Obewhere, O. A.; Dishari, S. K. *Lignin-based Materials for Energy Conversion and Storage Devices* in Sustainability Engineering Challenges, Technologies, and Applications, Editor: Tan, E. C. 1-60 (2023)
7. Acurio Cerda, K.; Kathol, M.; Purohit, G.; Zamani, E.; Morton, M. D.; Khalimonchuk, O.; Saha, R.; Dishari, S. K. *Cationic Lignin as an Efficient and Biorenewable Antimicrobial Material.* ACS Sustainable Chem. Eng. **11**, 10364-10379 (2023).
8. Obewhere, O.A.; Acurio Cerda, K.; Keloth, R.; Dishari, S. K. *"Implementing a Virtual STEM Camp for Middle- and High Schoolers in a Post-COVID Climate Leveraging Prio Experience.* ASEE PEER (2024).

Active interfaces driven by microtubule-based active matter

Dogic and Marchetti – University of California at Santa Barbara

Keywords: active matter, interfaces, liquid-liquid phase separation, wetting transitions.

Research Scope: Controlling interfacial structure and dynamics is key to creating diverse functional soft materials, ranging from lipid vesicles and lamellar phases to phase-separated systems and emulsions. Traditionally, interfacial control is accomplished through surface-modifying agents, such as surfactants and block copolymers. We study an entirely different non-equilibrium mechanism for controlling and shaping soft interfaces. By merging a phase-separating mixture of a microtubule-based active isotropic fluid and a passive fluid, we are exploring how activity provides a unique new handle for interfacial control. We are pursuing several aims. First, we study a model system of 1D active interfaces and associated liquid-liquid phase separation in quasi-2D geometries. Second, we are generalizing these studies to 2D interfaces that separate 3D bulk phases. Third, we study the behavior of active droplets and their interaction with a planar hard wall, with a particular focus on using active stresses to control droplet shape and interfacial wetting properties. All the aims merge experimental work with numerical simulations and theoretical modeling. We combine the unique features of microtubule-based active fluids with state-of-the-art microscopy techniques to visualize conformations of centimeter-sized interfaces, as well as the instantaneous configuration of the underlying active fluid with single-filament resolution. Combining such multiscale experimental data with theoretical modeling has the potential to decisively advance our understanding of how to shape and control soft interfaces through activity.

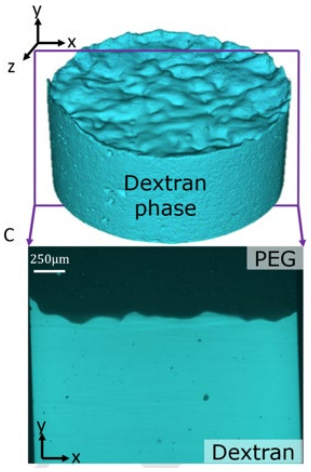

Fig. 1. Active interface separating microtubule-based active fluid and a passive phase.

Recent Progress: In an important advance we used a combination of experiments, numerical simulations, and analytical theory to characterize the structure and dynamics of active interfaces and associated active-liquid-liquid phase separation in quasi-2D confined samples[1]. This work identified four universal features of such novel non-equilibrium materials, which include giant interfacial fluctuations, non-inertial traveling waves, arrested phase coarsening, and formation of finite-sized active emulsions and activity-controlled wetting transitions.

In the initial study, the active liquid-liquid phases separated samples were strongly influenced by the frictional interactions between the interface and the confining walls. To eliminate such interactions, we developed a model system to visualize a macroscopic 3D active interface. Combining the unique feature of our microtubule-based active fluids with light-sheet imaging we

visualized the structure and fluctuations of millimeter-sized interfaces (**Fig. 1**). Experiments on bulk interfaces revealed several unexpected phenomena[2]. First, in the low-activity regime where the active/passive interface remains continuous, we observed that the active interface undergoes large deformations with distinct asymmetry. The interface had deep and narrow valleys of the passive phase protruding into the active phase and shallow and round peaks of the active phase protruding into the passive phase. Second, in the high-activity regime, the magnitude of the deformations increased and the interface folded on itself to envelop passive droplets (**Fig. 2**). The interface disintegration was also asymmetric; we observed frequent invagination of passive droplets by the active phase but never observed the reverse process of active droplets separating from the bulk active fluid and being ejected into the passive phase. On long time scales these processes created an active foam wherein an active fluid phase was perforated with droplets of the passive phase (**Fig. 3**). Both the asymmetric deformations and foam formation were not observed in the study on quasi-2D active interfaces illustrating the essential role of long-ranged hydrodynamic interactions in governing the fluctuations of bulk interfaces.

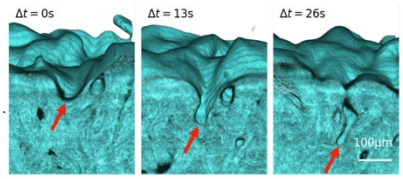

Fig. 2. Active interface separating microtubule-based active fluid and a passive phase.

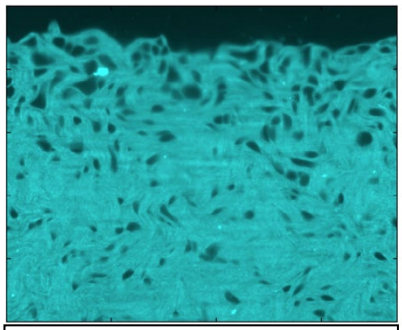

Fig. 3. Active foam phase formed by the disintegration of active interface.

To gain fundamental insight into these observations we developed a continuum hydrodynamics model of active interface and active LLPS in both 2D and 3D (**Fig. 4**). Numerical solutions of the hydrodynamic equations reproduced the asymmetric fluctuations of the interface and the formation of the active phase. Importantly, these efforts revealed a novel microscopic mechanism that underlies the asymmetry of active interfacial fluctuations and disintegrations. Our work showed that the soft interface breaks the spatial symmetry of the fundamental bend instability of extensile active nematics, which in turn creates interface-adjacent vortical flows that suppress the growth of upward protruding hills while enhancing and sharpening downward valley-like deformations (**Fig. 5**). These results have implications for any extensile active fluid that is confined by soft and deformable interfaces and membranes. For example, the cytoskeleton is a quintessential example of an out-of-equilibrium stress-generating network. In a cell, the cytoskeleton interacts with diverse membrane-less organelles and lipid bilayer membranes, driving their non-equilibrium fluctuations and associated processes such as endo- and

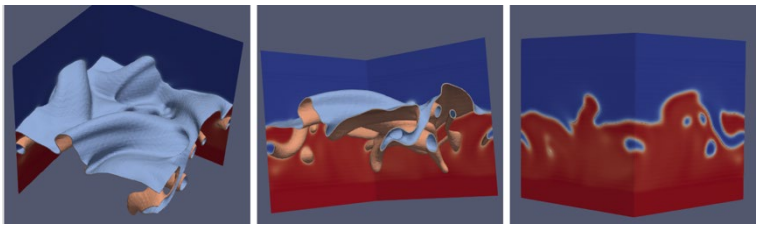

Fig. 4. Numerical simulations describe the fluctuations of a 2D soft interface separating bulk active and passive phase.

exocytosis. These comprehensive results describing experiment and theory on unconfined interfaces have been submitted for publication[2].

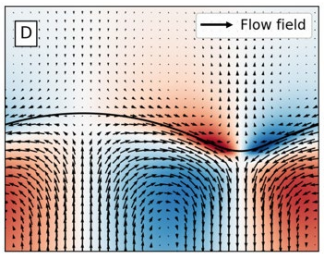

Fig. 5. The interface experiences asymmetric vortical flows, resulting in curvature.

The above-described experiments inspired subsequent theoretical modeling. Activity can drive surface waves at liquid crystal interfaces. The relaxational dynamics of a fluid interface coupled to an activity-driven liquid crystal sets up a non-reciprocal interaction between the interface fluctuations and the liquid crystalline dynamics leading to wave propagation. We developed a linearized theory to understand the spectrum of these interfacial waves[3]. We then used simulations of a two-phase model to measure these interfacial waves and verify the predictions of the linear theory. Similar wave propagation in experiments could provide a reliable and accurate handle to measure the bulk properties of an active fluid, and quantitatively connect them to continuum phenomenological models.

We have shown that in a phase-separated mixture of active and passive fluids, active flows can generically create mixing and suppress phase separation, by effectively decreasing the critical temperature[4]. In addition to understanding the mixing transition and its asymmetry, we found that at intermediate values of activity, active fluids generated by isotropic liquid crystal can lead to stretching of the active domains and result in a robustly percolated active phase. We have shown that it is possible to understand this percolated phase as a consequence of the activity-induced flow alignment of the liquid crystal orientation with fluid interfaces. This in turn leads to extensional flows creating a dynamical steady state with a percolating active phase perforated by large droplets of the passive phase (**Fig. 6**).

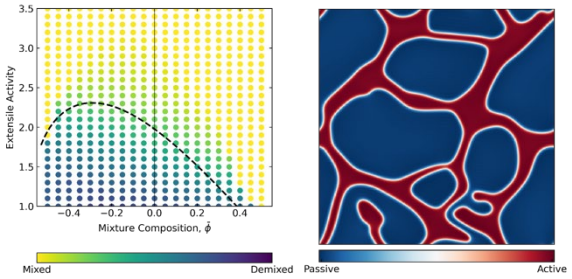

Fig. 6. (left) Active interface separating microtubule-based active fluid and a passive (right) activity leads to a dynamical steady state with arrested phase separation of a percolating active fluid.

In a complementary direction, we are using active interfaces as a novel probe to measure the defining properties of microtubule-based active fluids. In particular, active stress plays a central role in explaining how active matter transforms chemical energy from ATP hydrolysis into spontaneous mechanical motion in the form of turbulent-like flows. Nevertheless, it has been a significant challenge to experimentally measure the active stress. So far, the main approach has been to indirectly estimate active stress by quantifying the structure of the flows. We measured the velocity and vorticity fields of the flows and used their magnitude and structure to derive the strength of the active stresses. In parallel, we used the same sample and the unique properties of the active interface and the active wetting transition to independently measure the active stresses. The interface-based methods were consistent with each other but were quite distinct from the estimates based on characterizing the bulk flows. In particular, we found that interface-based

methods suggest that active stress continuously increases over the sample lifetime, while estimates based on bulk flows suggest that actin stress remains time-invariant. The cause of this discrepancy suggests a fundamental inconsistency in a widely studied hydrodynamic theory that is used to model extensile active fluids.

Future Plans: The above-described advances have relied on a synergistic combination of experiments, theory, and numerical modeling. They have significantly advanced our understanding of active interfaces and active liquid-liquid phase separation. We have several major goals for the near future. We aim to understand the discrepancy between active stresses estimated from the interface and bulk flows. One possibility is that the structure of the microtubule-based active fluid adjacent to the interface changes over the sample lifetime. So far, we have only been able to measure the flow velocity field in active phase-separated samples. We aim to develop a new high-resolution imaging method that will allow us to directly and simultaneously visualize the interface, the autonomous flow fields, and the local alignment (nematic order) of the microtubule filaments.

Over the next report period, we will also direct our efforts toward quantifying active wetting in 3D geometries, which is another intriguing yet poorly explained observation (**Fig. 7**). Experimentally, we observed that the contact between a hard wall and an active interface can be controlled by the activity of the active fluids. This leads to remarkable phenomena such as the interface climbing along a wall and working against gravity. Furthermore, we will also study dynamics in which the interface climbs along the wall and slowly falls back down under the influence of gravity. This is likely due to the coupling of the wall-induced wetting with traveling waves. These experimental observations demonstrate the need to develop a robust theoretical model of active wetting, an effort that is currently underway in our group

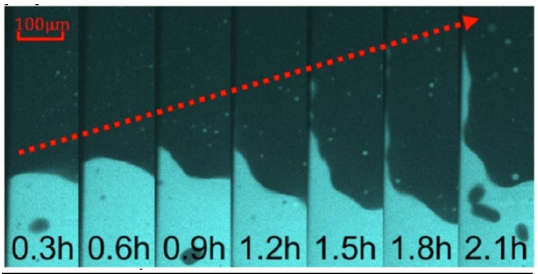

Fig. 7. (left) A sequence of images illustrates how activity changes the wetting angle that the active interface makes with a confining boundary.

Publications from DOE work:

1. R. Adkins, I. Kolvin, Z. You, S. Witthaus, M. C. Marchetti, Z. Dogic, "*Dynamics of active liquid interfaces*," Science **377,** 768 (2022).
2. L. Zhao, P. Gulati, F. Caballero, I. Kolvin, R. Adkins, M. C. Marchetti, and Z. Dogic "*Asymmetric fluctuations and self-folding of active interfaces*," https://arxiv.org/pdf/2407.04679.
3. P. Gulati, F. Caballero, I. Kolvin, Z. You and M. C. Marchetti, "*Nonreciprocal interactions drive capillary waves in active liquid crystals*," https://arxiv.org/pdf/2407.04196.
4. A. M. Tayar, F. Caballero, T. Anderberg, O. A. Saleh, M. C. Marchetti, Z. Dogic, "*Controlling liquid-liquid phase behavior with an active fluid"*, Nature Materials, **22**, 1401 (2023).
5. S. Ray, J. Zhang, and Z. Dogic, "*Rectified Rotational Dynamics of Mobile Inclusions in Two-Dimensional Active Nematics*," Physical Review Letters **130**, 238301 (2023).
6. M. Serra, L. Lemma, L. Giomi, Z. Dogic, L. Mahadevan, "*Defect-mediated dynamics of coherent structures in active nematics*," Nature Physics (2023)

Polymerization-driven active matter

Guillaume **Duclos**, Brandeis University, Waltham MA

Keywords: Active matter, actin, non-equilibrium turnover, flocking, reaction-diffusion

Research Scope

The rational design of biomimetic active materials from enzymes, nucleic acids, or proteins, has remained a challenge because of the multiscale nature of active matter: energy, injected at the particle scale, spontaneously propagates to larger length scales to drive collective behaviors. This inverse energy cascade uniquely endows active matter with remarkable self-organization capabilities. Here, we present how the non-equilibrium turnover of actin filaments can be leveraged as a tractable mechanism to investigate multiscale pattern formation and create a novel class of adaptive biomimetic materials. In these molecular materials, reaction-diffusion will be coupled to activity to mimic two fundamental features of morphogenesis: symmetry breaking and force generation.

Biomolecular active matter composed of purified proteins provides a promising route to bridge the length scale gap inherent to all active materials. These materials are simple, tunable, and more robust than living cells, making them prime candidates for engineering applications in soft robotics. Furthermore, the extensivity of the biomolecular landscape provides a myriad of proteins to power reconstituted materials in unique ways. To date, most of the experimental research in this field has focused on materials driven by molecular motors. However, these materials only mimic a fraction of what is observed in living matter because cells often use as well a variety of other processes to self-organize and move. Treadmilling polymers provide a unique and underexplored platform to investigate the multiscale self-assembly of active matter, unveiling uncharted territory for designing controllable adaptive materials.

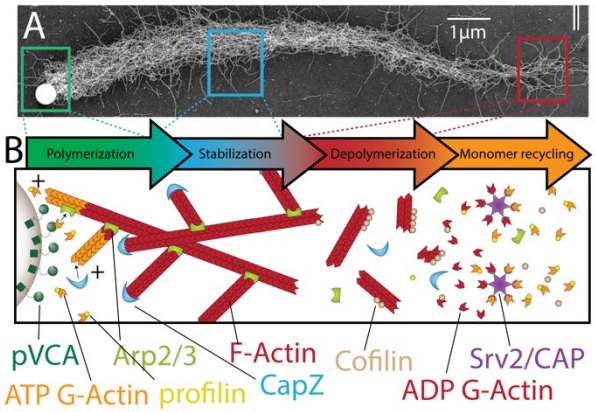

Fig. 1: Description of the model system. A) EM picture of a 0.5µm bead, Cameron et al.[1] B) Schematic of the four stages in the formation and turnover of an actin tail. Actin filaments nucleate from ATP-bound G-actin (left). Then ATP is hydrolyzed, F-actin is caped, and subsequently severed and dissembled. The released ADP-actin monomers undergo nucleotide exchange to replenish the pool of polymerization-competent ATP-G-actin (right).

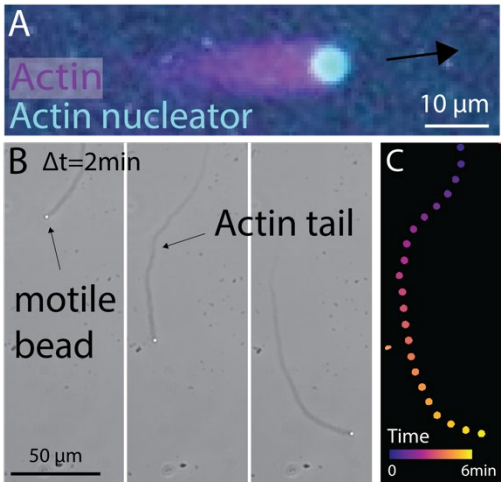

Our model system is inspired by how microbial pathogens such as listeria and shigella swim using actin from an infected host cell[2, 3]. In brief, we coat micron-sized polystyrene beads with pVCA, a protein that activates the polymerization of a branched actin network[4]. This growing actin shell spontaneously breaks symmetry, and the resulting asymmetric polymerization propels the bead forward[1] (**Fig. 2A**).

Fig. 2: Spontaneous motility *in vitro*. A) motile bead uniformly coated with pVCA (actin and pVCA are labeled). B) Time series of phase-contrast images of a 1.5 μm-diameter motile bead. C) Color-coded trajectory of the bead in figure B.

This model system provides a unique platform for uncovering new physics with actin-based materials that are fundamentally different from motor-based active matter. Preliminary experiments demonstrate rich emergent dynamics, including 1. spontaneous motility (**Fig. 2**); 2. synchronization of beating oscillations (**Fig. 3A)**; 3. flocking and giant density fluctuations (**Fig. 3C**); 4. active crystallization (**Fig. 3D)**. We show that these emergent behaviors are direct consequences of a generic coupling between reaction-diffusion and activity, which has been under-explored in biomimetic active matter.

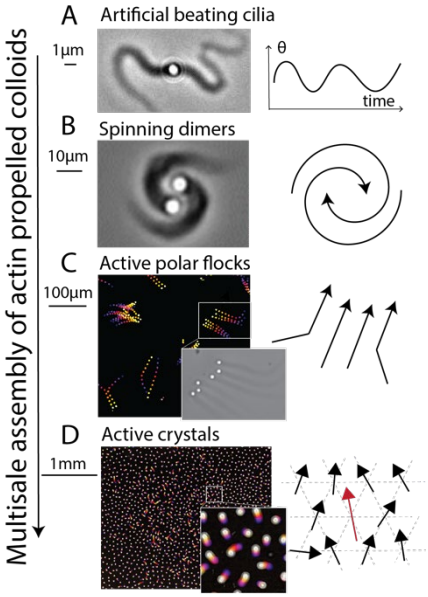

Fig. 3: Emergent behaviors at larger and larger length scales. Beads propelled by actin turnover exhibit unique emergent behaviors at different length scales when density is increased.

Recent Progress

We performed experiments with a dense suspension of beads propelled by polymerizing actin tails in quasi-2D confinement. We systematically varied bead density, bead diameter (from 1.5 μm to 10 μm), and confinement along the Z-axis. We identified flocking dynamics that were reminiscent of the patterns observed in nature in flocking birds, bacteria, and sperm cells, or in simulations of self-propelled particles with aligning interactions. Here, groups of beads moving in the same direction constantly merge and break apart as groups collide with each other, resulting in finite-size flocks instead of a global polar phase that spans the entire system (**Fig. 3C**). However, only larger beads flock (D>2.5μm). Smaller beads (D=1.5μm) are motile, interact sterically, and re-orient after colliding with each other, but do not flock. We hypothesized that a reaction/diffusion

mechanism is at the origin of this flocking transition: actin-propelled beads can sense the presence of their neighbors because they compete for actin monomers. Further, as there is a gap in length scale between the size of a monomer (4-7nm) and the size of the beads (1-10 μm), a gradient of actin monomer will result in non-uniform polymerization rate at the bead surface, which would lead to torque generation. Hence, the actin depletion between two motile beads could drive attractive interactions and flocking. Smaller beads would not be able to flock because they do consume enough actin to deplete the pool of monomeric actin.

We performed various experiments to test that hypothesis:

i) *Decreasing the actin polymerization rate inhibits flocking.* We decreased the pVCA surface coverage of the beads to decrease the actin polymerization rate. Densely covered beads flocked, while sparsely covered beads did not.

ii) *Decreasing actin diffusion rate promotes flocking.* We showed that increasing the viscosity of the surrounding fluid can promote flocking.

iii) *Beads accumulate along impermeable boundaries but not along permeable boundaries connected to an actin reservoir.* We performed experiments where motile beads were moving next to a boundary. We measured a significant enrichment of beads moving near the impermeable boundary compared to the permeable boundary connected to a reservoir. This experiment suggests that isolated actin-propelled beads can create and respond to asymmetric gradients of monomeric actin close to a wall.

Overall, the proposed research is novel in the following ways: 1) it leverages non-equilibrium turnover instead of molecular motors, which have been a standard in the field of active molecular materials over the past two decades; 2) emergent behaviors are governed by a coupling between reaction/diffusion and stress generation which, despite its fundamental relevance to morphogenesis, has been underexplored as a mechanism to power active materials; 3) the scale-separation between the characteristic sizes of actin monomers (nm), of a motile colloid (μm), and of the collective behaviors (mm) allow us to track how collective behaviors propagates through multiple length scales.

Future Plans

1. Future work will investigate how actin-propelled beads move in a linear gradient of protein (**Fig. 4**). One crucial prediction of our current hypothesis is that actin beads will perform anti-chemotaxis: they will move away from a source of actin.

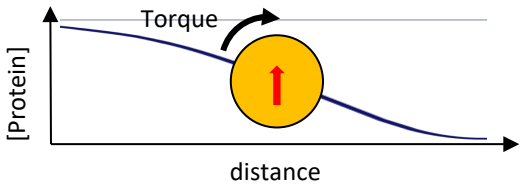

Fig 4: emergent antichemotaxis? (Future work) We predict that motile beads should turn towards the sink in a linear actin gradient. We will test that prediction using a microfluidic gradient generator

2. Future work will investigate the mechanisms that control the shape and size of the flocks (**Fig. 5**).

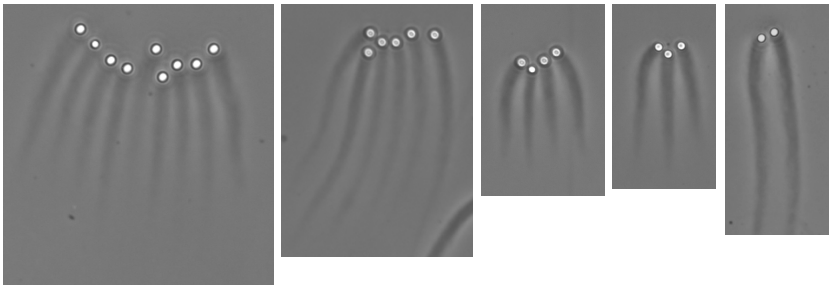

Fig. 5: Origin of flocks shape and size (Future work) Flocks have a stereotypic "U" shape

3. *What is the stability of the spinning dimers?* It is unclear what are the mechanisms that lead to the formation of a spinning dimers (**Fig. 6**) instead of a flock of beads moving in the same direction. Moreover, we do not know why only dimers emerge and not trimers or larger groups.

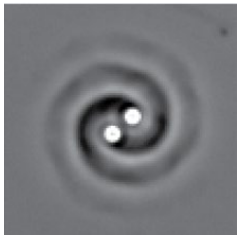

Fig. 6: Origin of stability of spinning dimmers (Future work)

References

1. Raz-Ben Aroush, D., Ofer, N., Abu-Shah, E., Allard, J., Krichevsky, O., Mogilner, A. and Keren, K., "*Actin Turnover in Lamellipodial Fragments*," Curr Biol **27**, 2963-2973 e2914 (2017).
2. Cameron, L. A., Footer, M. J., Oudenaarden, A. v. and Theriot, J. A., "*Motility of ActA protein-coated microspheres driven by actin polymerization,*" Proc. Natl. Acad. Sci. USA **96**, 4908-4913 (1999).
3. Marchand, J.-B., Moreau, P., Paoletti, A., Cossart, P., Carlier, M.-F. and Pantaloni, D., "*Actin-based Movement of Listeria Monocytogenes: Actin Assembly Results from the Local Maintenance of Uncapped Filament Barbed Ends at the Bacterium Surface,*" The Journal of Cell Biology **130**, 331-343 (1995).
4. Goldberg, M. B., "*Actin-based motility of intracellular microbial pathogens*," Microbiol Mol Biol Rev **65**, 595-626, table of contents (2001).
5. Loisel, T. P., Boujemaa, R., Pantaloni, D. and Carlier, M.-F., "*Reconstitution of actin-based motility of Listeria and Shigella using pure proteins,*" Nature **401**, 613-616 (1999).

Bio-inspired Materials Designs: Reactive, Functional Droplets and Smart Interfaces

Todd **Emrick**, Polymer Science & Engineering Department, University of Massachusetts, 120 Governors Drive, Amherst, MA 01003 tsemrick@mail.pse.umass.edu

Keywords: Functional polymers, fluid interfaces, dynamic surfaces, polymer zwitterions, smart droplets

Research Scope. Inspired by the sophistication with which biology assembles and utilizes soft materials and fluidic systems, the scope of this project encompasses the creation of new types of bio-inspired materials by efficiently connecting Nature's functionality with state-of-the-art synthetic methodology. With focus on the synthesis of functional polymers and their localization at fluid interfaces, our objective is to create polymeric and mesoscale materials that yield designer structures, such as soft, extended filaments and functional fluid droplets, that together exhibit morphologies and responsive features inspired by biological materials and processes. By strategically combining organic/polymer synthesis with the fabrication of mesoscale structures, materials opportunities arise from biological inspiration, such as the healing features of the immune system in which recognition, transport, and interfacial interactions are critically important.

Synthetic innovations guided by bio-inspired designs open access to novel, fundamental insights in materials research, including: *1) the synthesis of designer polymer surfactants that depart from conventional polymer structures by integrating functionality directly into zwitterionic sub-units and 2) the preparation of polymer-based multi-length scale and mesoscale structures that localize at fluid interfaces and exhibit stimuli-responsive properties owing to their polymeric constituents.* Insights gained from this scope of research are anticipated to advance emulsion-based systems, including those with triggered response while creating hybrid polymer structures spanning the nano-to-mesoscale. In essence, new synthetic methodology and focus on fluid-fluid and fluid-polymer interfaces is setup to produce innovative outcomes from simpler synthetic materials relative to biological systems, with potential to advance energy-efficient processes that exploit localization of functionality at interfaces. Progress along these lines will advance key areas pertaining to: 1) functional materials synthesis spanning multiple length scales; 2) precise isolation of reactivity at interfaces; and 3) energy-efficient routes to materials healing.

Recent Progress. Described here is recent progress on the synthesis of novel polymer zwitterions that yield dynamic surfaces and interfaces,[1] as well as the fabrication of mesoscale polymer-based materials containing functionality, size, and shape to promote their segregate to fluid interfaces in the form of functional droplets with extended appendages.[2] Our most recent synthetic design hinges on the ability to prepare functional zwitterions as products of successive ring-substitution and opening. For example, insertion of hydrophobic, reactive, and/or fluorophilic organic moieties into polar, hydrophilic zwitterions derived from nature (such as sulfobetaine (SB) and phosphorylcholine (PC)) sets up dynamic structures whereby disparate molecular subunits are forced into close contact and therefore segregate locally rather than macroscopically.

Figure 1 illustrates this concept for fluorinated sulfobetaine methacrylate polymers (FSBs), in which fluorocarbon moieties are attached directly to the zwitterionic components. An efficient two-step modification to the conventional sulfobetaine methacrylate monomer synthesis gave access to a series of polymer zwitterions containing varying extents of fluorocarbon character.

FSB methacrylates proved amenable to homo- and copolymerizations using reversible addition-fragmentation chain transfer (RAFT) conditions, affording polymers with molecular weights ranging from 5 to 20 kDa and with low molecular weight distributions. Thin films of FSB homopolymers on glass proved stable to aqueous environments and exhibited increasing hydrophobicity with fluorocarbon content, as well as remarkably large water contact angle hysteresis values that enable pinning of the water droplets on hydrophobic surfaces, reminiscent of the "petal-effect" found in nature.[3] FSB-containing copolymers in aqueous media demonstrated markedly reduced oil-water interfacial tension values, even with moderate (20-50 mol%) fluorocarbon incorporation.

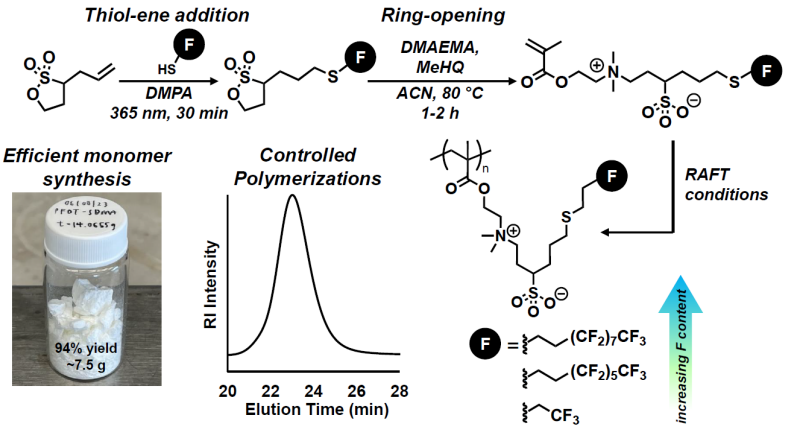

***Figure 1**. Synthesis of fluorinated sulfobetaine (FSB) monomers and polymers, in which fluorocarbon groups of various lengths are embedded directly into the sulfobetaine zwitterion moiety.*

The efficiency of this synthetic approach hinges on: 1) the high-yielding addition of thiol-terminated fluorocarbons to the allyl-substituted sultone, which proceeds quantitatively in minutes and 2) ring-opening of the sultone with DMAEMA that produces FSB monomers in ~90+% isolated yield without the need for chromatographic purification. Distinct from our recent papers on fluorinated choline phosphates (FCPs),[4,5] the thiol-ene approach to FSB polymers is conducted with improved synthetic efficiency while also contributing an additional level of hydrolytic stability owing to the sulfide linkage. The latter may prove important for future applicability in areas such as environmental remediation of perfluoroalkyl substances (PFAS).

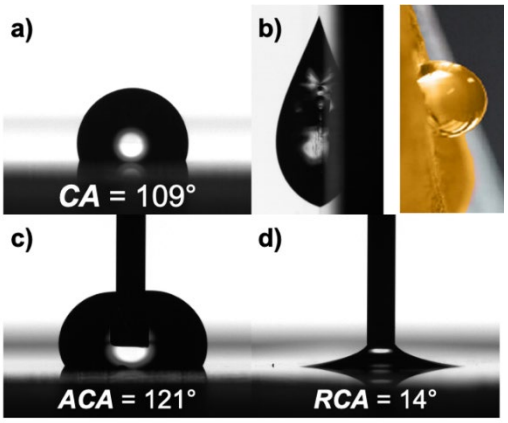

***Figure 2.** Wettability of FSB polymer surface: a) static water CA; b) water pinning at 90-degree tilt on FSB and on petal surface; c & d) large hysteresis between advancing and receding CA.*

The impact of covalently merging low-surface energy, hydrophobic fluorocarbons and hydrophilic zwitterions in FSBs was evident from their unique wetting properties, as illustrated in **Figure 2**. When prepared as thin films on glass, the static contact angle (CA) of water on FSB homopolymers with longer fluorocarbon groups was comparable to that of Teflon; for the lightly fluorinated FSB homopolymer with a trifluoromethyl group, the water CA was comparable to that of PSBMA. Moreover, the unique FSB structure enabled pinning of the droplets, as was evident in 90-degree tilt experiments, in which droplets of appreciable volume (~80 uL) remained static on the tilted surfaces, similar to the topological influence of rose petals and other water pinning hydrophobic surfaces. Dynamic CA measurements revealed moderate (~70°) to high (~115-120°) advancing values coupled with very low (~15°) receding CA values, indicating the dominance of

the fluorocarbon components at the air-polymer interface and dynamic response of the side chains, causing the interface is resist both wetting and dewetting. Notably, FSB homopolymers benefit from solubility profiles limited to fluorinated alcohols; as a result, simple FSB thin film coatings are robust and withstand prolonged exposure to aqueous environments without the need for sophisticated surface-grafting techniques.

Turning to mesoscale materials and interfaces, recent progress builds on our findings whereby integration of functional polymers into photolithographic methods yields ribbon-like mesoscale objects (**Figure 3**) that have an affinity for the fluid-fluid interface of droplets. This conceptual design is inspired by the multi-armed morphologies of dendritic cells, where the interface-adsorbed appendages extend radially outward from the droplet surface. These mesoscale polymer surfactants (MPSs) were prepared from thin polymer films containing reactive and functional moieties, specifically: 1) coumarin for (reversible) photocrosslinking; 2) triphenylsulfonium as a photoacid generator (PAG); and 3) *tert*-butyl ester pendent groups to trigger hydrophobic-to-hydrophilic switching. The photolithographic techniques we employed represent a new, scalable approach to robust, filamentous structures that may take on a variety of configurations, from straight filaments to helical structures. Importantly, these techniques do not require cleanroom access as they are conducted effectively simply under inert ($N_{2(g)}$) atmosphere at room temperature, with mask-alignment performed by hand and UV transformations accomplished in a benchtop UV box (UVP CL-1000M) equipped with 254 or 365 nm bulbs (power output of ~10 mW/cm^2). As detailed in our prior paper, these MPS structures adhere to the fluid interface of emulsion droplets,[2] affording a 'dendritic droplet' design in which the appendages may capture reagents from the solution phase, extend or retract, or even drive droplet motion.

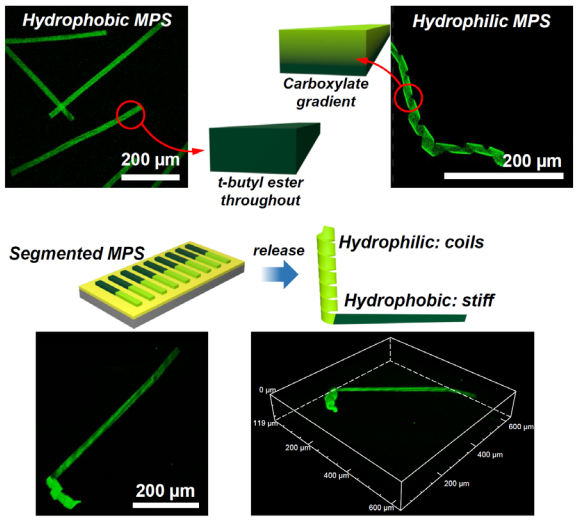

Figure 3. *Visualization of MPS segments by fluorescence confocal microscopy, showing straight (hydrophobic) and coiled (hydrophilic) structures emanating from their chemical structure and swelling in aqueous media.*

At present we are integrating dynamic polymer structures like FSBs into the mesoscale MPS concept, while simultaneously working towards next-generation MPS designs including multi-arm T- and Y-shaped objects. As illustrated in **Figure 4,** our photolithographic methods readily adapt to the preparation of MPS structures of arbitrary shape based on photomask geometry and AutoCAD Design software. In the example shown, a 40 mg/mL acetone solution of a protected zwitterionic copolymer was applied to a Si wafer by spin-coating and then crosslinked by photo-exposure. Dissolution of unexposed areas and release of the fully hydrophobic Y-shaped MPS into oil-in-water emulsions showed evidence of droplet wrapping, though mixtures of different MPS geometries (Y-shaped and linear) observed in the fluid phase are indicative of MPS breakage due to bending stress at the junction point and/or torque generated during fluid flow. As we proceed, we will systematically study multi-armed MPS structures by varying polymer film thickness (from ~50 to ~200 nm, dictated by polymer concentration in the spin-coating step) to evaluate tradeoffs between thicker (stronger) structures and thinner (more flexible) structures. Combining polymer

synthesis with MPS fabrication and mask design will yield multi-armed structures with well-defined hydrophobic and hydrophilic segments, such as shown in the figure for an MPS setup for interface wrapping with the red (hydrophobic) segments and extension of blue (hydrophilic) segments into the fluid. Inverting the hydrophobic and hydrophilic arrangement from that shown in the figure will yield droplets with multiple extending segments per wrapped segment, with peel-force and rheological characterization used to distinguish the properties of these multi-armed designs relative to linear structures.

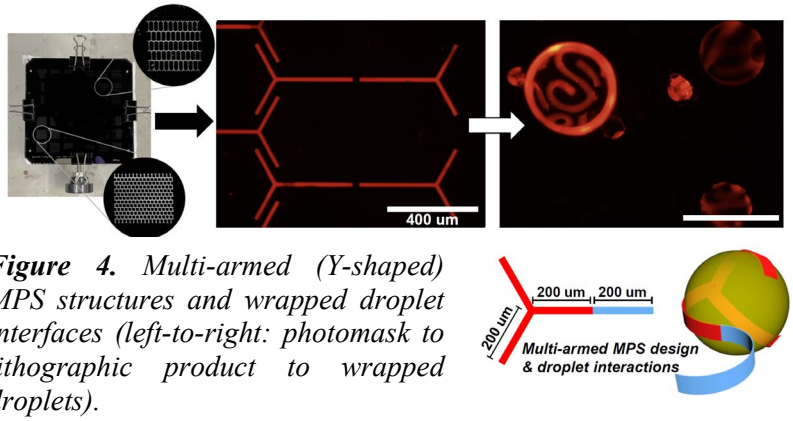

Figure 4. *Multi-armed (Y-shaped) MPS structures and wrapped droplet interfaces (left-to-right: photomask to lithographic product to wrapped droplets).*

Future Plans. Looking forward, we seek to couple innovative, bio-inspired syntheses of macromolecular materials with mesoscale materials fabrication methods to generate reactive, functional droplets, with advances hinging on tailoring surface and interfacial energies *via* chemical functionality. As we will build further on the FSB platform, replacement of fluorocarbon substituents with silanes and silicones offers opportunities to realize surfaces and interfaces with uniquely dynamic responses to their fluidic surroundings. At the same time, we will build on our dendritic droplet platform to yield asymmetric droplets (*i.e.*, where appendages extend from one distinct hemisphere), as well as droplets with appendages that function in surface cleaning at distances well beyond the droplet interface.

References

1. Steppan, C. G., Simon, L., Blackwood, C., & Emrick, T. (2024). Sulfobetaine Zwitterions with Embedded Fluorocarbons: Synthesis and Interfacial Properties. *ACS Macro Letters*, *13*, 761-767. DOI: 10.1021/acsmacrolett.4c00198.
2. Yang, Z., Snyder, D., Pagaduan, J. N., Waldman, A., Crosby, A. J., & Emrick, T. (2022). Mesoscale Polymer Surfactants: Photolithographic Production and Localization at Droplet Interfaces. *Journal of the American Chemical Society*, *144*(48), 22059-22066. DOI: 10.1021/jacs.2c09346.
3. Feng, L., Zhang, Y., Xi, J., Zhu, Y., Wang, N., Xia, F., & Jiang, L. (2008). Petal effect: a superhydrophobic state with high adhesive force. *Langmuir*, *24*(8), 4114-4119. DOI: 10.1021/la703821h.
4. Zhou, L., Triozzi, A., Figueiredo, M., & Emrick, T. (2021). Fluorinated Polymer Zwitterions: Choline Phosphates and Phosphorylcholines. *ACS Macro Letters*, *10*(10), 1204-1209. DOI: 10.1021/acsmacrolett.1c00451.
5. Zhou, L., Yang, Z., Pagaduan, J. N., & Emrick, T. (2023). Fluorinated zwitterionic polymers as dynamic surface coatings. *Polymer Chemistry*, *14*(1), 32-36. DOI: 10.1039/D2PY01197B.

BES-supported publications over past 2-years

1. Steppan, C. G., Simon, L., Blackwood, C., & Emrick, T. (2024). Sulfobetaine Zwitterions with Embedded Fluorocarbons: Synthesis and Interfacial Properties. *ACS Macro Letters*, *13*, 761-767. DOI: 10.1021/acsmacrolett.4c00198.
2. Snyder, D., & Emrick, T. (2024). Embedding Thiols into Choline Phosphate Polymer Zwitterions. *Macromolecular Rapid Communications*, *45*(8), 2300690. DOI: 10.1002/marc.202300690.
3. Zhou, L., Yang, Z., Pagaduan, J. N., & Emrick, T. (2023). Fluorinated zwitterionic polymers as dynamic surface coatings. *Polymer Chemistry*, *14*(1), 32-36. DOI: 10.1039/D2PY01197B.
4. Yang, Z., Snyder, D., Sathyan, A., Balazs, A., & Emrick, T. (2023). Smart droplets stabilized by designer surfactants: from biomimicry to active motion to materials healing. *Advanced Functional Materials*, *33*(52), 2306819. DOI: 10.1002/adfm.202306819**.**
5. Yang, Z., Snyder, D., Pagaduan, J. N., Waldman, A., Crosby, A. J., & Emrick, T. (2022). Mesoscale Polymer Surfactants: Photolithographic Production and Localization at Droplet Interfaces. *Journal of the American Chemical Society*, *144*(48), 22059-22066. DOI: 10.1021/jacs.2c09346.

Early Formation Stages and Pathway Complexity in Functional Bio-Hybrid Nanomaterials

PI: Lara A. **Estroff** [1]; Co-PIs: Elias Nakouzi [2] and Ulrich Wiesner [1]

[1]Department of Materials Science and Engineering, Cornell University, Ithaca, NY 14853

[2]Pacific Northwest National Laboratory, Richland, WA 99352

Keywords: Organic-inorganic hybrids, self-assembly, nanostructured materials, interfaces, crystallization

Program Scope

The current project is focused on using nanostructured organic and inorganic interfaces to guide assembly and crystallization pathways, resulting in materials with precisely-controlled structures across length scales, from the near-molecular all the way to the macroscopic scale. *The work focuses on three materials platforms to elucidate solution-based assembly pathways, with an increasing emphasis on the role of the solid-liquid interface composed of solvent molecules, polymer chains, and inorganic materials precursors and clusters.* In the first materials system, we are probing the early assembly stages in the formation of spherical amorphous silica nanoparticles by elucidating the role of "magic cluster" numbers in initial particle aggregation events, controlling surface chemistry by introducing hydrophobic patches, and manipulating particle topology to access rings, cages, and hollow particles by using surfactant self-assembly directed pathways. In the second system, we are investigating the role of the solid-liquid interface in directing the incorporation of secondary (nanoparticle) phases during crystallization. We are performing studies as a function of silica nanoparticle surface chemistry (e.g., functional groups, "patchiness", etc.) and topology, thereby connecting to the first materials system. Finally, in the third system, by inverting the approach taken in the second system, we are developing methods to elucidate the energy landscape associated with block copolymer self-assembly based nanostructured substrates in controlling nucleation and growth of inorganic materials. Here we are focused on elucidating the role of the solid-liquid interface during such growth phenomena. In all cases, we are interested in revealing the early stages in structure formation. We are striving to understand the "active" role of the solvent in directing hybrid assembly pathways, and importantly in mediating the "cross-talk" (information transfer) between organic templates and growing inorganic materials. To accomplish this goal, we are using two techniques ideally suited to probing molecular-scale features of interfaces important for determining assembly pathways in hybrid materials, but not yet well established in this line of research: High-performance liquid chromatography (HPLC) and three-dimensional atomic force microscopy (3D-AFM).

Recent Progress

Pathway complexity and early formation stages in amorphous silica nanostructures. We are developing novel high-performance liquid chromatography (HPLC) methods to study the earliest formation stages in, and surface chemical properties of, ultrasmall spherical dye-encapsulating inorganic silica-core poly(ethylene glycol) (PEG)-shell (core-shell) fluorescent silica nanoparticles (FSNPs) (**Fig. 1**). The elugram in (Fig. 1b) shows at least 9 peaks that are well resolved with the most intense peak being peak #7. We have tentatively assigned these peaks to FSNPs with different numbers of silica clusters assembled to form the silica particle core, as visualized in the particle rendering in Figure 1D (see red core built up from 5 clusters).

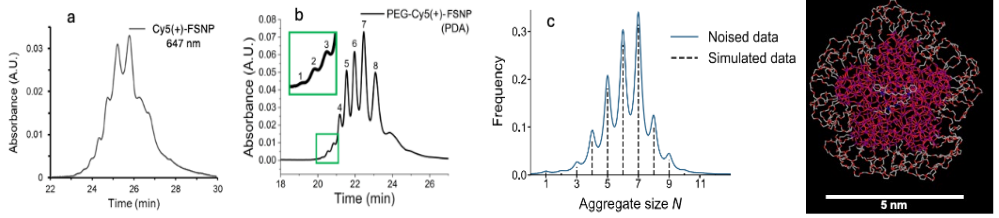

Fig. 1. Comparison of HPLC elugrams obtained from FSNPs using the original method (A) and the newly optimized advanced method (B). In (C) simulation results are shown using particles whose assembly behavior is governed by SALR interaction potentials. (D) Rendering of a PEG-ylated 5-6 nm diameter Cy5-dye encapsulating FSNP.

These results suggesting the most abundant particles forming around a core assembled from 7 clusters pose a puzzle. Theoretical studies into the origin of "magic" cluster numbers of spherical objects have suggested the first magical number to be 6 rather than 7. To solve this puzzle, we have worked with Prof. Julia Dshemuchadse (Cornell MSE). Simulations from her group suggest that the aggregation number 7 emerges when moving from hard sphere interactions between clusters to more realistic interparticle potentials combining short-range attractive (SA; from Si-O-Si bond formation between silica clusters) with long-range repulsive (LR; from electrostatic repulsion between negatively charged silica clusters) interactions (i.e., SALR interaction potentials). Particle aggregates with a pentagonal bipyramid-based structure emerge from this switch of interaction potentials (**Fig. 2**). Furthermore, quantitative analysis of the simulation results reveals that the most abundant aggregation number for such assemblies is 7, *i.e.*, a pentagonal bipyramid, consistent with our experimental HPLC results (compare **Fig. 1b,c**).

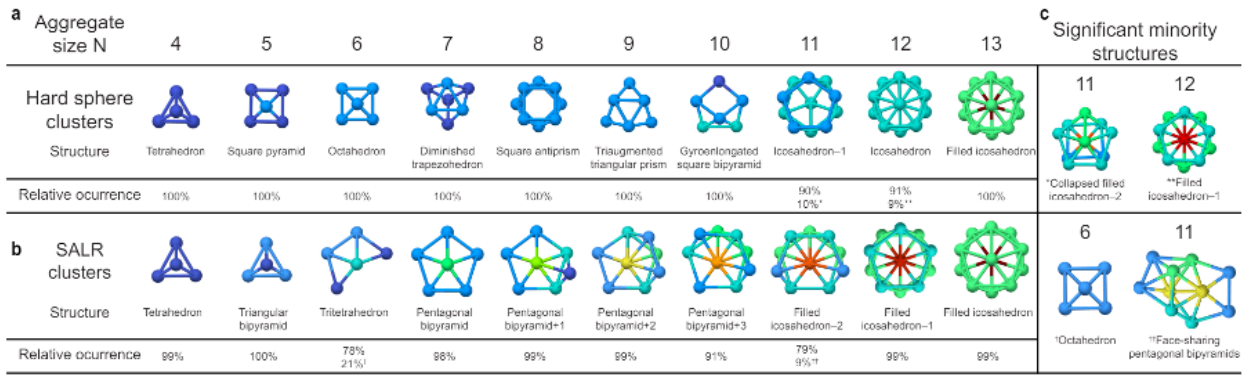

Figure 2: Comparing simulation results employing hard-sphere (top) versus SALR (bottom) interaction potentials and showing the emergence of pentagonal bipyramid structures (coordination #7).

Visualizing the interfacial solution structure at the calcite-solution-ligand interface. One of our primary goals is to measure the interaction potentials between ligand-coated particles and the calcite surface. To accomplish this objective, we are using the recently developed 3D atomic force microscopy (AFM) technique at PNNL. Here, Si-based AFM probes with oxide surface layers (i.e., silica) are functionalized with various ligands using azide-alkyne "click" chemistry. We acquired 3D force maps and force gradient data at the calcite interface in saturated calcium carbonate solutions using 5 types of probes: bare Si/SiO_2, PEG-coated, as well as the three target functional coatings: -OH (hydroxyl), $-NH_2$ (amine) and -COOH (carboxylic acid) (**Fig. 3**). While a detailed analysis is in progress, we can already report qualitative observations: 1) the data with the bare Si/SiO_2 probes is comparable with literature reports for calcite, providing a useful benchmark for the ligand datasets; 2) the -COOH coated probes experienced long-range interactions beyond 2 nm (**Fig. 3**, bottom row); 3) the functionalized probes revealed specific interactions at the calcite step edges as compared to the terraces; 4) we were able to resolve sub-nanometer features close to the calcite surface with the ligand-coated probes that correspond to solution structuring (**Fig. 3**, top row).

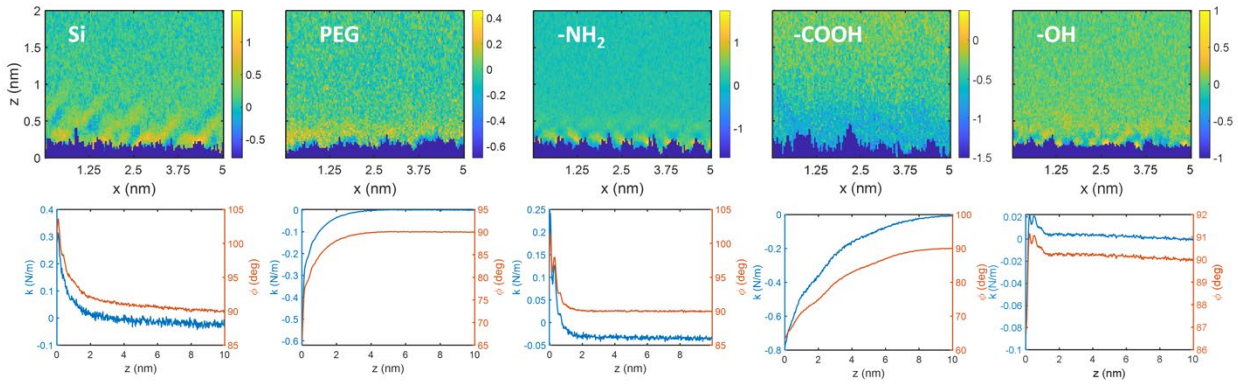

Figure 3. 3D AFM data of calcite surfaces imaged in saturated calcium carbonate solutions (1.5 mM $CaCl_2$ + 5 mM $NaHCO_3$) using functionalized silicon/silica tips. (Top row) Vertical slices from force maps acquired with various probes, including bare silicon/silica, PEG-ylated, and functionalized with amine, carboxylic acid, and hydroxyl terminations as described in the text. Colormaps indicate variations in force gradients (N/m) as nanoprobe navigates interfacial regions. (Bottom row) Corresponding average phase shift curves (orange) from force map raw data, which are converted to force gradient curves (blue). Data show long-range interactions corresponding to colloidal forces as well as short range oscillations that indicate solution structuring at the interface.

Surface reconstructions in hydrated, amphiphilic BCP thin films. In bulk BCPs, the interplay between enthalpic and entropic contributions of different blocks as well as their volume fractions gives rise to a variety of mesoscale morphologies. Thin film behavior differs from the bulk as a result of additional interfacial energy contributions to the free energy from film-substrate and film-air interfaces. We have evaluated polymer-solvent interactions and solvent-driven surface reconstructions via AFM analysis of amphiphilic BCP thin films upon exposure to DI water. We examined the differences in surface morphology, whole-film swelling, and force response in thin films of polystyrene-block-polyethylene oxide (PS-*b*-EO) and polystyrene-*block*-poly[(allyl glycidyl ether)-*co*-(ethylene oxide)] (PS-*b*-P[AGE-*co*-EO]) processed into standing-up cylinder morphologies perpendicular to the silicon surface (**Fig. 4**). We have not only analyzed the energetics of the driving forces of the BCP thin film surface reconfigurations but also probed the mechano-responsive nature of the dynamic top surfaces. Results show surface rearrangements via minimal tip-sample stimulation with broader implications for tuning of top surface hydrophilicity. Given the non-ionizable nature of the minority P(AGE-*co*-EO) block and the energetics of the underlying driving forces for chain mobility, this work shows how the elimination of unfavorable PS-water interfaces drives surface coverage and chain rearrangement. This work highlights effects of added complexity in BCP

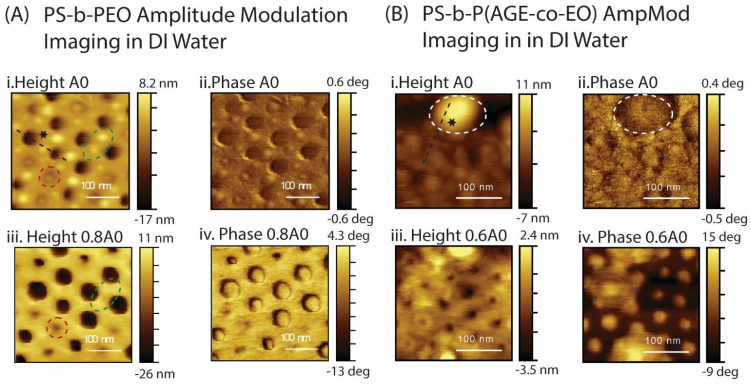

Figure 4. Amplitude Modulation AFM Imaging in water of (A) PS-*b*-PEO and (B) PS-*b*-P(AGE-*co*-EO) thin films after 1 hour incubation in DI water. Height (i,iii) and phase channel images at original amplitude setpoint A0 (i,ii) and reduced setpoints as shown (iii,iv).

thin film behaviors via random blocks and how those changes to local interfacial energies may drive larger scale film morphology reconstructions.

Future Plans.

Thrust 1 – We are building on our exciting results described earlier on magic cluster numbers in the silica core of FSNPs as highlighted via advanced HPLC methods and their quantitative understanding via coupling to simulation work in the group of Prof. Julia Dshemuchadse (Cornell MSE). The pentagonal bipyramidal structure of the clusters in the FSNP core is rather stable as one can think of it as assembled by 5 tetrahedra (one tetrahedron is constituted by the two touching beads above and below the plane of the pentagon, and two adjacent beads within the pentagonal plane). Preliminary simulations with different particle densities in the simulation box indeed all show the prevalence of this pentagonal bipyramidal structure. This suggests that the synthesis of such FSNP based nanomaterials, in contrast to many other nanomaterials, may not depend much on the concentration of the precursors and therefore may be scalable, a prerequisite for transfer of such nanotechnologies to application spaces requiring synthesis scale-up. We are currently performing HPLC experiments on FSNPs synthesized in different reaction volumes and from different precursor concentrations. If the simulation results are a correct prognostic, in HPLC using our advanced method these batches should show the prevalence of the cluster aggregates with magic number 7. Such a result would have substantial implications for synthesis scale-up, which has remained a major challenge in the applications of such nanomaterials.

Thrust 2 – We are continuing our analysis of the interaction potentials between ligand-coated probes and calcite surfaces and the solvent-structuring at the calcite-solution interface. We will extend our investigations to a different class of particle-surface interactions: namely friction forces, which could also be relevant to the outcomes of particle interactions. In this case, the functionalized probe is maintained at a constant height above the crystal surface and the lateral forces are measured as the probe navigates across the surface. The rationale for why this measurement is relevant to understanding nanoparticle incorporation is that particles (as represented by the functionalized tips) with stronger friction forces might be more conducive to incorporation within the calcite lattice, since they are more resistant to being "swept off" by a propagating step edge. In the second year, we will focus on correlating our bulk crystal growth experiments with the 3D AFM experiments as we endeavor to understand how the interfacial interactions between the functionalized particles, the solvent structuring, and the crystal surface all contribute to particle incorporation (or exclusion).

Thrust 3 – We will apply the 3D AFM techniques, which currently is in use only in Thrust 2, to characterize block copolymer thin films. Specifically, we will use 3D-force mapping to understand how the local nanoscale chemistry and topology of amphiphilic block BCP thin films determines the local polymer-solvent interfacial structure. Our goal is to connect local variations in repulsive and attractive forces to visualize nanoscale differences in hydrophilicity of the surface. We are trying to establish if and how such spatial variations in water structuring at these interfaces direct the nucleation and growth of inorganic materials on these thin films.

Publications Supported by BES 2022-2024

1) Lee, W. Y.; Chapman, D. v.; Yu, F.; Tait, W. R. T.; Thedford, R. P.; Freychet, G.; Zhernenkov, M.; Estroff, L. A.; Wiesner, U. B. Triblock Terpolymer Thin Film Nanocomposites Enabling Two-Color Optical Super-Resolution Microscopy. *Macromolecules* **2022**, *55* (21), 9452–9464. https://doi.org/10.1021/acs.macromol.2c01017.

2) Palin, D.; Kunitake, J. A. M. R.; Chang, M. P.; Sutter, S.; Estroff, L. A. Gel-Mediated Chemo-Mechanical Control of Calcium Carbonate Crystal Formation. *J Cryst Growth* **2023**, *602*, 126943. https://doi.org/10.1016/j.jcrysgro.2022.126943.

3) Yu, F.; Wiesner, U. The Emerging Field of Block Copolymer Self-Assembly-Directed Quantum Materials, *Polymer*, **2023**, *281*, 126063. 10.1016/j.polymer.2023.126063

4) Jacob A. Erstling, Nirmalya Bag, Thomas C. Gardinier, Ferdinand F. E. Kohle, Naedum DomNwachukwu, Scott D. Butler, Teresa Kao, Kai Ma, Melik Z. Turker, Grant B. Feuer, Rachel Lee, Nada Naguib, James F. Tallman, Henry F. Malarkey, Lieihn Tsaur, William L. Moore, Dana V. Chapman, Tangi Aubert, Saurabh Mehta, Richard A. Cerione, Robert S. Weiss, Barbara A. Baird, Ulrich B. Wiesner, "Overcoming Barriers Associated with Oral Delivery of Differently Sized Fluorescent Core-Shell Silica Nanoparticles", *Advanced Materials*, **2024**, *36*, 2305937, DOI: 10.1002/adma.202305937.

5) A. J. Drouhin, W. R. T. Tait, W. Moore, F. Yu, Y. Lee, J. Werner, R. B. van Dover, U. B. Wiesner, "Block copolymer self-assembly derived mesoporous magnetic materials with three-dimensionally (3D) co-continuous gyroid nanostructure", *Soft Matter*, **2024**, *20*, 2767, DOI: 10.1039/D3SM01622F.

6) P. Brahana, M. Zhang, E. Nakouzi, B. Bharti “Microplastics as ice nucleating particles”, *Nature Commun.,* under review.

Programmable dynamic self-assembly of DNA nanostructures

Elisa **Franco**, UCLA, and Rebecca **Schulman**, Johns Hopkins University**.**

Keywords: Dynamic assembly, polymerization, molecular circuits, biochemical energy

Research Scope

The development of artificial active biomolecular materials that can, like those in living systems, programmatically reorganize in a scalable manner to perform specified mechanical work is a grand challenge in materials science. Discerning how to direct precise operations efficiently is critical for energy science: mechanical operations offer the opportunity to vastly improve the efficiency of energy conversion, reliably store energy, direct material transport, and create lightweight, long-lasting materials and material systems. Understanding how to achieve these aims using biomolecular materials offers the opportunity to develop general principles for materials design without the need for exotic or limited raw materials. We are directly addressing this grand challenge by developing and demonstrating design principles for programming biomolecular materials to perform specific mechanical tasks through the collective interactions of molecular components, cofactors, and fuels, building on scientific developments of a multiphase research program within the BES Biomolecular Materials program. Our efforts combine experimental design, computational analysis, and simulations. They produce specific methods and general design principles for harnessing energy to do mechanical work and reprogram the structure of materials at multiple scales.

Recent Progress

Principles underlying assembly-driven deformation. Under what conditions is it possible to generate work from the passive self-assembly of monomers in confinement? To address this question, we have developed computational tools to analyze temporal pathways of polymeric assemblies that mimic DNA nanotubes adopted in our labs [1]. Polymer assembly is simulated through a patchy particle model of monomers embedded in a deformable vesicle. We have investigated how the mechanical properties, molecular features (e.g. monomer bond geometry and mobility), and the temporal schedule of monomer generation influence how growing nanostructure assemblies exert force on the confining vesicle and identify regions of parameter space in which directional forces are sufficient to deform the vesicle into a non-equilibrium shape.

Choosing the pathway of nanostructure assembly using biomolecular circuits to control monomer release. We recently developed mesoscale synthetic transcriptional circuits that programmatically control when multiple biomolecular outputs are produced and degraded [2]. We have now demonstrated how transcription circuits can control how biomolecular materials assemble because their outputs regulate when and how many components are available for assembly. We find that biomolecular outputs can control the availability of DNA monomers, and thus the pathway by which these monomers assemble into filaments in a manner consistent with

the predictions of quantitative models (Fig. 1) [3]. We developed transcription networks that release successive pulses of RNA regulators at precise times timing; these regulators activate or deactivate a particular population of DNA nanotube monomers, leading to successive assembly of nanotube populations whose composition evolves. We are now exploring how UV irradiation can also control nanotube growth by likewise activating monomers and have shown that modulating UV irradiation time (dosage) is an effective way to regulate nanotube growth rate. Combined with our theoretical studies, these results offer the opportunity to develop UV dose protocols that optimize the extent of vesicle deformation induced by DNA nanotube assembly, and thus more generally how to design and optimize far-from-equilibrium protocols for energy transduction via biomolecular material growth. UV-based growth control can also be combined with transcription-based growth control, leading to the development of biomolecular materials with the capacity to respond to multiple inputs.

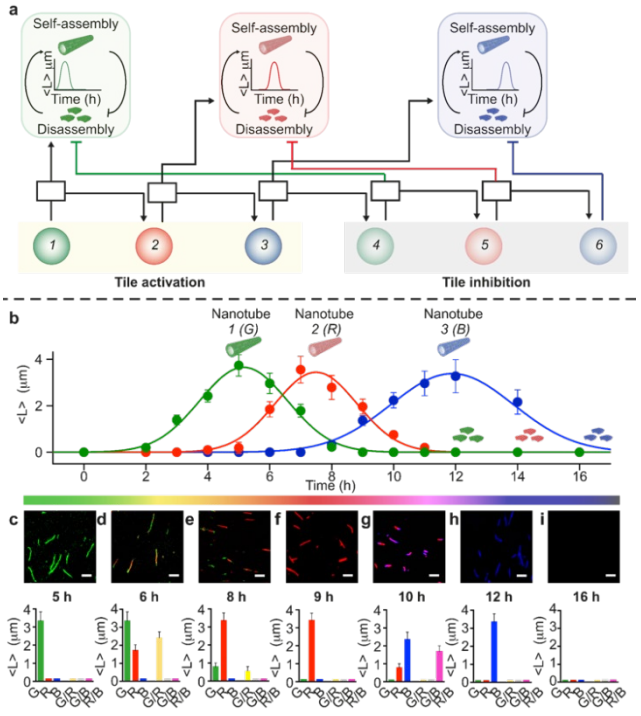

Figure 1: A cascade of artificial genes can robustly control the assembly and disassembly of distinct nanotube populations for extended periods of time [2]. Monomers are labeled with different fluorophores and are specifically controlled by the output of a particular gene. All monomers can coassemble. (a) Schematic of the system. (b) Average length of nanotubes decorated with distinct fluorophores (c) Representative microscopy images and bar charts showing the length of nanotube blocks of a particular monomer type. Scale bars 2.5 μm.

Biomolecular linear actuators. Inspired by the efficient and precisely controlled generation of force by actin polymerization at the cell membrane, we have developed a synthetic filament linear actuator that applies force to a load at its growing tip (Fig. 2). The actuator consists of DNA nanotubes with attached capping structures that can be displaced by polymerization or depolymerization. Monomers can be added or removed from the nanotube-cap interface because the flexible, multivalent interface structure transiently exposes portions of the nanotube's facet while remaining attached to the load. We are studying this process by pinning the ends of a filament to a surface to characterize the rate and extent of monomer insertion. In this case, monomer insertion or removal respectively, driven by the chemical potential, bends or stretches pinned filaments. The amount of work performed by these processes can then be measured by tracking changes in the configurational energy of filaments. We are using these measurements to determine the motor's stall force, by identifying filament configurations and chemical potential where there is no change in filament length, and the efficiency of the actuators by comparing the work they can perform to the required drop in chemical potential to perform this work. This simple,

specific, and highly programmable design offers a means of generating directional force using a generic mechanism, reversible molecular self-assembly. The principles developed here could thus potentially be adopted to create force-generating mechanical elements from any of the vast range of filaments that can grow *via* monomer attachment at the tip. And because the fuel consumed during force generation is specific to filament type, different types of filaments might be independently directed to expand and contract to precisely program material deformation by independently controlling their respective fuel concentrations.

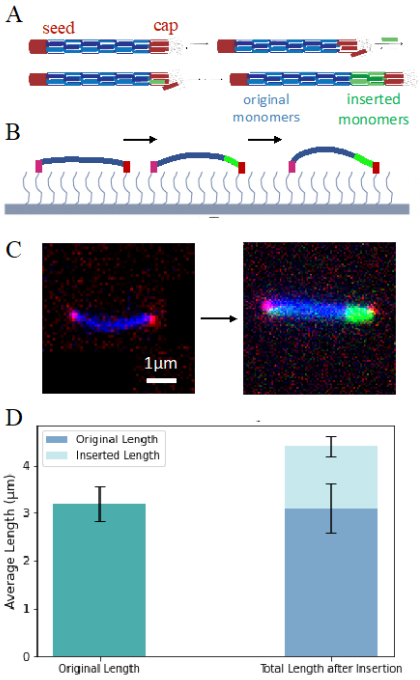

Figure 2: Filament linear actuators; A. Monomers attach to seeded DNA nanotubes during transient detachments of cap binding elements, over time moving the cap. B-C. Filaments pinned at both ends transduce the forces generated through growth to bending nanotubes, providing a means to measure force generation and actuator stall force. D. Ensemble measurements of the extent of insertion polymerization.

Semiflexible filament network architecture. Actin efficiently generates forces through directional growth when organized into crosslinked meshes, with optimal force generation occurring at a specific crosslinking angle. We have grown crosslinked DNA nanotube with control over crosslinking densities and angles enabling the exploration of the structure, mechanical properties, and force generation capacities of a whole class of new material structures (Fig. 3). Using rigid junction elements that we developed in a previous award cycle whose angle is precisely controlled by molecular sequence [4], we have assembled rigidly crosslinked nanotube structures and created a stochastic kinetic model that recapitulates their growth dynamics [5].

Future Plans

Transporting cargo using biomolecular filament linear actuators. We will demonstrate that linear actuators can perform work and actuator efficiency by measuring the rate at and extent to which nanotube linear actuators can lift a polystyrene bead (Fig. 4A). The work performed will be assessed as an increase in the potential energy of the bead, which is denser than the solvent. We will also build

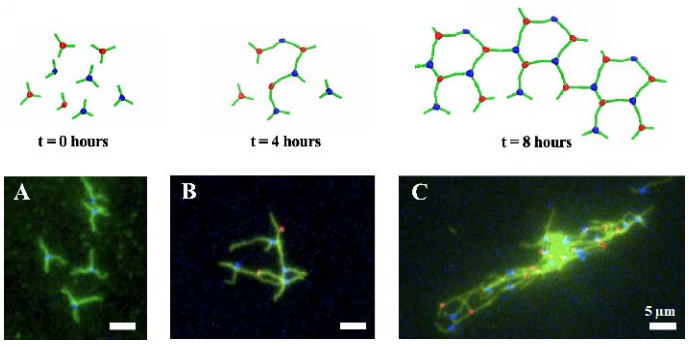

Figure 3: Assembly of rigidly crosslinked semiflexible filament (nanotube) networks; crosslink angle is controlled by multivalent seed structures and can be tuned using straightforward molecular design. The resulting materials have pores that are microns in diameter. Nanotubes grown from different types (red, blue) of seeds present ends that can undergo end-to-end joining. A-C Fluorescence micrographs of example networks after assembly times.

faster actuator systems assembling multiple filament actuators into chains (Fig. 4B). Bundling filament actuators should, correspondingly, increase actuator power. Filament actuators will therefore provide a laboratory for developing a class of linear actuators, mechanically active primitives for materials that could orchestrate material reconfiguration, repair, and the directed motion of different nanoscale or microscale components.

Programming the directions of forces applied by biomolecular materials. By forming networks of filament linear actuators using the methods described here, we will create contractile and extensible biomolecular materials whose dynamic restructuring is directed by the shrinking or growth of individual filaments. We will use the approaches developed in [1] to create protocols for efficiently generating forces using programmed modes of filament extension and contraction.

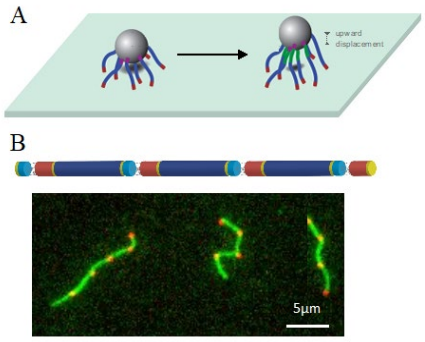

Figure 4: A. Insertion of monomers could displace cargo. B. Linear chains of monomers (top, design, bottom, fluorescence micrographs) could increase actuation speed.

Deforming vesicles using designed dynamic filament assembly processes. We will test whether, as predicted by our computational simulations, a vesicular compartment can be deformed by the gradual activation of DNA monomers and nanotube structures, thereby dissipating chemical energy to perform work (Fig. 5). The release of specific DNA monomers will be achieved through the combination of UV dosage as well as RNA transcription of distinct. These experiments will elucidate how passive assembly pathways can be used to perform work by optimizing the temporal features of the monomer release, thereby addressing the central question of our project.

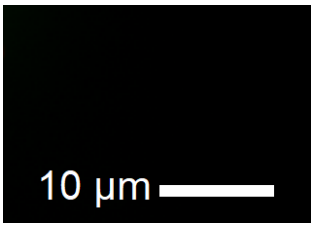

Figure 5: Fluorescence micrograph of lipid vesicles containing DNA nanotubes.

References

1. D. Osmanovic, and E. Franco, *Generating forces in confinement via polymerization.* arXiv preprint arXiv:2405.13270 (2024).
2. S. W. Schaffter, K.-L. Chen, J. O'Brien, M. Noble, A. Murugan, and R. Schulman. *Standardized excitable elements for scalable engineering of far-from-equilibrium chemical networks.* Nature Chemistry, **14**, 1224–1232 (2022). DOI: 10.1038/s41557-022-01001-3.
3. D. Sorrentino, S. Ranallo, F. Ricci, and E. Franco, *Developmental assembly of multi-component polymer systems through interconnected gene networks in vitro.* Accepted, Nature Communications. bioRxiv preprint 2024.03. 14.585044 (2024)

4. T. Jorgenson, A. Mohammed, D. Agrawal and R. Schulman. *Self-Assembly of Hierarchical DNA Nanotube Architectures with Well-Defined Geometries*, ACS Nano **17**, *1927-1936* (2016). DOI: 10.1021/acsnano.6b08008.
5. Y. Jiang, M. S. Pacella, S. Lee, J. Zhang, J. A. Gunn, P. Vallejo, P. Singh, T. Hou, E. Liu, and R. Schulman. *Hierarchical assembly and modeling of DNA nanotube networks using Y-shaped DNA origami seeds.* Nanoscale, **16**, 11688-11695 (2024). DOI: 10.1039/D4NR01066C

Publications

1. D. Sorrentino, S. Ranallo, F. Ricci, and E. Franco. *Developmental assembly of multi-component polymer systems through interconnected gene networks in vitro*, Accepted, Nature Communications. bioRxiv preprint 2024.03. 14.585044 (2024).
2. S. W. Schaffter, E. Kengmana, J. Fern, S. R. Byrne, and R. Schulman, *Strategies to Reduce Promoter-Independent Transcription of DNA Nanostructures and Strand Displacement Complexes*. ACS Synthetic Biology, online first, (2024). DOI: 10.1021/acssynbio.3c00726.
3. Y. Jiang, M. S. Pacella, S. Lee, J. Zhang, J. A. Gunn, P. Vallejo, P. Singh, T. Hou, E. Liu, and R. Schulman. *Hierarchical assembly and modeling of DNA nanotube networks using Y-shaped DNA origami seeds.* Nanoscale, **16**, 11688-11695 (2024). DOI: 10.1039/D4NR01066C.
4. D. Osmanovic and E. Franco, *Generating forces in confinement via polymerization.* arXiv preprint arXiv:2405.13270 (2024).
5. P. Moerman, H. Fang, T. Videbæk. W.B. Rogers, and R. Schulman. *A simple method to alter the binding specificity of DNA-coated colloids that crystallize.* Soft Matter, **19**, 8779-8789 (2023). DOI: 10.1039/D3SM01105D.
6. M. Rubanov, P. J. Dorsey, D. Scalise, and R. Schulman. *Sequential Activation of Spatially Localized Oligonucleotides*, ACS Materials Letters, **4**, 9, 1807–1814, (2023). DOI: 10.1021/acsmaterialslett.2c00286
7. H. Hall-Thomsen, S. Small, M. Gavrilov, T. Ha, R. Schulman, and P. Moerman. *Directing Uphill Strand Displacement with an Engineered Superhelicase*. ACS Synthetic Biology, **12**, 11, 3424–3432 (2023). DOI: 10.1021/acssynbio.3c00452.
8. J. Le, D. Osmanovic, M. A. Klocke, and E. Franco. *Fueling DNA Self-Assembly via Gel-Released Regulators*, ACS Nano, **16**, 16372 (2022). DOI: 10.1021/acsnano.2c05595.
9. S. W. Schaffter, K.-L. Chen, J. O'Brien, M. Noble, A. Murugan, and R. Schulman. *Standardized excitable elements for scalable engineering of far-from-equilibrium chemical networks.* Nature Chemistry, **14**, 1224–1232 (2022). DOI: 10.1038/s41557-022-01001-3.

Controlling Lattice Organization, Assembly Pathways and Defects in Self-Assembled DNA-Based Nanomaterials

Oleg **Gang** [1,2,3] and Sanat K Kumar,[1]
[1]Department of Chemical Engineering, [2]Department of Applied Physics and Applied Mathematics, Columbia University, New York, NY.
[3]Center for Functional Nanomaterials, Brookhaven National Laboratory, Upton, NY

Keywords: Self-assembly, DNA nanotechnology, superlattices, nanomaterials, inverse design

Research Scope

The project aims to establish the approaches for the assembly of prescribed nanoscale architectures and to uncover the principles of creating such systems. We develop platform methods for creating diverse large-scale and mesoscale 3D architectures for organizing nano-objects of several types (nanoparticles and proteins) using DNA-based assembly approaches. By utilizing liquid robotics, advanced characterizations, computational developments, and machine learning methods, we explore how to design and control efficiently and with low defects assembly of prescribed complex periodic nano-architectures, how to steer the system's assembly pathway, and how to control a lattice growth using thermodynamic factors and bond design. By combining assembly with detailed characterization and analysis, the project establishes approaches for creating designed nanoparticle-based materials with DNA-programmable architectures.

Recent Progress

The effect of anisotropic binding energies on morphology of the self-assembled lattices[1].

To understand the thermodynamic underpinnings of the self-assembly of DNA-grafted nanoparticles, our recent work investigated the self-assembly behavior of octahedral DNA frames. The DNA frames have complementary interacting vertices, which can result in the assembly of lattices with crystallographic symmetry determined by the valences of the DNA frames[2]. We demonstrated via computer simulations that assemblies with different three-dimensional (3D) crystalline morphologies can be formed depending on the relative strength of vertex-to-vertex

interactions in different directions, as shown in the morphology diagram in Figure 1. We developed a theoretical description based on the second-virial coefficient of patchy particles.

Complementing the theory and simulations, experimental studies were performed to investigate the assembly of octahedral DNA origami frames with varying binding energies. Electron microscopy imaging of the assembled domains validated the theoretical predictions and showed the correspondence of the distinct morphologies to the DNA interaction strengths in the three orthogonal directions. We are currently investigating octahedral nanoparticles with' asymmetric' inter-vertex interactions to further explore the controllability of the final assembly morphology via manipulating the directionality of inter-vertex interactions.

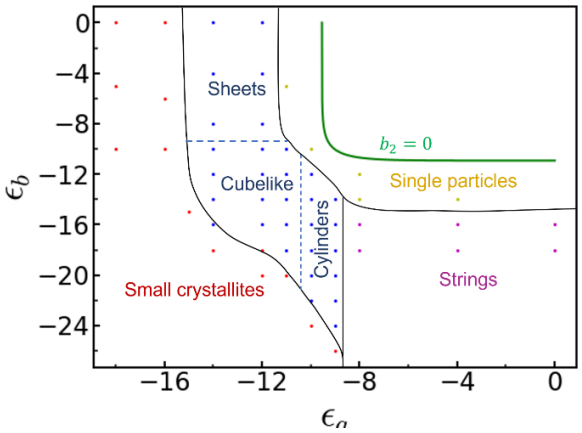

Figure 1. Crystal morphology diagram in the interaction energy, (εa, εb), space. The green line is the boundary between the regions of negative and positive second virial coefficient. Crystalline domains of three distinct morphologies: sheet-like, cube-like, and cylinder-like, all shown by the blue dots, where regions

1. Three-dimensional Nanoscale Metal, Metal Oxide and Semiconductor Frameworks through DNA-Programmable Assembly and Templating[3].

Controlling the three-dimensional (3D) nano-architecture of inorganic materials is imperative for enabling their novel mechanical, optical, and electronic properties. Modern technological advances in electronics, photonics, and sensing rely heavily on planar fabrication approaches offered by top-down lithographic methods. At the nanoscales, multi-step planar lithography and deposition methods have demonstrated a structural control with a resolution extending to ~30-100 nm. The technique, however, faces challenges of incorporating a broad class of materials and fabrication of 3D architecture. On the other side, self-assembly approaches offer a rich structural diversity in 3D that can be combined with inorganic templating, which allows for fabrication parallelization. However, these approaches typically do not offer ways to prescribe specific nanoscale architecture and the breadth of material systems is limited.

Ex-situ organic-inorganic hybridization techniques, including liquid-phase infiltration (LPI) and vapor-phase infiltration (VPI), are emerging as new methods for converting polymer templates into functional organic-inorganic hybrids and creating inorganic nanostructures. The infiltration techniques have also been shown to be valuable for creating a library of metals and metal oxides within polymeric structures. Given the structural designability of DNA-based nanomaterials, it would be advantageous to employ infiltration-driven hybridization processes to 3D DNA structures to convert them into organic-inorganic hybrids and inorganic nano-replicas.

We demonstrated the application of LPI and VPI for inorganic templating of large-scale DNA frameworks (Figure 2). The 3D templating, thus realized, allows us to achieve deep penetration into 3D nano-architectures and to apply these methods, separately or together, to form different functional metal and metal oxide frameworks based on the designed DNA scaffold frameworks. Sol-gel growth of silica on DNA frameworks[4] followed by the infiltration synthesis provides versatile and modular control over the spatial distribution and elemental composition of inorganic material incorporated into a framework superlattice. Incorporating single-element and multi-element coatings by exploiting LPI or VPI techniques, or their combination, preserves the underlying DNA lattice architecture while enabling a nanofabrication of 3D inorganic nanoscale frameworks.

By exploiting DNA-programmable assembly, we established a general approach for realizing designed 3D-ordered inorganic frameworks. Through inorganic templating of DNA frameworks by liquid- and vapor-phase infiltrations, we demonstrated successful nanofabrication of diverse classes of inorganic frameworks from metal, metal oxide, and semiconductor materials, and their combinations, including Zn, Al, Cu, Mo, W, In, Sn, Pt and composites such as aluminum doped zinc oxide, indium tin oxide and platinum/aluminum doped zinc oxide. The open 3D frameworks have features in the order of nanometers, with architecture prescribed by the DNA frames and self-assembled lattice. Structural and spectroscopic studies revealed the composition and organization of diverse inorganic frameworks, as well as the optoelectronic properties of selected materials.

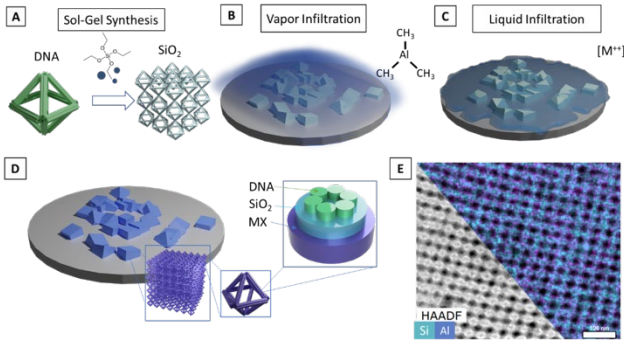

Figure 2. **Inorganic Templated Structures** (**A**) A silica 3D framework is formed from DNA framework. Templating of the framework is achieved either by (**B**) Vapor phase infiltration (VPI), where a vapor precursor such as trimethylaluminum (TMA) infiltrates the silica framework or (**C**) Liquid phase infiltration (LPI) whereby metal salt solutions infiltrate. (**D**) The resultant nanolattice is coated by metal/metal oxide (MX). (**E**) Scanning transmission electronic microscopy (STEM) cross-sectional high-angle annular dark-field (HAADF) imaging and energy dispersive spectroscopy (EDS) map of silica (blue) coated with alumina (purple) via vapor infiltration (scale bar 100 nm).

2. Inverse Design of Superlattices

We have developed a rational method of assembling hierarchically ordered lattices of DNA frames and nanoparticles through an inverse design approach. This design strategy considers the unique bond identities needed to achieve a desired structure through the inherent symmetry of the desired organization. First, we consider an arbitrarily defined, hierarchically ordered 3D structure that contains many nanocomponents as the target complexly organized lattice (Figure 3). The elementary building block is a DNA frame (termed material voxel) that may encapsulate a nano-particle or remain empty. In our study, the material voxel is an octahedral frame that can interact with six other voxels. The octahedra-formed simple cubic lattice defines a 3D cubic grid in which

nano-objects can be placed uniformly [2] or in simple patterns[5]. Interactions between voxels are specified using orthogonal DNA chromatic binding sequences. It is possible to make each bond in the desired metamaterial unique; however, the design and utilization of a large library of DNA binding sequences ("chromatic binding") can be quite taxing from a fabrication point of view. Additionally, complex materials with many components will suffer from kinetic restrictions, which limit the efficient assembly of the desired material. Instead, it is desired to minimize the number of unique voxels and interactions required to form the structure. We do this by leveraging local symmetries present in the desired structure, which results in the identification of a "mesovoxel" (a mesoscale structure with defined arrangement of voxels) and the set of unique voxels needed for a specific design (Fig. 3).

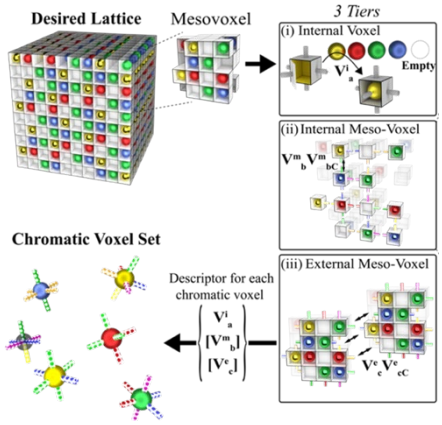

Figure 3. Inverse design of arbitrarily defined nanostructured materials through chromatic binding. Voxels are identified by an internal chromatic bond which loads functional nano-object and six external chromatic bonds which encode intervoxel interactions.

This developed strategy is a powerful tool for the design and assembly of complexly structured nanomaterials. We have successfully assembled several novel lattice architectures, including a nanoscale analog of a face-perovskite lattice, lattices with helical plasmonic nanoparticle arrangements, and organized planes of plasmonic nanoparticles with phonically relevant inter-planar spacings that are coupled with the arrangement of plasmonic nanoparticles within the planes. We use TEM or X-ray tomography to confirm the structure of designed lattices. Our experimental results were further confirmed by computational studies that provided insight into the nucleation and growth processes of the nanoscale systems with chromatic bonds.

Future Plans

In our future work, we will continue establishing predictive, practical and quantitative methods to design, assemble, and characterize DNA-programmable structures. We will integrate the assembly DNA-encoded methodology with inverse design strategy and machine learning methods to develop approaches for the prescribed assembly of DNA-based nanomaterials. Combining in-situ structural characterization using x-ray scattering and optical methods with ex-situ electron microcopy and tomography will permit the revealing of guiding phenomena, assembly pathways, and efficient design strategy. We will further use the established approaches for investigating how to control the multiscale organization of nanoparticles, how to direct the morphology of forming structures, and how to design and regulate an assembly pathway. Using our developments in 3D nanoscale imaging and scattering, we will investigate defects in complexly designed self-assembled systems and will correlate these findings with the system design (assembly motifs, bonds diversity, and strength) and with the assembly pathway. Through the application of ML/AI and computational methods, we will update the assembly design strategy, aiming to minimize

imperfections in DNA-assembled structures. The developed approaches will be applied to demonstrate a range of novel 3D organizations that can be assembled rationally.

References

[**1**] Adhikari et al., JACS, 2023. 145(36): p. 19578-19587; [**2**] Tian et al., Nat. Mat., 2020. 19(7): p. 789; [**3**] Michelson et al., Science Adv., 2024. 10(2): p. eadl0604; [**4**] Majewski et al., Science Adv., 2021. 7(12). [**5**] Wang, et al., Nat. Coom. 2021. 12(1)

Publications

1. Michelson, A., Minevich, B., Emamy, H., Huang, X. J., Chu, Y. S., Yan, H. F. & Gang, O. Three-dimensional visualization of nanoparticle lattices and multimaterial frameworks. *Science* 376, 203-+ (2022). https://doi.org:10.1126/science.abk0463

2. Dong, Y. X., Liu, J. L., Lu, X. Z., Duan, J. L., Zhou, L. Q., Dai, L. Z., Ji, M., Ma, N. N., Wang, Y., Wang, P., Zhu, J. J., Min, Q. H., Gang, O. & Tian, Y. Two-Stage Assembly of Nanoparticle Superlattices with Multiscale Organization. *Nano Letters* 22, 3809-3817 (2022). https://doi.org:10.1021/acs.nanolett.2c00942

3. Adhikari, S., Minevich, B., Redeker, D., Michelson, A. N., Emamy, H., Shen, E. R., Gang, O. L. & Kumar, S. K. Controlling the Self-Assembly of DNA Origami Octahedra via Manipulation of Inter-Vertex Interactions. *Journal of the American Chemical Society* 145, 19578-19587 (2023). https://doi.org:10.1021/jacs.3c03181

4. Logan, J. A., Michelson, A., Pattammattel, A., Yan, H. F., Gang, O. L. & Tkachenko, A. V. Symmetry-specific characterization of bond orientation order in DNA-assembled nanoparticle lattices. *Journal of Chemical Physics* 159 (2023). https://doi.org:10.1063/5.0168604

5. Mao, R. F., Minevich, B., McKeen, D., Chen, Q. Z., Lu, F., Gang, O. & Mittal, J. Regulating phase behavior of nanoparticle assemblies through engineering of DNA- mediated isotropic interactions. *Proceedings of the National Academy of Sciences of the United States of America* 120 (2023). https://doi.org:10.1073/pnas.2302037120

6. Michelson, A., Flanagan, T. J., Lee, S. W. & Gang, O. L. High-strength, lightweight nano-architected silica. *Cell Reports Physical Science* 4 (2023). https://doi.org:10.1016/j.xcrp.2023.101475

7. Liu, H., Matthies, M., Russo, J., Rovigatti, L., Narayanan, R. P., Diep, T., McKeen, D., Gang, O., Stephanopoulos, N., Sciortino, F., Yan, H., Romano, F. & Šulc, P. Inverse design of a pyrochlore lattice of DNA origami through model-driven experiments. *Science* 384, 776-781 (2024). https://doi.org:doi:10.1126/science.adl5549

8. Michelson, A., Subramanian, A., Kisslinger, K., Tiwale, N., Xiang, S. T., Shen, E., Kahn, J. S., Nykypanchuk, D., Yan, H. F., Nam, C. Y. & Gang, O. Three-dimensional nanoscale metal, metal oxide, and semiconductor frameworks through DNA-programmable assembly and templating. *Science Advances* 10 (2024). https://doi.org:10.1126/sciadv.adl0604

9. Arnon, Z.A., Piperno, S., Redeker, D.C., Randall, E., Tkachenko, A.V., Shpaisman, H., and Gang, O. Acoustically Shaped DNA-programmable Materials. *Nature Communications* (2024), accepted

10. Kahn, J.S., Minevich B., Michelson, A., Emamy, H., Kisslinger, K., Xiang, S., Kumar, S.K., Gang, O., Encoding Hierarchical 3D Architecture through Inverse Design of Programmable Bonds. ChemRxiv. (2022); doi:10.26434/chemrxiv-2022-xwbst

Data-driven learning of dissipation from microscopy of chemically active materials

Jason R. **Green**, University of Massachusetts, Boston

Joseph P. Patterson, University of California, Irvine

Keywords: Dissipative self-assembly, dynamic mode decomposition, liquid phase electron microscopy

Research Scope

Dissipative materials stand out in their potential to function dynamically, forming patterns and generating work. With supramolecular hydrogels, there is an opportunity to implement this functionality from the molecular scale by designing the chemical kinetics to control the number, lengths, and lifetimes of fibers assembled at the mesoscale. However, the dissipative processes involved can have a strong influence on the structure, function, and efficiency of the resulting materials. Our research program aims to establish the necessary framework for learning dissipation directly from experimental data, using theory and computation to guide further experimentation and material design. More specifically, we aim to measure dissipation in active supramolecular materials monitored through four specific aims: (i) quantify the structural dynamics of nanomaterials from in-situ electron microscopy, (ii) develop data-driven methods to measure the dissipation associated with material formation, (iii) train and GPU accelerate these methods on physically-relevant reaction-diffusion models, and (iv) validate our AI models of the dynamics against experimental data.

Recent Progress

Chemically active materials form complex spatiotemporal structures but also dissipate energy as heat, produce entropy, and waste free energy. Our program aims to learn how dissipative these structures are by applying nonequilibrium statistical mechanics and dynamic mode decomposition (DMD) to images from time-resolved microscopy. We have made progress along several fronts.

Dynamic mode decomposition for multiscale modeling and estimates of dissipation. At a high level, the algorithm systematically builds a dynamical model from high-dimensional data that captures predictable behaviors and identifies irrelevant noise. While it has been widely used for traffic flow and fluid dynamics, it has not yet been used as a technique to learn dissipation, so we have been adapting this algorithm and validating it against numerical simulations of model systems (assembling colloidal particles, damped oscillators, and Fickian diffusion). So far, we have shown that DMD can learn the energy dissipation rate in damped oscillators and the entropy production

rate in (i) Fickian diffusion and (ii) the nonequilibrium assembly of Lennard-Jones clusters interacting with a heat bath. These test cases are important groundwork for our aim to apply this approach to experimental and simulation images for chemically active materials at micron length and second timescales. In parallel with these benchmarks, we have continued developing our reaction-diffusion model for solitary, wave fronts (Figure 1). This model reproduces the behavior observed with liquid-phase transmission electron microscopy.

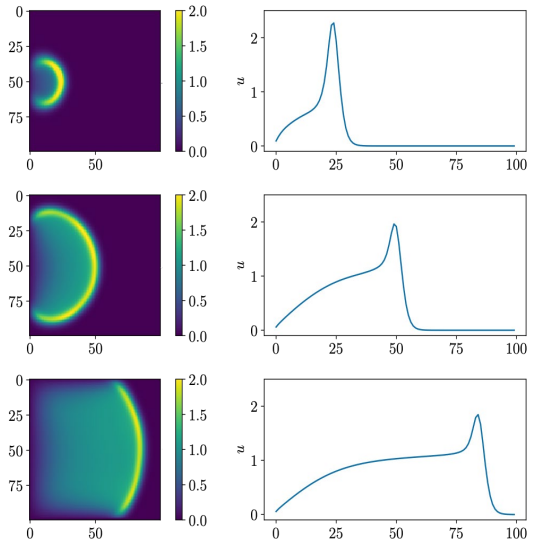

Figure 1. A model for a chemically-active supramolecular material (CSSC/CSH) generates solitary waves of active material in reaction-diffusion simulations. The wave front profile has

Quantify the structural dynamics of nanomaterials with in-situ electron microscopy. Because of their dynamic nature, ex-situ experimental analysis of these materials is challenging, sometimes impossible. As a result, the in-situ imaging methods we are using become essential. While structural changes in microscopy videos are often visually apparent, numerically quantifying the rate of change, temporal scale, and spatial scale of dynamic behavior is challenging. In a recent study, we developed a structural dissimilarity index measure (DSSIM) analysis as a general method of spatially and temporally quantifying dissipative structural dynamics in confocal microscopy videos. The DSSIM is a standard measure of the difference between two images, which compares variation in the mean, variance, and cross-correlation between local regions. DSSIM analysis has been widely adopted by the machine learning community as a metric to evaluate the performance of denoising and super-resolution models for microscopy datasets.

The experimental aim of this project is to quantify the structural dynamics of dissipative nanomaterials with in-situ electron microscopy. So far, we have collected preliminary data sets for an electrochemically active material (CSSC/CSH) with in-situ Liquid TEM. A several months effort was necessary to install a new holder cell in the instrument that will lead to improved images and temperature control. After processing data sets with DSSIM, we have begun analyzing the data with dynamic mode decomposition. To establish a workflow between theory and experiment and validate our DMD predictions, we are simulating transmission electron microscopy experiments with the open source package *ab*TEM. This simulation step provides an additional layer to investigate the impact of spatial and temporal resolution on measurements of dissipation with DMD.

GPU-accelerated supercomputing for data-driven discovery and multiscale simulations. Computationally, we are working to achieve a speedup in the timeline from hypothesis to corroboration by building a GPU accelerated codebase for our theory-informed ML techniques. GPU-accelerated codes are extremely effective at massively parallel linear algebra, making them well-suited to our theory and simulations. To parallelize our codes, we are collaborating with the cuNumeric team at NVIDIA. CuNumeric aims to provide 1-to-1 functionality with Numpy and specializes in optimizing Python programs with large datasets by spreading the computational load over multiple nodes. These libraries allow for immediate parallelization of our codes and a way to ultimately accelerate the materials design process. They are working to add all the linear algebra we need for our scientific objectives. Thus far, NVIDIA has implemented SVD and QR decompositions in cuNumeric. We are beginning to test these implementations numerically on single GPUs and our DMD code.

Future Plans

On the computational front, we plan to test the cunumeric NVIDIA implementation of SVD/QR on our algorithm for dynamic mode decomposition. While single CPU calculations are sufficient for the current development phase, we aim to scale up our methods for datasets that require multi-GPU computation. Some initial benchmarking and scaling will likely be necessary. In parallel, we plan to build on our success using DMD to predict entropy production and energy dissipation rates. An objective of our future work is to further develop the theory of DMD and demonstrate its ability to predict dissipation for reaction-diffusion simulations and simulated TEM images of nanoparticle self-assembly. We also propose to explore the parameter space of these systems, as well as the effects of shot noise from the TEM electron dose, to investigate the conditions where experimental data is likely to yield high fidelity measurements of dissipation.

References

1. W. S. Gibson, J. T. Mulvey, S. Das, S. Selmani, J. G. Merham, A. M. Rakowski, E. Schwartz, A. I. Hochbaum, Z. Guan, J. R. Green, J. P. Patterson, *Observing the dynamics of an electrochemically driven active material with liquid electron microscopy*, ACS Nano **18**, 11898 (2024).

2. P. J. Hurst, J. T. Mulvey, R. A. Bone, S. Selmani, R. F. Hudson, Z. Guan, J. R. Green, J. P. Patterson, *CryoEM reveals the complex self-assembly of a chemically driven disulfide hydrogel*, Chemical Science **15**, 1106 (2024).

A framework for exploring and controlling non-equilibrium coherent states in active fluids based on global phase space geometry

Piyush **Grover** (PI) and Jae Sung Park (co-PI), Mechanical and Materials Engineering, University of Nebraska-Lincoln

Michael M. Norton (Co-PI), School of Physics and Astronomy, Rochester Institute of Technology

Keywords: Active fluids, active turbulence, nonequilibrium steady states, pattern formation, reaction-diffusion

Research Scope

We are developing theoretical and computational tools using nonlinear dynamics theory to expose the *global phase space* of active fluids. In this project, we have showed that this infinite dimensional phase space in active nematics is populated by *Exact Coherent Structures* (ECS), which are exact solutions of the physical dynamics with distinct and regular spatiotemporal structure; examples include unstable equilibria, periodic orbits, and traveling waves. The ECSs are connected by dynamical pathways called invariant manifolds. Our main hypothesis is that active/mesoscale turbulence corresponds to a trajectory meandering in this phase space, transitioning between neighborhoods of the ECSs by traveling on the invariant manifolds.

A key objective is to develop a framework for predicting and classifying various classes of ECSs, and dynamical connections between them, as well as quantifying their robustness with respect to change in system parameters and geometry. The analysis will be based on exploiting various symmetries inherent in the active fluid systems, as well as the interplay between system symmetries and geometric properties of invariant manifolds. We will derive reduced-order representation of the phase space in terms of a directed graph, in which ECS are nodes, and dynamical connections are edges. This representation uncovers nontrivial relationships in phase space, which can be exploited to induce desired transitions using minimal external control input. We plan to verify the ECS hypothesis in the fully turbulent regime in simulations, as well as using existing data from active nematic experiments carried out at Brandeis University.

Another objective is to build upon the insights from the first objective to develop a theoretical and computational machinery for incorporating a controller into the material itself. This type of embedded or `endogenous' control is the defining feature of biological systems, where chemomechanical pathways orchestrate the dynamics of life at all scales. Motivating examples include morphogenesis, whereby feedback between chemical patterns and tissue structure leads to robust structure formation. Our goals include the design of a feed-forward controller in which a reaction-diffusion process patterns the active stress field with the goal of targeting a specific active nematic pattern, and design of two-way coupled reaction-diffusion processes to active flow dynamics that leverage active, directed transport of chemical signals and curvature sensing.

Recent Progress: Shadowing of exact coherent structures in pre-turbulent active flows: We have previously developed computational algorithms and an open-source computational toolbox (ECSAct) for efficient computation of various type of ECS for the 2D active nematic channel flow [1,2]. The toolbox also computes the stability of each ECS and enables the computation of dynamical connections between various pairs of ECS. Our recent work has focused on numerical investigation of the ECS hypothesis, which says that typical trajectories `shadow' various ECSs.

In the pre-turbulent regime at a single medium activity value, we have computed over 50 ECS. To verify the conjecture, we seeded thousands of trajectories along the unstable manifold of the unidirectional laminar flow solution. We constructed time-averaged *trajectory densities* in a 2D phase space projection. The trajectory density plot (Fig 1a) captures the transient statistics, and regions of high density in that plot are where trajectories spend the most time within the initial transient period before settling on an attractor. Many of such high density regions coincide with unstable (saddle-type) and stable ECS, hence providing evidence in support of our conjecture. To confirm that this *apparent* shadowing of unstable ECS indeed describes a feature of the full phase space dynamics, we compute a time-dependent symmetry-reduced distance between a trajectory and all ECSs in the full phase space. This symmetry-reduced distance (color gradient) is shown at a set of fixed timepoints (horizontal axis) and with respect to several ECSs (vertical axis) in Fig. 1b. Several shadowing events are clearly visible as horizontal red/black segments, where the symmetry-reduced distance is small.

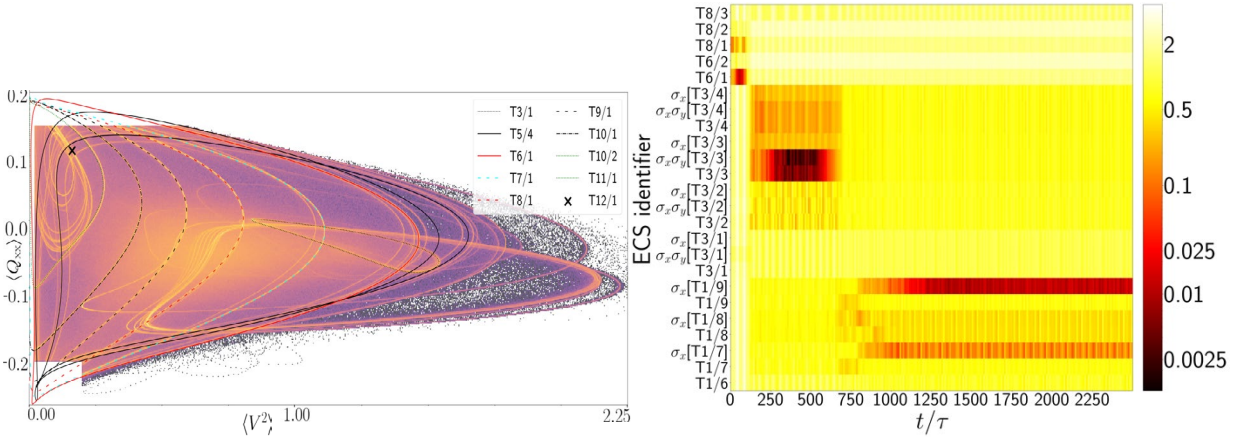

(a) (b)

Fig. 1. (a) A low-dimensional projection of trajectory 'densities' in the preturbulent regime, shown along with projections of various ECSs. The apparent overlap of high density regions (yellow) with unstable ECSs suggests the occurrence of shadowing. (b) The color gradient plot shows the distances between a time-dependent trajectory and a selection of ECSs in full phase space. The figure shows two shadowing events of unstable ECSs in black, and the trajectory eventually approaches an attractor (stable ECS).

Endogenous defect sensing in active nematics: We have previously proposed a reaction-diffusion defect sensing system for active nematics [3]. Recently, we have numerically quantified its performance in various ways. Briefly, our model of defect sensing operates by

creating a concentration field whose maxima and minima approximately coincide with topological defects of the active nematic within which it is embedded. The concentration field ρ (Fig. 2c) is created by deformation-activated reaction-diffusion dipoles that also orient perpendicular to the director. This emergent polar field (Fig. 2b) essentially turns half-integer defects into sources and sinks. There are multiple examples of tight coupling between chemistry and topology in biology; the system we develop possesses qualitatively similar features to a mechanism used by plants to organize root growth via active and coordinated transport of growth hormones [4,5,6].

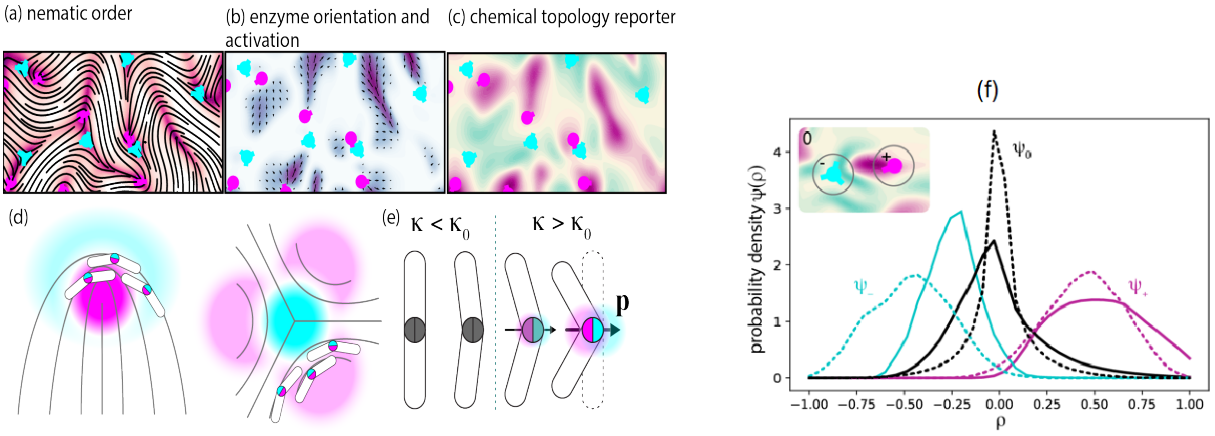

FIG 2: (a) Simulated active nematic field and corresponding (b) dipole strength and orientation, and (c) resulting chemical field ρ; (d,e) shows idealized behavior and schematic illustrating bend activation and orientation of reaction-diffusion dipoles. (f) Probability distribution functions of ρ in regions containing -1/2 defects (dark cyan), +1/2 defects (purple), or no defects (black) quantifies the performance of the defect detection system (solid) in the reaction-diffusion-dominated regime compared to diffuse charge density proposed in ref. [7] (dashed). Inset: regions are considered to belong to a defect if they fall within one nematic coherence length of a defect core.

The concentration field created by this source/sink distribution naturally diffuses and convects with the active flow, reducing the fidelity of the system (e.g. the correspondence between defect position and the labeling field). To help localize the field, we introduce a first-order degradation term and quantify performance as a function of diffusivity. In fig. 2f, we examine the distributions of ρ near +/- 1/2 defects and neutral regions. We see clear peaks for each region; however, the distributions are not entirely disjoint, indicating ambiguity. We found that ambiguity is minimized when the degradation reaction and diffusivity are both high compared to convection. In additional simulations, we find that adding phase separation dynamics to ρ dramatically increases correspondence to defects, demonstrating that mimicking biological phase separation to enhance signals can benefit engineered feedback loops in synthetic active matter.

Future Plans: Flow-reversal cycles and ECS shadowing in turbulent regime: While individual ECS lend structure to localized regions of phase space, the global structure is defined by connecting orbits between the ECS. We will exploit geometric/topological properties of invariant manifolds of ECS and the symmetries of the AN system to understand the origin and

robustness of different connecting orbits, as well as flow-reversal cycles discovered in our numerical work (Fig. 3a), and in experiments by others [8]. The other task is to compute quasiperiodic ECS that are conjectured to be shadowed in turbulent active nematic flows, and numerical verification of ECS hypothesis in the turbulent regime.

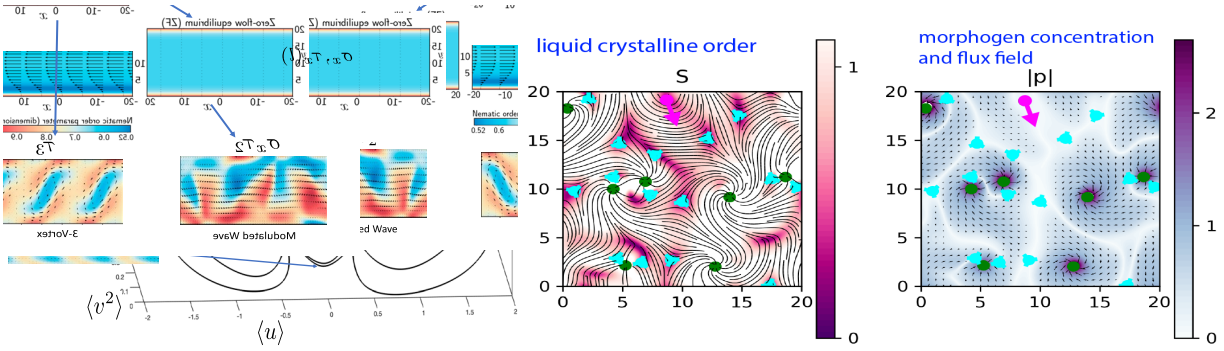

(a) (b) (c)

FIG 3: (a) 3D Phase space projection of a flow-reversal cycle, cycling between unidirectional right and left flowing steady states, with close approach to a lattice vortex state. (b) Active nematic with two-way coupling to an (c) actively pumped morphogen.

From Defect sensing to two-way chemomechanical coupling: We've begun exploring the behavior of systems in which two-way chemomechanical coupling is fully realized and creates new dynamical behaviors. Fig. 3(b,c) shows one such example where we expand on the plant morphogenesis inspiration described earlier by letting nematic extensile stresses arise only in regions of a high morphogen concentration. The morphogen is a species that is actively pumped by a polar field, which itself orients along morphogen gradients [4,5,6]. When coupling between nematic, polar, and concentration fields is high, typically motile nematic +1/2 defects spontaneously merge into a lattice of spiral +1 defects that drive local circulating flows. Our goal in the next years is to examine system behaviors as a function of forward and backward coupling between chemical and mechanical fields using our ECS toolbox.

References

1. C.G. Wagner, M.M. Norton, J.S. Park, and P. Grover**,** Exact coherent structures and phase space geometry of preturbulent 2D active nematic channel flow, Physical Review Letters, **128**.2: 028003 (2022)
2. C.G. Wagner, R.H. Pallock, M.M. Norton, J.S. Park, and P. Grover, Exploring regular and turbulent flow states in active nematic channel flow via Exact Coherent Structures and their invariant manifolds, Physical Review Fluids 8.12 (2023): 124401
3. M. M. Norton, and P. Grover, Mechanochemical Topological Defects in an Active Nematic, arXiv:2210.03796 (2022)

4. O. Leyser, “Plant hormones: Ins and outs of auxin transport,” Current Biology, vol. 9, pp. R8–R10, Jan. 1999.
5. E. Benková, M. Michniewicz, M. Sauer, T. Teichmann, D. Seifertová, G. Jürgens, and J. Friml, “Local, Efflux-Dependent Auxin Gradients as a Common Module for Plant Organ Formation,” Cell, vol. 115, pp. 591–602, Nov. 2003.
6. M. G. Heisler, O. Hamant, P. Krupinski, M. Uyttewaal, C. Ohno, H. Jönsson, J. Traas, and E. M. Meyerowitz, “Alignment between PIN1 Polarity and Microtubule Orientation in the Shoot Apical Meristem Reveals a Tight Coupling between Morphogenesis and Auxin Transport,” PLoS Biology, vol. 8, p. e1000516, Oct. 2010
7. M. L. Blow, S. P. Thampi, and J. M. Yeomans, “Biphasic, lyotropic, active nematics,” Physical Review Letters, vol. 113, no. 24, 2014.
8. Doré, Claire. Active nematic films under confinement: harnessing topological defects, shaping active flows and designing autonomous microfluidic machines. Ph.D. thesis, Université Paris sciences et lettres, 2022.

Publications (last 2 years)

1. C.G. Wagner, R.H. Pallock, M.M. Norton, J.S. Park, and P. Grover, Exploring regular and turbulent flow states in active nematic channel flow via Exact Coherent Structures and their invariant manifolds, Physical Review Fluids 8.12 (2023): 124401
2. C.G. Wagner, M.M. Norton, J.S. Park, and P. Grover**,** Exact coherent structures and phase space geometry of preturbulent 2D active nematic channel flow, Physical Review Letters, **128**.2: 028003 (2022)
3. M. M. Norton, and P. Grover, Mechanochemical Topological Defects in an Active Nematic, arXiv:2210.03796 (2022)
4. T. E. Bate, M. E. Varney, E. H. Taylor, J. H. Dickie, C.-C. Chueh, M. M. Norton, and K.-T. Wu., Self-mixing in microtubule-kinesin active fluid from nonuniform to uniform distribution of activity. Nature Communications **13**, 6573 (2022)
5. A.M. Ibarra and J.S. Park, Transition to turbulence in viscoelastic channel flow of dilute polymer solutions,
   Journal of Fluid Mechanics, 976 (2023): A28
6. C.G. Wagner and P. Grover, Exact Coherent Structures for Active Matter (**ECSAct v1.0**): Open-source library available at https://github.com/DynamicalSystemsLab-UNL/ECSActV1.0 (2023)

Bioinspired Design of Dissipative Self-assembly of Supramolecular Materials Zhibin **Guan**, University of California, Irvine, Irvine, CA 92697 (zguan@uci.edu)

Keywords: dissipative self-assembly, active materials, electrical fuel, supramolecular materials, coacervates

Program Scope

The main goal of this project is to mimic nature's out-of-equilibrium self-assembly processes to create active materials using redox chemistry. Fuel-driven, out-of-equilibrium assemblies like microtubules and actin filaments are essential for many cellular functions, including transport, motility, proliferation, and morphogenesis. These natural processes have inspired the design of synthetic self-assembled systems powered by chemical fuels. However, existing chemical-fueled dissipative assemblies face significant challenges, such as the use of harsh and toxic fuels, waste production, low fueling efficiency due to nonproductive background reactions, and a lack of precise spatiotemporal control. These issues significantly impede the further development of active materials for practical applications. With the support of DOE, this project aims to address these challenges by developing an out-of-equilibrium self-assembly system using a mild chemical, electrochemical, and photo redox reaction networks. During this review period, we have developed a fully electrically fueled dissipative self-assembly system that is waste-free, highly sustainable, and capable of precise spatiotemporal control. Furthermore, by using light and electricity as non-invasive, spatiotemporally controllable energy sources, we demonstrate precise control over the dissipative self-assembly of supramolecular materials. Most recently, we have developed a fully electrically fueled dissipative self-assembly of active coacervate system.

Recent Progress

1. Fully electrically fueled dissipative self-assembly of active nanofibers

During this review period, we developed a waste-free, fully electrically fueled dissipative self-assembly system by coupling two electrocatalytic cycles (*J. Am. Chem. Soc.,* **2023**, *145*, 3727–3735; DOI: 10.1021/jacs.2c13140). The anodic cycle generated a catalytic oxidant ($[Fe(CN)_6]^{3-}$) that initiated fiber self-assembly, while the cathodic cycle produced a catalytic reductant ($[MV]^{+\bullet}$) that triggered disassembly. This system achieved transient fiber assembly through the controlled application of electrical voltage, balancing oxidation and reduction for continuous dynamic self-assembly. This integration allowed precise spatiotemporal control and sustained operation over an extended period. Compared to chemical-fueled systems, our electrically fueled approach produces no waste and maintains a homeostatic active state indefinitely. This platform offers a promising foundation for exploring other redox-active supramolecular assemblies, potentially leading to future bioelectronic applications.

2. Dual light and electrical fuels provide precise control of dissipative self-assembly

In another study, we combined light and electricity as clean, spatiotemporally controllable fuels to precisely regulate the morphology of dissipative self-assembly of a perylenebisimide glycine (PBIg) building block in a self-contained solution (*Chem. Eu. J.* **2023**, *29*, e202300347; DOI: 10.1002/chem.202300347). Electrochemical oxidation served as the positive fuel to promote PBIg self-assembly, while photoreduction acted as the negative fuel to induce disassembly. By programming these counteracting fuels, we controlled the self-assembly of PBIg into various morphologies. Additionally, using both light and electrical fuels simultaneously created dynamic instability and morphological changes, resulting in asymmetric assemblies with curvatures. This precise control over self-assembly could have future applications in programming complex active materials and designing pharmaceutical reagents with specific morphologies. This is the first report of utilizing both light and electricity to fuel a dissipative self-assembly system. By sequencing photoreduction and electrochemical oxidation, we achieved diverse aggregate morphologies for the same building block without changing the solution composition. The dual fuel system also induced morphological changes to asymmetric assemblies with curvatures. Such control over supramolecular assemblies in self-contained systems may have future applications in programming complex active materials and formulating pharmaceutical reagents with desired morphologies.

3. Dissipative self-assembly of active coacervates fueled by electricity

In a recent study, we successfully developed a dissipative self-assembly of active coacervates fueled by electricity. In this study, we applied our e-fueled, waste-free, sustainable route to fuel a liquid-liquid phase-separation (LLPS) self-assembly of a redox-sensitive short peptide. Informed by our previous studies of redox-fueled dissipative self-assembly of active fiber materials, this system employs a thiol-to-disulfide redox interconvertion for generating dissipative coacervates. Specifically, electrochemical oxidation creates $[Fe(CN)_6]^{3-}$ at the anode which oxidizes a dipeptide derivative FF-SH to FFssFF, leading to LLSP into coacervate droplets. Simultaneously, $[MV]^{+\bullet}$ formed at the cathode reduces FFssFF back to FF-SH, resulting dissipation of the coacervate droplets. Applying an electrical potential to reach steady state, we were able to establish an dissipative self-assembly of active coacervates (**Figure 1a**).

Furthermore, we demonstrated that the dissipative coacervates can recruit a separate, redox inactive dipeptide (isoleucine-phenylanaline, IP) and induce its secondary self-assembly inside of the coacervate droplets (**Figure 1b**). We added IP to the FF-SH buffer solution with the IP bulk concentration below its critical assembly concentration (C_c). Without coacervation, there was no self-assembly of IP in the bulk solution. In contrast, upon applying an electrical potential to the system dissipative coacervation of FF-SH/FFssFF occurred, recruiting and enriching IP in the coacervates and inducing its secondary assembly. Confocal fluorescence microscopy images

clearly show the formation of FFssFF coacervates were able to recruit IP dipeptide and induced IP secondary assemblies that autofluorescence.

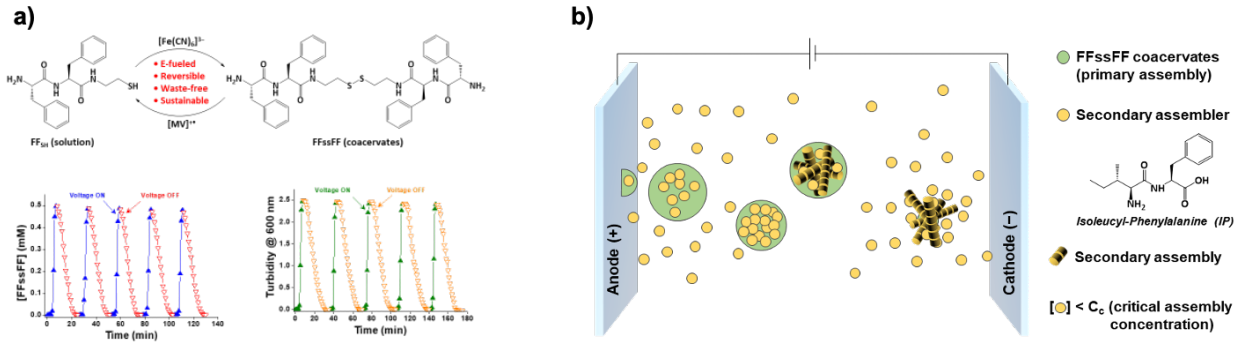

Figure 1. Dissipative self-assembly of active coacervates fueled by electricity. a) Kinetics for active coacervate formation and dissipation upon electrochemical oxidation and reduction. b) Schematic illustration of using active coacervates to recruit IP dipeptide and induce its secondary assembly inside of the coacervates.

Future Plans

In our further study, we will continue investigating the dissipative coacervate system. One particular focus is on demonstrating the capability of dissipative coacervates for recruiting and transporting molecular cargoes.

Publications in year 2022-2024 (which acknowledge DOE support):

1. Gibson, W.; Mulvey, J. T.; Das, S.; Selmani, S. Merham, J. V.; Rakowski, A. M.; Schwartz, E.; Hochbaum, A.; Guan, Z.; Green, J. R.; Patterson, J. P. "Observing the Dynamics of an Electrochemically Driven Active Material with Liquid Electron Microscopy" *ACS Nano* **2024**, *18*, 11898–11909; https://pubs.acs.org/doi/10.1021/acsnano.4c01524.
2. Wei, H.; Pascual-Herrero, H.; Selmani, S.; Marroquin, S.; Reginato, G. D.; Guan, Z.; Ragan, R. "Nanoantennas Report Dissipative Assembly in Oscillatory Electric Fields" *J. Colloid Interface Sci.* **2024**, *666*, 629-638; https://www.sciencedirect.com/science/article/pii/S0021979724007124?via%3Dihub
3. Song, Y. M.; Selmani, S.; Freites, J. F.; Guan, Z.; Tobias, D. J. "Multiscale Molecular Dynamics Simulations of an Active Self-Assembling Material" *J. Phys. Chem. B* **2024**, *128*, 1266–1274; https://pubs.acs.org/doi/10.1021/acs.jpcb.3c06572.

4. Castro, J.; Westworth, X.; Shrestha, R.; Yokoyama, K.; Guan, Z. "Efficient and Robust Dynamic Crosslinking for Compatibilizing Immiscible Mixed Plastics through In Situ

Generated Singlet Nitrenes" *Adv. Mater*. **2024**, 2406203; https://onlinelibrary.wiley.com/doi/10.1002/adma.202406203.

5. Yokoyama, K.; Guan, Z. "A Vitrimer Acts as a Compatibilizer for Polyethylene and Polypropylene Blends" *Angew. Chem., Int. Ed.* **2024**, e202317264; https://onlinelibrary.wiley.com/doi/epdf/10.1002/anie.202317264.
6. Hurst, P. J.; Mulvey, J.; Bone, A. R.; Selmani, S.; Hudson, R. F.; Guan, Z.; Green, J. R.; Patterson, J. P. "CryoEM reveals the complex self-assembly of a chemically driven disulfide hydrogel" *Chem. Sci*. **2024**, *15*, 1106–1116; https://pubs.rsc.org/en/content/articlepdf/2024/sc/d3sc05790a
7. Barpuzary, D.; Hurst, P.; Patterson, J.; Guan, Z. "Waste Free Fully Electrically Fueled Dissipative Self-assembly System" *J. Am. Chem. Soc.* **2023**, *145*, 3727–3735. https://pubs.acs.org/doi/10.1021/jacs.2c13140
8. Chen, C.; Guan, Z. "Precise Control of Dissipative Self-assembly by Light and Electricity" *Chem. E. J.* **2023**, *29*, 9, e202300347. https://doi.org/10.1002/chem.202300347
9. Jo, H.; Selmani, S.; Sim, S.; Guan, Z. "Sugar-Fueled Dissipative Living Materials", *J. Am. Chem. Soc.* **2023**, *145*, 811–1817. https://pubs.acs.org/doi/full/10.1021/jacs.2c11122
10. Tretbar, C. A.; Castro, J.; Yokoyama, K.; Guan, Z. "Fluoride-Catalyzed Siloxane Exchange as a Robust Dynamic Chemistry for High-Performance Vitrimers", *Adv. Mater.* **2023**, 2303280. https://onlinelibrary.wiley.com/doi/10.1002/adma.202303280

Machine learning approaches to understanding and controlling active matter

Michael F. **Hagan**, Brandeis University (Principal Investigator)
Seth Fraden, Brandeis University (Co-Investigator)
Pengyu Hong, Brandeis University (Co-Investigator)
Zvonimir Dogic, University of California Santa Barbara (Co-Investigator)

Keywords: Active matter, Machine learning, data-driven methods, optimal control, deep learning

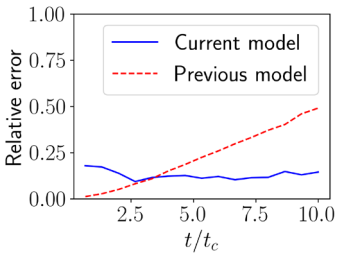

Fig. 1. Deep learning (DL) based model-free forecasting of active nematics. Comparison of error between predicted and ground truth number of defects for the new transformer-based model and the previous model.

Research Scope: In Aim 1, we develop model-free control protocols that redirect active materials to arbitrary new states. We combine experimental data, Deep Learning (DL), and deep reinforcement learning (DRL) to develop a model-independent framework that predicts and controls the dynamics of 3D active materials. The framework does not require the knowledge of the underlying microscopic mechanisms, but leverages the symmetries of the system. In Aim 2, we develop model-predictive control protocols that target preset dynamics. We use optimal control theory to identify spatiotemporal sequences of light-generated activity or crosslinks that direct the dynamics of 3D active matter toward a predetermined steady state. We use the identified control protocols and their efficacy to understand the statistical properties of active stresses and their causal influence on the emergent dynamics. In Aim 3, we combine data-driven approaches to improve physics-based models of active materials. These models describe experiments with higher accuracy, while also revealing how active stresses cascade across scales to generate collective dynamics and functionalities, without a priori knowledge of the microdynamics.

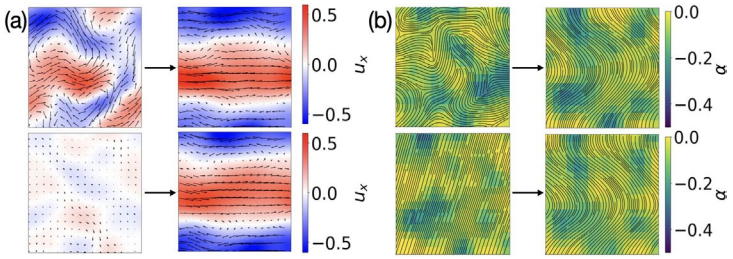

Fig. 2. Deep reinforcement learning (DRL) to control light-activated active nematics. The plots show the initial and final (a) velocity profiles and (b) director field (lines) and activity profile (color map).

Recent Progress: (1) DL tools to measure director and velocity fields from experiments. Our DL tool for generating director fields and identifying defects from experimental fluorescence data was published [1]. It outperforms existing tools and eliminates the need for quantitative polarization microscopy. Traditional Particle Imaging Velocimetry (PIV) techniques yield low-resolution velocity profiles in our systems, unsuitable for data-driven methods. Thus, we adapted a DL-based unsupervised optical flow model to extract flow fields from active nematic image sequences [2]. This framework provides velocity profiles with higher resolution and accuracy than PIV. We anticipate it will become a widely used ML tool in soft matter and beyond.

(2) Model-free forecasting. Our previous work [3] constructed Long-Short Term Memory based models to predict active nematic dynamics but struggled with long-term accuracy. We developed a new model that integrates a transformer and reduced-dimension discrete latent space learning. The model first encodes experimental input frames into a compact latent space, and then uses a transformer-like model to predict future states in this space, which are then decoded back to the input space. Preliminary results show significantly improved long-term accuracy compared to previous models (Fig. 1).

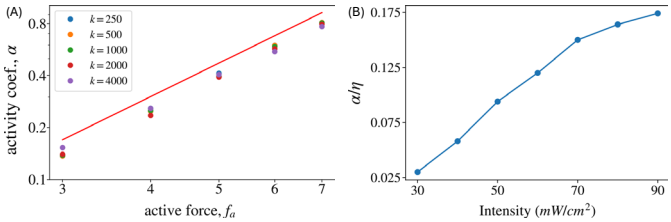

Fig. 3. Data-driven model discovery for 2D dry and light-activated nematics. (A) Activity coefficient as a function of microscopic parameters (bending modulus, k, and active force, f_a) for simulations of dry active nematics. **(B)** The fit coefficient of the activity term, α / η, as a function of the applied light intensity in experiments on light-activated active nematics with spatially varying light profiles.

(3) Model-free control with deep reinforcement learning (DRL). We are developing a DRL framework to control active nematics into new states. We trained a DRL agent to determine spatiotemporal active stress patterns to achieve desired flow states, such as a coherent flow in one direction along a "channel" in a bulk system without confining boundaries (Fig. 2). The DRL agent takes the current system state (director, flow, and activity fields) as input and adjusts the active stress pattern to move the system closer to the target state.

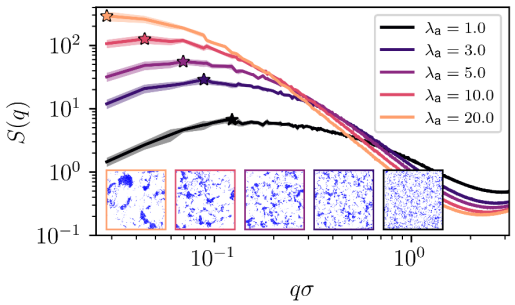

Fig. 4: Simulations of hard sphere self-assembly driven by spatiotemporally correlated active noise, with varying correlation length λ_a and time scale τ_a. Structure factor showing how the emergent length scale of assemblies depends on the active noise correlation length, for correlation timescale $\tau_a = 10$. A snapshot is shown for each curve.

(4) Model-predictive control with optimal control theory: We developed an optimal control theory framework for active fluids. For polar active fluids, we computed protocols that move asters along a predetermined distance and direction, flip the direction of polar flocks, and transform a flock into an aster [4]. For active nematics, we demonstrate controllability of the director and velocity fields into arbitrary target states, including those that are not basins of attraction without control (in preparation).

(5) Data-driven model discovery: We adapted Sparse Identification of Nonlinear Dynamics (SINDy), to determine the equations that capture the system's time evolution, from experiments and computational data. Building on our successful implementation of SINDy on experimental data from 2D MT-based 'wet' active nematics [5], we obtained preliminary equations for 'dry' active nematics (with negligible hydrodynamic interactions), using data from particle-based simulations. Significantly, the physics governing these systems are less understood than for the wet case. We obtain a flow equation of $u = \alpha_0 \nabla . Q + \alpha_1 \nabla \rho$ and a Q-tensor equation of $\partial_t Q = -\lambda_c u \cdot \nabla Q - \lambda_\Omega (\Omega \cdot Q - Q \cdot \Omega) + \lambda_E \left(E - \frac{Tr[E]I}{2} \right) - \lambda_{EQ} (E : Q) Q$. Importantly, SINDy quantitatively estimates key coefficients as a function of microscopic simulation parameters (Fig.

3a). *Wet active nematics with spatially varying activity.* We applied SINDy to light-activated active nematics with spatially varying activity profiles, and obtained a relationship between the active stress and the applied light intensity (Fig. 3b). This is key for implementing optimal control and feedback control in experiments.

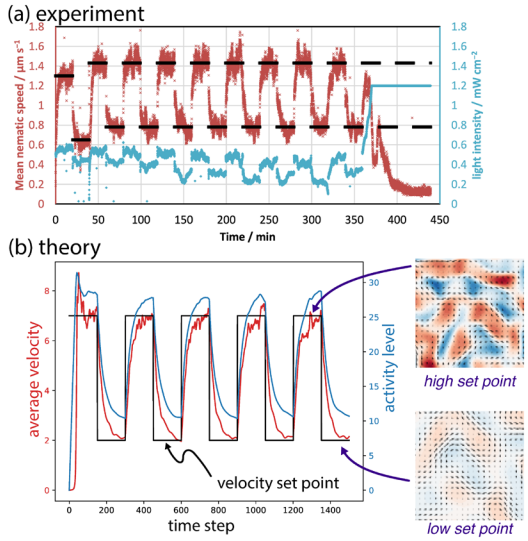

Fig. 5: PI control of light-activated 2D active nematics in (a) experiments and (b) simulations.

(6) Computational approach to simulate viscoelastic networks and self-assembling materials in active fluids. A major challenge in active fluids is to harness their intrinsically chaotic flows to manipulate soft materials to form patterns on desired time and length scales. Motivated by this goal, and the active composite system (Fig. 4), we devised a novel efficient computational approach to model soft materials advected by active fluids with orders of magnitude reduced computation time, by treating the fluid as a spatiotemporally correlated noise field. Our simulations show that modulating the correlation length and time of this noise field tunes the transport properties of suspended tracer particles. Moreover, the spatial correlations of the field lead to novel forms of organization in multiparticle suspensions. Hard spheres form clusters, whose size can be tuned by changing the active noise correlation length and time (Fig. 4). Similarly, the scale of stress fluctuations in elastic networks can be tuned by modifying the active noise parameters. Our results provide insight into the interplay between active fluid time/length scales and emergent driven assembly behaviors. More broadly, our approach efficiently simulates diverse active fluids and other systems with spatiotemporally correlated noise.

(7) Proportional-Integral (PI) control of active nematics in experiments and theory. We implemented closed-loop feedback control of the speed of light-activated active nematics (Fig. 5). The nematics are imaged in a light microscope and the average speed is measured in real time using our optical flow framework. The PI controller sets the light intensity that is projected onto the sample. Remarkably, the speed is controlled within 10% accuracy over 5 hours (Fig. 5a), while the uncontrolled sample reduces speed by 100% over the same period due to aggregation. We qualitatively understand the experimental PI-controlled nematics by implementing analogous PI control in a canonical PDE model of nematohydrodynamics (Fig. 5b**)**. Both experiment and simulation exhibit classical behaviors of P and PI-controlled systems (e.g. steady-state velocities below the set point (droop) for P control, and overshoot and oscillations for PI-control).

(8) Active composite experiments: By integrating the MT-based active fluid within a passive elastic network we observe a hierarchical self-organized process of remarkable complexity (Fig. 6). The passive component, composed of filamentous actin (F-actin) crosslinked by fascin, forms

a large bundled network with tunable mechanics. We create a well-defined interpenetrating double network by first polymerizing actin around a MT network that lacks activity. In the absence of activity, this network is static, demonstrating that thermally induced fluctuations are negligible. The release of caged ATP initiates MT-based active flows, which drive reorganization of the passive actin network across a hierarchy of length scales. At the shortest length scales, the active flows power collisions between adjacent bundles, forming new connections through fascin-mediated crosslinking. These rearrangements develop a coarsened and disordered network of actin bundles. Over time, the reorganization of crosslinkers and filaments at the microscale generates an elastic network with structural features that are distinct from passively-formed networks. As a connected network is formed, the overall shape of the connected structure separates from the walls of the chamber, contracting toward the midplane. At intermediate times and length scales, the emerging elastic network exhibits local in-plane deformations at scales associated with the disordered active driving, and out-of-plane deformations of the actin sheet on scales similar to the flowing microtubule bundle structures. Finally, the presence of a connected network allows for interactions at longer ranges than the scale of the correlated active flow. On the millimeter scale, the entire actin network undergoes persistent system-size self-shearing oscillations.

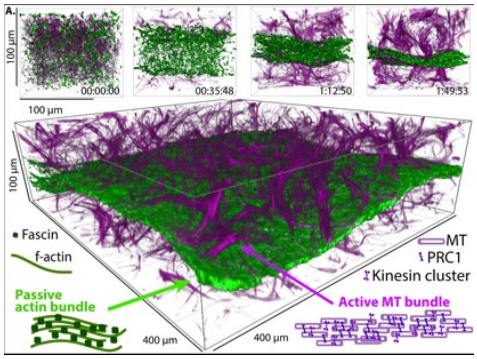

Fig. 6: Active composites: 3D actin network embedded in MT-based active fluid. The active fluid controls the formation, structure, mechanics, shape, and dynamics of the actin network, leading to diverse structures, including elastic membrane-like sheets.

Future Plans: DRL: We will extend the DRL to handle more varied initial conditions. We will combine the DL forecaster with the DRL technique to allow machine learning-driven model-based feedback control. We will extend the forecaster and RL technique to 3D. **PI-Control:** We will quantitatively compare experiment and simulation behaviors of PI controlled nematics under varying control parameters. Key measurements will be the steady state value of the controller, the time constant associated with reaching steady state, and statistical properties of the velocity fluctuations about the steady state (such as correlation times and power spectra). **Data-driven model discovery:** We will build on the application of our SINDy implementation to data from systems with spatiotemporally varying activity profiles (Fig. 3b) to identify appropriate models. We will apply the optical flow and SINDy frameworks to 3D active isotropic and active nematic systems. **Light-activated nematics experiments and theory:** We are working to eliminate the aggregation in the light sensitive motors. Once this is accomplished, we will build on the success in implementing PI control, by using our optimal control [4, 6] and DRL (Fig. 2) frameworks to enable more complex feedback control protocols. Using these results, we will create controllers that aim for activity patterns leading to arbitrary emergent behaviors, including coherent flows that perform work. **Active composites:** The complex dynamics of active composites is not understood. We will apply a suite of the above-described techniques to elucidate their quantitative models.

Publications

1. Joshi, C., Ray, S., Lemma, L. M., Varghese, M., Sharp, G., Dogic, Z., Baskaran, A. & Hagan, M. F. Data-Driven Discovery of Active Nematic Hydrodynamics. *Phys. Rev. Lett.* **129**, 258001, (2022).
2. Lemma, L. M., Varghese, M., Ross, T. D., Thomson, M., Baskaran, A. & Dogic, Z. Spatio-temporal patterning of extensile active stresses in microtubule-based active fluids. *PNAS Nexus* **2**, doi:10.1093/pnasnexus/pgad130 (2023).
3. Li, Y., Z. Zarei, P.N. Tran, Y. Wang, A. Baskaran, S. Fraden, M.F. Hagan, and P. Hong, A machine learning approach to robustly determine director fields and analyze defects in active nematics. *Soft Matter*, 2024. 20(8): p. 1869-1883, https://doi.org/10.1039/D3SM01253K (2024).

4. Tran, P.N., S. Ray, L. Lemma, Y. Li, R. Sweeney, A. Baskaran, Z. Dogic, P. Hong, and M.F. Hagan, Deep-learning Optical Flow Outperforms PIV in Obtaining Velocity Fields from Active Nematics. *arXiv.2404.15497*, https://doi.org/10.48550/arXiv.2404.15497 (2024).

Cited References

1. Li, Y., Z. Zarei, P.N. Tran, Y. Wang, A. Baskaran, S. Fraden, M.F. Hagan, and P. Hong, *A machine learning approach to robustly determine director fields and analyze defects in active nematics.* Soft Matter, 2024. **20**(8): p. 1869-1883.
2. Tran, P.N., S. Ray, L. Lemma, Y. Li, R. Sweeney, A. Baskaran, Z. Dogic, P. Hong, and M.F. Hagan, *Deep-learning Optical Flow Outperforms PIV in Obtaining Velocity Fields from Active Nematics.* arXiv.2404.15497, 2024.
3. Zhou, Z., C. Joshi, R. Liu, M.M. Norton, L. Lemma, Z. Dogic, M.F. Hagan, S. Fraden, and P. Hong, *Machine learning forecasting of active nematics.* Soft Matter, 2020.
4. Ghosh, S., C. Joshi, A. Baskaran, and M.F. Hagan, *Spatiotemporal control of structure and dynamics in a polar active fluid*. 2024: arXiv.2405.07942.
5. Joshi, C., S. Ray, L.M. Lemma, M. Varghese, G. Sharp, Z. Dogic, A. Baskaran, and M.F. Hagan, *Data-Driven Discovery of Active Nematic Hydrodynamics.* Physical Review Letters, 2022. **129**(25): p. 258001.
6. Norton, M.M., P. Grover, M.F. Hagan, and S. Fraden, *Optimal Control of Active Nematics.* Physical Review Letters, 2020. **125**(17): p. 178005.

Chemically fueled dissipative assembly of complex molecular architectures

C. Scott **Hartley** and Dominik Konkolewicz, Department of Chemistry and Biochemistry, Miami University

Keywords: Nonequilibrium, carbodiimides, polymer networks, self-assembly, systems chemistry

Research Scope

Many of the remarkable behaviors of biological materials, such as actuation, self-healing, and replication, derive from complex networks of chemical reactions that operate out of equilibrium. In many cases, these systems are driven by the hydrolysis of ATP, which acts as a chemical "fuel". Inspired by nature's example, abiotic reaction networks based on the same principles are currently being developed, yielding materials and molecular machines with time-dependent behavior.[1]

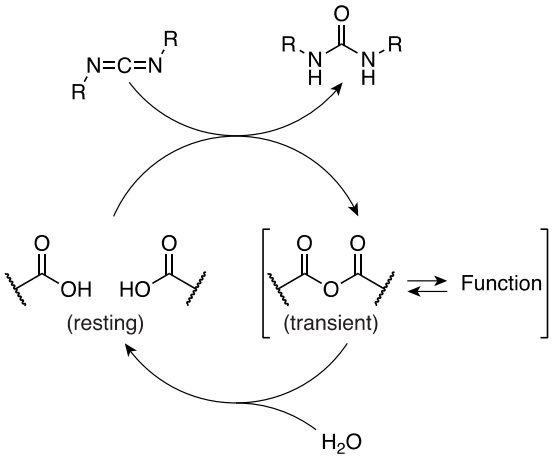

Scheme 1. Treatment of aqueous carboxylic acids with carbodiimides gives transient anhydrides.

Controlling reaction rates within a network is challenging, thus it is important to develop fuel reactions that can be used broadly. The hydration of carbodiimides is among the most versatile of the abiotic fuel reactions developed so far.[2] In its simplest form, shown in Scheme 1, carbodiimides couple aqueous carboxylic acids to anhydrides, resulting in a transient covalent bond. This simple chemistry has been applied to a wide range of functional systems, from molecular motors to responsive polymer materials.

The goal of this project to develop methods to control out-of-equilibrium chemical reaction networks and to exploit them in the design of new functional materials. We currently have three Specific Aims: (1) to develop catalysts to control the rates of anhydride formation, hydrolysis, and exchange in nonequilibrium systems; (2) to develop polymer network hydrogels with both persistent and transient dynamic bonding; and (3) to couple fuel chemistry to phase transitions in materials for amplified responses. The progress reported below is mostly for the previous funding period.

Recent Progress

Transient reinforcement of pre-crosslinked polymer networks. A key focus of our work has been polymer networks where carboxylic-acid-containing monomers are transiently crosslinked on treatment with EDC, a common water-soluble carbodiimide. We had previously demonstrated systems that undergo sol–gel–sol transitions through the temporary crosslinking of dissolved polymer chains.[3] We realized, however, that, for many functional systems, initially solid materials that undergo autonomous changes in mechanical properties may be of more use. We therefore prepared polymer network hydrogels from acrylamide (Am) and acrylic acid (AA) crosslinked with *N*,*N*′-methylene bisacrylamide (MBAm). On treatment with EDC, these materials give increases in their storage moduli (G') of up to an order of magnitude, as shown in Figure 1. Because these materials are solids and remain solids when treated with fuel, they are suitable for new functional behavior: two pieces temporarily adhere when treated with EDC at their interface (with the amount of EDC dictating the adhesion time), and patterns of temporary changes in properties can be induced by spraying films with EDC solution through a mask.

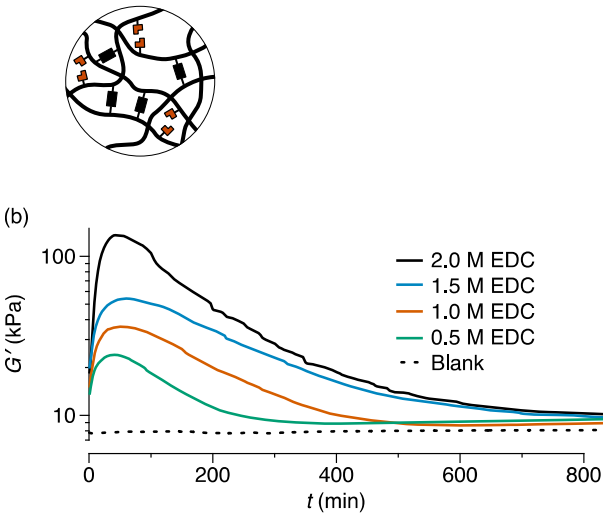

Figure 1. (a) Transient anhydride crosslinking (orange) of polymer networks with permanent MBAm crosslinks (black). (b) Change in storage modulus over time on treatment with EDC.

Network architecture effects in transient polymer networks. The polymer networks discussed above are architecturally simple; they are single networks (SNs) that, on treatment with EDC, also give SNs (but with a higher crosslink density, Figure 1a). Polymer network architecture is, however, well known to have substantial effects on mechanical properties; for example, interpenetrated networks (IPNs), which comprise two or more polymer networks that are intertwined but not covalently connected, can exhibit greatly improved mechanical properties.[4] In principle, transient bond formation can effect transitions between network architectures. We therefore prepared more-complex precursor materials, that, beginning as semi-interpenetrated networks (semi-IPNs), would yield either IPNs or single networks on treatment with the fuel.

On treatment with EDC, the performance of materials beginning as semi-IPNs is on some level

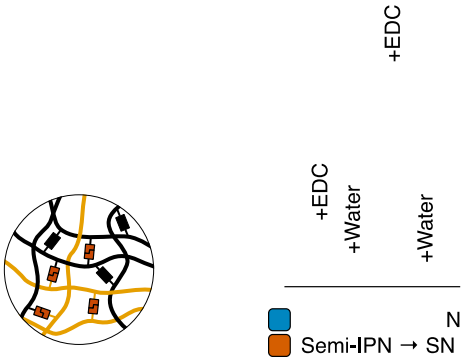

Figure 2. Polymer network architecture effects on fracture energy.

"worse" than that of SNs, with substantially smaller increases in *G′*. Remarkably, despite this behavior, semi-IPNs that form transient IPNs give much improved resistance to compressive strain and much higher fracture energies (resistance to fracture). Figure 2 shows the best case examined, where the material's fracture energy increases by an order of magnitude when EDC is added (compared to roughly twofold increases in systems giving SNs). Consequently, we found that damaged materials that give IPNs on fueling reach much higher strains before breaking compared to analogous SN materials (or the same materials without EDC).

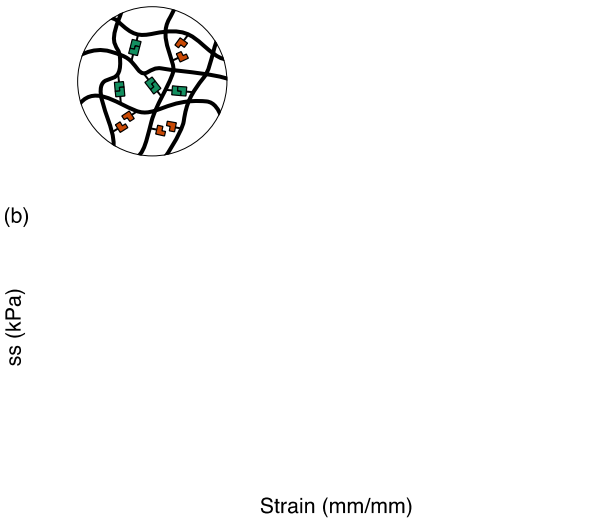

Figure 3. (a) Polymer network hydrogels with both persistent (green) and transient (orange) exchanging crosslinks. (b) Self-healing of a Zn^{2+}-containing system on treatment with water or EDC.

Mixed static/transient dynamic polymer network materials. We are currently exploring the properties of polymer networks that combine transient anhydride crosslinks with persistent dynamic crosslinks (i.e., that exist in the material at rest). Instead of MBAm, the polymers include terpyridine (tPy) monomers that provide dynamic crosslinks through coordination to metals. The hydrogel properties are dependent on the metal used, with, for example, Ni^{2+} forming more stable gels than Zn^{2+}, which gives more stable gels than Cu^{2+}. Importantly, we have found that the metal–ion coordination and anhydride formation and hydrolysis are compatible, with the expected increases in *G′* on treatment of the gels with EDC. Because of the persistent metal–ion coordination crosslinks, these materials are inherently self-healing, as shown in Figure 3. Fueling with EDC provides a boost in mechanical properties while the material self-heals, although not an improvement in its final properties.

Transient polymerization. Transient polymers play important roles in biochemical systems (e.g., actin networks and microtubules). Taking these systems as inspiration, many abiotic transient supramolecular polymers have been reported.[5] We have proposed that transient *covalent* polymers complement these systems by enabling new methods of characterization (e.g., GPC) and easier control over assembly kinetics. These systems are also fundamentally different as the rates of assembly and disassembly are comparable to the rates of fuel consumption (as opposed to supramolecular systems where assembly is generally much faster). We have recently demonstrated the first examples of simple transient covalent polymers, formed by treatment of dibenzoic acid monomers with EDC. Monomer structure, solvent, reactant concentrations, and temperature allow the rates of disassembly to be controlled over orders of magnitude (hours to weeks).

Carbodiimide–pyridine adducts. While there have been significant efforts to control the rate of deactivation (hydrolysis) in carbodiimide-activated systems, the rate of activation (anhydride

formation) has received limited attention. We discovered that a derivative of EDC, mEDC, shown in Figure 4a, undergoes the reversible formation of adducts with pyridine derivatives. These adducts are inert to carboxylic acid; thus, pyridines temporarily deactivate the carbodiimide, reducing its effective concentration in solution. This both slows the rate of activation (anhydride formation) and provides a reservoir of carbodiimide to extend lifetimes. We have demonstrated this with a simple sol–gel–sol polymer system, as shown in Figure 4b. Compared to EDC (which does not form the adduct), for mEDC with 4-methoxypyridine the time to reach peak modulus is increased by 86% and the lifetime is increased by 43%.

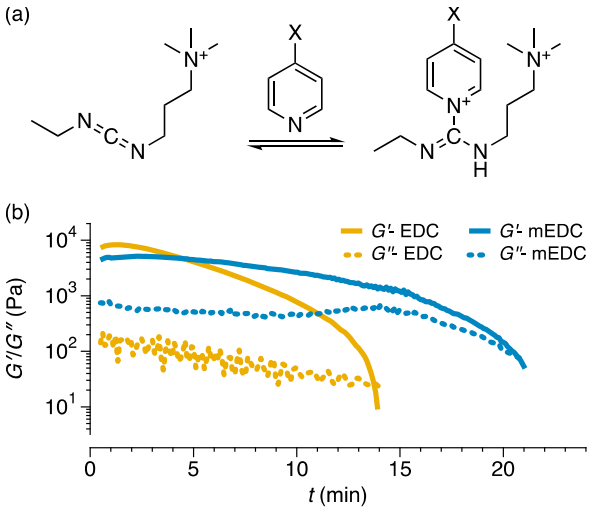

Figure 4. (a) Adduct formation from mEDC and pyridine derivatives. (b) Rheological comparison of transient gel formation from a soluble polymer using either mEDC with 4-methoxypyridine, which gives adduct, or EDC, which does not.

Future Plans

Catalysts for carbodiimide-driven reaction networks. We are examining different catalysts that can be used to control the activation, deactivation, and exchange processes for carbodiimide-driven anhydride formation. The role of exchange in particular is an underappreciated aspect of these systems.

Pluripotent polymer networks. We are continuing our examination of polymer hydrogels with both persistent and transient exchanging crosslinks. We are specifically interested in controlling the relative rates of exchange in these systems so as to achieve synergy and enhanced function (e.g., self-healing, fracture resistance). These same materials are also expected to respond to transient acids in addition to carbodiimides, which we will exploit in a distinct self-healing mechanism.

Phase-transition-induced changes in network materials. Finally, following a productive discussion at a previous program meeting, we are exploring how transient anhydride formation in polymer systems can be coupled to phase transitions for amplified responses to the fuel. Specifically, we will be looking at poly(NiPAm) with different loadings of maleic acid. Treatment with carbodiimide should give a change in hydrophobicity that lowers the lower critical solution temperature (LCST).

References

1. L. S. Kariyawasam, M. M. Hossain, and C. S. Hartley, *The Transient Covalent Bond in Abiotic Nonequilibrium Systems*, Angew. Chem., Int. Ed. **60**, 12648–12658 (2021).

2. P. S. Schwarz, M. Tena-Solsona, K. Dai, and J. Boekhoven, *Carbodiimide-Fueled Catalytic Reaction Cycles to Regulate Supramolecular Processes*, Chem. Commun. **58**, 1284–1297 (2022).

3. O. J. Dodo, L. Petit, C. W. H. Rajawasam, C. S. Hartley, and D. Konkolewicz, *Tailoring Lifetimes and Properties of Carbodiimide-Fueled Covalently Cross-Linked Polymer Networks*, Macromolecules **54**, 9860–9867 (2021).

4. J. P. Gong, Y. Katsuyama, T. Kurokawa, and Y. Osada, *Double-Network Hydrogels with Extremely High Mechanical Strength*, Adv. Mater. **15**, 1155–1158 (2003).

5. A. Sharko, D. Livitz, S. D. Piccoli, K. J. M. Bishop, and T. M. Hermans, *Insights into Chemically Fueled Supramolecular Polymers*, Chem. Rev. **122**, 11759–11777 (2022).

Publications

1. C. W. H. Rajawasam, C. Tran, M. Weeks, K. S. McCoy, R. Ross-Shannon, O. J. Dodo, J. L. Sparks, C. S. Hartley, and D. Konkolewicz, *Chemically Fueled Reinforcement of Polymer Hydrogels*, J. Am. Chem. Soc. **145**, 5553–5560 (2023).

2. M. A. S. N. Weerasinghe, O. J. Dodo, C. W. H. Rajawasam, I. O. Raji, S. V. Wanasinghe, D. Konkolewicz, and N. De Alwis Watuthanthrige, *Educational Series: Turning Monomers into Crosslinked Polymer Networks*, Polym. Chem. **14**, 4503–4514 (2023).

3. C. W. H. Rajawasam, O. J. Dodo, M. A. S. N. Weerasinghe, I. O. Raji, S. V. Wanasinghe, D. Konkolewicz, and N. De Alwis Watuthanthrige, *Educational Series: Characterizing Crosslinked Polymer Networks*, Polym. Chem. **15**, 219–247 (2024).

4. I. O. Raji, O. J. Dodo, N. K. Saha, M. Eisenhart, K. M. Miller, R. Whitfield, A. Anastasaki, and D. Konkolewicz, *Network Polymer Properties Engineered Through Polymer Backbone Dispersity and Structure*, Angew. Chem., Int. Ed. **63**, e202315200 (2024).

5. C. W. H. Rajawasam, C. Tran, J. L. Sparks, W. H. Krueger, C. S. Hartley, and D. Konkolewicz, *Carbodiimide-Driven Toughening of Interpenetrated Polymer Networks*, Angew. Chem., Int. Ed. **63**, e202400843 (2024).

6. N. K. Saha, W. S. Salvia, D. Konkolewicz, and C. S. Hartley, *Transient Covalent Polymers Through Carbodiimide-Driven Assembly*, Angew. Chem., Int. Ed., in press.

7. W. S. Salvia, G. Mantel, N. K. Saha, C. W. H. Rajawasam, D. Konkolewicz, C. S. Hartley, *Controlling Carbodiimide-driven Reaction Networks through the Reversible Formation of Pyridine Adducts*, ChemRxiv, DOI: 10.26434/chemrxiv-2024-qrl52 (2024).

Transport and Molecular Discrimination in Biomimetic Artificial Water Channels for Lanthanide Separations

Manish **Kumar**; Department of Environmental and Chemical Engineering, The University of Texas at Austin.

Keywords: Membrane, lanthanides, supramolecular channel, rare earth elements, pillar[5]arene.

Research Scope: Rare earth elements (REEs), encompassing seventeen metallic elements including fifteen lanthanides along with scandium and yttrium, are indispensable for modern industries and high-tech devices.[1] They play a vital role in renewable energy systems, energy-efficient infrastructure materials including in batteries for electric cars, energy-efficient lighting, display panels, and magnets for wind turbines,[2] medical imaging,[3] petroleum refining,[4] and defense applications.[5] The extensive use of REEs in day-to-day life, combined with their unstable supply chains, has led to a rapidly increasing demand for these critical elements. Demand for some of these elements is estimated to grow by more than 2600% by 2035.[6] Five REEs (Y, Nd, Eu, Tb, and Dy) have been highlighted by the U.S. Department of Energy and the European Commission as at risk for supply disruption and criticality because of their frequent use in low-carbon and green energy technologies, such as wind turbines, electric vehicles, and LEDs.[7, 8] However, the domestic production of these critical elements has declined significantly, while their extraction from natural ores is expensive, energy-intensive, and environmentally harmful.[9] Size-based separation is ineffective due to the nearly identical sizes of lanthanides. To address these challenges, we proposed an affinity-based biomimetic separation technique that utilizes specific ligands for lanthanides. In this study, we have developed supramolecular channels (**Figure 1**) based on a pillar[5]arene scaffold with appended diphenyl phosphine oxide ligands (DPP) and these channels demonstrate remarkable selectivity for lanthanides over commonly found monovalent metal ions (≥18) during electrochemically driven (voltage clamp) transport measurements. These channels exhibit promising selectivity towards medium lanthanides, such as Europium ions, showing a 20-fold preference over heavy lanthanides (Yb^{3+}) and a 41-fold preference over light lanthanides (La^{3+}), while effectively excluding all measured monovalent and divalent ions, including protons. The exceptional selectivity of these channels is attributed to their highly hydrophobic side chains and DPP functional groups, which enable the dehydration of medium lanthanides. Additionally, the oxygen atom positioned above the central ring acts as a selectivity filter. Overall, this novel class of channels presents excellent potential as building blocks for sustainable lanthanide separation membranes.

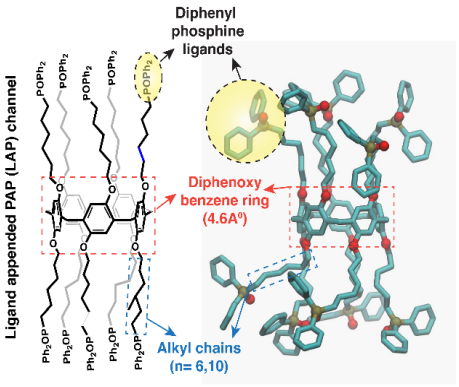

Figure 1 The biomimetic artificial channel proposed combines lanthanide selective filter with selective nanoconfined transport was seen in selective ion channels such as KcsA by decorating DPP ligands at the channel entrance created around the pillar[5]arene central ring .

Recent Progress:

Our overall objective is to discover and design artificial ion channels that could interact and selectively transport metal ions of interest, and then incorporate them into scalable membranes that are manufacturable, robust, and selective (**Figure 2**). We have been successful in synthesizing pillar[5]arene-based channels appended with DPP ligands, referred to as LAP5 channels (**Figure 1**). Ion transport activity and ion-ion selectivity was then measured across the lipid bilayer as a model system. In order to quantify the ion-ion selectivity of these channels, we used patch clamp ion current measurements to determine selectivity under applied potential gradients (**Figure 3**). In this setup, we painted planar lipid bilayer membrane containing multiple channels that separates two chambers with appropriate metal chloride solution to evaluate the electrochemically driven transport of various ions across these channels (**Figure 3A**). In general, under applied potentials, the measured currents for K^+, La^{3+}, and Yb^{3+} ions were close to their background levels (**Figure 3B**), indicating limited transport through the channels. However, noticeable currents were observed for Eu^{3+} ions (**Figure 3B-C**). The selectivity of LAP5n6 for Eu^{3+} over La^{3+} was determined to be 41.4, indicating a preference for the middle lanthanides over the light lanthanides (**Figure 2C**). Similarly, the selectivity of Eu^{3+} over Yb^{3+} was found to be 21.4, suggesting a preference for the mid lanthanides over the heavy lanthanides. These channels also showed high selectivity for Eu^{3+} ions over alkali metal ions with a Eu^{3+}/K^+ selectivity of ~ 18. These selectivity values represent much higher than those observed for single stage solvent extraction (< 3.0) and are the first values reported for a custom designed lanthanide channel.

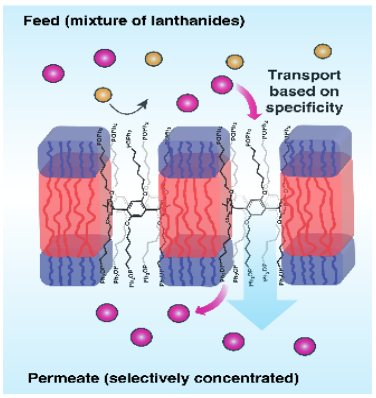

Figure 2. Schematic of continuous solvent-free lanthanide separation by selective transport

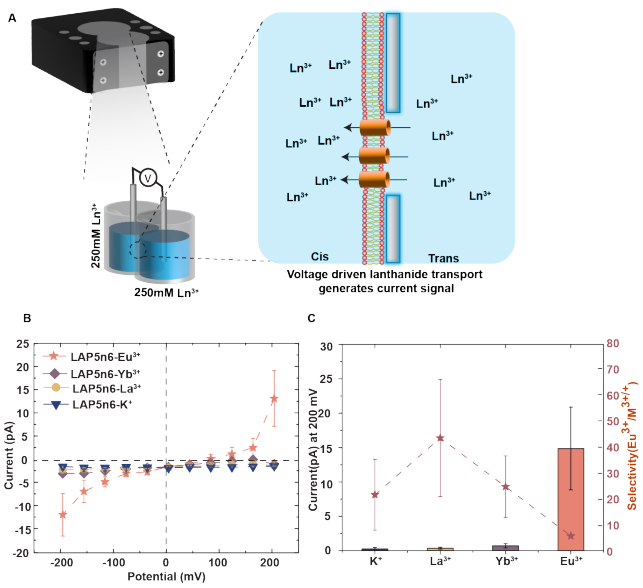

Figure 3: Patch clamp measurements performed on LAP5 channels embedded in painted lipid bilayers. A. Schematic representation of patch clamp apparatus used for conducting measurements **B** Voltage sweeps conducted with various ions provide confirmation of the selectivity of the LAP5n6 channel **C.** Summarized ion/ion selectivity values show high Eu^{3+}/La^{3+}, Eu^{3+}/Yb^{3+} and Eu^{3+}/K^+ selectivity

We have developed a scalable approach for the fabrication of a 3-dimensionally interconnected membrane (refer to as artificial tissues) through simple processing via droplet interface bilayer formation and centrifugation followed by 3D printing (**Figure 4A**). In our experimental setup,

(**Figure 4A**), the tissues were sandwiched between hydrogel layers with appropriate electrolytes on each side and a potential is applied across the membrane. These membranes, composed of 3-dimensionally interconnected lipid/polymeric bilayers, were non-conductive without ion channels (**Figure 4B)**. By successfully incorporating ion channels into the membrane, an ion conductive pathway can be formed. Consequently, an ion-selective membrane can be fabricated if an ion-selective channel is inserted into these membranes. Our initial findings with gramicidin A (gA) incorporated lipid/polymeric artificial tissue membrane showed a significant K^+ ion transport (**Figure 4B**) as compared to the control membrane. Surpassingly, a peptide channel showed significant transport discrimination between heavy and mid lanthanides such as Yb^{3+} and Eu^{3+} ions (**Figure 4C**).

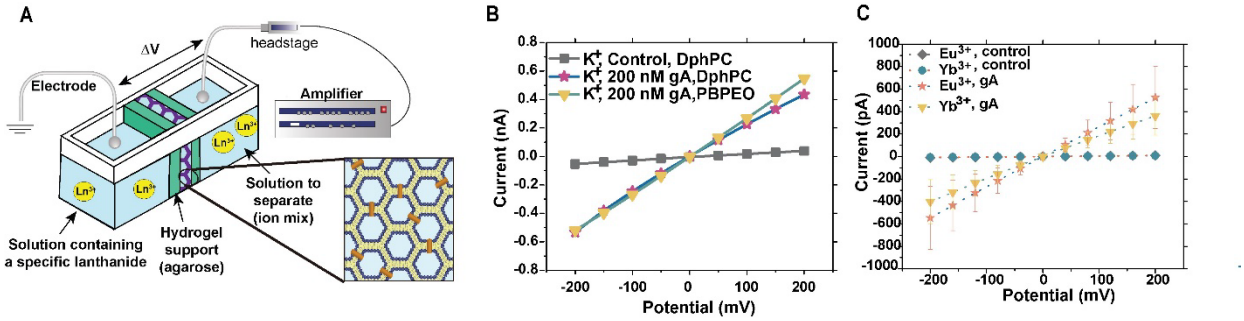

Figure 4. A artificial tissue membrane is utilized to evaluate the compatibility of channels with membranes and their transport properties. A. Schematic representation of the experimental set up to test the artificial tissue membrane's efficiency for ion separation.; **B**. gA incorporated artificial tissue membrane (made form lipid or polymers) showed significant K^+ ion transport as compared to the control membrane, **G.** Peptide incorporated artificial tissue membrane showed transport discrimination between heavy (Yb^{3+}) and medium (Eu^{3+}) lanthanides.

However, integrating LAP5 channels into these membranes proved challenging due to low compatibility and precipitation during fabrication. To overcome this, we pursued two strategies: constructing channels with more stable pore architectures and designing membrane-compatible channels. We synthesized a variant with shorter arms and enhancing the stability of the channel's backbone by connecting macrocycle rings through click chemistry (**Figure 5A**), which showed distinct Li^+ transport activity with transporting 3.7 $\times 10^7$ Li^+ ions/channel/sec. Nonetheless, the precipitation issue persisted. To improve membrane compatibility, we incorporated tryptophan amino acids into the channel's architecture which demonstrated high insertion efficiency and stability within the

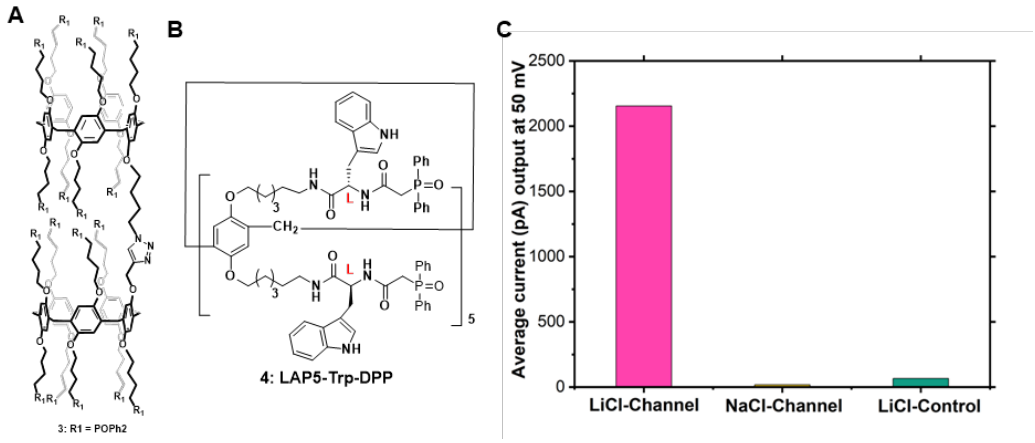

Figure 5. A-B. Chemical structure of stable LAP5 channels **3** and Amino acid attached LAP5 channels **4, C.** The channel **4** showed high Li-selectivity at a rate ≥ 100 times higher than Na^+ ions

membrane (**Figure 5B**). These channels exhibited a Li^+ transport rate over 100 times higher than Na^+ ions under applied potential (**Figure 5C**). Our ongoing work aims to optimize the integration of these channels into artificial tissue membranes and evaluate their performance for efficient critical metal ion separation.

Future Plans: Our path moving forward will be completed by working on two distinct goals: fundamental transport studies and use inspired fundamental membrane research.

Fundamental transport studies: The fundamental studies that will be conducted involve conducting research to deepen our understanding of design and development of artificial ion channels that have the required selectivity for lanthanides. In the past year, we have employed multiple approaches, such as molecular dynamics simulations and iterative methods like test-redesign-test, to identify and evaluate lanthanide and lithium selective ion channels. These channels were investigated for their ability to transport ions and examined the selectivity of ion-ion interactions across the lipid bilayer membrane, which serves as a representative model system. However, the low membrane compatibility of these channels poses a challenge for potential scale-up applications. Therefore, in the upcoming year, our primary focus will be on developing more robust and membrane-compatible rigid architectures for highly selective artificial ion channels. We are also aiming to perform lanthanide ion separations from mixed ion experiments to understand transport behavior and the impacts of the unique water-filled membrane architecture of aspects of transport such as concentration polarization.

Use inspired membrane research: The use inspired work part focuses on utilizing this knowledge to eventually lead to practical solutions and innovations. Our ultimate goal is to develop a continuous and efficient separation process that is energetically efficient and environmentally friendly. Therefore, in the coming years, our focus would remain on fabricate scalable, stable, and selective artificial tissue membranes for separating critical metal ions. Therefore, we will design and synthesize various amphiphilic di-block polymers though anionic polymerization. An iterative approach will be adopted to discover an appropriate polymer to fabricate channel compatible stable artificial tissue membranes. The lanthanide discrimination of these channel incorporated scalable membrane will be investigated.

References

(1) Cheisson, T.; Schelter, E. J. Rare earth elements: Mendeleev's bane, modern marvels. *Science* **2019**, *363* (6426), 489-493.
(2) Bomgardner, M. M. The struggle to mine rare earths. *CHEMICAL & ENGINEERING NEWS* **2015**, *93* (30), 36-39.
(3) Bottrill, M.; Kwok, L.; Long, N. J. Lanthanides in magnetic resonance imaging. *Chemical Society Reviews* **2006**, *35* (6), 557-571.
(4) Vogt, E. T.; Weckhuysen, B. M. Fluid catalytic cracking: recent developments on the grand old lady of zeolite catalysis. *Chemical Society Reviews* **2015**, *44* (20), 7342-7370.
(5) Humphries, M. *Rare earth elements: the global supply chain*; Diane Publishing, 2010.
(6) Alonso, E.; Sherman, A. M.; Wallington, T. J.; Everson, M. P.; Field, F. R.; Roth, R.; Kirchain, R. E. Evaluating Rare Earth Element Availability: A Case with Revolutionary Demand from Clean Technologies. *Environmental Science & Technology* **2012**, *46* (6), 3406-3414. DOI: 10.1021/es203518d.
(7) Joint Research, C.; Institute for Energy and, T.; Tercero, E.; Bryson, R.; Chapman, A.; Tzimas, E.; Moss, R.; Ostertag, K.; Thompson, P.; Morley, N.; et al. *Critical metals in the path*

towards the decarbonisation of the EU energy sector : assessing rare metals as supply-chain bottlenecks in low-carbon energy technologies; Publications Office, 2014. DOI: doi/10.2790/46338.
(8) Chu, S. *Critical materials strategy*; DIANE publishing, 2011.
(9) Navarro, J.; Zhao, F. Life-cycle assessment of the production of rare-earth elements for energy applications: a review. *Frontiers in Energy Research* **2014**, *2*, 45.

PUBLICATIONS

The following three manuscripts are under preparation/submitted

1. Harekrushna Behera, Tyler J Duncan, Laxmicharan Samineni, Hyeonji Oh, Chenhao Yao, Venkat Ganesan, Manish Kumar "*Bioinspired Super Selective Lithium Membrane Channels" Manuscript is under preparation*

2. Harekrushna Behera, Tyler J Duncan, Laxmicharan Samineni, Hyeonji Oh, Venkat Ganesan and Manish Kumar "*Voltage-gated lanthanide selective supramolecular membrane channels" Manuscript is under revision*

3. Tyler J. Duncan, Harekrushna Behera, Michael F. Meng, Zidan Zhang, Nico Marioni, Meron Tadesse, Manish Kumar and Venkat Ganesan "*Side-chain and ring-size effects on permeability in Artificial Water Channels." Manuscript is under preparation*

CONFERENCES

1**. Harekrushna Behera,** Tyler J Duncan, Laxmicharan Samineni, Hyeonji Oh, Venkat Ganesan and Manish Kumar. "*Lithium Selective Artificial Ion Channels for Lithium Separation"* Oral presentation at North American Membrane Society 2024, Santa Fe, NM, United States.
2. **Duncan, T.**; Behera, H.; Kumar, M.; Ganesan, V.. *Ion-ion Separations in Biomimetic Water Channels* Oral presentation at. North American Membrane Society 2024, Santa Fe, NM, United States.
3. **Harekrushna Behera,** Tyler J Duncan, Laxmicharan Samineni, Hyeonji Oh, Venkat Ganesan and Manish Kumar. "*Biomimetic Supramolecular Channels for Sustainable Extraction of Rare Earth Elements"* Oral presentation at North American Membrane Society 2023, Tuscaloosa, Alabama.
4. **Tyler Duncan**, Harekrushna Behera, Laxmicharan Samineni, Manish Kumar, Venkat Ganesan "*Ln (III) Selectivity in Biomimetic Ligand-appended Channels"* Oral presentation at American Physical Society Meeting 2023, Las Vegas, Nevada.

INTELLECTUAL PROPERTY

We have submitted two disclosures based on the outputs of this project. The first has now been filed as a PCT patent

1. (Provisional Patent Application 63/502,796) Behera, H.; and Kumar, M. Synthetic Ion Channels And Methods Of Making And Using Thereof. University of Texas at Austin (2023)
    a. PCT/US2024/029989

2. (Provisional Patent Application. UT Ref 8281KUM) Fica, A.; and Kumar M. Network Materials and Methods of Making and Using Thereof. University of Texas at Austin (2024)

Bio-mimetic material design based on principles of disorder

Andrea J. **Liu**; The University of Pennsylvania and Sidney R. **Nagel**; The University of Chicago
Keywords: Training; Memory; Landscape; Disorder; Networks

Research Scope

Our previous results have opened up new ways of thinking about how to design or train bio-inspired functionality into disordered matter. They raised a number of fundamental questions. In particular, training a mechanical network alters its energy landscape. Does the energy landscape contain imprints of the function that the network was trained to perform? If so, can we use physical properties of the system to deduce how the function was attained?

As enlightening as these studies are for novel ways of creating function in ordinary matter, however, the molecules relevant for life operate under very different conditions. The complexity of molecular structure has not yet been reproduced in the models used in learning or training in function. Studies of training have been performed for matter that has no internal stresses and which is athermal, that is at zero temperature. One goal is to confront the question of whether pre-stress, temperature, long-range interactions, or angle-bending forces can be accommodated into the training and learning protocols that have been proposed so far. If they are not, then the question emerges of whether those protocols can be augmented or changed to accommodate these ubiquitous features of living matter. Such understanding would also make it possible to use analogous training in more complicated forms of purely physical systems.

The concept of training assumes that the material is capable of storing a memory of its history so that it is able to retain the information and use it in its future behavior. Thus, the ways in which information can be stored in a material is important for learning how to train and implement behavior. Another goal is to address these two related issues: training complex, interacting systems and understanding how information is stored, *i.e.*, memory, in a material.

Recent Progress

Spring networks can be trained to develop a function that is inspired by protein allostery where binding a molecule creates a conformational change elsewhere in the protein. We consider the case in which a strain applied to one location in a network generates a specified strain at a designated target. Previously the PIs showed that this response can be trained. They define a cost function that is proportional to the square of the difference between the actual and desired response at the target. To minimize this cost function, they adjust "adaptive degrees of freedom," namely the spring constants and/or equilibrium lengths of the springs. At T=0, the network must minimize the mechanical energy so that the forces exerted by the springs on each node balance. This "double gradient descent" process simultaneously minimizes the cost function with respect to adaptive degrees of freedom while minimizing the energy with respect to the physical node positions. Adjusting the adaptive degrees of freedom, however, changes the energy landscape.

This alteration of the energy landscape leaves imprints that show if the system has been trained. Liu analyzed the physical Hessian, whose eigenvalues and eigenvectors correspond to the normal frequencies and modes of vibration. Compared to generic untrained networks, trained networks have more low-frequency modes; these modes align with the function for which the system was trained [1]. Liu established a connection between the physical and learning Hessians. The learning Hessian has been shown in deep neural networks to characterize the decision

boundary in classification tasks, so it is known to contain information about what has been learned. Those results show that the physical Hessian can also be used to extract information about what is learned. The great advantage of the physical Hessian is that it can be measured or calculated *without knowing what has been learned* and without specifying or applying inputs or outputs.

Liu has also found that by applying the maximally localized Wannier function analysis, developed in quantum condensed matter, to the eigenmodes of the physical Hessian, one can extract the key learning degrees of freedom responsible for the learned task. Thus, the fact that electrical learning networks are physical systems opens a window to the microscopic (individual edge-level) origins of the learned collective function. This window does not exist for artificial neural networks, which are not physical objects and therefore do not have physical Hessians. This work is being written up now.

Understanding that memories are encoded in the low frequency modes [1] has led the PIs to extend their studies of network allostery to *cooperative binding*. Their earlier work trained networks to produce a desired strain at an output location in response to an input strain elsewhere. They now consider the case of cooperative binding, where a strain applied at either location produces a desired strain at the other location. Until now they had neglected the effects of noise. Proteins, however, are subject to thermal noise. The PIs have found that the effects of temperature can be estimated theoretically based on a normal mode analysis, using ideas from [1]. The low eigenmodes of the physical Hessian encoding the learned function are the least robust to temperature. To increase thermal stability one must therefore raise these low eigenmodes. To accomplish this they developed new training approaches. These protein-function-inspired results have implications for material science at the nanoscale or below.

In related work, Liu used persistent homology to understand the collective response of the system to inputs. She previously applied this to fluidic networks and obtained quantitative understanding of learned response. She has now generalized this analysis to mechanical networks. The challenge is that persistent homology analysis alone is not useful; it must be coarse-grained to provide useful insight. She has now done this in a way that connects to existing insight in the protein allostery literature and applied it to real proteins.

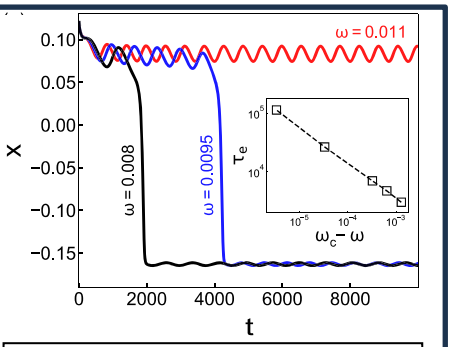

Position *vs.* time for a dynamical hysteron driven at different frequencies. The black and blue curves take multiple cycles before falling into the global minimum; the red curve is above the critical frequency at which the system remains in the less- favorable (upper) well. From [3].

Evolution in time-varying environments leads to adaptable biological systems that quickly switch function. There is the possibility of creating a wide range of materials which can also be trained for adaptability. By periodically switching targets, Nagel can teach a material to perform incompatible functions with minimal changes in parameters [2]. The results reveal physical principles that enable adaptability. Moreover, bistable objects that are pushed between states by an external field are often used to study memory formation. Such systems, called hysterons, are typically treated quasistatically. Nagel generalized this to dynamics in tunable bistable systems [3] as shown in the figure where there is competition between following the energy minimum versus following the configuration path. Oscillatory forcing leads to transients lasting many cycles, not possible for quasistatic hysterons.

Memory formation in many fluid instabilities draw inspiration from biology such as proportionate growth found in viscous fingering. There, pattern growth changes after onset. Nagel introduced a technique [4] to probe a new length scale associated with pressure gradients around the interface. Another form of memory is seen in the dynamics of contact-line motion. In an analogy with fluid flow, the PIs generalized their approach for training mechanical systems that minimize energy to include low Reynolds number flow networks as well as resistor networks. Both must satisfy Kirchhoff's laws with no net current at any node, just as there is no net force anywhere in a mechanical network. Liu's results for the physical Hessian described above [1] were derived in sufficient generality to cover fluid, resistor as well as mechanical networks.

These results confirm there is much to be gained by applying biological ideas to experiments on physical systems. Liu introduced laboratory electrical resistors networks that self-adjust with local rules to minimize the cost function that measures the difference between the actual and desired response. As shown in the figure, this prototype performs tasks such as linear regression and classification. One advantage of these "physical learning neural networks" is that once trained, they use physics to perform inference (to calculate the output in response to input voltages), since physics solves Kirchhoff's law at every node on its own. This greatly lowers the energy cost of inference, so that the second-generation nonlinear analog networks [5], not been optimized for energy efficiency and built on breadboards, consume only 10 pJ per adjustable parameter per inference. This is within striking difference of digital neural networks on Qualcomm AI chips (among the most energy-efficient chips available). Liu finds that the networks can learn multiple tasks simultaneously if trained simultaneously and identified the important time scales that control memories of multiple tasks.

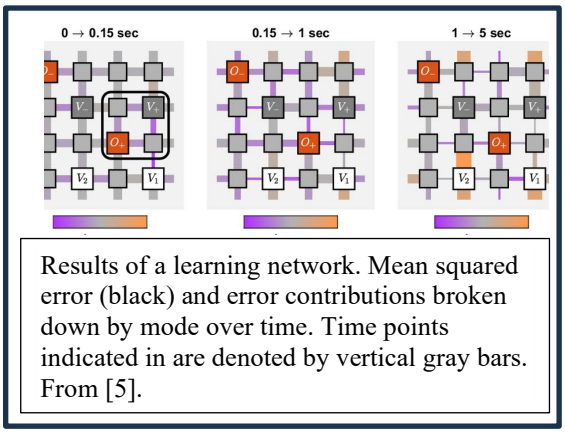

Results of a learning network. Mean squared error (black) and error contributions broken down by mode over time. Time points indicated in are denoted by vertical gray bars. From [5].

Future Plans

The mode frequency is related to curvature of the energy landscape. The PIs have a record of investigating this landscape by a variety of means. Of most interest is Liu's earlier work on the size of basins of attraction in jammed packings. Nagel is investigating a new form of order in the distribution of basin sizes. This has implications for how perturbations can ever find a way to form a periodic orbit.

The PIs have both considered the case of pre-stress in networks. Liu is looking specifically at the under-coordinated case. Nagel is developing a theory for how to include prestress and prestrain into the response of an over-coordinated network. This theoretical advance will give us additional insight into the way in which generalized networks respond to stresses and show what are the limits of training in these functional materials that take inspiration from biological cellular networks.

Liu is extending the theoretical framework of coupled learning. The coupled learning local rule projects onto the direction of gradient descent in the cost function, so it minimizes the cost function without using the global process of gradient descent. However, it is currently restricted to physical systems whose physical degrees of freedom minimize a Lyapunov function that is either the energy (as in mechanical networks) or the dissipated power (as in flow/electrical networks). Liu is working on extending coupled learning to systems with non-reciprocal

interactions. For example, consider a set of coupled chemical reaction equations, where the dynamics are controlled by the reaction kinetics but the influence of one species on the rate of change of another is not reciprocal. The PIs will apply this approach to such systems to understand how to construct systems that maintain homeostasis as so many biochemical reaction networks do.

The PIs are studying how temperature fluctuations interfere with cooperative binding above a crossover temperature determined by the low eigenmodes of the physical Hessian. They plan to study how different training methods might control whether the system develops allostery (where a regulatory site controls binding at another site, but not vice versa) vs. cooperative binding (where either site controls binding at the other site).

The PIs will continue their studies into how memories can be formed in materials. Their joint discovery of the powerful tool of introducing transient degrees of freedom will be adapted to new situations where ground states need to be determined in a rugged energy landscape especially in the case where the particles are polydisperse. Nagel will also follow up on work that measures the distribution of the volumes of attraction in monodisperse sphere packings. This has led to insight about the organization of jammed systems and in particular about how a jammed system evolves when perturbed such as when sheared. They will see to what extent the polydisperse case can be thought of as a perturbation about the monodisperse situation. The dominant question is how can a many-particle disordered material *ever* return to the same state when sheared enough so that it visits many different ground states.

References

[1] M. Stern, A. J. Liu, V. Balasubramanian, *PRE* **109**, 24311 (2024), "Physical effects of learning."

[2] M.J. Falk, J. Wu, A. Matthews, V. Sachdeva, N. Pashine, M. Gardel, S. R. Nagel, A. Murugan, *PNAS* **120**, e2219558120 (2023) "Learning to learn by using non-equilibrium training protocols for adaptable materials."

[3] C. W. Lindeman, V. F. Hagh, C. I. Ip, S. R. Nagel, *PRL.* **130**, 197201 (2023) "Competition between energy and dynamics in memory formation."

[4] S.D. Gowen, T.E. Videbæk, S.R. Nagel, *PRF* **9**, 053902 (2024) "Measurement of Pressure Gradients near the Interface in the Viscous Fingering Instability."

[5] S. Dillavou, B.D. Beyer, M. Stern, A.J. Liu, M.Z. Miskin, D.J. Durian, *PNAS* (in press), "Machine learning without a processor: emergent learning in a nonlinear analog network."

Publications

1. M. Stern, A. J. Liu, V. Balasubramanian, *"Physical effects of learning"* PRE **109**, 24311 (2024).

2. M. Stern, S. Dillavou, D. Jayaraman, D. J. Durian, A. J. Liu, *"Training self-learning circuits for power-efficient solutions,"* APL Mach. Learn. **2**, 016114 (2024).

3. C. Arinze, M. Stern, S. R. Nagel, A. Murugan, *"Learning to self-fold at a bifurcation,"* Phys. Rev. E **107**, 025001, (2023).

4. C. W. Lindeman, V. F. Hagh, C. I. Ip, S.R. Nagel, *"Competition between energy and dynamics in memory formation,"* Phys. Rev. Lett. **130**, 197201, (2023).

5. M. J. Falk, J. Wu, A. Matthews, V. Sachdeva, N. Pashine, M. Gardel, S.R. Nagel, A. Murugan, "*Learning to learn by using non-equilibrium training protocols for adaptable materials,"* PNAS **120**, e2219558120, (2023).

6. C. W. Lindeman, S.R. Nagel, *"State-and-rate friction in contact-line dynamics,"* Phys. Rev. E **107**, 065111, (2023).

7. A. J. Liu, S. R. Nagel, *"Twenty-five years of the jamming phase diagram,"* Nature Reviews Physics **5**, 630-631, (2023).

8. S. D. Gowen, T. E. Videbæk, S.R. Nagel, *"Measurement of Pressure Gradients near the Interface in the Viscous Fingering Instability,"* Phys. Rev. Fluids B, 053902, (2024).

9. V. F. Hagh, S. R. Nagel, A. J. Liu, M. L. Manning, E. I. Corwin *"Transient learning degrees of freedom for introducing function in materials,"* PNAS **119** (19) e2117622119 (2022).

Understanding and Informed Manipulation of Functional Dynamics on the Nanoscale Through Integrated Experiments and Computation

Erik **Luijten**; The University of Illinois and Qian **Chen**; Northwestern University

Keywords: Nanoparticle self-assembly, patchy nanoparticles, electric field effects, liquid-phase transmission electron microscopy

Research Scope

This project revolves around an experimental–computational collaboration that aims to bridge the nanoscopic length-scale gap by studying and replicating nanoscopic functional dynamics found in living systems within synthetic materials to leverage their macroscopic properties. Specifically, we focus on understanding the fundamental mechanisms underlying the dynamics of nanoparticles (NPs) and exploiting this understanding to manipulate the aggregation of such particles into materials with tunable and responsive structures and properties. The NP dynamics we investigate are inspired by biological systems and driven by chemical fuels or external fields. In the previous funding cycle, our team demonstrated significant advances in directly imaging large assemblies of NPs with unprecedented spatial and temporal resolution using liquid-phase transmission electron microscopy (TEM). These observations have been partnered with advanced computational methods to extract mechanistic insights. In this project, we build on these efforts and synthesize patchy NPs with designed surface charge patterns that will subsequently be steered by external energy input. We integrate the unique real-space observations of nanoscale dynamics by liquid-phase TEM with predictive capabilities achieved by modeling diffusional dynamics, dielectric polarization effects, charge regulation (i.e., the dynamic response of surface ionization of NPs), and hydrodynamic flow fields. The procedures and insights thus developed will ultimately be used to realize scaled-up assemblies composed of patchy NPs through new pathways. Additionally, we aim to achieve real-space understanding of the relationship between the design of charged patchy NPs and their functional dynamics, as well as the modulation of this relationship upon assembly, i.e., under dynamic, non-dilute, non-equilibrium conditions, which are particularly unexplored on the nanoscale. Thus, the success of the proposed research will impact a multitude of DOE biomolecular materials program initiatives, including the design of bioinspired materials capable of functioning in harsh and non-biological environments, the development of predictive models through a closely knit in-situ feedback loop with experiments, and scaled-up manufacturing.

Recent Progress

During this reporting cycle, we have made major progress in experimentally capturing, analyzing, and understanding nonequilibrium assembly dynamics in NP systems where experimental imaging has not been possible with nanometer resolution. Simultaneously, we have gained extensive insights into hydrodynamic modeling of active swimmers and spinners and the collective behaviors that can be harnessed from their activity. These efforts are detailed in the following.

1. Colloidal synthesis and nanoscopic imaging of self-propelled ultra-small catalytic nanomotors

Ultra-small "nanomotors" (<100 nm) are highly desirable functional nanomachines due to their size-specific advantages over their larger counterparts. They have a large relative surface area permitting efficient catalysis and a sufficiently small size for breaking through biological barriers, attracting increasing attention for applications spanning nanomedicine, directed assembly, active sensing, and environmental remediation. While there are extensive studies on motors larger than 100 nm, the design and understanding of ultra-small nanomotors have been scant due to the lack of high-resolution imaging of their propelled motions with orientation and shape details.

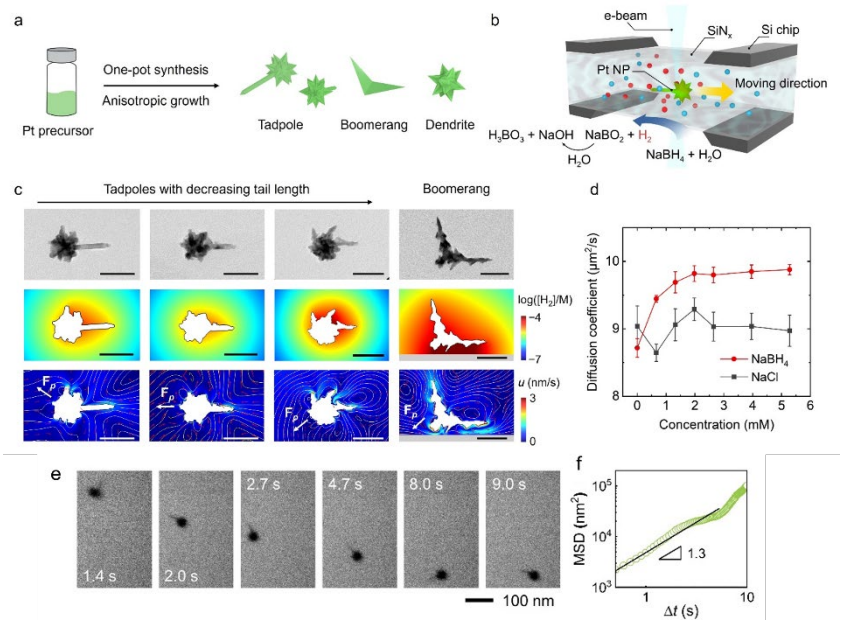

Fig. 1. Colloidal synthesis of Pt U-motors and finite-element simulation of the chemical gradient surrounding them in the presence of NaBH4 fuel. (a) Schematic illustration showing the one-pot synthesis of Pt NPs. (b) Schematic illustration showing the tracking of the self-propelled motion of Pt NPs in a liquid chamber for TEM imaging. (c) TEM images of Pt NPs (top) and simulated diffusio-osmotic flow around them (bottom). Scale bars: 50 nm. (d) Diffusion coefficients of Pt NPs in NaBH4 and NaCl solutions measured by dynamic light scattering (DLS). (e) Time-lapse liquid-phase TEM images, (f) MSD on a log–log scale and fit (black line) of the diffusion exponent, and (g) centroid position trajectory overlaid with particle orientation of a Pt NP motor.

Here we report the design of U-motors based on colloidally synthesized Pt NPs, which can be powered by catalyzing the decomposition of the $NaBH_4$ fuel in aqueous solution, and achieve the direct imaging of their propelled motions with shapes resolved under liquid-phase transmission electron microscopy (TEM). Based on finite element analysis (FEA), through $NaBH_4$ decomposition, a H_2 gradient can be generated around Pt NPs of asymmetric shapes (e.g., tadpoles and boomerangs) and propel the NPs into directional motion. This design of U-motors is verified by our liquid-phase TEM imaging, where Pt NPs exhibit directed motion with diffusion exponents as high as 1.4 (Fig. 1). The nanometer resolution imaging allows us to map the orientation and centroid positions of NPs, where a high correlation is consistently found between the NPs' orientation and moving direction, matching our FEA prediction based on experimentally resolved NP shapes. This agreement supports the hypothesis that self-diffusiophoresis induced by the local concentration gradient of catalyzed reaction products serves as the major propulsion mechanism, which fundamentally originates from the nanoscopic shape asymmetry of NPs. Meanwhile, other mechanisms such as

self-electrophoresis and ionic self-diffusiophoresis may also contribute to the propulsion of these U-motors. Control experiments using unfueled NPs in NaCl solution show a considerable decrease in the fraction of active NPs undergoing propelled motion. Studying the trajectories of more than 180 NPs, we find that NPs require directional driving forces to counteract randomized Brownian force. This work demonstrates the integration of colloidal synthesis of U-motors, simulation of the propulsion mechanism, and liquid-phase TEM imaging of the propelled motions. Such combination invites future efforts in designing, understanding, and modulating U-motors that are batch synthesized from solution and are promising candidates for broad applications, including intracellular sensing and delivery, pollutant detection and degradation, and controlled self-assembly.

2. Swarming NP superlattices driven by non-reciprocal interactions.

Swarming is an "intelligent," collective behavior where many individuals (typically more than ten) consume energy to coordinate movement or mechanical work, maintaining intricate patterns and communication of information. Extensive research on micron-sized colloids has shown that swarming relies on non-reciprocal interactions, achievable in non-equilibrium conditions driven by external energy, often through symmetry-breaking fluid flows. This breaks Newton's third law and has applications in drug delivery, cell transportation, and photochromic inks. However, for NPs, despite their advantages, designing non-reciprocal interactions and realizing swarms remains unexplored territory. NPs offer unique properties for device miniaturization, crossing biological barriers, multifunctionality, and scalable colloidal synthesis.

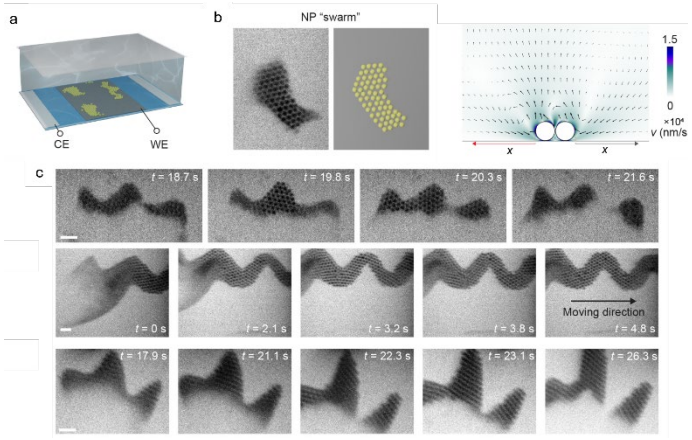

Fig. 2. Experimental design to realize NP swarm. (a) Schematic of the SiN_x microchip with patterned electrodes for liquid-phase TEM imaging. (b) Liquid-phase TEM image and cartoon of a typical NP superlattice swarm (left) and finite-element calculation showing the unbalanced flow surrounding NPs (right). (c) Typical time-lapse liquid-phase TEM images of wavy NP swarm with single-particle resolution under an electric field, showing highly reconfigurable assembly, highly dynamic sinusoid-like pattern, and wavy pattern. Scale bars: 500 nm in (c).

We have realized for the first time the implementation of nonreciprocal interactions in NPs and direct imaging of their swarms in solution at nanometer resolution using liquid-phase TEM coupled with electric biasing. The NPs that we focus on are the simplest for demonstration purposes, namely gold nanospheres (GNSs), but we extend the principles to representative anisotropic NP, gold nanorods (GNRs), whose swarming behaviors are also observed (Fig. 2). The key to realizing non-reciprocal interactions is to achieve nonuniform

polarization of NPs vertical and close to a conductive substrate (i.e., working electrode). Traditionally this has been achieved in a parallel electrode configuration for micron-sized colloids, which is not technically possible within a liquid-phase TEM holder. Instead, we optimize a design of coplanar electrodes with well-controlled dimension and position to induce this effect. By doing so, a non-reciprocal equilibrium charge electro-osmotic (ECEO) flow is generated around the NPs that pushes them to laterally interact and concentrate near the substrate, leading to swarming superlattice patterns. Single NP tracking shows that both bulk and surface particles share similar diffusivity and contribute almost equally to frequent reconfiguration, which contrasts with the equilibrium assemblies of GNSs in the absence of a field. All these principles translate to GNRs, which also form swarms, but with even richer lattice structures owing to the additional degree of freedom provided by shape anisotropy. Our work demonstrates the first step toward realizing, understanding, and potentially manipulating nonequilibrium collective behavior of NPs, opening a route toward nanoscale intelligent materials.

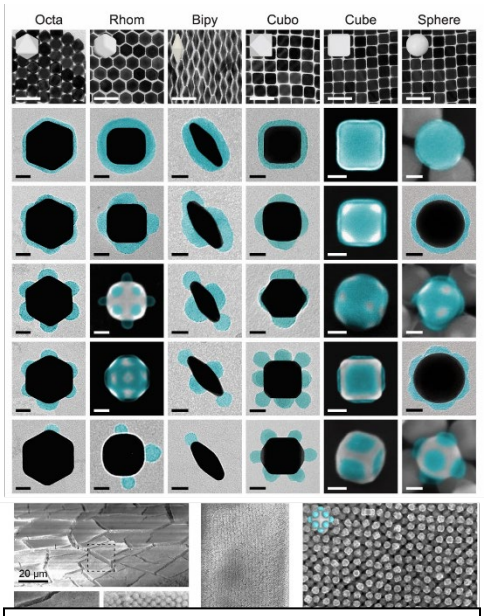

Fig. 3. TEM images of different patchy NPs created via the stencil method, as well as their large-scale assembly. Scale bars: Top: 100 nm & 20 nm (enlarged)

3. Synthesis and large-scale assembly of patchy NPs using selective ion masking

We have greatly expanded the library of patchy NPs synthesized with the aid of selective ion masking. Patterning NPs with patches with predictive control over patch size, shape, placement, and number is a holy grail of NPs assembly research, potentially applicable in nanorobots, targeted delivery, and assembly into optical and mechanical metamaterials. However, patterning at the nanometer scale remains challenging, in particular when creating large-scale, uniform particles with intricate patch patterns. This often leads to low-quality and inhomogeneous patches on the NPs, resulting in low yields and a lack of large-scale assembly. To provide a versatile and definitive method for controlling patch patterning, we designed a new platform enabling precise nanoscale patch-patterning, inspired by "stencil" methods. In our design, the iodine adatoms "mask" gold NP surfaces to induce selective polymer grafting to be "painted" on NP surfaces with controlled patterns and sizes which were previously not accessible. This method generates highly uniform patchy NPs at high yield, allowing us to achieve large-scale assembly of patchy NPs into ordered porous crystals for the first time (Fig. 3).

Future Plans

In the coming cycle we plan to achieve a more thorough understanding of electric-field driven assembly, extending our methods to nanoparticles of different shapes and attaining

predictive modeling of their behavior. We will also proceed toward scaled-up assembly, uncovering collective optical and mechanical properties.

Publications

1. Z. Lyu, L. Yao, Z. Wang, C. Qian, Z. Wang, J. Li, C. Liu, Y. Wang, Q. Chen, Nanoscopic Imaging of Self-propelled Ultrasmall Catalytic Nanomotors, *ACS Nano* **18**, 14231 (2024).

2. T. Curk and E. Luijten, Phase separation and ripening in a viscoelastic gel, *Proc. Nat. Acad. Sci. (USA)* **120**, e230465512 (2023).

3. G. R. Burks, L. Yao, F. C. Kalutantirige, K. J. Gray, E. Bello, S. Rajagopalan, S. B. Bialik, J. E. Barrick, M. Alleyne, Q. Chen, C. M. Schroederm Electron Tomography and Machine Learning for Understanding the Highly Ordered Structure of Leafhopper Brochosomes. Biomacromolecules **24**, 190 (2023).

4. B. Luo, Z. Wang, T. Curk, G. Watson, C. Liu, A. Kim, Z. Ou, E. Luijten, and Q. Chen, Unravelling Crystal Growth of Nanoparticles. *Nat. Nanotechnol.* **18**, 589 (2023).

5. Z. Lyu, L. Yao, W. Chen, F. C. Kalutantirige, and Q. Chenm Electron Microscopy Studies of Soft Nanomaterials. *Chem. Rev.* **123**, 4051 (2023).

6. A. Kim, T. Vo, H. An, P. Banerjee, L. Yao, S. Zhou, C. Kim, D. J. Milliron, S. C. Glotzer, Q. Chen, Symmetry-Breaking in Patch Formation on Triangular Gold Nanoparticles by Asymmetric Polymer Grafting. *Nat. Commun.* **13**, 6774 (2022).

7. Z. Wang, C. Liu, Q. Chen, In-Situ Imaging of Nucleation and Growth of Superlattices from Nanoscale Colloidal Nanoparticles. *J. Cryst. Growth* **601**, 126955 (2022).

8. L. Yao, H. An, S. Zhou, A. Kim, E. Luijten, and Q. Chen, Seeking Regularity from Irregularity: Unveiling the Synthesis-Nanomorphology Relationships of Heterogeneous Nanomaterials Using Unsupervised Machine Learning. *Nanoscale* **14**, 16479 (2022).

Manuscripts in preparation:

Z. Wang et al., Qian Chen, Direct Imaging of Swarming Nanoparticle Superlattices Driven by Non-Reciprocal Interactions.

G. Watson, E. Luijten, Emergent nonreciprocity in multicomponent chiral fluids.

A. Kim, et al., Q. Chen, “Atomic Stencil” for Precise Polymer Patch Formation on Gold Nanoparticles.

Developing Backmappings for Protein Sidechains and Water Compatible with Reweighting

Jacob I. **Monroe**, Ralph E. Martin Department of Chemical Engineering, University of Arkansas, Fayetteville, AR

Keywords: Coarse-graining, backmapping, molecular simulation, statistical mechanics, variational autoencoders

Research Scope

In materials science and engineering, rational design of materials that change their properties in response to their environment remains a grand challenge. Many such materials exist in nature, often composed of self-assembling peptides or proteins and exhibiting hierarchical and multiscale structures that contribute to their ability to adjust their behavior. Design of these materials could be accelerated through improved computer simulations that take into account information across many length scales. Our work brings us closer to such simulations by developing techniques that seamlessly switch between resolutions over the course of a simulation by learning probabilistic backmappings. These machine-learned backmapping models are capable of recovering fine-grained atomistic coordinates from coarse-grained (CG) representations of a system, which accelerate simulations by removing some atoms and lumping others together into coarser beads with modified interactions. Our most recent work focuses on learning backmappings from CG representations of proteins and water. While each is investigated separately here, both will be necessary for studying materials composed of self-assembling proteins, as inclusion of water is crucial for capturing important interactions, such as hydrophobic attractions.

Recent Progress

Our recent research in developing backmappings for protein sidechains and water has been enabled through the development of a general software library for learning backmappings of molecules. This code base is highly modular and allows for rapid implementation of state-of-the-art machine learning techniques such as autoregressive normalizing flows,[1] which are necessary for learning the complex probability densities associated with molecular degrees of freedom. In general, our backmappings do not directly produce the locations of atoms removed during coarse-graining, but instead predict their probability densities conditional on the CG structure. Based on prior work,[2] we typically predict atom locations in internal molecular coordinates consisting of bond lengths, bond angles, and torsion angles, or bond-angle-torsion (BAT) coordinates. This is a natural representation for molecules and allows more rapid training through the learning of simpler conditional distributions compared to rectangular coordinates. The software supporting creation and training of these probabilistic models will be made available to the public in tandem with related journal publications.

The CG protein representation is inspired by the centroid representation used in the protein modeling and analysis software Rosetta. Specifically, all-atom structures are converted to a CG representation involving all backbone atoms, as well as the β-carbon of a sidechain and a CG bead at the center of mass of all sidechain atoms. To emulate partially decoded structures, a random set of residues are selected to have their sidechain atoms preserved. The internal BAT coordinates of sidechain atoms of each target CG bead to decode are also stored, along with one-hot vectors describing the identities of all atoms and CG beads within the training example.

The full sidechain decoding process is shown schematically in Fig. 1. It takes all particle locations and first defines a local environment around the CG bead to be decoded. Based on this local environment, the algorithm predicts probability distributions for the BAT coordinates of sidechain atoms. This occurs iteratively for each residue in a protein, using a different trained model for each residue type. As residues are decoded, samples are drawn from the predicted probability distribution and added to the coordinates used to determine the local environments of subsequently decoded CG beads, making the overall model autoregressive. The resulting models have been trained on data mined from the RCSB Protein Databank.[3] By design, both in terms of architecture and training, models are transferable to any peptide or protein system and chosen simulation force field (parametrization of atomic level interactions).

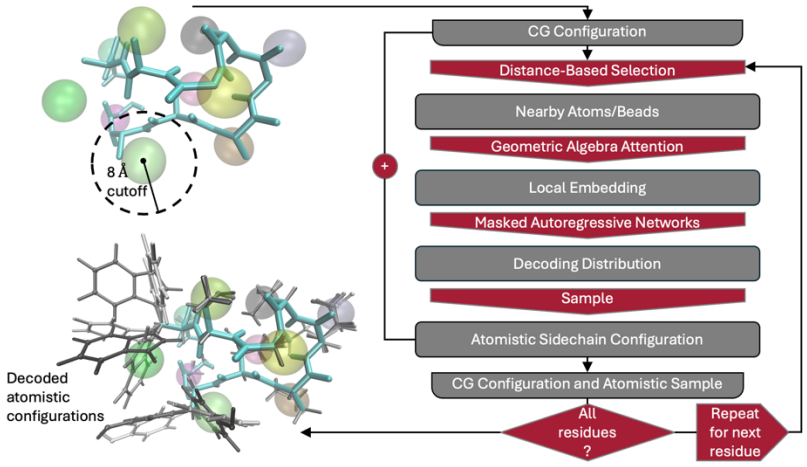

Figure 9: Schematic demonstrating the decoding process from CG representations of proteins (backbone atoms shown in blue and CG beads shown as colored spheres) to all-atom representations (shades of gray indicate independently sampled configurations). Red blocks indicate operations or layers within the model while gray blocks represent outputs of those operations.

Multiple sampled configurations are shown in Fig. 1, demonstrating that new all-atom configurations are produced through the decoding procedure. Fig. 2 demonstrates that the samples produced for models decoding aspartic acid, tryptophan, and arginine sidechains produce distributions of important dihedrals that match the training set. Further, these distributions depend on the specific training example passed into the model, indicating sensitivity to the local environment. As sidechains become larger or more flexible, however, this sensitivity to the local environment decreases, as indicated in Fig. 2b-c.

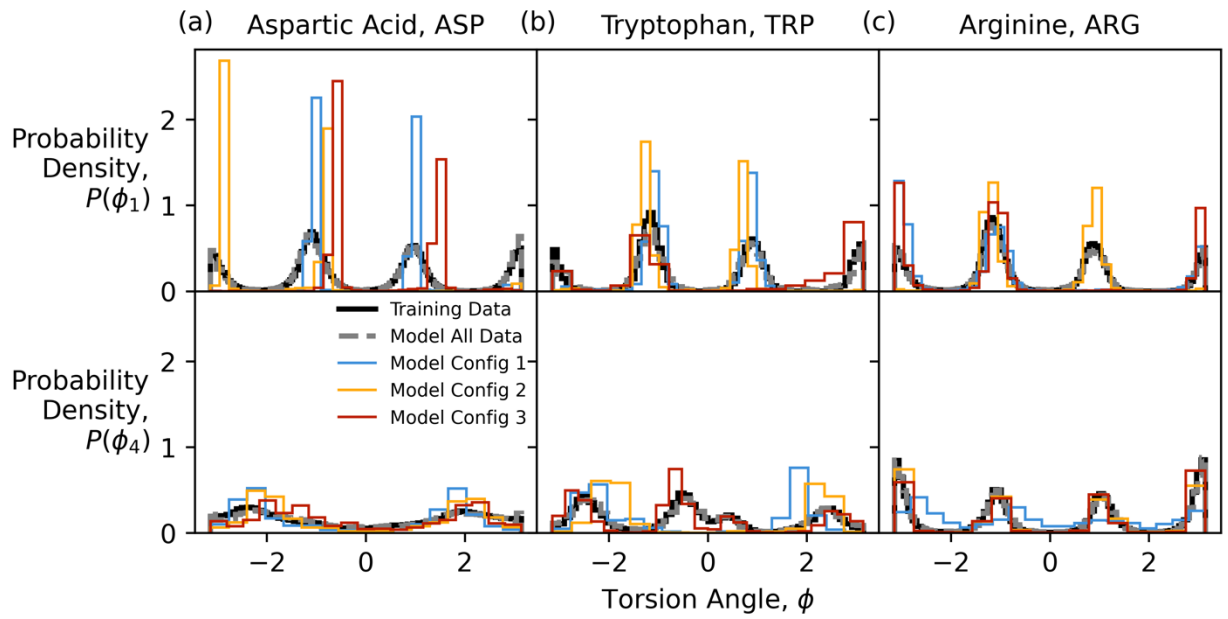

Figure 2: Probability densities of the 1st and 4th sidechain dihedral angles in internal coordinates are shown for aspartic acid (a), tryptophan (b), and arginine (c) residues. Training data is shown as a sold black curve while model-generated data from all training examples is shown in dashed gray. Distributions over 10,000 samples from decoding distributions predicted from 3 different training examples are shown as solid-colored curves.

An important aspect of our overall backmapping model is the presence of a calculable conditional probability associated with an all-atom structure given a CG representation. This allows for exact reweighting of generated all-atom configurations to ensure sampling of a specific thermodynamic ensemble or force field. This makes our model unique amongst recent efforts in protein backmapping, while it still performs at the state of the art based on recently developed metrics for bond lengths, atomic overlaps, and diversity of generated structures.[4] To assess reweighting of our model-generated structures, along with its efficiency compared to standard molecular simulation techniques, we have performed a detailed analysis with the miniprotein chignolin.

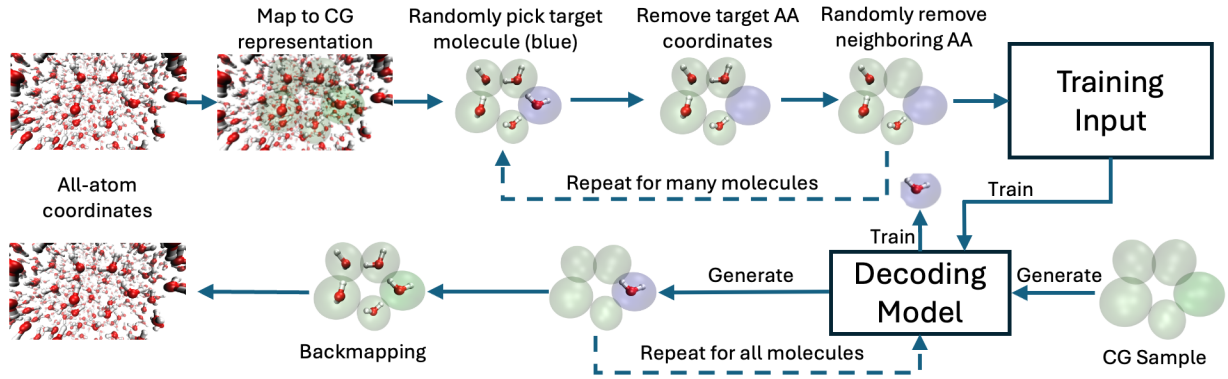

Figure 3: Schematic demonstrating the procedure for generating training inputs (top row) and for generating AA configurations from CG samples (bottom row).

A similar approach is taken in our backmapping models of water, as shown in Fig. 3. In this case, we use a CG representation that fully encodes the translational degrees of freedom of the molecule through its center of mass. All that remains to be predicted is the rigid-body rotation of the atomistic water based on its local environment. The probability distribution of these rotations, conditioned on the local environment, is what our backmapping model is trained to predict. To specify the orientation in a manner independent of the global coordinate system, the axes of rotation are defined by the vectors connecting the CG bead to be decoded to the two nearest CG beads. As an example, the molecule with its CG bead representation shaded blue in Fig. 3 will be decoded, with gray molecules having been identified as within its local environment. The rotational coordinates of the blue molecule will be saved as the target while random nearby molecules have had their atoms removed and are only represented by CG beads. During decoding of the full system, each water CG bead is decoded in turn. To assess transferability of our trained backmapping, we explore its ability to reproduce the correct ensemble of orientations given data at different temperatures and densities. We also investigate the ability to backmap from simulations of CG models of water with varying abilities to reproduce the unique thermodynamic properties of water.

Future Plans

After completing analysis of our backmapping models for protein sidechains and water, we will continue to expand our expertise and understanding of such backmappings through application to other systems. The overarching goal is to develop models that can explore the relationships between microscopic structure and conductivity in conjugated polymer systems used in flexible electronics. In this area, there is a critical need to understand how deformation (e.g., stretching) of these materials impacts mesoscale structure and in turn conductivity at a molecular level. Reaching this goal will require consideration of a series of systems of increasing complexity. Our protein sidechain models will be extended to CG models that also coarse-grain the backbone, then applied to self-assembling dipeptides with electrically conductive properties. Water models will proceed to higher levels of coarse graining that map multiple waters to single CG beads, as well as to heterogeneous environments involving ionic species and proteins.

References

1. Papamakarios, G., Nalisnick, E., Rezende, D. J., Mohamed, S. & Lakshminarayanan, B. *Normalizing flows for probabilistic modeling and inference*. J. Mach. Learn. Res. **22**, 1–64 (2021).

2. Monroe, J. I. & Shen, V. K. *Learning Efficient, Collective Monte Carlo Moves with Variational Autoencoders*. J. Chem. Theory Comput. **18**, 3622–3636 (2022).

3. Berman, H. M., Westbrook, J., Feng, Z., Gilliland, G., Bhat, H., Weissig, H., Shindyalov, I. N. & Bourne, P. E. *The Protein Data Bank*. Nucleic Acids Res. **28**, 235–242 (2000).

4. Jones, M. S., Shmilovich, K. & Ferguson, A. L. *DiAMoNDBack: Diffusion-Denoising Autoregressive Model for Non-Deterministic Backmapping of Cα Protein Traces*. J. Chem. Theory Comput. **19**, 7908–7923 (2023).

Publications

N/A

Electrostatic Driven Self-assembly Design of Functional Nanostructures

Monica **Olvera de la Cruz** (Northwestern University)

Keywords: membranes, Ionic conductivity, diffusiophoresis, microcompartments, electrolytes

Research Scope

The design of molecules and conditions to generate functional biomimetic structures, requires an understand of the basic principle that govern their functionalities. By assembling heterogeneous molecules one can mimic the organization and function of specific biomolecular assemblies such as bacterial microcompartments. We propose to design and characterize the organization of heterogeneous molecules with polar, non-polar, and charged groups including proteins and amphiphiles, into specific nanostructures with broken symmetries to explore biomimetic and new functionalities.

Recent Progress

Bacterial microcompartments (BMCs) allow bacteria to survive in harsh environments by limiting toxicity and improving enzymatic pathway flux. The microcompartment consists of a shell made of many proteins that encapsulates the enzymatic machinery necessary to enable safe and efficient bacterial metabolism. BMCs attract reactants and sequester intermediate reactions. The goal of the team is to design various shell morphologies form amphiphilic molecules to mimic and optimize BMCs functions including chemotaxis and self-ionic diffusiophoresis. Regarding the structure, our work revealed a robust patterning mechanism present in multicomponent shells which captures the observed morphologies of bacterial microcompartments (BMCs). The shell protein distribution mediated by Gaussian curvature provides direct insights into the distribution of the protein specific charge on the shell [1]. Such surface features in turn play an important role in the chemotactic movement of components inside cells and can be utilized in the design of synthetic vesicles for targeted and optimized cargo transport. The team employed a continuum model of multi-component elastic shells where the morphology and component patterning depend on the competition of mean and Gaussian bending energies. When a weak interfacial line tension

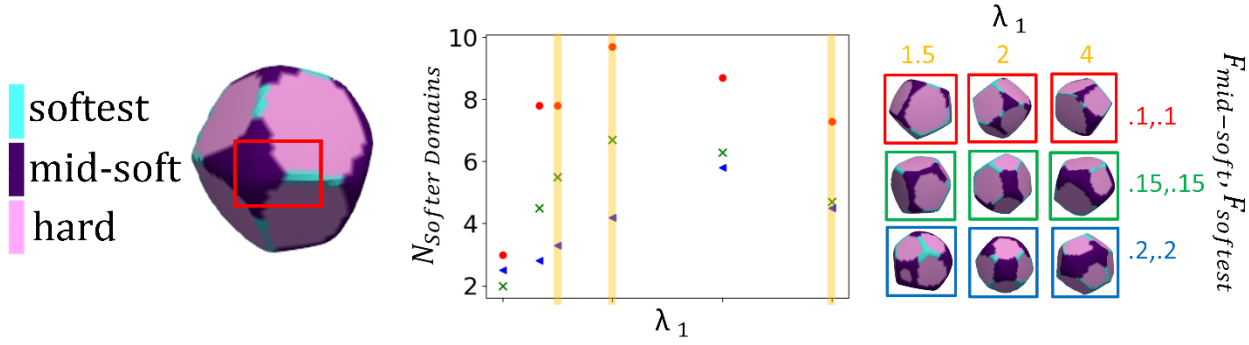

Fig. 1: Pattering and morphology of multicomponent elastic shells. The number of softer domains (mid-soft and softest) plotted as a function of their bending rigidity ratio λ_1 for different component fractions F.

is present, the two softer components separate into subdomains that are patterned by the Gaussian curvature. We show that this degree of fractionation is maximized when the bending rigidity of the mid-soft component is approximately twice that of the softest component (see Fig. 1).

Quantifying the prevalence of micro- and nano-scale transport mechanisms is crucial to the long-standing efforts in understanding the spatial organization and functionality of components inside cells. We showed that self-propulsion of chemically active nanoparticles is achieved and enhanced through asymmetry in the surface charge of the particle [2]. This lends formative insight into the underlying physical principles that regulate chemotactic motion of intracellular matter such as organelles, vesicles, and enzymes. Moreover, these findings suggest novel avenues for the design of synthetic nanomotors and vesicles that provide optimized and targeted cargo transport in ionic media. We developed a hydrodynamic model for ionic self-diffusiophoresis that quantitatively analyzes and determines the velocity of nanosized particles with surface asymmetries. We showed that asymmetry in the surface charge distribution introduces an additional mode of self-propulsion for chemically active particles that produce ionic species. We found that directed propulsion is achieved through surface charge asymmetry even when ionic flux is uniform on the particle's surface (see Fig. 2).

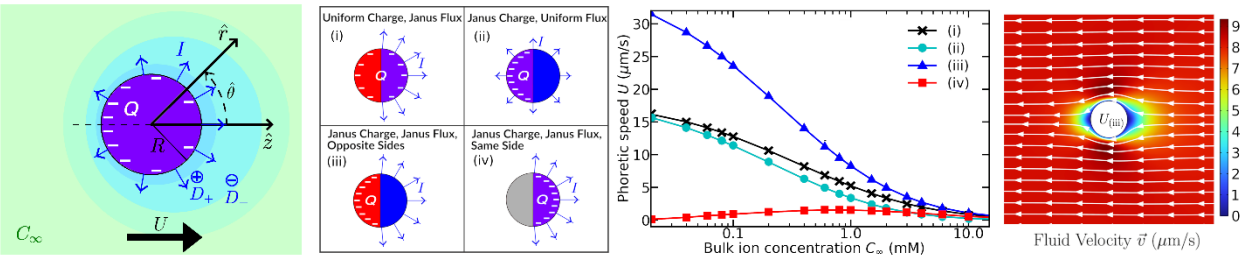

Fig. 2: Enhanced phoretic self-propulsion of Janus nanoparticles. The propulsion speed plotted as a function of bulk ion concentration for four different combinations of surface charge Q and ion flux I asymmetries.

We have also modelled diffusiophoresis-induced chemotaxis observed in enzymic bacterial microcompartments (BMCs) subject to both external bulk-imposed and internal generated chemical gradients via consumption of the reactant inside a spherical cell/vesicle environment (in preparation). When surface consumption is added to the system, we found that a stagnation plane exists in the vesicle at which the effects from bulk and nucleus (consumption) gradients cancel and the chemotactic rates reduces to zero. Another interesting finding is the blockage effects is only related to the relative scaling of the sizes of the vesicle, the blocker and the location of the BMC.

Ions in confinement have demonstrated nonlinear conductivities. The channel formed in the interstitial space in layered materials inhibits ion conduction. Applications of these layered materials include biomimetic properties such as neural activity with voltage spiking and synaptic potentiation. These functionalities depend on interactions among the ions and the interfaces formed at the junctions of the layered materials. We studied the physical principles of ionic transport

driven by external electric fields of an electrolyte solution confined in slit-like channels consisting of surfaces separated by distances that fit only a few water layers. The interaction between ions is significantly affected by the surfaces' induced polarization: the interaction is of a much shorter range in confinement by conductive surfaces than between non-polarizable surfaces, which results in ionic currents and conductivities higher in conductive slit channels than in dielectric ones [3].

Electric fields are ubiquitous in biological membrane systems, often arising due to ionic concentration gradients across a membrane or between different extracellular regions. These fields can exert important effects on membrane structure and function. We found that normal and lateral electric fields have different effects on lipid membrane mechanical properties [4]. Normal fields cause asymmetries in these properties. We derived a relation between cohesive energy and bending rigidity which provides a simple, useful way to estimate bending rigidity from a simple cohesive energy determination. We also determined changes in membrane tension under external fields. We found that normal electric fields decrease membrane tension and bending rigidity, while lateral fields increase both (Fig. 3). Normal fields change the bilayer in an asymmetric way. They cause different changes to bending rigidity on the top and bottom leaflets. This may lead to instabilities or buckling behavior. By combining rough interfaces with asymmetric ion valences (2:1), we created patterns of interfacial net charge which mirror the interfacial geometry. This has implications for designing interfaces for applications such as nanofluidic neuromorphic computing.

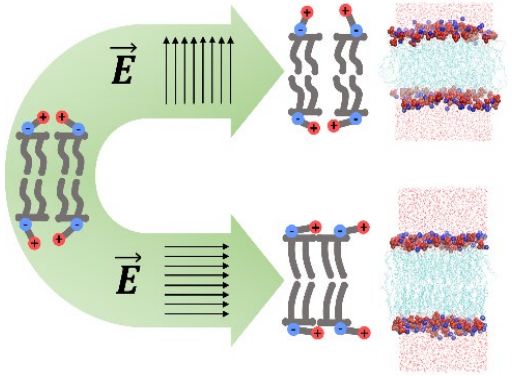

Fig. 3: Changes in tension under lateral fields are largely caused by changes in dipole-dipole interactions. Normal fields change the bilayer in an asymmetric way.

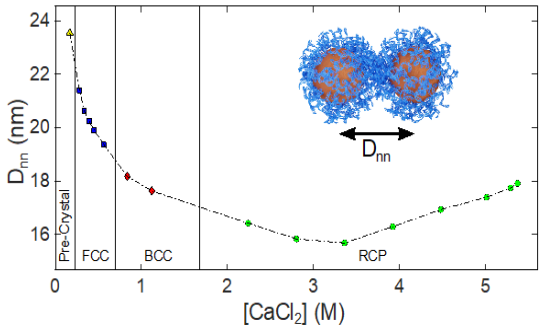

Fig. 4: Structure and interparticle separations, D_{nn}, for DNA-NPs assembled in $CaCl_2$.

We demonstrated that calcium chloride (CaCl2) induces attractive forces between DNA-NPs, resulting in the formation of face-centered cubic (FCC) crystals that transition to body-centered cubic (BCC) structures as the salinity increases due to a reduction of the hydration shells of the DNA and over screening (Fig. 4), that is, an apparent increases in the range of repulsions between like-charged surfaces [5].

Acid-base equilibria directly influence the functionality and behavior of peptides, proteins and charge regulates macroion particles. We have analyzed the charge regulation of ionizable groups in a suspension colloidal particle via Brownian Dynamics and Monte Carlo simulations.

We observed that as pH increases, particles functionalized with acid groups, change their arrangement from face-centered cubic (FCC) packing to a disordered state due to charge polydispersity arising from an increase in pH. The also studies the size, shape, and charge of amphiphilic assemblies in different solution ionic conditions. Charge regulation of the ionizable groups in such structures, is described through ionization/deionization effective equilibrium constants *pK*, which are distinct from the ionization/deionization equilibrium constants for isolated ionizable groups in dilute solutions since apparent *pK* values are affected by the size, shape and aggregation number of assemblies. We combined X-ray scattering and nonlinear Poisson-Boltzmann theory to predict the degree of ionization in assemblies of amphiphilic molecules with ionizable groups (Fig. 5) without any adjustable parameters (in preparation).

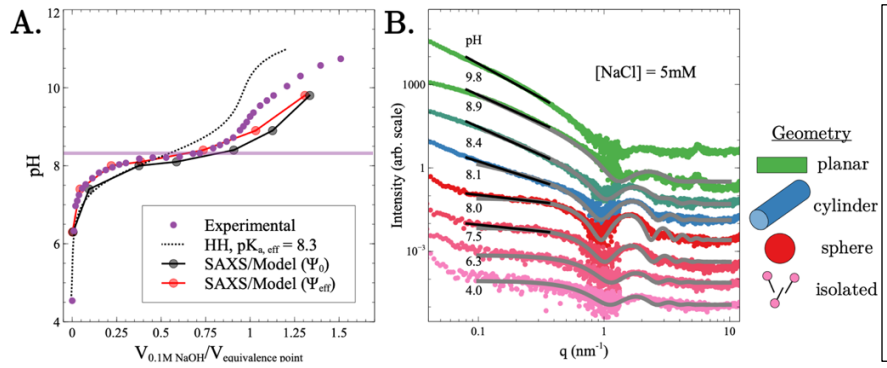

Fig.5: (A)Titration data for 4 mM $C_{16}K_2$ in 5 mM NaCl (purple circles). Titration curves based on SAXS-derived (B) size of shape data ((red circles), nonlinear Poisson-Boltzmann theory (black circles), and previous model (dotted curve).

Future Plans

We plan to investigate cooperative behaviors in a system of multiple active nanoparticles that have asymmetric surface charge and ionic flux. For many-particle systems, we plan to study emergent patterns and collective dynamics using field theoretic approaches. As an outcome, we expect to form a quantitative understanding of the key physical mechanisms governing chemotactic motion and self-organizing structures in charged systems, and provide robust schemes for optimal transport and assembly. We will assemble experimentally microcompartments of amphiphiles co-assembled with enzymes to validate the models.

We will continue developing approaches to include both dielectric mismatch [3]and charge regulation [5] to analyze ions in confinement with non-faly surfaces as well as amphiphilic and protein-based aggregates responsive to pH changes accurately.

References

1. C. Waltmann, A. Shrestha and M. Olvera de la Cruz, *Patterning of multicomponent elastic shells by Gaussian curvature*, Phys. Rev. E **109**, 054409 (2024)
2. A. Shrestha and M. Olvera de la Cruz, *Enhanced phoretic self-propulsion of active colloids through surface charge asymmetry*, Phys. Rev. E **109**, 014613 (2024)
3. F. Jimenez-Angeles, A. Ehlen, and M. Olvera de la Cruz, *Surface polarization enhances ionic transport and correlations in electrolyte solutions nanoconfined by conductors* Faraday Discuss. **246**, 576-591 (2023)

4. N. Pogharian, P. M. Vlahovska, M. Olvera de la Cruz, *Effects of Normal and Lateral Electric Fields on Membrane Mechanical Properties*, J. Phys. Chem. B (under review).
5. R. J. Reinertsen, S. Kewalramani, F. Jimenez-Angeles, S. Weigand, M. Bedzyk, M. Olvera de la Cruz, *Re-expansion of Charged Nanoparticle Assemblies in Concentrated Electrolytes*, PNAS **121**, e231653712 (2024)

Publications

1. C. Waltmann, N. W. Kennedy, C. E. Mills, E. W. Roth, S. P. Ikonomova, D. Tullman-Ercek, M. Olvera de la Cruz, *Kinetic growth of multi-component microcompartment shells*, ACS Nano **17**, 15751 (2023)
2. R. J. Reinertsen, F. Jimenez-Angeles, S. Kewalramani, M. Bedzyk, M. Olvera de la Cruz, *Transformations in crystals of DNA functionalized nanoparticles by electrolytes*, Faraday Discussions **249**, 408 (2023)
3. L. López-Flores and M. Olvera de la Cruz, *Induced phase transformation in ionizable colloidal nanoparticles*, Eur. Phys. J. E **46**, 122 (2023)
4. A. Aggarwal, E. Kirkinis, M. Olvera de la Cruz, *Thermocapillary migrating odd viscous droplets,* Phys. Rev. Lett. **131**, 198201 (2023)
5. E. Kirkinis and M. Olvera de la Cruz, *Activity-induced propulsion and separation of passive chiral particles in liquids*, Phys. Rev. Fluids **8**, 023302 (2023)
6. Y. Lin, M. Olvera de la Cruz, "Colloidal superionic conductors" PNAS **120**, 15 (2023)
7. R. J. Reinertsen, S. Kewalramani, F. Jimenez-Angeles, S. Weigand, M. Bedzyk, M. Olvera de la Cruz, *Re-expansion of Charged Nanoparticle Assemblies in Concentrated Electrolytes*, PNAS **121**, e231653712 (2024)
8. C. Waltmann, A. Shrestha and M. Olvera de la Cruz, *Patterning of multicomponent elastic shells by Gaussian curvature*, Phys. Rev. E **109**, 054409 (2024)
9. A. Shrestha and M. Olvera de la Cruz, *Enhanced phoretic self-propulsion of active colloids through surface charge asymmetry*, Phys. Rev. E **109**, 014613 (2024)
10. N. Pogharian, A. P. dos Santos, A. Ehlen, and M. Olvera de la Cruz, *Electric Fields Near Undulating Dielectric Membranes,* J. Chem. Phys. **160**, 094704 (2024)

Transport Mechanisms in Active and Biomolecular Materials

Ahmad K. **Omar**, Department of Materials Science and Engineering, University of California, Berkeley

Keywords: active matter, nucleation, capillary fluctuations, odd transport

Research Scope

Living and biological systems across an outstanding range of length scales can display dynamical properties that appear fundamentally different from those of conventional synthetic materials. The breaking of parity and time-reversal symmetry at the microscale frees biomolecular materials from the constraints these symmetries impose on the transport coefficients of traditional "passive" systems. Indeed, from the chiral motion of starfish embryos that generate "odd" transport coefficients to the predator-prey interactions among microorganisms resulting in traveling states, the living world motivates the need to advance our fundamental understanding of active transport mechanisms. Such an understanding could pave the way towards the design of next-generation materials with novel dynamical properties that could improve performance and potentially unlock new applications. Taking inspiration from a variety of recent experiments characterizing biomolecular material transport, this research leverages theory and computation to develop a microscopic understanding of some of the exotic dynamical properties exhibited by these materials. We address theoretical questions surrounding the origins of odd diffusion, explore the implications of violating Newton's third law on multicomponent diffusion, and develop a theory for the dynamics of active interfaces and nucleation. Alongside these theoretical advancements, we build and develop tools for the characterization of these transport coefficients that can be used in both computational and experimental settings. Moreover, as the line between structure and dynamics is blurred for these out-of-equilibrium systems, we will explore the implications of these transport mechanisms on material structure and stability.

Recent Progress

The statistical mechanics of equilibrium interfaces has been well-established for over a half century. In the last decade, a wealth of observations have made increasingly clear that a new perspective is required to describe interfaces arbitrarily far from equilibrium. These include the reports of a *negative surface tension* of active liquid interfaces despite the interface appearing stable. Beginning from microscopic particle dynamics that break time-reversal symmetry, we have systematically derived the interfacial dynamics of coexisting motility-induced phases. Doing so allows us to identify the athermal energy scale that excites interfacial fluctuations and the nonequilibrium surface tension that resists these excitations. Our theory identifies that, in contrast to equilibrium fluids, this active surface tension contains contributions arising from nonconservative forces which act to suppress interfacial fluctuations and, crucially, is distinct from the mechanical surface tension of Kirkwood and Buff (see Fig. 1). We find that the interfacial stiffness scales linearly with the intrinsic activity of the constituent active particle trajectories, in

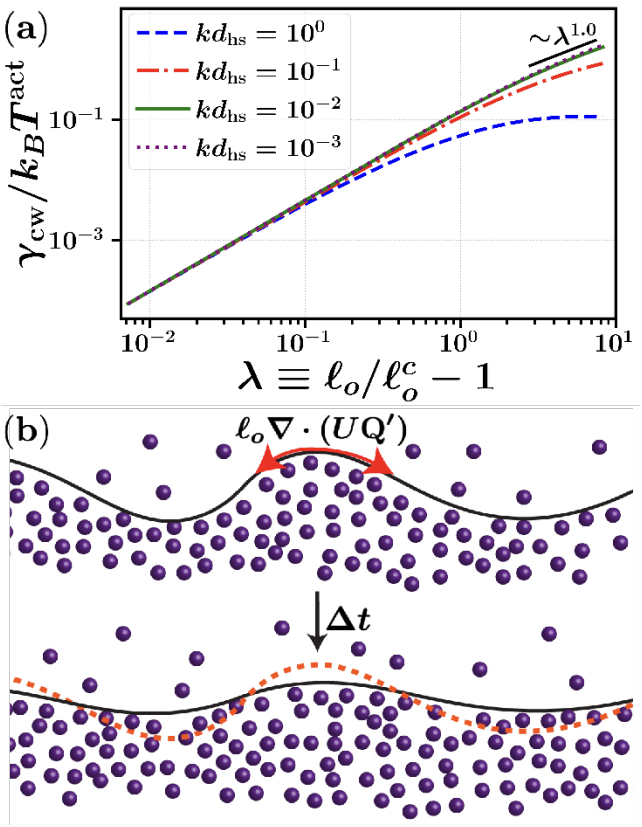

Figure 1: (a) Dynamically derived dimensionless surface tension as a function of the activity (ℓ_o) relative to its critical value (ℓ_o^c) and spatial wavevector magnitude (k). (b) Nematic flows result in a positive surface tension.

separation, we find that nucleation proceeds in a qualitatively similar fashion to equilibrium systems, with concepts such as the Gibbs-Thomson effect and nucleation barriers (see Fig. 2) remaining valid. We further demonstrate that the recovery of such concepts allows us to extend classical theories of nucleation rates and coarsening dynamics to active systems upon using the mechanically-derived definitions of the nucleation barrier and surface tensions. *Three distinct surface tensions* (see Fig. 3) -- the mechanical, capillary, and Ostwald tensions -- play a central role in our theory. While these three surface tensions are agreement with simulation data. We demonstrate that at wavelengths much larger than the persistence length, the interface obeys surface area minimizing Boltzmann statistics with our derived nonequilibrium interfacial stiffness playing an identical role to that of equilibrium systems.

We were able to build on our interfacial fluctuation perspective to develop a theory for nucleation and growth of nonequilibrium fluids. Homogeneous nucleation, a textbook transition path for phase transitions, is typically understood on thermodynamic grounds through the prism of classical nucleation theory. However, recent studies have suggested the applicability of classical nucleation theory to systems far from equilibrium. We have formulated a purely mechanical perspective of homogeneous nucleation and growth, elucidating the criteria for the properties of a critical nucleus without appealing to equilibrium notions. Applying this theory to active fluids undergoing motility-induced phase

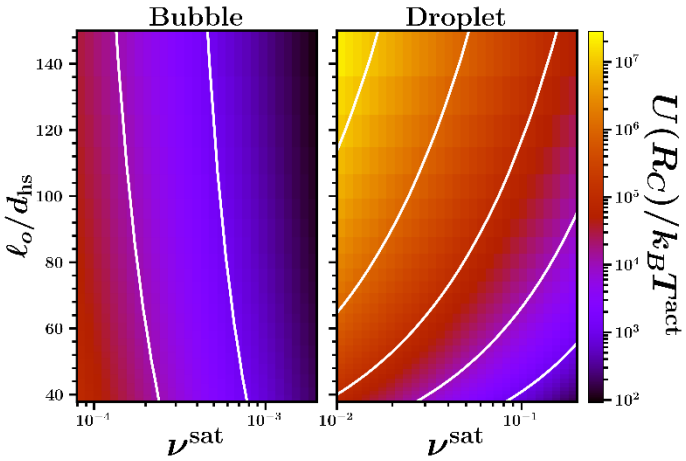

Figure 2: Dynamically derived dimensionless active nucleation barrier for bubbles and droplets as a function of the dimensionless activity ($\ell_o/d_{\rm hs}$) and dimensionless saturation density ($\nu^{\rm sat}$).

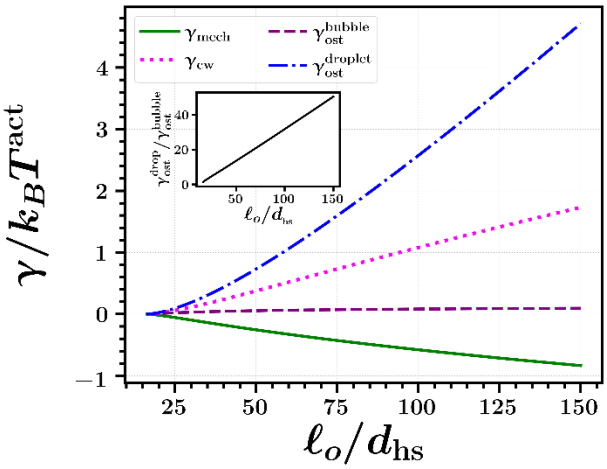

Figure 3: The *three* surface tensions of out-of-equilibrium fluids with an additional distinction between the Ostwald tensions of bubbles and droplets. *At equilibrium, all of these tensions are identical.*

identical in equilibrium, our work highlights the distinctive role of each tension in the stability of active interfaces and the nucleation and growth of motility-induced phases.

Finally, while in the above instances we have derived both the equations-of-motion and expressions for the material properties, there are instances in which theories for transport coefficients require numerical guidance. Measuring the transport coefficients of passive materials from computer simulation is facilitated by Onsager's celebrated regression hypothesis (and the resulting Green-Kubo relations) which posits a fundamental connection between macroscopic transport phenomena and the average relaxation of spontaneous microscopic fluctuations. This relaxation, however, is agnostic to *odd transport phenomena*, in which fluxes run orthogonal to the gradients driving them. To account for odd transport, we have generalized the regression hypothesis, postulating that macroscopic linear constitutive laws are, on average, obeyed by microscopic fluctuations, whether they contribute to relaxation or not. From this "flux hypothesis," Green-Kubo and reciprocal relations follow, elucidating the separate roles of broken time-reversal and parity symmetries underlying various odd transport coefficients. As an application, we derive and verify the Green-Kubo relation for odd collective diffusion in chiral active matter, first in an analytically-tractable model and subsequently through molecular dynamics simulations of concentrated active spinners.

Future Plans

Nonreciprocal interactions are ubiquitous in the natural and living world and can endow systems with properties that have no analogue in passive materials. A familiar example of a nonreciprocal interaction is the so-called "predator-prey" interaction whereby one entity (the predator) feels an attractive force towards the other (the prey) while the other is repelled. These effective nonreciprocal interactions can emerge from a host of complex factors and can have far-reaching implications on collective phenomena, phase transitions, and pattern formation. In the living world, examples range from the interactions amongst bacteria at the microscale to the dynamics of animal herds at the macroscale. Synthetic systems with nonreciprocal interactions have also been increasingly realized, with nonreciprocity emerging in systems as diverse as dusty plasmas, colloidal suspensions, and even solid metameterials. The understanding of the dynamics and structure of multiscale living systems and leveraging nonreciprocal interactions in synthetic materials will require a fundamental understanding of both the origins and implications of these effective interactions.

Effective forces acting on particles of interest have long been known to shape the structures and properties of condensed matter systems. These forces emerge from the coarse-graining of degrees of freedom, such as other species present within the system. When the coarse-grained degrees of freedom are in equilibrium the structure of the effective forces is severely restricted: the one-body forces (e.g., fluctuating Brownian and dissipative forces acting on solute upon coarse-graining a molecular solvent) must satisfy the fluctuation-dissipation theorem (FDT) and many-body forces (e.g., the pairwise depletion force between larger solutes upon coarse-graining smaller solutes) must be conservative and consistent with Newton's third law.

Coarse-graining degrees of freedom that are out of equilibrium unlocks a new range of possibilities. In a nonequilibrium environment, one-body forces need not satisfy FDT with these "active"' forces resulting in novel phase transitions and collective phenomena. A driven environment may also generate effective *nonreciprocal* many-body forces. The consequences of violating interaction reciprocity on transport phenomena and phase behavior remain unclear (especially in comparison to those of one-body active forces) and have motivated the development of a variety of phenomenological theoretical perspectives. This research effort *aims to develop the framework for multicomponent active diffusion and reveal the macroscopic consequences of violating microscopic reciprocity*. If successful, the development of a statistical mechanical framework for multicomponent active transport would allow for an understanding of how microscopic nonreciprocity can generate transport properties and dynamical phases that are unachievable for passive materials. This framework will enable the *prediction* of these novel properties from microscopic considerations, a crucial first step in the design of materials with next generation transport properties.

Publications

1. L. Langford and A. K. Omar, *Theory of Capillary Tension and Interfacial Dynamics of Motility-Induced Phases*, arXiv:2308.08531 (2024).

2. C. Hargus, A. Deshpande, A. K. Omar and K. K. Mandadapu, *The Flux Hypothesis for Odd Transport Phenomena*, arXiv:2405.08798 (2024).

3. L. Langford and A. K. Omar, *The Mechanics of Nucleation and Growth and the Surface Tensions of Active Matter*, arXiv:2407.06462 (2024).

Biomolecules for non-biological things: Peptide 'Bundlemer' design for model colloidal particle creation and hierarchical solution assembly

Darrin J. **Pochan**, Materials Science and Engineering, University of Delaware

Christopher J. Kloxin, Materials Science and Engineering/Chemical and Biomolecular Engineering, University of Delaware

Jeffrey G. **Saven**, Department of Chemistry, University of Pennsylvania

Keywords: peptides, self-assembly, nanoparticle, computational design

Research Scope

A solution-assembled system comprising computationally designed coiled coil bundle motifs, also known as 'bundlemers', will be discussed as model colloidal particle systems. The molecules and nanostructures are non-natural amino acid sequences and provide opportunities for controlled solution behavior and arbitrary nanostructure creation with peptides. With control of the display of the amino acid side chains (both natural and non-natural) throughout the peptide bundles, desired physical and covalent (through appropriate 'click' chemistry) interactions are designed to control interparticle interactions in solution, which involve both individual bundlemer particles as well as polymers of connected bundlemers. Physical, interbundlemer stacking is observed between particles to form liquid crystal phases. The individual bundlemer building blocks are responsive to varying salt and pH, since computational design is used to design bundlemers with different net charge character to manipulate their interactions in solution. Patches of interaction can be designed on the surface of the particles to dictate their physical interaction in solution and to provide control of interparticle assembly (e.g., crystalline-like lattice vs. amorphous aggregation). Included in the discussion will be new peptide molecule design, hierarchical assembly pathway design, control of nanostructure, and liquid crystal formation.

Recent Progress

Recent results involve bundlemer covalent 1-D chains with short, monodispersed lengths produced from the conjugation of bundlemers with parallel symmetry as well as physical 1-D chains (and consequent liquid crystal formation) from the stacking of new, single charge bundlemer designs. In order to form monodisperse chains, we took advantage of computationally designed coiled coil designs for bundlemer formation. These are distinct from previously studied

D_2 symmetric (antiparallel) tetrahelical bundles. One can have desired covalent 'click' chemical reactive groups on one end of the assembled bundlemer particle. Therefore, the bundlemer designs provide for anisotropic display of the functional groups. When two bundlemers are reacted together via a thiol-Michael click reaction, one bundlemer with cysteines as the N-terminal amino acid and the other bundlemer with a maleimide functionality placed at the N-terminus of the constituent peptides, they form bundlemer rods. Small-angle x-ray scattering (Figure 1) clearly shows rigid cylinders in solution with homogeneous length of ~8 nm, which is precisely the nanostructure that would form from the click conjugation between the bundlemer building blocks. Concentrated solutions show the formation of lyotropic liquid crystal phases with the monodisperse, short bundlemer rods.

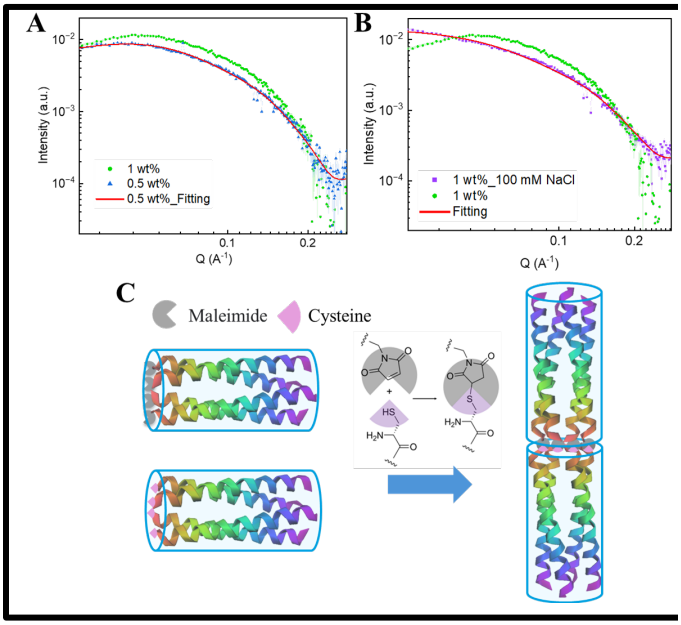

Figure 1. A) Prll_1a dibundlemer SAXS at 0.5 wt% and 1.0 wt% with the 0.5 wt% data fit with a cylindrical rod form factor with a radius of ~1.5 nm and a length of ~8 nm. B) The addition of 100 mM NaCl to the 1.0 wt% sample eliminates the interparticle structure factor for the 1.0 wt% rod smaple allowing a cylindrical rod form factor fit. C) Schematic of the thiol-Michael covalent Prll_1a dibundlemer rod formation.

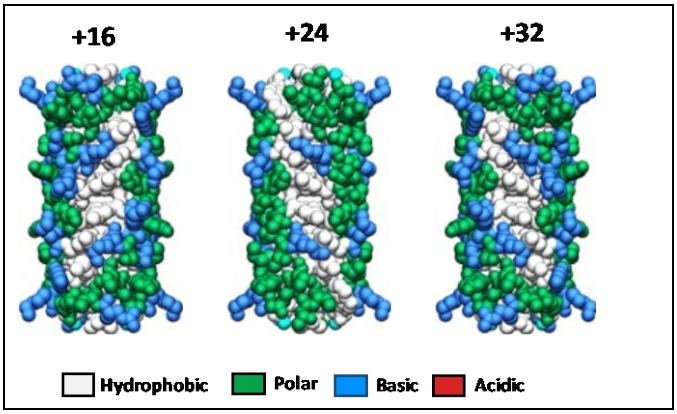

Figure 2. Renderings of new single charge bundlemer particles with varying net charge that contain no acid amino acid residues and, therefore, no attractive electrostatic patches on the particle surfaces.

Other recent designs include homotetrameric bundlemers with antiparallel (D_2 symmetric) packing but with peptides that include only one charge type (only acidic residues vs only basic residues) to make 'single charge type' particles (Figure 2) as opposed to the typical mixed charge character of typical, natural proteins. This single charge character produces particles in solution that are purely repulsive electrostatically as opposed to proteins with mixed charges that produce patches of attractive interparticle interactions. The laterally repulsive particles also stack in an end-to-end fashion producing hexagonal columnar liquid crystal phases at very low concentrations where equivalently charged mixed charge systems produce only soluble aggregates in solution, highlighting the unique behavior of the single charge system.

The other main area of discussion is the solution assembly of bundlemer building blocks into 2-d and 3-d lattices through designed, interparticle interactions. Specifically, mixtures between oppositely charged bundlemers are created to use electrostatic interactions to form nanostructure. Comparisons were made between mixtures of bundlemers with both positively and negatively charged amino acids within the individual bundlemers (what we call "mixed charge" bundlemers with a desired net charge) vs. mixtures using the bundlemer designs that only have one type of charged residue within their peptide primary sequence (what we call "single-charge bundlemers"). The desired display of charged groups was observed to have pronounced effects on the nanostructure formed via electrostatic complexation.

Future Plans

Future focus will be the extent to which we can control the assembly behavior by using new bundlemer designs with display of desired sets of charged amino acids, different amino acid side chains (e.g., natural bases or acids vs non-natural ionic side chains), and different bundlemer symmetries (e.g., antiparallel coiled coils vs parallel). Furthermore, our ability to control the solution behavior of the bundlemers containing a single type of charged amino acid will be studied and compared to mixed-charge particles where we hypothesize greater dispersion and interparticle repulsion of the single-charge constructs vs the mixed-charge sequences, which have patches of charge that may facilitate to aggregation.

Publications

1. J. E. Meisenhelter, N. R. Petrich, J. E. Blum, A. R. Weisen, R. Guo, J. G. Saven, D. J. Pochan, C. J. Kloxin. *Impact of Peptide Length and Solution Conditions on Tetrameric Coiled Coil Formation.* Biomacromolecules **25**, 3775–3783 (2024).
2. S.S. Patkar, Y. Tang, A.M. Bisram, T. Zhang, J.G. Saven, D.J. Pochan, and K.L. Kiick, *Genetic Fusion of Thermoresponsive Polypeptides with UCST-type Behavior Mediates 1D Assembly of Coiled-Coil Bundlemers*. Angew. Chem. Int. Ed., **62**, e202301331 (2023).
3. G.A. Taggart, A. Guliyeva, K. Kim, G.P.A. Yap, D.J. Pochan, T.H. Epps, and E.D. Bloch, *Monitoring the Solution Persistence of Porous Coordination Cages with Diffusion NMR Spectroscopy and Cryogenic Transmission Electron Microscopy.* The Journal of Physical Chemistry C, **127**, 2379-2386 (2023).
4. R. Guo, N.J. Sinha, R. Misra, Y. Tang, M. Langenstein, K. Kim, J.A. Fagan, C.J. Kloxin, G. V. Jensen, D. J. Pochan, and J.G. Saven, *Computational Design of Homotetrameric Peptide Bundle Variants Spanning a Wide Range of Charge States.* Biomacromolecules **23**, 2022, 1652-1661 (2022).
5. N. J. Sinha, R. Guo, R. Misra, J. Fagan, A. Faraone, C.J. Kloxin, J.G. Saven, G.V. Jensen, and D.J. Pochan, *Colloid-like Solution Behavior of Computationally Designed Coiled Coil Bundlemers*. J Colloid Interf Sci **606**, 1974-1982 (2022).
6. K. Kim, C.J. Kloxin, J.G. Saven, and D.J. Pochan, *Nanofibers Produced by Electrospinning of Ultrarigid Polymer Rods Made from Designed Peptide Bundlemers.* ACS Appl Mater Inter **13**, 26339-26351 (2021).

7. N. J. Sinha, Y. Shi, Y. Tang, C.J. Kloxin, J. G. Saven, A. Faraone, G. V. Jensen, and D. J. Pochan, *Intramolecular Structure and Dynamics in Computationally Designed Peptide-Based Polymers Displaying Tunable Chain Stiffness.* Phys Rev Mater **5**, 095601 (2021).
8. N. J. Sinha, C. J. Kloxin, J. G. Saven, G. V. Jensen, Z. Kelmane, and D. J. Pochan. *Recombinant expression of computationally designed peptide-bundlemers in Escherichia coli.* Journal of Biotechnology **330**, 57-60 (2021).

Adaptive Nonequilibrium Design of Biological Metamaterials: Theoretical Constraints and Practical Strategies

Grant M. **Rotskoff**

Keywords: nonequilibrium control, self-assembly, reinforcement learning, metamaterials

1. Research Scope:

Our poster presents progress on the development of a comprehensive theoretical and computational framework for understanding and controlling nonequilibrium self-assembly. We seek to bridge the gap between basic theoretical results and the practical design of nanomaterials using experimental control. This problem is inherently multiscale, spanning from molecular interactions to emergent material properties, and integrates theory from optimal transport and stochastic thermodynamics. We present results that constrain thermodynamic and information-theoretic entropy in systems driven far from equilibrium. We derive bounds on dissipation, speed, and accuracy of control protocols, and explore their implications for biomaterial design [1]. Our approach combines analytical methods [1,2], numerical simulations [3], and machine learning techniques [1-3]. We develop minimal models that capture essential physics while remaining tractable, and we employ advanced computational methods to explore complex, many-body systems. We exemplify these bounds in the context of growing F-actin networks [3] and self-assembly of passive particles in a chiral active bath [4].

2. Recent Progress

We derived a lower bound on the dissipated work in generic nonequilibrium control problems that extends the "Wasserstein speed limits" to the more realistic setting of imprecise experimental control [1]. This result generalizes and refines previous thermodynamic speed limits by accounting for imperfect control, a ubiquitous scenario in practical applications. The bound is asymptotically tight and reduces to known results in the limit of perfect control. Importantly, it provides meaningful constraints even when the target distribution is not fully realized, making it particularly relevant for experimental and computational studies of material assembly. We demonstrate the utility of this bound for various systems, illustrating that it provides a more precise metric of efficient control protocols. Our analysis reveals fundamental trade-offs between dissipation, speed of transformation, and accuracy of the final state, providing a unifying framework for understanding the costs of nonequilibrium control.

To test these ideas in the setting of biomolecular material design, we developed a minimal model of branched actin network growth under dynamic force protocols, inspired by recent experiments on reconstituted systems. Our model captures key features of actin polymerization, branching, and capping, as well as the force-dependent growth dynamics observed experimentally. Using this model, we demonstrated that external feedback control during network assembly can encode growth-dependent properties into the resulting structure, leading to tunable mechanical responses.

We employed multi-task reinforcement learning to optimize control protocols, enabling access to regions of configurational space that are inaccessible through uncontrolled growth. Our analysis also reveals how spatially heterogeneous density profiles emerge from the interplay between applied forces and network reorganization. These heterogeneous structures exhibit metamaterial-like properties, with mechanical responses that can be precisely tuned by modulating the growth conditions. We quantified these effects through detailed studies of the network's elastic properties and response functions.

Through a combination of large-scale molecular dynamics simulations and continuum modeling, we elucidated the microscopic mechanisms by which chiral active particles induce effective interactions between passive solutes. Our work reveals that odd diffusive dynamics, arising from the breaking of time-reversal and parity symmetries, play a crucial role in generating long-range attractive forces that can drive robust assembly. We developed a minimal continuum model based on odd hydrodynamics that captures the essential physics of this phenomenon. Our model accurately predicts the density profiles and force generation observed in detailed simulations across a wide range of parameters, including particle density, activity, and chirality.

3. Future Plans:

Building on these results, we are investigating the modulation of force-sensitive bonds, known as “catch bonds” to design metamaterials. We will focus on the biological context of sarcomere self-assembly, which is the fundamental contractile units of muscle tissue. This system presents an intricate example of multiscale, force-sensitive assembly that is critical to biological function and offers inspiration for synthetic adaptive materials. We will investigate how these molecular-scale features influence the macroscopic assembly and mechanical properties of the sarcomere.

References

1. Klinger, J.; Rotskoff, G. M. Computing Nonequilibrium Responses with Score-Shifted Stochastic Differential Equations. arXiv June 20, 2024. http://arxiv.org/abs/2406.14752 (accessed 2024-06-23).
2. Klinger, J.; Rotskoff, G. M. Universal Energy-Speed-Accuracy Trade-Offs in Driven Nonequilibrium Systems. arXiv February 27, 2024. http://arxiv.org/abs/2402.17931 (accessed 2024-02-29).
3. Chennakesavalu, S.; Manikandan, S. K.; Hu, F.; Rotskoff, G. M. Adaptive Nonequilibrium Design of Actin-Based Metamaterials: Fundamental and Practical Limits of Control. *Proceedings of the National Academy of Sciences* **2024**, *121* (8), e2310238121. https://doi.org/10.1073/pnas.2310238121.

4. Batton, C. H.; Rotskoff, G. M. Microscopic Origin of Tunable Assembly Forces in Chiral Active Environments. *Soft Matter* **2024**, *20* (20), 4111–4126. https://doi.org/10.1039/D4SM00247D.

Publications

1. Batton, C. H.; Rotskoff, G. M. Microscopic Origin of Tunable Assembly Forces in Chiral Active Environments. *Soft Matter* **2024**, *20* (20), 4111–4126. https://doi.org/10.1039/D4SM00247D.
2. Liu, K.; Rotskoff, G. M.; Vanden-Eijnden, E.; Hocky, G. M. Computing Equilibrium Free Energies through a Nonequilibrium Quench. *The Journal of Chemical Physics* **2024**, *160* (3), 034109. https://doi.org/10.1063/5.0176700.
3. Chennakesavalu, S.; Rotskoff, G. M. Data-Efficient Generation of Protein Conformational Ensembles with Backbone-to-Side-Chain Transformers. *J. Phys. Chem. B* **2024**. https://doi.org/10.1021/acs.jpcb.3c08195.
4. Chennakesavalu, S.; Manikandan, S. K.; Hu, F.; Rotskoff, G. M. Adaptive Nonequilibrium Design of Actin-Based Metamaterials: Fundamental and Practical Limits of Control. *Proceedings of the National Academy of Sciences* **2024**, *121* (8), e2310238121. https://doi.org/10.1073/pnas.2310238121.
5. Chennakesavalu, S.; Toomer, D. J.; Rotskoff, G. M. Ensuring Thermodynamic Consistency with Invertible Coarse-Graining. *J. Chem. Phys.* **2023**, *158* (12), 124126. https://doi.org/10.1063/5.0141888.
6. Chennakesavalu, S.; Rotskoff, G. M. Unified, Geometric Framework for Nonequilibrium Protocol Optimization. *Phys. Rev. Lett.* **2023**, *130* (10), 107101. https://doi.org/10.1103/PhysRevLett.130.107101.

Bending Controlled 2D Crystal Morphology and Impact on Vesicle Shapes

Maria M. **Santore** and Gregory M. Grason Department of Polymer Science and Engineering , University of Massachusetts, Amherst, MA 01003.

Keywords: elasticity, assembly, two dimensional colloids, crystallization

Research Scope

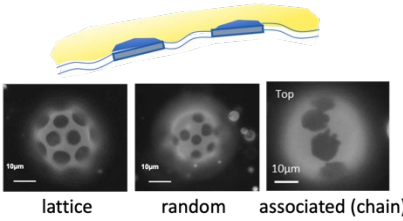

Figure 1. Schematic of 2D fluid-solid composite and examples of solid element configurations.

This program integrates theory and experiment to facilitate the discovery and understanding of elasticity-driven patterning mechanisms in flexible ultrathin composite sheets and to realize these mechanisms in materials such as elastic lamellae that act as 2D composites due to their coexisting fluid and solid (often crystalline) phases or regions. 2D fluid-solid composites exhibit sought-after properties not achieved with either classical solid sheets such as graphene, no matter how thin or flexible, nor by canonical fluid membranes themselves. For instance their fluid-solid composite character enables the thin sheets in this program to reversibly assume a variety of complex contours having non-zero Gaussian curvature, thereby accessing shapes not achievable with thin solid films which bend only cylindrically. In addition, the composites in this program reversibly assemble their solid constituents in arrays and other patterns in response to mechanical stimuli, and can switch between patterns and spacing with mechanical triggers. Examples include regular hexagonal lattices, parallel stripes, or interconnected networks where the hierarchy and connectivity of the structure spans length scales up to that of the system, typically many tens of microns. Notably solid domains, once created, comprise a chemically and materially fixed set of building blocks from which different patterns assemble, accessing many material properties from a fixed composition.

This program exploits the 4nm-thick lamellae of giant unilamellar phospholipid vesicles containing fluid and solid domains as a platform to establish mechanisms of pattern formation. These two-phase biomolecular membranes have 2D fluid regions with integrated 2D solids both with bending and stretching elasticity. The fluid regions flow freely via in-plane shear while the solid domains have large in-plane moduli that effectively eliminate shear deformation. Thus, solid shear elasticity underlies the geometrically nonlinear coupling between Gaussian curvature and in-plane strain of 2D sheets. Extensive analytical and finite element modeling combines with experiment to develop a predictive framework for understanding and guiding their complex functions.

Recent Progress

Overview. Comparison of simulation and experiment reveal how bending energy, distributed between the fluid membrane and a single solid domain, which nucleates and grows as a crystal within a fluid membrane, influence the growing crystal shape. Current work further translates the mechanism of combined fluid and solid elasticity to processing strategies that enable crystals of different shapes and sizes to be produced at small but regular scale on vesicles of different sizes. These translate to processing maps to produce different single solid domain shapes on vesicles of different size. The bending energy, arising predominantly from curvature of the 2D fluid, varies depending on shape constraints that are externally imposed and on the positions of compact solid domains relative to one another, leading to phase transitions in assembly and touch-sensitivity of assembly patterns. Major theory advances explore the relationship between the presence of a rigid circular solid domain and the shape of a vesicle.

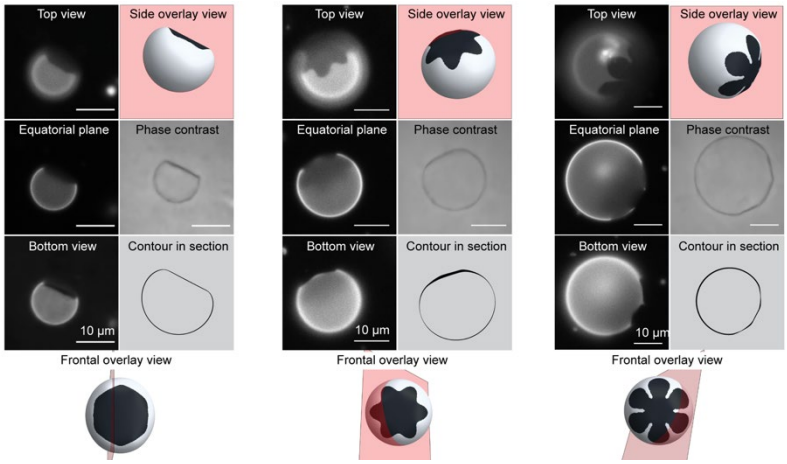

Figure 2. Observed and computed vesicle and crystal shapes.

Processing Strategies to Exploit Bending in Selection of Crystal Shapes. We demonstrated how the total energy (bending energy plus line energy) selects the preferred solid domain morphology, employing finite element computations and an experimental model of giant unilamellar vesicles of 30% DPPC and 70% DOPC along with a tracer dye that resides in the fluid phase, revealing solid crystals that appear dark.[1] At elevated temperatures this composition produces a one phase fluid membrane that, upon cooling to room temperature, nucleates and grows membrane-integrated rigid crystals of 6-fold symmetry which are nearly pure in DPPC. The relatively low DPPC content favors the nucleation of a single crystal of ~13% area fraction in each giant unilamellar vesicle, enabling a systematic study of factors influencing their morphology. Comparison of experimental images with Surface Evolver-computed elastic energy optimizing shapes established the distinct importance of bending energy in both fluid and crystal phases, a substantial departure from prior studies of colloidal crystal growth from suspension onto curved templates[2] and related theory.[3] While the strain energy of a crystal forced to assume a shape having non-zero Gaussian curvature is large enough to shift the crystal growth away from such morphologies, crystals grown in large vesicles were observed to produce flower petal like protrusions while compact domains were found on small vesicles. This opposes expectations, for instance the curvature dependence of templated colloidal crystals.[2] The explanation that larger vesicles experience higher tension, increasing the impact of bending energy, provides an inroads for scalable processing and separation strategies to produce differently shaped crystals.

An engineering model, taking into consideration thermal membrane contractions during cooling (tending to increase membrane tensions) and water loss due to membrane permeation (tending to relax tension, and incorporating the membranae area expansion modulus, coefficient of thermal expansion, and permeability, was developed to predict the evolution of membrane tension for vesicles of different sizes, subject to different cooling histories prior to and during thee nucleation and growth of solid crystals. From this model, we demonstrated 1) how the cooling rate and vesicle size influenced tension even before entry into the two phase region, such that the shapes of crystals were predetermined by history even before they grew large enough to be visible in a fluoresce microscope, and 2) that while, at any given moment during cooling, tension is continuous in vesicle size, for a wide range of realistic membranae properties, small and large vesicles exhibit qualitative different overall behaviors. Smaller vesicles reach a tension plateau and large vesicles experience sharply increasing tensions to the point at which vesicles must surely rupture but could experience burst- reseal processes. The low tension plateau limits the tension experienced by small vesicles, enabling the growth of compact domains while the large vesicles, with higher tensions produce vesicles with 6-fold protrusions, with star and flower shapes. 3) We demonstrated agreement between predicted and measured tensions; 4) we created a processing state space maps combining the vesicle size and cooling rate as they variables, comparing experimental morphology and lines of iso-tension; and 5) we demonstrated the impact of the different membrane properties on the impact of cooling rate and vesicle size on the distribution of shapes expected. This new understanding of tension history and the influence of the fluid membrane phase on the ultimate morphology of a growing crystal provides a means to create desired building blocks for studies of their assembly and, more broadly a potential means of producing and purifying ultrathin crystals at modest scale.

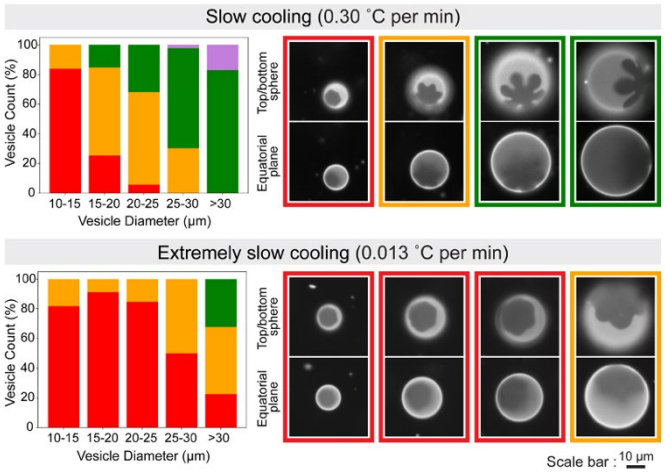

Figure 3. Influence of cooling history on crystal shape.

<u>Emergent Shape Space of Composite Vesicles with Single, Rigid, Compact Domains.</u> Towards an understanding of the assembly of compact rigid domains in fluid sheets or membranes, modeling was undertaken to probe the preferred shapes of vesicles containing single small flat circular solid domains. An analytical treatment centering on a Helfrich energy and combining inflation volume and surface energy terms was employed to probe the minimal energy shapes of axisymmetric vesicles having a fixed volume and total area, and a solid domain occupying a fixed vesicle area fraction.[4] The energies of non-axisymmetric shapes were computed using Surface Evolver, a finite element treatment. These results depart dramatically from the well-establish, canonical case of axisymmetric homogenous vesicles,[5] whose ground states remain *prolate* for inflations exceeding 0.65 reduced volume and *oblate* at highly underinflated volumes below this value. Because of the

redistribution of Gaussian (and mean) curvature required by the slid domain, on composite vesicles oblate shapes are generally preferred in vesicles containing disc-shaped solid domains. Indeed, the introduction of the solid disk into the membrane was shown to shift the oblate-prolate competition in favor oblate shapes, such that, depending on the area fraction of the solid domain, the transition between the two shape classes is substantially altered. The preference for oblate shapes increases with solid area fraction while, for solid discs of 10-15% of the total area, corpuscular vesicle shapes develop when vesicles are substantially deflated. Here, these new theoretical results parallel common experimentally observed shapes, in Figure 4. Further computation reveals that, with vesicle deflation, there is an increased capacity for irregular vesicle shapes and for a small solid domain to break axisymmetry. Moreover, new parameters are identified linking the elastic energy, tension, and length scale of bending at the domain edge in the asymptotic high inflation limit. In addition to establishing the reduced set of parameters that govern the accessible shape space of single round rigid domain vesicles, our theory identifies conditions that give the greatest configurational stability versus those which are highly sensitive to slight perturbations, with both being potentially useful.

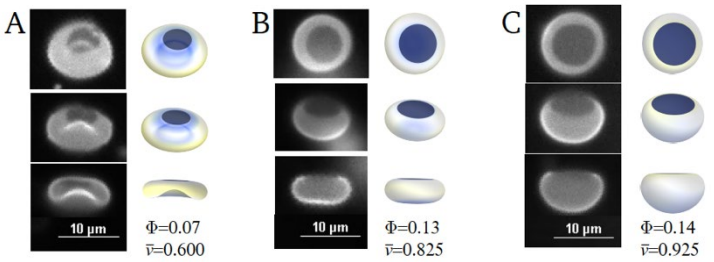

Figure 4. Observed and predicted influence of a single round domain on vesicle shape.

Future Plans

While much recent effort has advanced our understanding of the shapes of single solid domains within vesicles, the impact of the fluid membrane elastic on the solid domain morphology, and the presence of one solid domain on the shapes of closed fluid membranes, we anticipate next steps will focus on the impact of elasticity on the morphology, interactions, and assembly of multiple solid domains within single vesicles.

References

1. H. Wan, G. Jeon, W. Y. Xin, G. M. Grason, and M. M. Santore, *Flower-shaped 2D crystals grown in curved fluid vesicle membranes*. Nature Comm **15**, 3442 (2024).

2. G. N. Meng, J. Paulose, D. R. Nelson, and V. N. Manoharan, *Elastic Instability of a Crystal Growing on a Curved Surface*. Science **343**, 634-637 (2014).

3. C. Kohler, R. Backofen, and A. Voigt, *Stress Induced Branching of Growing Crystals on Curved Surfaces*. Phys Rev Lett **116**, (2016).

4. J. Geon, J. Fagoni, H. Wan, M. M. Santore, and G. M. Grason, *Shape eqilibria of vesicles with rigid planar inclusions*. Soft Matter (2024).

5. U. Seifert, K. Berndl, and R. Lipowsky, *Shape transformations of vesicles - phase diagram for spontaneous curvatue and bilayer coupling models*. Physical Review A **44**, 1182-1202 (1991).

Publications

H. Wan, G. Jeon, W. Y. Xin, G. M. Grason, and M. M. Santore, *Flower-shaped 2D crystals grown in curved fluid vesicle membranes*. Nature Comm **15**, 3442 (2024).

J. Geon, J. Fagoni, H. Wan, M. M. Santore, and G. M. Grason, *Shape eqilibria of vesicles with rigid planar inclusions*. Soft Matter (2024) accepted, in press. https://arxiv.org/abs/2404.09355

H. Wan, G. Jeon, W., G. M. Grason, and M. M. Santore, *Thermal Preconditioning of Membrane Stress to Control the Shapes of Ultrathin Crystals*. Soft Matter, in review. http://arxiv.org/abs/2407.05228

W. Xin, and M. M. Santore, Bending-Driven Patterning of Objects in Lipid Membranes: Colloidal Assembly in Elastic 2D Fluids, Proceedings of the National Academy of Science, in review. https://arxiv.org/abs/2402.15068

Computationally designed coiled coil 'bundlemers' as model colloidal nanoparticles for solution assembly and materials design

Jeffery **Saven**, , Darrin **Pochan**, & Christopher Kloxin

Keywords: Colloids, Self-assembly, Computational design, Peptidic Materials

Research Scope

We describe the creation of targeted nanomaterials using computationally designed peptide coiled coil nanoparticles, or "bundlemers", with controllable particle size and shape coupled with customizable surface amino acid residue display. The bundlemer is a model nanoparticle that is used to study of peptidic particle solution behavior and complex colloidal stability. Specifically, we focus on the importance of the patterning of charge and hydrophobicity on the surface of the particles to understand the importance of spatial display of interparticle interactions on solution assembly toward programmed nanomaterials. While physical (noncovalent) interactions are a driving force for solution assembly, we also use covalent interactions to stabilize and polymerize nanostructures that result from physical interactions during solution self-assembly.

Bundlemer nanoparticles are designed de novo using theory and computational modeling, which is not contingent on known natural proteins and allows programmability using natural and unnatural amino acids with low molecular weight sequences. The computational modeling and design, peptide synthesis and modification, conjugation chemistry, and materials characterization create processes that afford materials with protein-like, molecular scale definition and nanometer scale structure through simple solution assembly. This work addresses the encoding of materials structure and function into constituent molecular structures and properties. Potential applications include new liquid crystal phase formation exclusively from peptidic molecular assemblies and three-dimensional lattices with crystalline-like symmetry, defined nano-porosity, and tailorable chemical functionality.

Recent Progress

The effort has resulted in the prediction of a series of peptides that were designed to produce homotetrameric coiled coil particles with antiparallel symmetry but with fine-tuned net

charge. With computationally designed bundlemer particles, bundle charge can be varied in well-defined increments via designed positioning of ionizable amino acids side chains. For a sufficiently stable bundle, this variation can be achieved without varying the backbone structure or hydrophobic core of the protein. Such variation of only the exterior amino acids allows for the creation of a series of building blocks with finely-tuned differences in net charge and charge patterns. The computational design approach has been used to identify exterior residues where ionizable amino acids are particularly probable. We introduced constraints in the calculations to specify a net overall charge of the sequences. Making amino acid substitutions based on the calculated probabilities and repeating the calculation provides an approach to iteratively identify a series of bundles with targeted charges. Charge state is determined by the expected charge states (at pH 7) of ionizable amino acid residues. To specify charge, we employed combinations of the natural amino acids: glutamic acid, aspartic acid, lysine, and arginine (having charges of -1, -1, +1, and +1, respectively in units of the electron charge). Via an iterative process of design, synthesis, and characterization, we identified sets of bundle-forming peptides having varying net charge, from -8 to +8 per peptide or -32 to +32 per tetrameric bundle building block. The folding and assembly of these individual coiled coils were experimentally confirmed. The antiparallel symmetry also was confirmed through successful end-to-end covalent conjugation of the building blocks into long, rigid chains through reaction of properly functionalized N-termini of two bundlemer populations in a binary reaction mixture. This series of peptide particle designs afforded us the ability to explore the solution behavior of these particles with the same size and shape but with surface charge altered with individual amino acid precision. This work relied on the complete, collaborative skills of all members with new particle computational design (Saven), synthesis and folding studies (Kloxin and Pochan), covalent click 1-D linking, and solution characterization of individual bundlemers and 1-D polymeric chains (Pochan).

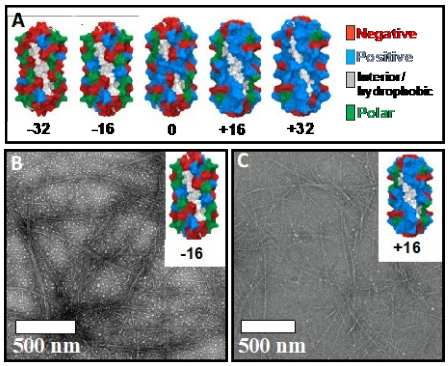

Figure: A) Bundlemer design with targeted net charge. Putative charge shown is that of designed homotetrameric coiled coil. B) Negatively stained TEM of long chains made from covalent conjugation of the -16 bundlemer building block via the N-termini of the constituent peptides. C) Negatively stained TEM of long chains made from covalent conjugation of the +16 building block through the N-termini of the constituent peptides.

Future Plans

Targeted, designed materials discovery will leverage designed physical (noncovalent) interactions for solution phase assembly. These include: liquid crystal materials obtained from solutions of bundlemer particles that contain carefully controlled charge type, net charge, and charge distribution; lattices formed via the interparticle assembly of bundlemers; and assemblies resulting from mixtures of distinct bundlemers.

Publications

1. Y. Ning, S. Yang, D.-B. Yang, Y.-Y. Cai, J. Xu, R. Li, Y. Zhang, C. R. Kagan, J. G. Saven, C. B. Murray. *Dynamic Nanocrystal Superlattices with Thermally Triggerable Lubricating Ligands*. J. Am. Chem. Soc. **146**, 3785–3795 (2024).
2. J. E. Meisenhelter, N. R. Petrich, J. E. Blum, A. R. Weisen, R. Guo, J. G. Saven, D. J. Pochan, C. J. Kloxin. *Impact of Peptide Length and Solution Conditions on Tetrameric Coiled Coil Formation.* Biomacromolecules **25**, 3775–3783 (2024).
3. S. S. Patkar, Y. Tang, T. Zhang, A. M. Bisram, J. G. Saven, D. J. Pochan, K. L. Kiick*, Genetically Fused Resilin-like Polypeptide–Coiled Coil Bundlemer Conjugates Exhibit Tunable Multistimuli-Responsiveness and Undergo Nanofibrillar Assembly.* Biomacromolecules **25**, 2449–2461 (2024).
4. S. S. Patkar, Y. Tang, A. M. Bisram, T. Zhang, J. G. Saven, D. J. Pochan, K. L. Kiick *Genetic Fusion of Thermoresponsive Polypeptides with UCST-type Behavior Mediates 1D Assembly of Coiled-Coil Bundlemers.* Angew. Chem. Int. Ed. **62**, e202301331 (2023).
5. J. A. Villegas, N. J. Sinha, N. Teramoto, C. D. Von Bargen, D. J. Pochan, J. G. Saven *Computational Design of Single-Peptide Nanocages with Nanoparticle Templating.* Molecules **27**, 1237 (2022).
6. R. Guo, N. J. Sinha, R. Misra, Y. Tang, M. Langenstein, K. Kim, J. A. Fagan, C. J. Kloxin, G. Jensen, D. J. Pochan, J. G. Saven *Computational Design of Homotetrameric Peptide Bundle Variants Spanning a Wide Range of Charge States.* Biomacromolecules **23**, 1652–1661 (2022).
7. N. J. Sinha, R. Guo, R. Misra, J. Fagan, A. Faraone, C. J. Kloxin, J. G. Saven, G. V. Jensen, D. J. Pochan. *Colloid-like solution behavior of computationally designed coiled coil bundlemers.* J. Colloid Interface Sci. **606**, 1974–1982 (2022).

Synthesizing functionality in excitonic systems using DNA origami

Gabriela S. **Schlau-Cohen** (PI), Department of Chemistry
Mark Bathe (co-PI), Department of Biological Engineering
Adam P. Willard (co-PI), Department of Chemistry
Massachusetts Institute of Technology

Keywords: DNA nanotechnology, excitonic materials, solar energy conversion

Research Scope

Our research program aims to establish a class of DNA-based materials that enable programmable exciton dynamics. The functional breadth of electronic excited states, *i.e.*, excitons, is remarkably rich. For example, chlorophyll can function in multiple ways, performing nanoscale energy transfer, facilitating charge separation, and undergoing rapid non-radiative decay. Natural systems select amongst these functions via precise positioning of chlorophyll within their protein scaffolds. This position-dependent functionality can be achieved in synthetic systems by using DNA origami architectures as scaffolds for molecular chromophores. The structural variety and geometric precision afforded by higher-order DNA origami architectures enable the development of bioinspired excitonic systems with broad and tunable functionalities that mimic or potentially exceed those found in Nature. DNA-based excitonic systems have been demonstrated previously, yet have employed a limited number of DNA structural motifs. In turn, these motifs demonstrate limited control over chromophore positioning and interchromophoric coupling, and so studies thus far have focused on exciton transport efficiency alone. We are advancing in the complexity and precision of these structures to enable the investigation of other fundamental functions in exciton dynamics, such as charge separation, singlet fission, and non-radiative decay.

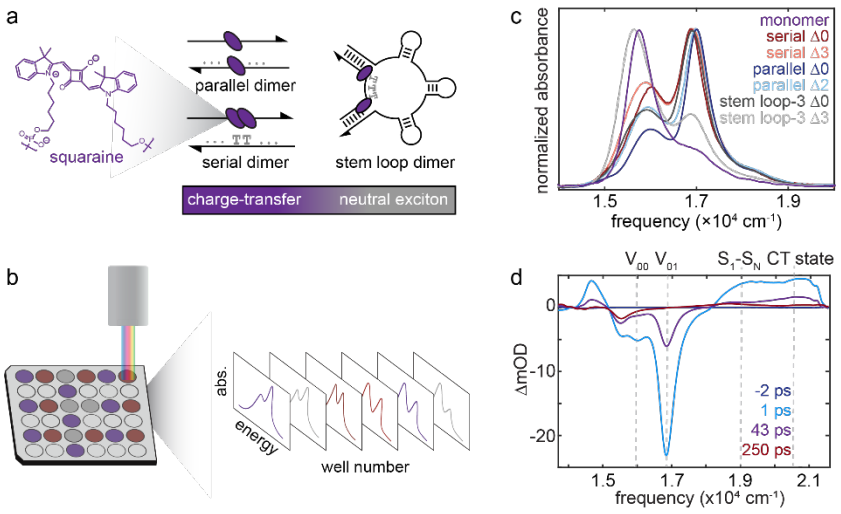

Figure 1. Exploring charge-transfer coupling in DNA-chromophore assemblies. (A) Schematic of DNA-squaraine assemblies. (B) High-throughput screening of DNA-squaraine constructs to rapidly sample excitonic properties. (C) Absorption spectra of squaraine monomers and dimer duplexes and stem loop constructs. (D) Femtosecond transient absorption spectra for the stem loop-3 constructs dimer upon excitation centered at 17,700 cm^{-1}.

Recent Progress

A major focus of the project has been optimizing chromophore geometry for photoproduct selection. In recent work, we have demonstrated the ability to selectively drive charge transfer, form excimers, and program pathways for electronic energy migration.

Activating charge transfer formation in strongly-coupled dimers using DNA scaffolds. Excitonic systems are typically regulated by long-range Coulombic coupling and short-range charge transfer coupling. Here, we leverage variable DNA-chromophore constructs to tailor the interplay between the types of couplings through the examination of a zwitterionic squaraine dye (Figure 1A).[1] We developed a method to perform a high-throughput screening of the excitonic properties, which we leveraged to rapidly characterize ~50 constructs with steady-state absorption and emission spectroscopy (Figure 1B). These steady-state measurements revealed the formation of strongly-coupled dimers possessing a charge transfer state (Figure 1C). We further investigated this state via transient absorption spectroscopy (Figure 1D). The strongly-coupled squaraine dimer exhibits symmetry-breaking charge transfer. Despite extensive previous studies, charge transfer had not been previously achieved in squaraine dimers. This work demonstrates that DNA scaffolds offer the potential to control the interplay of intermolecular couplings, which allows the selection of distinct photochemical and photophysical processes.

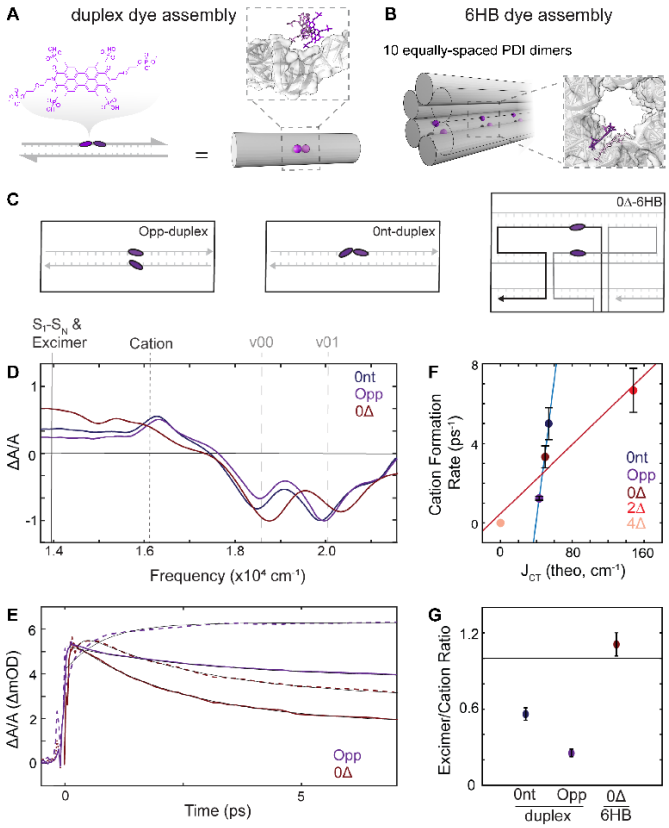

Figure 2. (A) Duplex and (B) 6HB dimers. (C) Illustration of strongly-coupling dimers in duplex and 6HB constructs. (D) TA spectrum collected at τ=3 ps of duplex dimers with 0 nucleotide spacing (0nt; blue) and opposite (opp; purple) configurations, as well as an opp-6HB dimer (0Δ; red). (D) Kinetic traces for PDI cation (dashed) and excimer (solid) in opp-duplex- and 0Δ 6HB-dimers. (F) Comparison of cation formation rate for duplex and 6HB assemblies with varied Coulombic coupling. (G) Excimer-cation sub-population ratios for duplex and 6HB assemblies.

Sculpting photoproducts with DNA origami. The geometry of coupled chromophores dictates the nature of their intermolecular interactions and, thus, the emergence and propagation of excited electronic states. Previously, DNA-based systems had been limited to the building blocks of DNA origami, which have included duplexes and DX-tiles. Here, we introduce six-helix

bundles (6HBs), a DNA origami scaffold, and leverage the additional geometric control offered by this more complex structure to program specific couplings in dimers of a prototypical molecular sensitizer, perylene diimide (PDI). We templated PDI dimers to DNA scaffolds of varied structural complexity: duplexes and 6HBs (Figure 2A-C).[2] Transient absorption (TA) spectroscopy revealed that the structural complexity of the DNA scaffold can modulate the formation and dynamics of excitonic product states. TA spectra and kinetic traces illustrate that duplex scaffolds facilitate predominantly charge transfer coupling, while 6HBs can also generate excimer states (Figure 2D-G). These findings suggest that DNA nanophotonic materials can steer emergent photophysics in designer photovoltaic and optoelectronic devices.

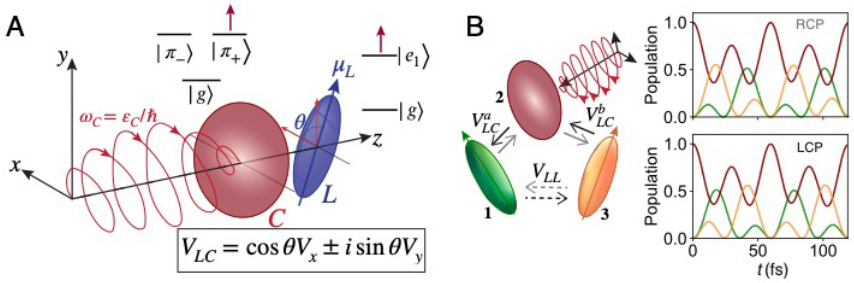

Figure 3. (A) Generation of complex-valued coupling through the interaction between a symmetric circular molecule and an asymmetric linear molecule. (B) Using light polarization to manipulate the direction of exciton flux in a three-dye cycle.

Investigating the role of complex-valued coupling for energy transfer. The tendency of excitons to migrate or delocalize within a network of chromophores is mediated by the intermolecular couplings. Unique modes of control over exciton dynamics can be achieved when elements of this network are complex-valued. This includes the ability to direct the flow of excitons to turn in specific directions within cyclic or branching circuits. Little was known, however, about how to generate complex-valued coupling (CVC) in realistic multichromophoric excitonic systems. We have developed a strategy for designing excitonic circuits that exhibit complex-valued coupling elements and proposed a simple molecular motif capable of yielding CVCs and, in principle, directing the flow of excitons in multichromophoric systems.

Our approach to generating CVCs relies on control over the phase of excitonic wavefunctions. We achieve phase control through the interactions of highly symmetric molecules, such as porphyrins, and circularly polarized laser pulses, which are capable of selecting one of two delocalized complex exciton states based on light pulse polarization. The coupling of these complex exciton states to low-symmetry linear chromophores includes complex components (see Figure 3A). We utilized theoretical modeling to demonstrate control over exciton flux in three-dye cycles (Figure 3B)[3] and in chomophore networks with branching linear dye pathways.

In addition to the development of excitonic building blocks, we have also used DNA to organize our architectures into higher order assemblies.

Enhancing energy transport through exciton delocalization in DNA-templated chromophore arrays. In natural photosynthetic proteins, delocalized excitons are thought to mediate highly efficient energy transport—yet how, or even whether, delocalization facilitates energy transfer has been challenging to test systematically and optimize experimentally. To probe the effect of exciton delocalization on long-range energy transduction, we exploit the synthetic programmability of DNA nanostructures to design molecular photonic wires (MPWs) capable of strong, intermediate, and weak intermolecular coupling between templated Cy3 chromophores (Figure 4A).[4] For each MPW, we characterized transport time across the bridge through both experimental time-resolved fluorescence measurements and numerical simulations executed using a site-based microkinetic model. The experimental and theoretical results exhibit strong agreement (Figure 4B). Intermediate intermolecular coupling between the Cy3 subunits reduced transport time by 70%, thereby facilitating MPW function and increasing the distance scale over which energy can be transduced.

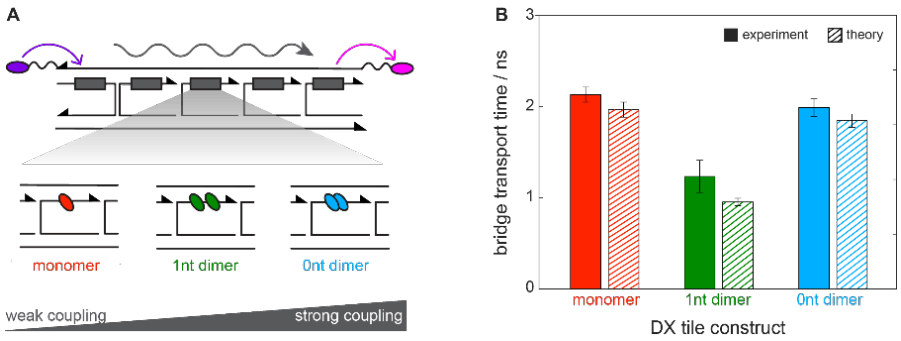

Figure 4. Engineering delocalization for energy transport. (A) Schematic of DX tile photonic wires. A series of subunits of Cy3 (grey) monomers, coupled dimers separated by one or zero nucleotides (nt) are scaffolded on a DX tile with a donor (Atto 425, purple) and an acceptor (Cy5, pink) at opposing ends. (B) Experimental and theoretical transport time across the photonic wire.

Other projects. Work is also ongoing on other DNA-based excitonic structures, including excimeric systems, systems with multiple strongly coupled chromophores, and enhanced 2D energy transport as well as materials using non-canonical nucleic acid structures.

Future plans

Our ongoing and planned work focuses on fundamental photophysics and photochemistry and their translation into higher-order structures for solar energy conversion, fluorescence assays, and computing. The development of such properties will allow for the incorporation of new functionality into these nanoscale materials.

References

1. S. M. Hart, J. L. Banal, M. A. Castellanos, L. Markova, Y. Vyborna, J. Gorman, R. Häner, A. P. Willard, M. Bathe, and G. S. Schlau-Cohen, *Activating Charge-Transfer State Formation in Strongly-Coupled Dimers Using DNA Scaffolds,* Chem. Sci. **13**, 13020-13031 (2022).

2. J. Gorman*, S. M. Hart*, T. John, M. A. Castellanos, D. Harris, M. F. Parsons, J. L. Banal, A. P. Willard, G. S. Schlau-Cohen, M. Bathe. *Sculpting photoproducts with DNA origami.* Chem, **10**, 1553-1575 (2024). *These authors contributed equally.

3. M. A. Castellanos, and A. P. Willard, *Imaginary Excitonic Coupling: Toward Directional Exciton Flux in Organic Semiconductors*, submitted.

4. W. Chen*, M. N. Scott*, J. L. Banal, C. Brooks, X. Wang, S. M. Hart, A. Dodin, M. Bathe, A. P. Willard, and G. S. Schlau-Cohen, *Exciton Delocalization Enhances End-to-End Resonance Energy Transfer in DNA Scaffolded Molecular Photonic Wire*, in preparation. *These authors contributed equally.

Publications.

1. M. A. Castellanos, and A. P. Willard, *Imaginary Excitonic Coupling: Toward Directional Exciton Flux in Organic Semiconductors*, submitted.

2. J. Gorman*, S. M. Hart*, T. John, M. A. Castellanos, D. Harris, M. F. Parsons, J. L. Banal, A. P. Willard, G. S. Schlau-Cohen, M. Bathe. *Sculpting photoproducts with DNA origami.* Chem, **10**, 1553-1575 (2024). *These authors contributed equally.

3. S. M. Hart, J. Gorman, M. Bathe, and G. S. Schlau-Cohen, *Engineering Exciton Dynamics with Synthetic DNA Scaffolds,* Acc. Chem. Res., 159-166 (2023).

4. S. M. Hart, X. Wang, J. Guo, M. Bathe, and G. S. Schlau-Cohen, *Tuning Optical Absorption and Emission Using Strongly Coupled Dimers in Programmable DNA Scaffolds*, J. Phys. Chem. Lett. **13**, 1863-1871 (2022).

5. S. M. Hart, J. L. Banal, M. A. Castellanos, L. Markova, Y. Vyborna, J. Gorman, R. Häner, A. P. Willard, M. Bathe, and G. S. Schlau-Cohen, *Activating Charge-Transfer State Formation in Strongly-Coupled Dimers Using DNA Scaffolds,* Chem. Sci. **13**, 13020-13031 (2022).

Principles of self-navigation for cell-sized gliders

William **Shih**, Dana-Farber Cancer Institute, Wyss Institute for Biologically Inspired Engineering at Harvard, Harvard Medical School

Keywords: DNA nanotechnology, self-navigation, molecular motors, self-organization, self-assembly

Research Scope

Biological systems illustrate how matter can be self-organized and undergo adaptation, maintenance, and repair across length scales through dissipative processes involving large collections of agents. One class of such systems involves the cooperative action of teams of molecular motors acting on arrays of motor binding sites; examples include muscle contraction, cytoplasmic streaming, chromosome segregation, and cytokinesis. A major challenge is to elucidate design principles that enable us to program similarly sophisticated behaviors from synthetic materials towards future capabilities in advanced manufacturing, lightweight self-repairing materials, and energy capture, transfer, and storage. We seek to determine how custom patterning of nanometer-scale features on propelled micrometer-scale objects can be harnessed to realize predictable submillimeter-scale trajectories. Guided by our theory and simulation results [1], we are exploring an experimental model system based on micron-sized “gliders" that self-navigate across a macroscopic “arena”. The latter will be implemented as a sector of a glass coverslip randomly coated with dynein motor proteins engineered with LEF1 domains to walk on DNA instead of microtubules [2]. In turn, the gliders will be self-assembled from DNA into cell-

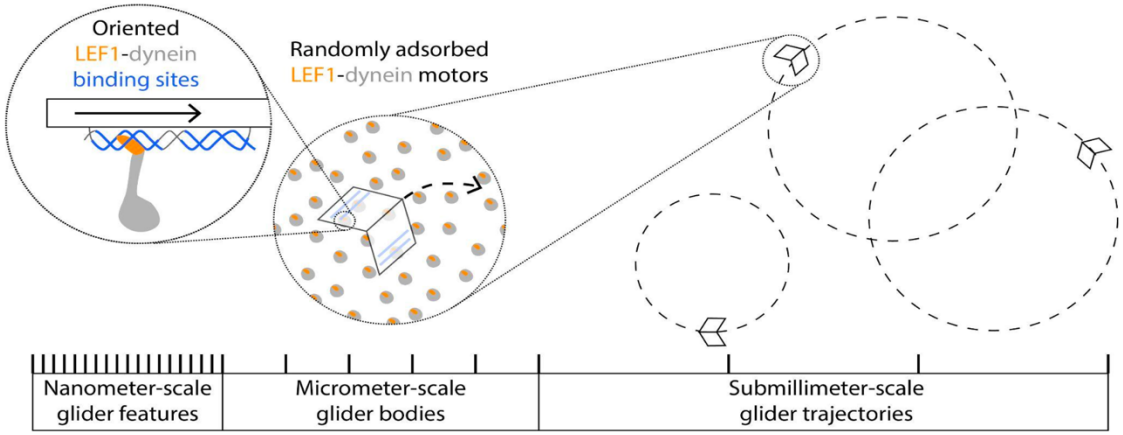

Figure 1 LEF1-dynein-surfing, cell-sized “gliders” self-assembled from DNA as a model system for self-organization of active matter across scales. LEF1-dynein motors, which operate on DNA instead of microtubules, randomly decorate an “arena” hosted on a glass coverslip. Micron-scale gliders undergo directed motion driven by these motors. The precise positioning and orientation of motor-binding sites and frictional brushes on the body of a glider determine its submillimeter-scale trajectory (e.g. brush gradient creates turning).

sized structures programmed by controlled orientation and positioning of LEF1-dynein binding sites and other features on their bodies [3–5]. Conversely, micrometer-resolution printing of

features on the arena, such as frictional elements or depots for cargo pick-up and drop-off, can render glider navigation responsive to non-uniformities in the local environment. As benchmarks for testing and refining our understanding of relevant design principles for dynein-surfing gliders, we propose to implement four distinct macroscopic trajectories: (i) rotation, (ii) circular paths, (iii) refraction at interfaces with a step in friction, and (iv) forward-and-reverse cyclic translation between depots.

Recent Progress

We have hired a postdoctoral fellow to lead the experimental progress this project, Dr. Florian "Katzi" Katzmeier. Dr. Katzmeier is an outstanding young biophysicist who completed his PhD studies at Technical University of Munich working with Professor Fritz Simmel. Dr. Katzmeier's most striking work was on using AC electric fields to generate hydrodynamic flows on asymmetric particle dimers, that could be steered by remote control. He has excellent experience in building and working with microscope, as well as performing analysis and computer simulations. We were not able to hire Dr. Katzmeier until mid-April of this year (2024), so that he could wrap up the studies from his dissertation research.

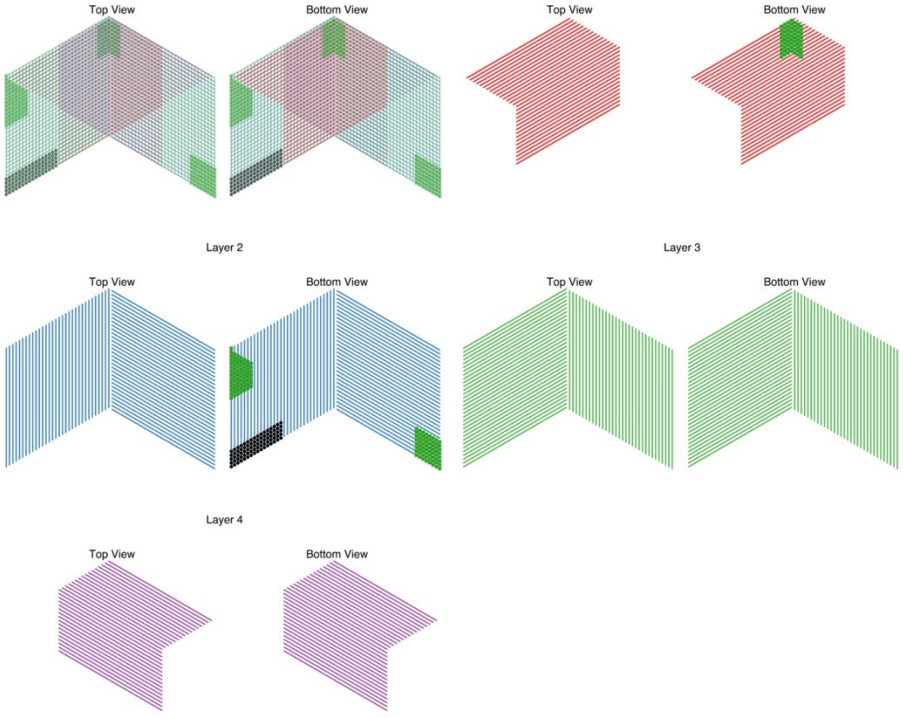

We have made important advances in developing a solid-phase assembly method for building crisscross origami megastructures such as gliders. This approach involves capture of a DNA-origami seed on a magnetic microparticle or nanoparticle, and then subsequent growth of the megastructure

Figure 2 Design of crisscross origami chevron that is ~800 nm across. There are four distinct layers of crisscross origami slats. Slats only interact with slats above and below, and don't interact with neighbors on the same layer. Layers 2 and 3 define adjacent diamond structures, each composed of 64 slats. Layers 1 and 4 serve to bind the two diamonds together to form a micron-scale chevron that could be resolvable using diffraction-limited epifluorescence microscopy.

following addition of component slats. Then a magnet can be used to sequester the particles away from the bulk solution, enabling multiple rounds of slats to be applied in sequence, and also enabling several rounds of washing to remove stray slats.

We have successfully demonstrated self-assembly of chevron shapes that are ~800 nm across (Fig. 3). These structures are sufficiently large that their orientation can be resolved using diffraction-limited fluorescence microscopy. Thus crisscross origami can be seen as a means to enable characterization of nanotechnological structures using lower-cost light microscopy, as opposed to molecular microscopy that requires more expensive TEM or AFM microscopes.

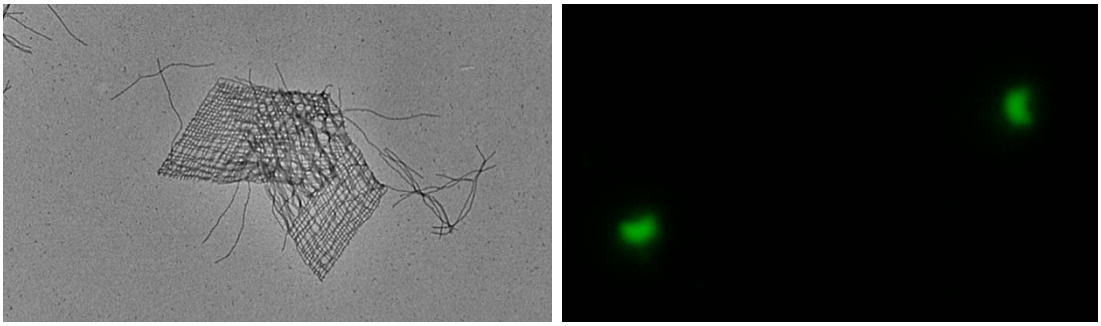

Figure 3 Left, transmission electron micrograph of a self-assembled chevron megastructure using crisscross origami polymerization. This structure is ~800 nm across its largest dimension. Right, diffraction-limited epifluorescence microscopy of chevron megastructures labeled by YOYO-1 intercalating dye.

Future Plans

In the upcoming year, our major goals are to (1) refine assembly of the chevron-shaped crisscross megastructures using our solid-phase approach and (2) demonstrate motility of DNA origami structures using modified dyneins. These will be key steps to enable generation of the goals as outlined above. A challenge for this project is the apparent nonspecific binding of the engineered dyneins to M13-based DNA origami nanotubes. We are considering modifications to the dyneins and/or the gliders in order to address this challenge. For example, the dyneins could be functionalized with a weak DNA substrate for competitive inhibition of binding with off-target sites. Alternatively, gliders could be coated with a steric brush that weakens the binding of the dyneins, such that only the specific binding will be strong enough for significant interaction.

References

Wintersinger CM, Minev D, Ershova A, Sasaki HM, Gowri G, Berengut JF, Corea-Dilbert FE, Yin P, Shih WM. Multi-micron crisscross structures grown from DNA-origami slats. *Nat Nanotechnol.* 18, 281–289 (2023).

Minev D, Wintersinger CM, Ershova A, Shih WM. Robust nucleation control via crisscross polymerization of highly coordinated DNA slats. *Nat Commun.* 12, 1741, 2021.

Douglas, S. M., Chou, J. J. & Shih, W. M. DNA-nanotube-induced alignment of membrane proteins for NMR structure determination. *Proc. Natl. Acad. Sci. U. S. A.* 104, 6644–6648, 2007.

Ibusuki R, Morishita T, Furuta A, Nakayama S, Yoshio M, Kojima H, Oiwa K, Furuta K. Programmable molecular transport achieved by engineering protein motors to move on DNA nanotubes. *Science*. 375, 1159–1164, 2022.

Ross, T. D., Osmanović, D., Brady, J. F. & Rothemund, P. W. K. Ray Optics for Gliders. *ACS Nano* 16, 16191–16200 (2022).

Publications

We have no publications supported by BES yet; we're still in our first year of funding.

Bio-inspired Polymer Membranes for Resilience of Electrochemical Energy Devices

Meredith N. **Silberstein**, Sibley School of Mechanical and Aerospace Engineering, Cornell University

Keywords: polyelectrolytes, electric field, dialysis, mechanical properties

Research Scope

Like biological cell membranes, polymer membranes for electrochemical energy storage and conversion devices must control ion transport and be mechanically robust. Biological membranes are constantly assessing evolving "operating" conditions such as electric field and optimizing their function by dynamically adjusting their material state; the current generation of synthetic polymer membranes are static. Synthetic membrane performance and durability can be dramatically improved by imbuing the membrane with the ability to sense and adapt to the local electrochemical environment. One key enabler of biological self-regulation is ionic interactions. We are applying this biological concept to modulating ionic crosslinking within synthetic polymers (Figure 1).

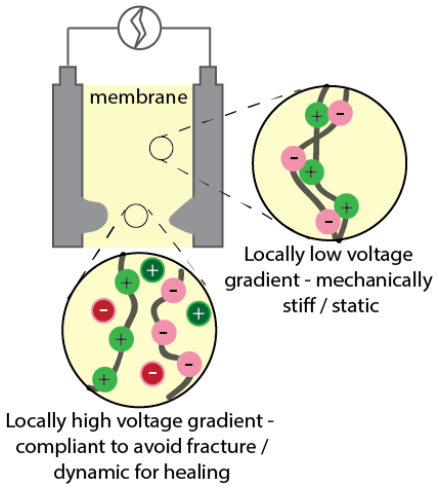

Figure 1. Concept schematic for electric field-dependent mechanical properties in ionically-functionalized polymers.

The scope of this program is to discover the fundamental physical mechanisms for self-regulation of polymers and gels under electric fields by focusing on the following three aspects: (I) The influence of an external electric field on the strength of ionic bonds between polymer chains and how this interaction depends on concentration of ionic bonds, any solvent, free ions, polymer backbone rigidity, chemical details of the polymer; (II) How ionic bond strength and concentration among linear polymer chains influences polymer mechanical properties and self-healing for different polymer backbone rigidities and chain lengths; (III) Complete mechanical property dependence on electric fields by adding to I and II, key coupled aspects such as polymer reconfiguration guided by locally high electric field gradient. We are approaching this unexplored concept computationally, utilizing molecular dynamics (MD) simulations and constitutive modeling and validating our findings using synthesis, solution-based experiments, spectroscopy, and mechanical testing.

Recent Progress

We have built upon our knowledge gained in previous grant periods in terms of how ionic interactions govern mechanical properties, to design polymer gels with strongly salt concentration-dependent mechanical properties (Figure 2)[1,2]. In each case we synthesize the material near the salt saturation threshold and then dialyze out the salt by soaking the gel in water. We have demonstrated through control experiments that the differences in stiffness and strength are not due to changes in water content. Further, there is a substantial opacity change associated with this dialysis as the material conformation internally changes. An underlying mechanism of tight polyelectrolyte domain aggregation with reduced salt content was recently reported upon by another group, with their interpretation also supported by molecular dynamics simulations [3].

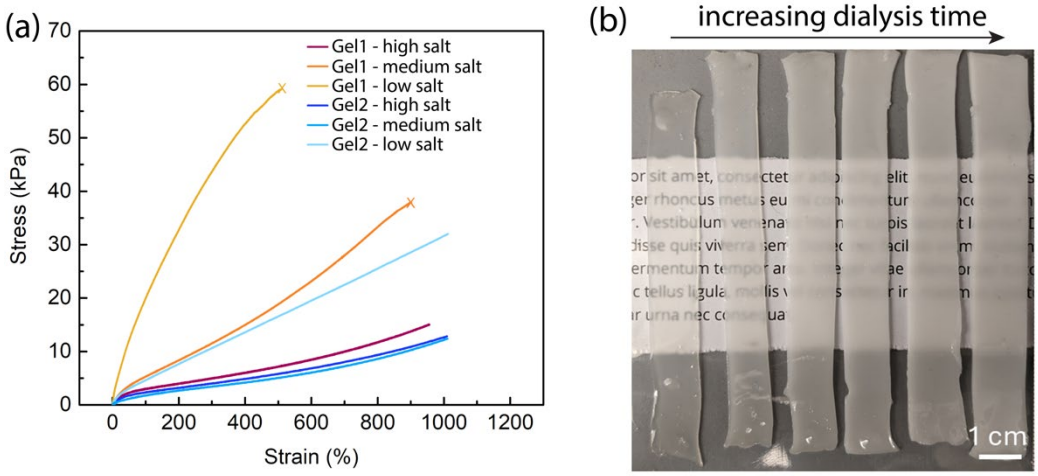

Figure 2. Conventional dialysis control of mechanical properties. (a) Salt dependent tensile mechanical properties for two gel formulations, identical in chemical but varying in molecular weight, at three different salt concentrations. (b) Change in opacity of Gel1 initially synthesized with high salt as it is soaked in DI water for increasing time periods.

We next used the Gel1 – high salt formulation to demonstrate electric field-based stiffness modulation (Figure 3). We use a mechanism of electrodialysis, whereby the salt is driven out of the gel and severely inhibited from returning by using selective transport membranes. By applying a nearly constant current over 30 minutes, we were able to more than double the initial stiffness of the gel. This current can only be sustained by a corresponding voltage that is over the threshold for water splitting at the electrodes. As in the traditional dialysis case, we were able to show that this property change is not due to loss of water. When current is run in the opposite direction, there is a noticeable, though smaller, decrease in stiffness, which we believe is primarily attributable to pH changes in the gel. We used both FTIR and scanning electron microscopy to demonstrate the salt content change in the gel. Finally, we were able to demonstrate the progressive nature of this electrodialysis process and corresponding property change by conducting compression tests at different time points (not shown). This work is comprehensively described in our in-preparation manuscript.

In parallel to, and in support of this experimental effort, we have developed a reduced order modeling framework that can efficiently capture the transport of multiple ion species through

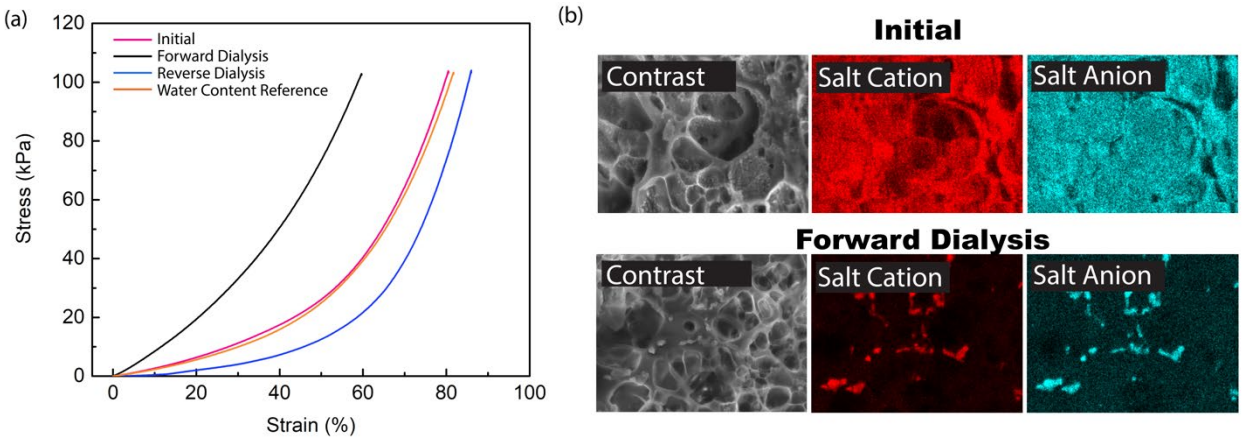

Figure 3. Electrodialysis property modification. (a) Compressive mechanical properties before and after application of an electric current for 30 minutes either in the forward or reverse direction. Since evaporation occurs over 30 minutes, a reference curve with matched water content is provided. (b) Scanning electron microscopy analysis of gel structure and salt content before and after application of electrodialysis that demonstrates the removal of salt ions.

stacks of polymers in response to electronic and ionic boundary conditions, as well as the associated current, voltage, and ion concentration changes. This modeling framework is in the spirit of equivalent electrical circuit modeling and has been developed within an open-source equivalent circuit modeling software tool for easy integration with similar modeling approach. However, we have taken a materials centric view, with all of the underly effective components naturally resulting from the composition and geometry of the materials (*e.g.* Figure 4), as well as the interface between materials. This tool will enable facile design of polymer assemblies for controlling and processing ion transport - a task that tends to be difficult because of the diversity of ionic species (compared to just electrons and holes in electronic devices), the partially selective transport of ions through different polymers whose characteristics changes with ion concentrations, and the range of relevant length and time scales.[4] The details of the model are in a second in preparation manuscript. For this particular application, we have customized the relevant material properties based on a combination of values available in literature

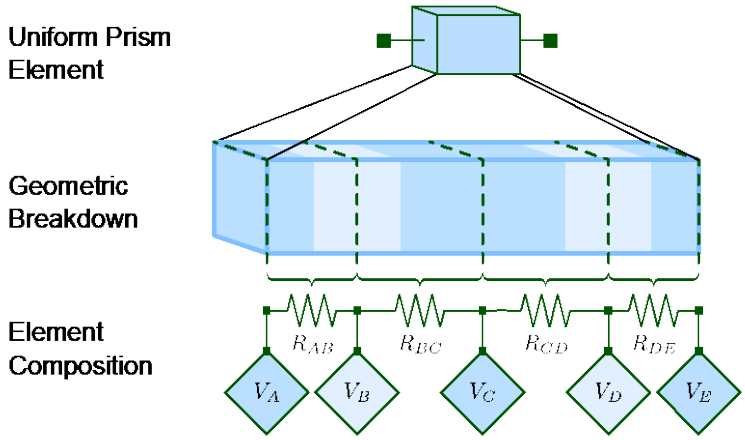

Figure 4. Prismatic material element within our newly developed reduced order modeling framework that captures how a materials scientist would think about synthesizing a device. We treat this element as a series of volumes (V_I) and resistors (R_{IJ}) that can capture the behavior of the element within an ionic system / ionic circuit.

and our own measurements taken with electrochemical impedance spectroscopy. We have also included electrochemical generation of protons and hydroxide anions, as well as their recombination resulting in charge annihilation. Our reduced order model was used to help design our polymer stack. Further, it shows that while electrodialysis can effectively alter salt content in our gel, a large fraction of the current in our system consists of protons and hydroxide anions. The simulations suggest that there should be substantial pH changes – a finding that we were able to verify experimentally (Figure 5).

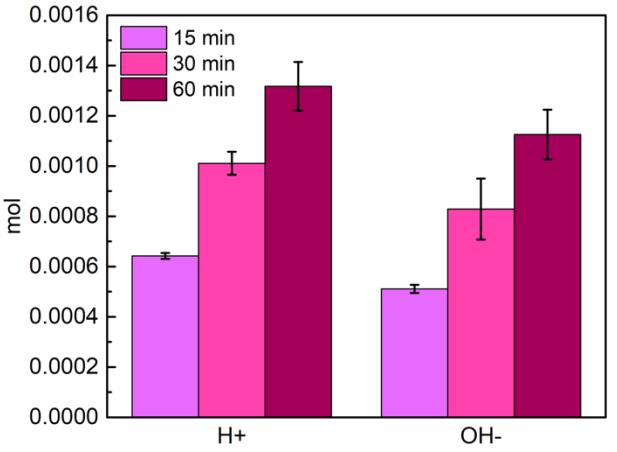

Figure 5. Proton and hydroxide anion change measured in materials adjacent to Gel1 after different durations of current application, confirming our mechanistic understanding predicted by the reduced order model.

Future Plans

This grant funded period ends in August 2024. We are therefore focused primarily on completing and submitting the two manuscripts described within our recent progress section. Additionally, we are exploring (1) whether the stiffness modulation mechanism discovered here can be used in an autonomously regulating system, and (2) whether the electrodialysis approach can also be used to influence the rate of self-healing from damage.

References

1. H. Cai, Z. Wang, N.W. Utomo, Y. Vidavsky, and M.N. Silberstein, *Highly Stretchable Ionically Crosslinked Acrylate Elastomers Based on Polyelectrolyte Complexes*, Soft Matter **18**, 7679 (2022).

2. Z. Wang, H. Cai, and M.N. Silberstein, *A Constitutive Model for Elastomers Tailored by Ionic Bonds and Entanglements*, Mechanics of Materials **179**, 104604 (2023).

3. J.E. Sayed, A. Mukherjee, S.E. Aani, N. Vengallur, M. Koch, A. Giuntoli, and M. Kamperman, *Structure–Property Relationships of Granular Hybrid Hydrogels Formed through Polyelectrolyte Complexation*, Macromolecules **57**, 3190–3201 (2024).

4. N. Bosnjak, M. Tepermeister, and M.N. Silberstein, *Modeling coupled electrochemical and mechanical behavior of soft ionic materials and ionotronic devices.* Journal of the Mechanics and Physics of Solids **168**, 105014 (2022).

Publications

1. H. Cai, Z. Wang, N.W. Utomo, Y. Vidavsky, and M.N. Silberstein, *Highly Stretchable Ionically Crosslinked Acrylate Elastomers Based on Polyelectrolyte Complexes*, Soft Matter **18**, 7679 (2022).

2. Z. Wang, H. Cai, and M.N. Silberstein, *A Constitutive Model for Elastomers Tailored by Ionic Bonds and Entanglements*, Mechanics of Materials **179**, 104604 (2023).

3. F. Aubrecht, K. Orme, A. Sau, H. Cai, T. Ranathunge, M.N. Silberstein and B. McDonald, *Ion-Specific Interactions Engender Dynamic and Tailorable Soft Matter Properties in Biomimetic Cationic Polyelectrolytes*, Angewandte Chemie Volume, provisionally accepted 2024.

4. H. Cai, M. Tepermeister, and M.N. Silberstein, *Modulating Mechanical Properties of a Semi-Interpenetrating-Network Hydrogel With Mobile Ions Via an Electric Field,* in preparation.

5. M. Tepermeister and M.N. Silberstein, *Lumped Element Ionic Material and System Modeling*, in preparation.

Biomimetic Strategies for Field-Driven Defect Annealing in Microparticle Crystals

Michael J. **Solomon** and Sharon C. Glotzer, University of Michigan Ann Arbor

Keywords: crystallization, annealing, confocal microscopy, Brownian dynamics simulation, colloids

Project Scope

The purpose of this project is to seek scientific principles that expand our understanding of defect annealing to produce high-quality crystals in materials self-assembled from microscale building blocks. Our guiding inspiration is life's capacity to create high-quality crystal structures from microscopic building blocks, yielding materials that produce important functional properties like structural color. To discover such principles, we have developed techniques based on electric field assisted self-assembly to anneal defect structures in colloidal crystal monolayers of microparticle spheres and disks. We resolve the spatiotemporal evolution of these structures at the single-particle level by confocal microscopy and use computational simulation to yield mechanistic understanding of the annealing pathways. The fundamental questions this project addresses are: (1) How does the orientation-dependence of an applied electric field couple to the fundamental lattice symmetry of colloidal crystals? (2) How may such electric fields be configured to generate rapid transitions between different, high quality crystal phases of anisotropic colloids? (3) How does the shape of an active particle affect its dynamics and defects in a crystal lattice comprised of passive colloids? These scientific questions motivate a work plan comprised of specific aims in which we study the effects of field symmetry on the annealing of local and global defects of colloidal crystals; measure the quality of switchable liquid crystals generated by anisotropic colloids with reconfigurable orientation; and characterize the effects of active ellipsoids on crystal defect structures and dynamics. The scientific outcome of this work are new principles that enable the coupling of fields sculpted in space and time to specific features of colloidal crystals—including their symmetry and the anisotropic particle shape of their building blocks—to control the quality of their order both locally and globally. The impact on basic energy sciences are governing principles that translate into new strategies for spatiotemporal control of annealing in self-assembled materials comprised of microscale building blocks like colloids, polymers, and proteins, with implications for structural color and thermal management materials.

Recent Progress

We report our recent progress in probing: (1) the relationship between defect structure and grating diffraction structural color optical response in self-assembled colloidal crystals; (2) the reconfigurable optical response of discoid liquid crystals under field-induced change in orientation; (3) the annealing colloidal crystals by means of rotating electric fields [1].

Defect control in electrophoretic deposition of colloids and its effect on grating diffraction structural color. Iridescent structural colors arise from well-organized colloidal crystals that can

diffract visible light. One mechanism of structural color that generates a prismatic effect is by grating diffraction from 2D colloidal arrays. These colloidal arrays are here manufactured by direct current electric field induced electrophoretic deposition and self-assembly on a solid substrate. The defects present principally as grain boundaries, and their abundance can be controlled by the applied current density (from 1.6 – 310 μA/cm^2) and ion concentration (from 0.01 – 10 mM). Different operating conditions yield materials with liquid, polycrystal, and surface-bound states. The self-assembled colloids have global six-fold crystal bond order ψ_6 varying from 0.45±0.05 to 0.95±0.01 and grain number density n_g ranging from 0 to 100 per 0.01 mm^2 area. The electrophoretic deposition and assembly behavior are modeled by molecular dynamics (MD) simulation, which predicts the dynamic behavior and structural properties of the crystals. The grating diffraction structural color of the colloidal crystals shows strong dependence on crystal quality, including correlation with both ψ_6 and n_g. For example, about 2.5 times stronger diffraction intensity was detected for crystals with ψ_6 = 0.95 compared to those with ψ_6 = 0.45 (Figure 1). Applying finite-difference time domain (FDTD) simulation of structures realized by MD simulation confirms these correlations and identifies the specific roles of these two quantities on the optical response. Specifically, low grain number density reduces the structural color uniformity while greater ψ_6 increases the peak intensity, an indication of a trade-off in design for structural color with implications in applications such as coatings.

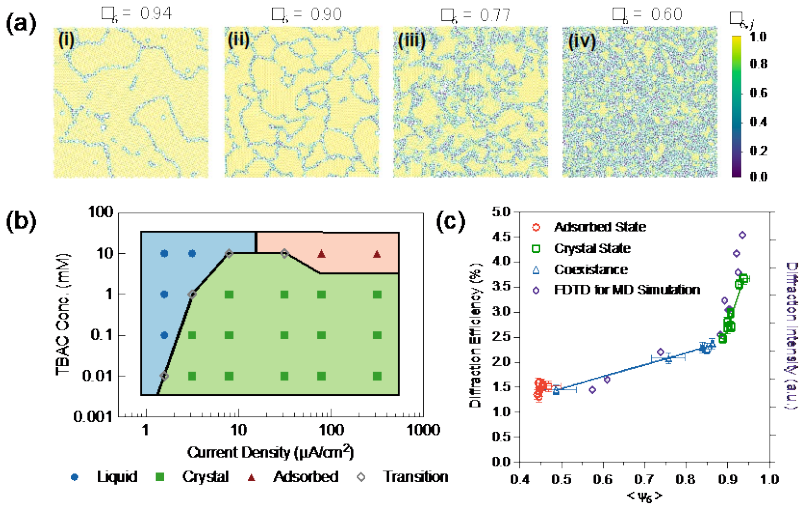

Figure 1. (a) Images show polycrystals with different crystal qualities. (b) State diagram of self-assembled colloids under different operating conditions. (c) Measured structural color intensity for various crystal qualities [2].

Reconfigurable optical response of colloidal discoid liquid crystals by reversible switching between planar and homeotropic alignment. We applied a combination of direct current (DC) and alternating current (AC) electric fields to reconfigure the liquid crystal orientation of colloidal discoids between planar and homeotropic alignment, thereby yielding control of the material's structural color response. We self-assemble 4-μm sulfate-modified polystyrene discoids dispersed in an isopropanol-water mixture into a monolayer crystal. The self-assembly is accomplished by

applying electric fields between two conductive coverslips separated by a 120-µm spacer. The discoids initially undergo gravitational and electrophoretic deposition on the bottom substrate in a DC field of 0.50 V. They adopt homeotropic alignment, with minor axis symmetry oriented perpendicular to the substrate. Adding an AC-component (1 kHz) to the DC field switches the discoids to planar alignment, with minor axis symmetry oriented parallel to the substrate. The orientation switching is reversible and reaches the maximum change at $V_{AC} \geq 0.50$ V (Figure 2). The diffraction efficiency of the crystal also shows a significant shift in the peak wavelength and intensity upon reconfiguration. The change in optical response upon the switch from planar to homeotropic alignment occurs within 100 s and can be maintained for at least 10 on/off cycles.

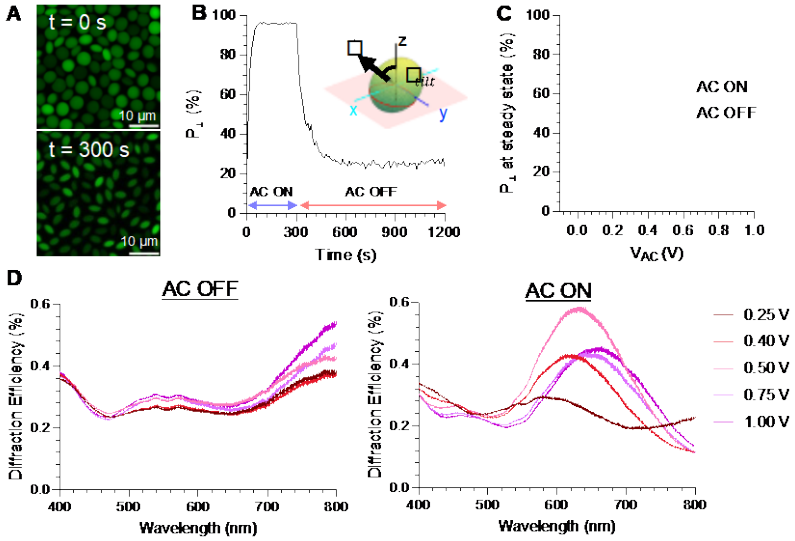

Figure 2. Effect of on/off AC electric field cycle on colloidal discoid liquid crystals as shown by discoid orientation (A-C) and spectral response (D). We use confocal microscopy to image the discoid orientation (A) as a function of time, during which AC field is turned on for 300 s and turned off for 900 s. The discoid orientation is quantified by the percentage of discoids with $\theta_{tilt} > 45°$ ($P_\perp$), where θ_{tilt} is the angle between the particle director (minor axis for discoids) and the z-axis perpendicular to the substrate (B). The steady-state $P_\perp$ after AC is turned on is maximized at 0.50 V and greater, while the steady-state $P_\perp$ after AC is turned off is similar for all voltages (C). The diffraction efficiency of the colloidal crystals at an angle of 10° from normal shows greater peak intensity at a longer wavelength after AC is turned on (at 0.40 V and greater), compared to after AC is turned off (D) [3].

Colloidal crystal annealing by rotating AC electric fields. Rapidly self-assembled colloidal crystals contain defects, such as grain boundaries, dislocations, and vacancies. Colloidal self-assembly by external fields is widely used but these methods are prone to yield abundant defects. Annealing by means of periodic external stimuli allows the particles to reorganize, overcome free energy barriers and explore lower free energy states. In this study, we explore an annealing strategy using rotating AC electric fields to convert polycrystals to a single crystal grain. The electric fields were applied to counter-pairs of electrodes in a 6-fold coplanar device and rotationally cycled at a constant period, τ. In the first phase of assembly, dipole-dipole interactions and dielectrophoresis compact particles into a hexagonal polycrystal with defects. In the second phase, the cyclic rotation

deforms the crystal along different directions; this motion accomplishes defect rearrangement and progressive migration of grain boundaries to edges. We analyzed the annealing process by confocal microscopy and calculate the global ψ_6 order parameter and Voronoi area for individual particles (Figure 3). In addition, we found a cycling period τ that optimizes the average hexatic order parameter, ψ_6. This annealing approach significantly improves the efficiency of annealing and ultimately generates a defect-free crystal in an open loop control system.

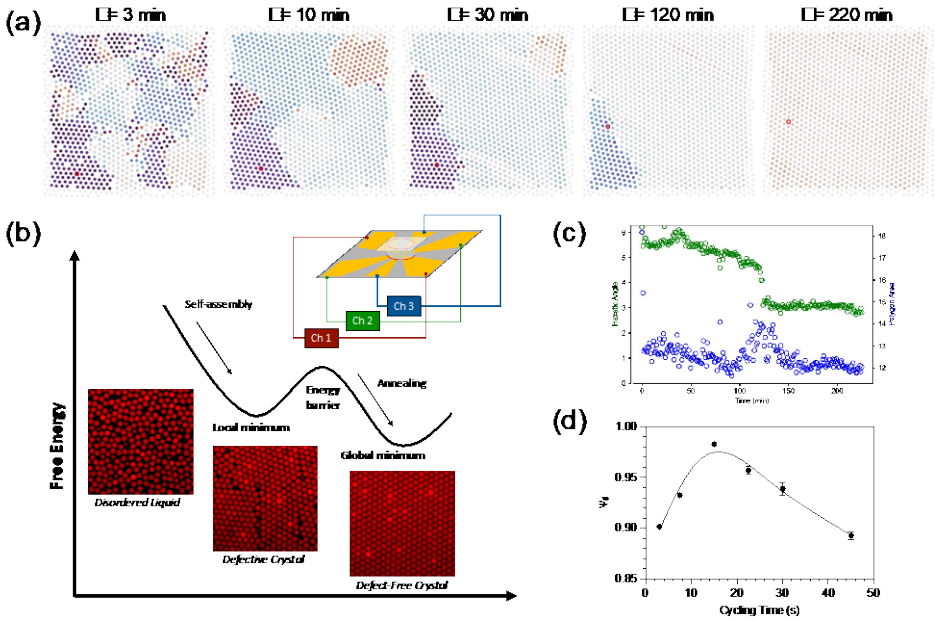

Figure 3. (a) Single particle tracking during the annealing process as labeled by the red circle. (b) conceptual view of free energy change during annealing and device schematic. (c) Single particle hexatic phase angle and Voronoi area change with time of annealing. (d) Optimum cycling period that yields greatest ψ_6.

Future Plans

Next steps in this project include: (1) changing the symmetry of the rotating electrode system from 6-fold to 5- and 7-fold to study the effect of alignment of field and crystallographic axes on crystal quality and annealing; (2) controlling the tilt angle of colloidal discoid liquid crystals by manipulating the orientation of the aligning field; (3) introducing active colloids of anisotropic shape into the crystals to assess their effect on the local structure of passively self-assembled materials.

References

1. Tianyu Liu, Syahidah Mohd Khairi, Chih-Mei Young, and Tim Moore performed research reported in this extended abstract.

2. Liu, T., C-M Young, T.C. Moore, S.C. Glotzer and M.J. Solomon, "Defect control in electrophoretic deposited colloids and the effect on grating diffraction structural color," in preparation (2024).

3. Mohd Khairi, S. and M.J. Solomon, "Reconfigurable optical response of colloidal discoid liquid crystals by reversible switching between planar and homeotropic alignment," in preparation (2024).

Publications supported by BES in the last two years

1. Liu, T. and M.J. Solomon, "Reconfigurable Grating Diffraction Structural Color in Self-Assembled Colloidal Crystals," *Small* **19** 2301871 (2023). DOI: 10.1002/smll.202301871

2. Saud, K.T. and M.J. Solomon, "Microdynamics of active particles in defect-rich colloidal crystals," *J. Colloid Interface Science.* **641** 950-960 (2023). PMID: 36989821; DOI: 10.1016/j.jcis.2023.03.025

3. Liu, T., T. Liu, F. Gao, S.C. Glotzer, and M.J. Solomon, "Structural Color Spectral Response of Dense Structures of Discoidal Particles Generated by Evaporative Assembly," *J. Phys. Chem B* **126** 6 1315-1324 (2022). DOI: 10.1021/acs.jpcb.1c10015.

Far-from-equilibrium topological defects on active colloids in nematic liquid crystals for bio-inspired materials assembly

Kathleen J. **Stebe**, Chemical and Biomolecular Engineering, University of Pennsylvania

Keywords: Topology, reconfigurable materials, physically intelligent systems, emergent interactions, embedded energy

Research Scope

Active colloidal particles in nematic liquid crystals (NLC) provide diverse routes for materials manipulation. The particles' shape and surface chemistry can be tailored to generate companion topological defects. The particles' motion can generate new modes of motion and nemato-elastic interactions. We develop active colloidal systems that embed and dynamically reconfigure information in their nematic liquid crystalline milieu, generating a suite of interactions for manipulation of passive colloidal building blocks or colloidal cargo.[1,2]

Recent Progress

In this funding year, we have established that micro swimmer dynamics in NLC differ fundamentally from those in isotropic fluids via two major effects. First, NLCs generate broken symmetries under symmetric perturbations. Second, NLCs generate far from equilibrium topological defects whose energy can be harnessed for propulsion. These effects dramatically expand the suite of swimmer motions that generate translation in NLC.

1. The Scallop Theorem Does Not Constrain Micro-swimmers in NLC.

The constraints imposed by the scallop theorem on micro-swimmers moving with negligible inertia in Newtonian fluids must be reconsidered for NLC. The scallop theorem states that non-reciprocal motions of micro-swimmers' bodies are required to generate translation. For this reason, in nature and in biomimetic systems, micro-swimmers rely on helical flagellar rotation or complex body motions to generate thrust. However, by examining rotating homogeneous spherical colloids, we find that highly symmetric motions—including purely axisymmetric rotation and reciprocal motions—drive translation in NLC. The key to this finding is the anisotropic spatial arrangement of nematogens generated by the symmetric flows. The NLC itself generates broken symmetries and elastic stresses that drive motion, expanding the palette of motions that generate net thrust.

In experiment, nematic liquid crystal filled cells are prepared from two microscope slides separated by 50 μm gap defined by particle spacers that are afixed by a UV polymerizable glue (NOA 68). The inner surfaces of the glass substrates are coated with polyimide PI2555 (HD MicroSystems) and rubbed unidirectionally to impose planar alignment on the nematic director. Unless otherwise noted, the NLC pentylcyanobiphenyl (5CB) is studied. Ferromagnetic nickel coated glass spheres (Cospheric; radius 2.5 μm $\leq a \lesssim$ 15 μm) are coated with N-dimethyl-N-octadecyl-3-aminopropyl-trimethylsilyl chloride (DMOAP) to impose homeotropic (perpendicular) anchoring of the liquid

crystal molecules at their surface. The spheres are dispersed in NLC and injected into the cell. An external magnetic field B is applied to the cell using two pairs of Helmholtz coils arranged to generate a uniform rotating magnetic field ~10mT at the center of the domain, well below field strengths that alter NLC orientation. The spheres' motion is observed using a Zeiss Axio Vert A1 inverted microscope recorded by a FLIR camera. Trajectories are tracked via a Mathematica code.

Purely axisymmetric rotation of spheres drives translation

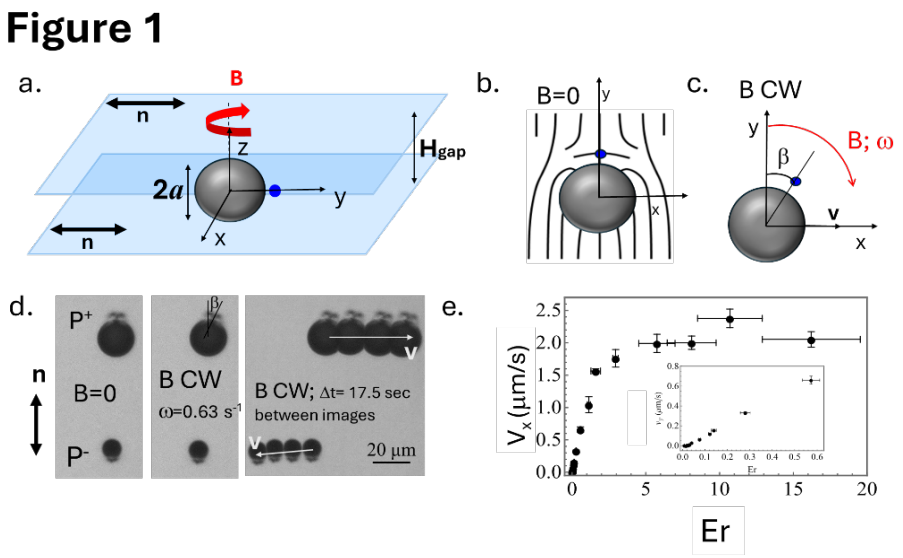

The experiment is shown schematically in Fig 1a. The sphere forms a topological companion defect (shown schematically as the blue dot) that aligns parallel to the far field nematic director **n** along the y axis with polarization P^+ or P^- with equal probability. The colloid with dipolar defect configuration has an associated distortion in the nematic director **n(x)** that is symmetric about the y axis at equilibrium (Fig 1b). Steady rotation of the sphere around the z-axis at angular frequency ω causes the dipolar defect to shift away from the y-axis to an angle β (Fig 1c and d). The resulting broken symmetry generates unbalanced elastic stresses that force the particle to translate. Particles move with velocity **v** in the x direction for dipole polarity P^+ rotated CW; P^- move in the opposite direction (Fig. 1d). The translation speed is linear in the frequency ω for slow rotations and saturates at high frequencies that challenge the visco-nematic relaxation timescale $\tau_R=\gamma a^2/K$ or for Ericksen numbers $Er= \omega\tau_R$ large compared to unity (Fig 1e). As expected, such translation is absent in isotropic fluids (confirmed in experiment, not shown). Analysis predicts this translation; a force balance on the defect equating viscous drag and elastic restoring forces predicts the angular displacement of the defect β. An evaluation of elastic stresses on the sphere within Leslie Ericksen theory predicts the translational velocity **v**. The direction and strength of translation is also predicted to differ from one nematic liquid crystal to another owing to their different balances of Leslie viscosities; these differences are confirmed in experiment.

Reciprocal motion of spheres generates translation in nematic liquid crystals. We force reciprocal rotation of the spheres by sweeping **B** over an angle 2θ in an oscillatory fashion, alternating between CW and CCW directions (Fig 2a). The dipole defect is displaced periodically by this alternating field from one side of the sphere to the other. The resulting elastic field drives their translation roughly parallel to the nematic director while the defect leads the way (Fig 2b). The speed is roughly an order of magnitude slower than in the axisymmetric rotation of the sphere. As the field's angular frequency increases, the sphere moves faster. The motion along the nematic director is ballistic while perpendicular to that is oscillatory with zero net displacement. The defect oscillates with the external field and its amplitude increases in higher amplitudes of field oscillation. Spheres experiencing the reciprocal rotation in the NLC N-(4-Methoxybenzylidene)-4-butylaniline (MBBA; Sigma Aldrich) show the same qualitative behavior, while those in a mixture of 4′-Heptyl-4-biphenylcarbonitrile (7CB) and 4-octyl-4-biphenylcarbonitrile (8CB) with 1:1 ratio (Sigma Aldrich) migrate in the opposite direction consistent with prediction.

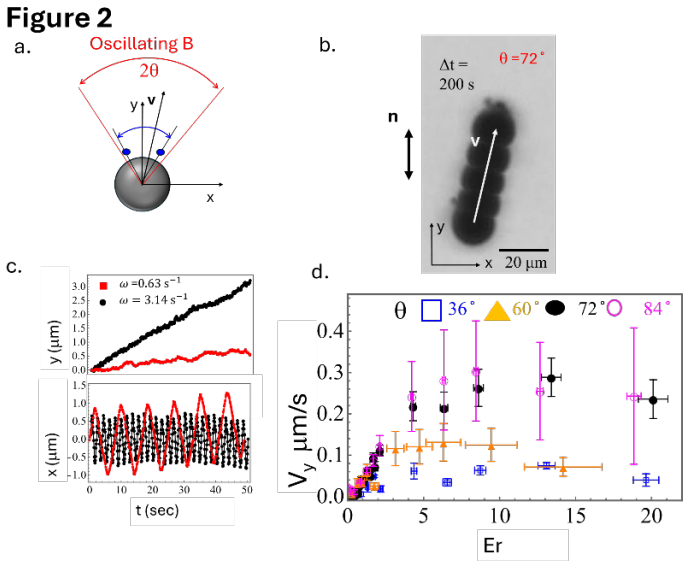

Defect swim stroke as topological instability that powers swimming. Disks are fabricated from SU-8 epoxy resin using standard lithographic methods (diameter $2a$= 75μm, height H_{disk}~30 μm). The surfaces are sputtered with thin films of nickel, treated with DMOAP to impose homeotropic anchoring and released from the substrate. The resulting disks are ferromagnetic and have hybrid anchoring: random planar on the SU-8 face, homeotropic on all nickel and DMOAP coated surfaces. We introduce the hybrid ferromagnetic disk colloids in NLC to the domain (Fig. 3a), with H_{gap} between plates of ~50μm. Upon quenching into the nematic phase, the planar disk face adopts oriented planar anchoring like that of the bounding surfaces. The disks have a companion defect, a disclination loop (Fig 3b), which undergoes periodic transformations as the

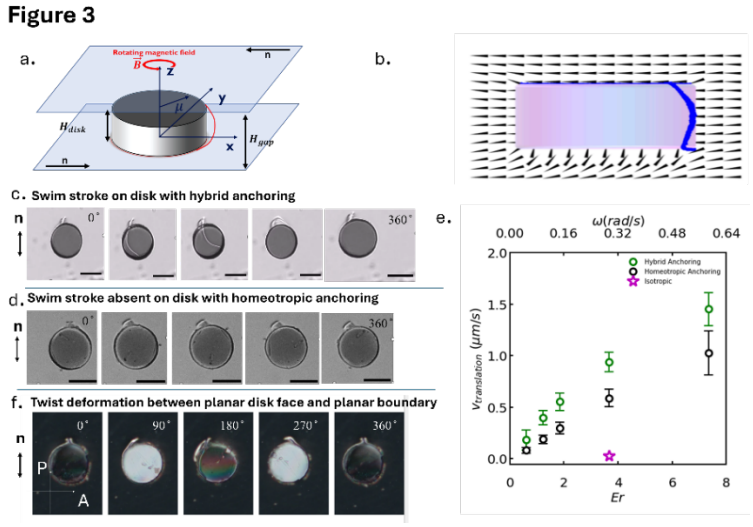

disk rotates. The disclination loop elongates along the disk's edge, depins, and sweeps across its body, performing a "swim stroke" that powers disk swimming (Fig 3c). An all-nickel disk with uniform homeotropic anchoring also translates when rotated in the domain but performs no swim stroke. Its speed is roughly half that of the disk with swim stroke, indicating that the defect swim stroke powers swimming via an elastic storage and release mechanism (Fig 3e). The planar disk face begins with its director aligned with the bounding surface. As the disk rotates, it twists the nematic director field above the disk, storing elastic energy. This twist is evident in images of the rotated disk taken under crossed polarizers (Fig 3f). We explain the swim stroke in terms of a defect instability driven by strong twist of nematogens between the disk and bounding surfaces.

Implications Prior work on swimming in NLC using e.g. bacteria in lyotropic LC has found that swimmers move, assemble, and disassemble[3] along trajectories that are strongly biased by the NLC director and defect locations. Pattern anchoring on boundaries can bias swim directions away from sites of bend, and toward sites of splay. Directed swimming can be harnessed to develop polarized jets of swimmers at sites of splay[4], and swimmers moving in non-trivial paths generated by hydrodynamic interactions[5]. In these studies, the bacteria swim via flagellar generation of thrust, which obeys the scallop theorem for Newtonian fluids and is influenced by broken symmetries in the NLC generated by confinement and patterning. We show that absent patterning, the NLC itself generates directed thrust even from highly symmetric forcing and can add additional power via elastic energy released via instabilities of topological defects.

Future Plans We are currently focusing on: 1. The role of colloid shape in biasing defect location, broken symmetries and colloid motion; dimers of active colloids. 2. Patterned surfaces to generate standing arrays of topological defects for active colloid-defect interactions/ reconfiguration. 3. Patterned defects loaded with passive colloids and/or defect active molecules will be used for assembly/ reconfiguration.

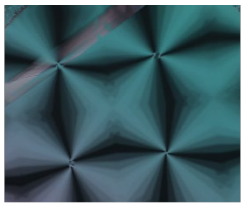

Figure 4 Patterned boundary for reconfigurable defect arrays

References

1. T. Yao, Ž. Kos, Q. X. Zhang, Y. Luo, E. B. Steager, M. Ravnik, and K. J. Stebe, *Topological defect-propelled swimming of nematic colloids* Science Advances **8**, eabn8176 (2022).

2. T. Yao, Ž. Kos, Q. X. Zhang, Y. Luo, F. Serra, E. B. Steager, M. Ravnik, and K. J. Stebe, *Nematic Colloidal Micro-Robots as Physically Intelligent Systems* Advanced Functional Materials **32**, 2205546 (2022).

3. P.C. Mushenheim, R. R. Trivedi, H. H. Tuson, D. B. Weibel, and N. L. Abbott, *Dynamic self-assembly of motile bacteria in liquid crystals* Soft Matter **10**, 88 (2014).

4. M. M. Genkin, A. Sokolov, O. D. Lavrentovich, and I. S. Aranson, *Topological defects in a living nematic ensnare swimming bacteria* Physical Review X **7**, 011029 (2017).

5. T. Turiv, R. Koizumi, K. Thijssen, M.M. Genkin, H. Yu, C.Peng, Q.H. Wei, J.M. Yeomans, I.S. Aranson, A. Doostmohammadi, and O.D. Lavrentovich, *Polar jets of swimming bacteria condensed by a patterned liquid crystal*. Nature Physics, **16,** 481 (2020).

Publications

Two publications in preparation.

Materials Exhibiting Biomimetic Carbon Fixation and Self Repair: Methanotrophic Materials

Michael S. **Strano**, Carbon P. Dubbs Professor of Chemical Engineering, Massachusetts Institute of Technology, Department of Chemical Engineering.

Co-author: Jimin Kim, Postdoctoral researcher, Massachusetts Institute of Technology, Department of Chemical Engineering**.**

Keywords: carbon fixation, material repair, polymer synthesis, methane oxidation.

Research Scope

Synthetic Methanotrophic systems that produce valuable polymer materials at ambient conditions: Anthropogenic methane emissions to the atmosphere significantly contribute to climate warming. Its concentration has tripled to 1900 ppb since pre-industrial times, making it the second largest contributor to climate warming. However, the low temperature and concentration of these emission streams make them difficult to address by currently proposed methane oxidation routes, which rely on high temperatures or pressures to drive methane oxidation rapidly and efficiently. We have introduced a novel tandem catalytic system, combining alcohol oxidase with iron-modified ZSM-5 that functions as a synthetic methanotrophic system capable of partially oxidizing methane at ambient temperatures and pressures, producing chemically useful intermediates for polymer material synthesis. Our results show that the methane-to-formaldehyde selectivity can exceed 90% at room temperature and 0.5 atm of CH_4 and air. The generated formaldehyde intermediate was rapidly incorporated into a growing urea polymer, with a material growth rate exceeding 5.0 mg g_{cat} hr^{-1} under ambient conditions, surpassing rates observed in many cultured methanotrophic bacteria systems. Recently, we have investigated the performance of the systems under even leaner atmospheres of methane. Additionally, we have examined the atomic configuration of the active centers of iron-modified ZSM-5 and explored the strategies to enhance the stability of this tandem catalysis.

Recent Progress

The activity of Fe-ZSM-5/AOX hybrids under low partial pressure and system robustness for industrial application: One major source of methane emission is the natural gas infrastructure. Recently, satellite imaging was introduced to precisely pinpoint where high concentrations of methane emissions are coming from, revealing that a small number of 'super-emitters' are responsible for a significant share of methane emissions in these gas and oil infrastructures (*1*). These point sources were, for instance, undetected leaks from pipelines, temporary venting, or abandoned sites, which are all diluted with air under ambient pressure. These dilute sources, which comprise up to one-quarter of emissions, are the focus of our application scenario to effectively reduce methane emissions. There are numerous literature reports highlighting great selectivity and production rates from zeolite-based studies; however, many systems were found to operate at high

pressures due to the low solubility of methane, which cannot be directly applied to scenarios involving diluted or even 1 atm methane sources.

Therefore, to probe the performance of these catalytic systems for methane oxidation in the presence of even leaner streams of methane emissions, methane oxidation reactions were performed with partial pressures of the gas in the air all the way down to 4.8%—below the gas' flammability limit in the air of 5%. The results are shown in Figure 1. At these lower partial pressures, we observed the reaction products still accumulated, though in lower quantities. Additionally, partial pressure methane (20% CH_4 and 80% air) yielded the highest product accumulation. This is due to more dissolved oxygen in the reaction solution, allowing for greater H_2O_2 production from alcohol oxidase, where its reaction is limited by oxygen availability.

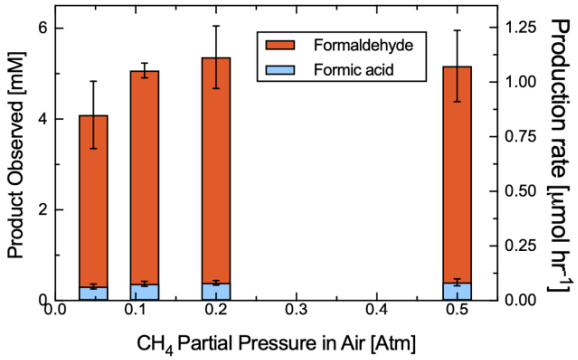

5/AOX under varying partial pressure of methane. Each reaction was run under an atmosphere of 4.8%, 11.1%, 20%, and 50% of CH_4 and balanced with air. 1.0 mg of each of the Fe-ZSM-5 and the SiO_2-AOX catalysts were suspended in 5.0 mL of KBS buffer in a capped 40.0 mL reaction vessel initially loaded with 100 mM of methanol. The reactions were run for 24 hours.

In addition, the effects of impurities of various co-pollutants in emission streams on the activity of the chemo-enzymatic system were investigated, and the performance of catalysts was confirmed compatible with the co-pollutants, including longer alkanes and longer alcohols. The fresh and used chemocatalysts after the methane oxidation reaction were characterized with multiple material characterization tools, including XPS, STEM, and UV-Vis spectroscopy, and the chemical and physical properties of catalysts were unchanged after the reaction. Thus, these results show that our system could be a promising and potential solution to abate methane emissions with their widespread applications in emission streams at lower partial pressures.

Enhancing the stability of the chemo-enzymatic system by regulating hydrogen peroxide: To make this system a feasible route for large-scale methane abatement, the system's stability could be further improved. Particularly, the stability of the enzyme used in the study was hindered by the accumulated H_2O_2. For instance, 5 mM of H_2O_2 was experimentally verified to decrease the enzymatic activity in 2 hours of exposure. Thus, in the host microorganism, *Pichai Pastoris,* another enzyme, catalase expression is imperative (*2*). By adding the catalase in the AOX-SiO_2 solution, which breaks hydrogen peroxide into oxygen and water, the formaldehyde generation was 30 times higher. Thus, fast consumption of H_2O_2 is important for stability, and Fe-ZSM-5, which consumes hydrogen peroxide for methane oxidation, can alleviate this issue. As preliminary data, adding a 10 times higher mass of Fe-ZSM-5 to the system increased the total carbon product accumulation nearly three times with the AOX-SiO_2 loading. Further, the accumulation of the

products was a function of the initial loading of methanol and the ratio between the volume of liquid solution and headspace gas mixture. Therefore, optimizing the ratio between Fe-ZSM-5 and AOX-SiO_2 and batch process parameters could provide a potential solution to enhance the stability of the enzymatic system while maximizing the accumulation of the desired product.

Future Plans

Synthetic Methanotrophic systems that produce valuable polymer materials at ambient conditions: We have confirmed that the system could operate at low methane partial pressures, and the catalysts were reusable and recyclable after the reaction. In order to enhance the system stability, the accumulated hydrogen peroxides need to be removed rapidly and this can be achieved by adjusting the mass ratio of the two catalysts. We will further enhance the current batch-type system by adopting a microfluidic flow reactor design for a continuous process, where the catalysts are embedded on a membrane, and the reaction solution flows beneath, while the gas reactants, a mixture of methane and oxygen, flow above of the catalyst membrane. By adopting the flow reactor design, the concentration of H_2O_2 can be efficiently regulated, and the low solubility of the gas reactants can also be alleviated.

References

1. R. M. Duren, A. K. Thorpe, K. T. Foster, T. Rafiq, F. M. Hopkins, V. Yadav, B. D. Bue, D. R. Thompson, S. Conley, N. K. Colombi, C. Frankenberg, I. B. Mccubbin, M. L. Eastwood, M. Falk, J. D. Herner, B. E. Croes, R. O. Green, C. E. Miller, California's methane super-emitters. *Nature*. **575** (2019), doi:10.1038/s41586-019-1720-3.
2. F. S. Hartner, A. Glieder, Regulation of methanol utilisation pathway genes in yeasts. *Microb. Cell Fact.* **5**, 1–21 (2006).

Publications

1. D. J. Lundberg, J. Kim, D. Parviz, and M. S. Strano, *Mitigation of ventilation air methane (VAM) using novel methanotrophic coating materials: a technical analysis*, Environmental Research Letters, 18,11,114039 (2023)

2. Zhang, J. F. Yang, S. Yang, A. M. Brooks, V. B. Koman, X. Gong, and M. S. Strano, *Colloidal State Machines as Smart Tracers for Chemical Reactor Analysis*, Advanced Intelligent Systems, 2300130. (2023)

3. D. J. Lundberg, D. Parviz, H. Kim, M. Lebowitz, R. Lu, and M. S. Strano, *Universal Kinetic Mechanism Describing CO2 Photoreductive Yield and Selectivity for Semiconducting Nanoparticle Photocatalysts*, Journal of the American Chemical Society, 144, 30, 13623-13633. (2022)

4. J. F. Yang, T. A. Berrueta, A. M. Brooks, A. T. Liu, G. Zhang, D. Gonzalez-Medrano, S. Yang, V. B. Koman, P. Chvykov, L. N. LeMar, M. Z. Miskin, T. D. Murphey, and M. S. Strano. *Emergent microrobotic oscillators via asymmetry-induced order*, Nature Communications, 13, 5374 (2022)

5. G. Zhang, J. Yang, D. Gonzalez-Medrano, M. Z. Miskin, S. Yang, V. B. Koman, Y. Zeng, S. X. Li, M. Kuehne, A. T. Liu, A. M. Brooks, and M. S. Strano. *High Energy Density Picoliter Zn-Air batteries for Colloidal Robots and State Machines*, in review (2024)

6. D. J. Lundberg, J. Kim, Y. Tu, C. Ritt, and M. S. Strano, *Concerted Methane Fixation at Ambient Temperature and Pressure by Enzymatic Fe-ZSM-5 Catalytic Coupling*, minor revision in Nature Catalysis. (2024)

7. H. Kim, D. J. Lundberg, D. Parviz, M. Chen, and M. S. Strano, *Tailoring CO_2 Photocatalytic Activity and Selectivity using Tunable Tungsten Oxide Materials*, in preparation

8. H. Kim, M. Chung, Y. Cho, J. Park, D. J. Lundberg, G. He, D. Parviz, J. Kong, H. J. Kulik, K. Manthiram, and M. S. Strano, *Defect Control of Monolayer Boron Nitride on Copper (hBNO/Cu) for High CO_2 Reduction Selectivity toward Methane*, in preparation.

Materials Exhibiting Biomimetic Carbon Fixation and Self Repair: Methanotrophic Materials

Jimin Kim, Postdoctoral researcher, Massachusetts Institute of Technology, Department of Chemical Engineering.

Co-author: Michael S. **Strano**, Carbon P. Dubbs Professor of Chemical Engineering, Massachusetts Institute of Technology, Department of Chemical Engineering.

Keywords: carbon fixation, material repair, polymer synthesis, methane oxidation, urea synthesis.

Research Scope

Sustainable production and upcycling of urea from the environment as an intermediate for polymer materials at ambient conditions: Urea ($CO(NH_2)_2$) is a crucial chemical intermediate for capturing formaldehyde into the urea-formaldehyde polymer and preventing the over-oxidation of carbon products in our synthetic methanotrophic system. Urea comprises two-thirds of the total mass in the final polymer material. Large-scale production of urea is typically carried out by combining ammonia and carbon dioxide at high temperatures and pressures (*1*). Furthermore, the "Haber-Bosch" method, which predominates in industrial ammonia production (with 42% of ammonia used for urea synthesis (*2*)), is energy-intensive, operates in extreme circumstances, and accounts for more than 2% of the world's energy consumption and emissions today. Thus, there is a strong motivation for more sustainable urea production under mild conditions, not only for our synthetic methanotrophic systems operating at ambient conditions but also for the general supply of urea. Concurrently, urea is a major nitrogen waste product of mammalian metabolism. For example, human urine contains approximately 300 mM of urea, and removing urea from the waste streams is a crucial issue for alleviating water pollution (*3*, *4*). Therefore, we currently seek sustainable urea sources for polymer production at ambient conditions through: 1) the co-reduction of carbon dioxide and nitrate into the catalytic urea synthesis and 2) the upcycling of high-concentration urea from human urine.

Recent Progress

Co-reduction of carbon dioxide and nitrate for sustainable synthesis of urea: Urea is a nitrogen source in urea-formaldehyde, a polymer product of synthetic methanotrophs, comprising two-thirds of the total mass, with nitrogen constituting approximately 40 at%. To sustainably synthesize urea, the catalytic coupling of nitrate and carbon dioxide was studied in an electrochemical reactor. Analytical methods for quantifying NH_3 and urea were optimized for a reliable standard curve with $R^2 > 0.999$. A spray coating method was introduced to enable a microscopically homogeneous loading of catalysts on a carbon fiber template. Solvothermal synthesized indium hydroxide nanocubes were spray-coated onto carbon fiber electrodes, and the homogeneous deposition of catalysts was confirmed by SEM-EDX mapping, which doubled the faradaic efficiency toward urea synthesis. Various electrochemical parameters including applied potential, electrolyte pH,

and electrolyte cations, were tuned in order to study the mechanism and kinetics of the catalytic reactions. With such an optimization, the systems yielded 40% urea selectivity and 13.4 $\mu g/cm^2$ h of yield, which is comparable to the reported literature and a good starting point for integration with the methane-oxidizing chemistry of synthetic methanotrophs.

Upcycling of urea in human urine for polymer production: It was brought to our attention that while urea can be synthesized from nitrate and carbon dioxide, urea is present in human urine and is a crucial waste product that needs to be removed from waste liquid to prevent water pollution. Currently, various urea removal technologies via adsorption, membrane separation, and hydrolysis are proposed, but there is no established method for recovery of the chemical. In this project, we aim to upcycle urea waste from human urine samples into the urea-formaldehyde polymer. As preliminary data, pooled human urine was purchased, and the urea concentration of the sample was directly measured at ~200 mM with an assay compatible with urine. The urine was then diluted with a blank phosphate solution to vary the concentrations of urea and decrease the biological molecules contained in urine, which could potentially degrade the activity of the alcohol oxidase and Fe-ZSM-5 catalysts. The result is shown in Figure 2, and it shows that the desired product could be directly synthesized from waste liquid. The system was performed even better in urine samples compared to the control with added urea. Under 50% of urine conditions, the system achieved 68 % selectivity toward methylene diurea (MDU), a monomer for urea-formaldehyde polymerization, and 1.024 M g_{cat}^{-1} day^{-1} of productivity, which is 200% and 62% higher than the control that contained the same concentration (100mM) of added urea. These results indicate that our synthetic methanotrophic systems can be utilized as a potential route for the removal and upcycling of urea from the waste liquid, simultaneously addressing the methane emissions.

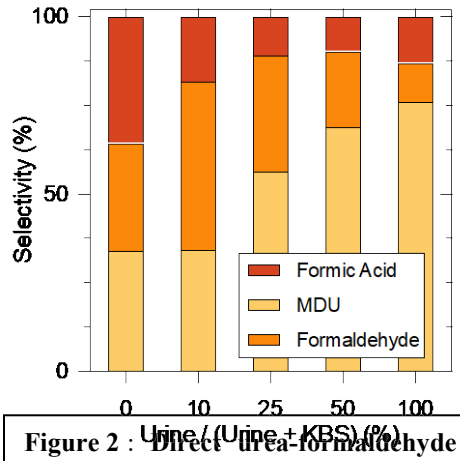

Figure 2 : Direct urea-formaldehyde synthesis from human urine. Each reaction was run under an atmosphere of 50% CH_4 and 50% air. 2.5 mg of Fe-ZSM-5 and 2.5 mg of SiO_2-AOX catalysts were suspended in 1.0 mL of urine and phosphate buffer solution (KBS) mixture with varying ratios in a capped 40.0 mL reaction vessel initially loaded with 100 mM of methanol. 100 mM of urea was added to the 100% KBS solution. The reactions were run for 24 hours.

Future Plans

Sustainable production and upcycling of urea from the environment as an intermediate for polymer materials at ambient conditions: With the optimized urea-producing chemistry, we plan to integrate urea-producing and methane-oxidizing chemistry in one reactor, turning greenhouse gases and nitrates into the polymer product. On the cathodic side, carbon dioxide and nitrates are coupled into urea, while on the anodic side, oxygen is produced from water to provide substrate for hydrogen peroxide generation by alcohol oxidase. The substrates for the polymer synthesis are

methane, water, carbon dioxide, and nitrate in the absence of air. In this scheme, our system will be further expanded into synthetic "anaerobic" methanotrophs. For the upcycling of urea from urine samples, based on the preliminary data and observed activity of the catalytic system in human urine samples, we will further investigate the long-term operation of synthesis and the removal and recovery efficiency of urea.

References

1. M. Muhyuddin, G. Zuccante, P. Mustarelli, J. Filippi, A. Lavacchi, L. Elbaz, Y. H. Chen, P. Atanassov, C. Santoro, Electrochemical urea production using carbon dioxide and nitrate: state of the art and perspectives. *Energy Environ. Sci.*, 3739–3752 (2024).

2. X. Zhu, X. Zhou, Y. Jing, Y. Li, Electrochemical synthesis of urea on MBenes. *Nat. Commun.* **12**, 1–9 (2021).

3. M. K. van Gelder, J. A. W. Jong, L. Folkertsma, Y. Guo, C. Blüchel, M. C. Verhaar, M. Odijk, C. F. Van Nostrum, W. E. Hennink, K. G. F. Gerritsen, Urea removal strategies for dialysate regeneration in a wearable artificial kidney. *Biomaterials*. **234**, 119735 (2020).

4. D. Weerakoon, B. Bansal, L. P. Padhye, A. Rachmani, L. James Wright, G. Silyn Roberts, S. Baroutian, A critical review on current urea removal technologies from water: An approach for pollution prevention and resource recovery. *Sep. Purif. Technol.* **314**, 123652 (2023).

Publications

1. D. J. Lundberg, J. Kim, D. Parviz, and M. S. Strano, *Mitigation of ventilation air methane (VAM) using novel methanotrophic coating materials: a technical analysis*, Environmental Research Letters, 18,11,114039 (2023)

2. Zhang, J. F. Yang, S. Yang, A. M. Brooks, V. B. Koman, X. Gong, and M. S. Strano, *Colloidal State Machines as Smart Tracers for Chemical Reactor Analysis*, Advanced Intelligent Systems, 2300130. (2023)

3. D. J. Lundberg, D. Parviz, H. Kim, M. Lebowitz, R. Lu, and M. S. Strano, *Universal Kinetic Mechanism Describing CO2 Photoreductive Yield and Selectivity for Semiconducting Nanoparticle Photocatalysts*, Journal of the American Chemical Society, 144, 30, 13623-13633. (2022)

4. J. F. Yang, T. A. Berrueta, A. M. Brooks, A. T. Liu, G. Zhang, D. Gonzalez-Medrano, S. Yang, V. B. Koman, P. Chvykov, L. N. LeMar, M. Z. Miskin, T. D. Murphey, and M. S. Strano. *Emergent microrobotic oscillators via asymmetry-induced order*, Nature Communications, 13, 5374 (2022)

5. G. Zhang, J. Yang, D. Gonzalez-Medrano, M. Z. Miskin, S. Yang, V. B. Koman, Y. Zeng, S. X. Li, M. Kuehne, A. T. Liu, A. M. Brooks, and M. S. Strano. *High Energy Density Picoliter Zn-Air batteries for Colloidal Robots and State Machines*, in review (2024)

6. D. J. Lundberg, J. Kim, Y. Tu, C. Ritt, and M. S. Strano, *Concerted Methane Fixation at Ambient Temperature and Pressure by Enzymatic Fe-ZSM-5 Catalytic Coupling*, minor revision in Nature Catalysis. (2024)

7. H. Kim, D. J. Lundberg, D. Parviz, M. Chen, and M. S. Strano, *Tailoring CO_2 Photocatalytic Activity and Selectivity using Tunable Tungsten Oxide Materials*, in preparation

8. H. Kim, M. Chung, Y. Cho, J. Park, D. J. Lundberg, G. He, D. Parviz, J. Kong, H. J. Kulik, K. Manthiram, and M. S. Strano, *Defect Control of Monolayer Boron Nitride on Copper (hBNO/Cu) for High CO_2 Reduction Selectivity toward Methane*, in preparation.

Superstructures and Dynamics in Functional Supramolecular Assemblies

Samuel I. **Stupp**, Department of Materials Science and Engineering, Department of Chemistry, Department of Biomedical Engineering, Department of Medicine, Simpson Querrey Institute for BioNanotechnology, Northwestern University, Evanston, Illinois 60208, USA

Keywords: Supramolecular polymers, dynamics, organic ferroelectrics

Research Scope

Cells rely on compartmentalization to perform functions across length scales. At the largest scale, the very existence of the cell is defined by the separation between the cytoplasm and the extracellular environment by a lipid membrane. Within the cytoplasm, organelles with distinct metabolic and transport functions are also enclosed by lipid bilayers. In these examples, the compartmentalization occurs via encapsulation by membranes, but interestingly membranes are not always used by biology for compartmentalization. Within cell membranes, we find microdomains on the order of 10–200 nm known as lipid rafts, in which signal receptors are segregated. Also the cell nucleus undergoes phase transitions between condensed and loose states, this way regulating gene transcription. It has been suggested that these examples of liquid–liquid phase separation (LLPS) occur as a result of incompatibility between two fluid-forming materials such as hydrophilic and lipophilic domains or condensed and dilute phases. LLPS is also often mediated by a third component that preferentially interacts with one of the components such as cholesterol–sphingolipid interactions or histone–DNA complexation. These biological examples are all highly dynamic, despite having a high degree of order in their structures.

Inspired by the ways cells compartmentalize and organize their components, we investigate here the reversible formation of synthetic superstructures composed of dynamic assemblies of molecules. In our previous research funded by the DOE Biomolecular Materials program, we observed the growth of ordered arrays of filamentous nanostructures in water driven by repulsive electrostatic interactions as well as the formation of superstructures of these assemblies enabled by the dynamic exchange of molecules to allow optimal cohesion between the molecules.[1–5] We explore here how supramolecular dynamics, crowding, and polar structure can drive supramolecular assemblies of small molecules to form superstructures. From the functional perspective of novel soft materials, we propose to investigate the potential of these superstructures in tandem catalysis aided by the internal dynamics of individual nanoscale assemblies. Another functional objective proposed is to investigate if polar assemblies can play a role in superstructure formation and if these structures can amplify ferroelectric behavior.

Recent Progress

We recently investigated the ability of anionic biomacromolecules to induce hierarchical assemblies in negatively charged peptide amphiphile (PA) supramolecular nanofibers. Specifically, we found that negatively charged polysaccharides, such as alginate and hyaluronic acid, can drive self-assembly of PAs (such as $C_{16}V_3A_3E_3$) into hierarchical structures specific chemical interactions between these components (see Figure 1a). Polarized optical microscopy reveals that the nanofibers are strongly aligned within the bundles and that addition of 150 mM NaCl and 3 mM KCl significantly increases birefringence intensity. Furthermore, confocal microscopy show that the size of the bundles increases with added salt. Solution small-angle X-ray scattering (SAXS) patterns of these mixtures in water showed Bragg that are consistent with a highly ordered 2D hexagonal lattice (i.e., q/q^* ratios of $1{:}\sqrt{3}{:}\sqrt{4}{:}\sqrt{7}{:}\sqrt{9}{:}\sqrt{12}$, where q^* is the principal peak position). Increasing the solution pH caused a modest increase in the spacing, likely due to increased electrostatic repulsion. Interestingly, increasing the concentration HA polymer resulted in a decrease in spacing, which we expect if the polymer is acting as a crowding agent. These porous networks can be stabilized as bulk gels by ionic crosslinking with divalent cations like calcium and the confined spaces that emerge could be useful scaffolds for enzymatic catalysis.

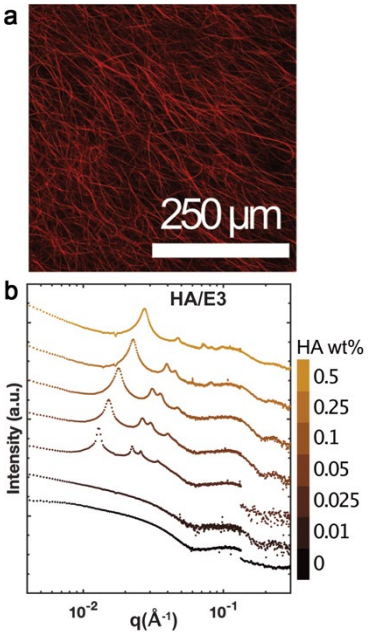

Figure 1. (a) Confocal micrographs of bundles formed by hyaluronic acid (HA) and $C_{16}V_3A_3E_3$ PA in water at pH 6.8 (PA molecules were labeled with TAMRA). (b) Solution small-angle X-ray scattering patterns of 0.5 wt % $C_{16}V_3A_3E_3$ PA and 0–0.5wt % HA (collected at the Advanced Photon Source).

In a second project, we have very recently developed a ferroelectric material that is inspired by the commonly used macromolecule poly(vinylidene fluoride) (PVDF) but using a small molecule containing only six structural units of rather than the thousands in the polymer. We found that conjugating VDF oligomers to a tetrapeptide with a strong propensity to assemble into β-sheet structures led to the formation of nanoscale ribbons in water that acquire ferroelectric polarization. Furthermore, the β-sheet secondary structure programs thermodynamic stability in the all-*trans* conformation of the VDF hexamer, which is required to obtain the ferroelectric polymorph. When an external electric field is applied during the casting of the film, the hydrogen bond axes of the β-sheets (which are parallel to the long axis of the ribbons) gain macroscopic alignment that is either parallel or anti-parallel to the electric field. This stabilizes the two possible bistable orientations of the VDF dipoles under the influence of the external electric field without

disrupting the highly favorable hydrogen-bonding pattern of the β-sheets. This is an important factor in the high polarization observed in the OVDF-PA supramolecular systems. We therefore conclude that both the low coercive fields and high polarization in the systems investigated benefit from the nature of peptide assemblies combined with the characteristic dynamics of supramolecular polymers. Furthermore, variations in the peptide sequence also yield "relaxor" phases in which small ferroelectric domains generate strong electromechanical actuation.

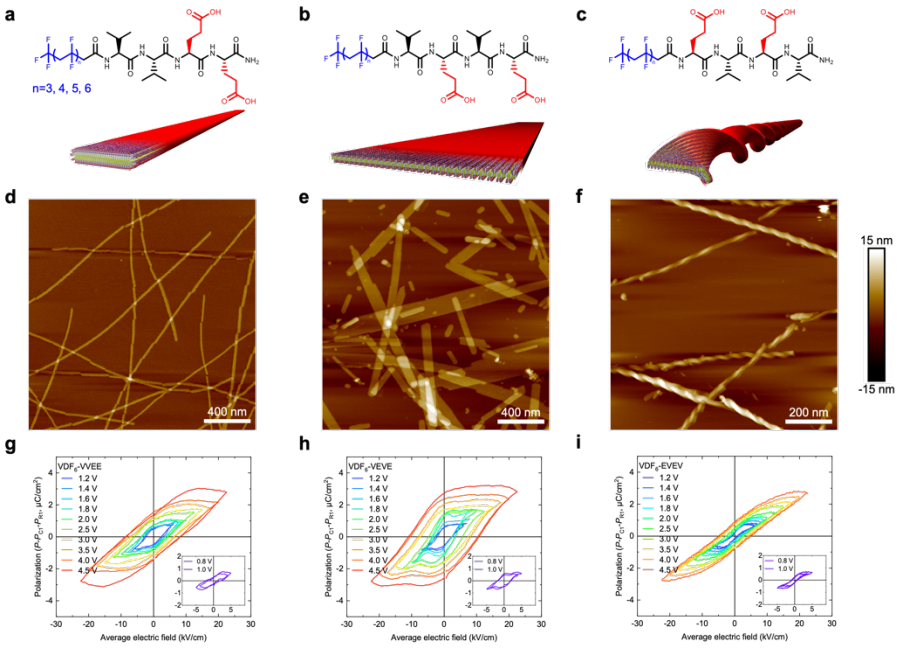

Figure 2. Chemical structures and molecular graphics illustrations of supramolecular architectures of the OVDF-PAs containing hydrophobic segments with three to six VDF repeat units and the peptide sequences VVEE (a), VEVE (b), and EVEV (c). Liquid AFM images of VDF_6-VVEE (d), VDF_6-VEVE (e), and VDF_6-EVEV (f) cast from 20 mM aqueous solutions after annealing. Polarization versus electric field (P-E) loops of VDF_6-VVEE (g), VDF_6-EVEV (h), and VDF_6-VVEE (i).

This biomolecular approach using peptides enables facile organization of ferroelectric nanodomains with a strongly preferred polar axis defined by hydrogen bonding along the long axis of the nanoribbon. The functionality of the supramolecular materials includes a strong electroactive response and a coercive field that is two orders of magnitude lower than that in fluoropolymers. We conclude that these attractive properties are linked to the collinear axes of β-sheet hydrogen bonding and the two bistable states of the multiaxial ferroelectric and also to the inherent dynamics of molecules within supramolecular polymers. These features generate long range cooperativity among molecular dipoles and at the same time the motion of monomers bonded noncovalently and reversibly facilitates polarization switching. Having access to single ferroelectric nanostructures such as the peptide amphiphile ribbons investigated here could lead to ultra-low power devices that take advantage of transient negative capacitance to overcome the theoretical limit of the so-called "Boltzmann tyranny".

Future Plans

We will continue to investigate the formation of bundles of aligned PA filaments by the addition of a macromolecular crowding agent. Our preliminary results show that addition of non-ionic macromolecular crowding agents, such as PEG or dextran, will bring the assemblies closer to each other without electrostatic screening from charged groups. We will explore the use of polymeric crowding agents to control the dimensions of supramolecular bundles to encapsulate enzymes in a confined environment to increase their catalytic activity to potentially create solar fuels. Furthermore, colocalizing several different enzymes within the bundles could enhance their ability to catalyze multiple reaction steps in the same material.

Due to the spontaneous polarization parallel to the long axis of the ferroelectric PA ribbons, we expect that electrostatic forces between the dipoles will cause the adjacent ribbons to align in an antiparallel fashion. The spacing between the ribbons should depend on the concentration of the PA molecules and the crowding agent. The bundling of antiparallel ferroelectric microcrystals is expected to generate antiferroelectric superstructures characterized by a distinctive double hysteresis loop. The combination of external electric fields and crowding agents could be necessary to obtain superstructures with macroscopic polarization and ferroelectric behavior. Ferroelectricity of the PA structures not only depends on the β-phase crystallization in the OVDF tail region but is also affected by the coupling among the crystal domains. Applying an external field to the solution should cause ferroelectric domains to align in the same orientation. The anisotropic nature of the PA assemblies should also drive them to orient parallel to the electric field, which is the preferred orientation for the OVDF tail dipole and PA hydrogen bonds. This will enable the formation of larger domains within the bundles through the coupling of dipoles from the individual ribbons and generate enhanced ferroelectric polarization.

References

1. J. H. Ortony, C. J. Newcomb, J. B. Matson, L. C. Palmer, P. E. Doan, B. M. Hoffman, and S. I. Stupp, *Internal Dynamics of a Supramolecular Nanofibre*, Nature Materials **8**, 812 (2014).
2. R. Freeman, M. Han, Z. Álvarez, J. A. Lewis, J. R. Wester, N. Stephanopoulos, M. T. McClendon, C. Lynsky, J. M. Godbe, H. Sangji, E. Luijten, and S. I. Stupp, *Reversible Self-Assembly of Superstructured Networks*, Science **362,** *362*, 808 (2018).
3. J. R. Wester, J. A. Lewis, R. Freeman, H. Sai, L. C. Palmer, S. E. Henrich, and S. I. Stupp, *Supramolecular Exchange among Assemblies of Opposite Charge Leads to Hierarchical Structures*, Journal of the American Chemical Society **142**, 12216 (2020).
4. Z. Álvarez, A. N. Kolberg-Edelbrock, I. R. Sasselli, J. A. Ortega, R. Qiu, Z. Syrgiannis, P. A. Mirau, F. Chen, S. M. Chin, S. Weigand, E. Kiskinis, and S. I. Stupp, *Bioactive Scaffolds with Enhanced Supramolecular Motion Promote Recovery from Spinal Cord Injury*, Science **374**, 848 (2021).

5. A. N. Edelbrock, T. D. Clemons, S. M. Chin, J. J. W. Roan, E. P. Bruckner, Z. Alvarez, J. Edelbrock, K. S. Wek, and S. I. Stupp, *Superstructured Biomaterials Formed by Exchange Dynamics and Host–Guest Interactions in Supramolecular Polymers*, Advanced Science **8**, 2004042 (2021).

Publications

1. A. Dannenhoffer, H. Sai, E. P. Bruckner, L. Đorđević, A. Narayanan, Y. Yang, X. Ma, L. C. Palmer, and S. I. Stupp, *Metallurgical Alloy Approach to Two-Dimensional Supramolecular Materials*, Chem **9** 170 (2023).
2. S. I. Stupp and L. C. Palmer, *New Frontiers in Supramolecular Design of Materials,* MRS Bulletin **49**, 478, (2024)
3. M. H. Sangji, S. R. Lee, H. Sai, S. J. Weigand, L. C. Palmer, and S. I. Stupp, *Self-Sorting vs. Co-Assembly in Peptide Amphiphile Supramolecular Nanostructures*, ACS Nano **18**, 15878 (2024).
4. R. Emmanuele, H. Sai, J.-S. Chen, D. J. Morrow, L. Đorđević, D. J. Gosztola, S. W. Hla, S. I. Stupp, and X. Ma, *Lattice Symmetry-Guided Charge Transport in Two-Dimensional Supramolecular Polymers Promotes Triplet Formation*, Advanced Science (2024) Early View. DOI: 10.1002/advs.202402932
5. S. A. Egner, M. Agrawal, H. Sai, L. C. Palmer, and S. I. Stupp, *Functional Design of Peptide Materials Based on Supramolecular Cohesion,* In revision.
6. Y. Yang, H. Sai, S. A. Egner, R. Qiu, L. C. Palmer, and S. I. Stupp, *Peptide Programming of a Supramolecular Vinylidene Fluoride Ferroelectric Phase,* In revision.

Protein Self-Assembly by Rational Chemical Design

F. Akif **Tezcan**, University of California, San Diego

Keywords: Protein-Based Materials, Dynamic/Stimuli-Responsive/Self-Healing Systems, Weaving/Interlocking Topologies, Protein-Polymer Interface

A. Research Scope. Our research aims to develop design strategies to control protein self-assembly and to construct dynamic/functional protein-based materials. To circumvent the challenge of designing extensive non-covalent interfaces for controlling protein self-assembly, we have endeavored to develop a chemical bonding toolkit (metal coordination, disulfide linkages, computationally prescribed non-covalent bonds, DNA hybridization, host-guest interactions, etc.) to mediate protein-protein interactions. The initial focus of our DOE-funded program was to establish design strategies for obtaining desired structures such as discrete (*i.e.,* finite) or 0-, 1-, 2- and 3D (*i.e.,* extended) protein assemblies with crystalline order. While we still pursue such methodology development for designing new protein *structures* (see section B.1), a considerable fraction of our ongoing efforts center on designing protein-based materials with new *functions/properties*. In the last two-year funding period, our particular goals have been as follows: (1) to construct hierarchical and spatially patterned polymer-integrated protein crystals (PIX) that are adaptive, stable, self-healing and capable of selectively taking up biological macromolecules toward fabricating multifunctional biomaterials, (2) to design 2- and 3D protein arrays with interlocking/woven topologies, which–like their macroscopic counterparts–are proposed to have superior mechanical properties, (3) to design *de novo* protein scaffolds capable of autocatalytic isopeptide bond formation (toward the generation of stable, covalently-linked protein-based materials), and (4) to design dissipative protein architectures, which, like natural cytoskeletal assemblies, require constant energy input/consumption for maintaining their self-assembled states.

B. Recent Progress. Our progress on polymer-integrated protein crystals (PIX) and their uses in selective biomolecular uptake/release as well as in coupling enzymatic activities were summarized in our poster presentation/abstract last year (Publications 2 and 7). Therefore, we will focus here on the construction of topological woven protein assemblies and two new research elements aimed to design new types of dynamic/functional protein assemblies.

B.1. Designing protein building blocks for the bottom-up construction of 2- and 3D materials with woven/interlocked topologies (unpublished): Designing covalent and non-covalent interactions at protein interfaces has been a major focus in protein-based materials research (including our group) that led to the development of discrete and extended protein assemblies. In these "conventional" protein assemblies, each protein is typically considered as a positionally rigid building block, chemically connected to its neighbors. However, one kind of bond that has been critically underexplored in protein assemblies is the mechanical bond. In mechanical bonds, one or more building blocks are mechanically interlocked, such that they can move freely within the topological limits set by their mechanically bonded partners, yet breaking of a covalent bond is necessary for their full dissociation. Such woven protein materials–just like their macroscopic textile counterparts–are expected to have superior mechanical properties.

Using ApoCyt-RIDC1 (an engineered, heme-free variant of cytochrome cb_{562}, a four-helix bundle protein) as building block, we explored different strategies to assemble protein weaves. In the presence of Zn^{2+}, ApoCyt-RIDC1 assembles into D_2 symmetric tetramers composed of two

pairs of interlacing V-shaped protein monomers, with each tetramer resembling the crossover points of a molecular weave (**Fig. 1a**) We established conditions in which ApoCyt-RIDC1 crystallizes in an arrangement reminiscent of a chain-link weave. Next, we installed cysteine residues at strategic points at the vertex of the V-shaped dimer, as well as at its arms, providing the functional groups to connect the protein monomers to topologically interlocked, "infinitely-linked" threads. Crystallographic evidence confirmed the presence of a disulfide bond at one of the desired sites (positions 81 at the vertices), however, the cysteines placed at the second site (positions 51 in the arms) were found to have an orientation incompatible with disulfide bond formation (**Fig. 1b**). Regardless of this lack of continuous covalent linkage throughout the "threads", we still examined if the resulting partially disulfide-linked crystals would be robust and display dynamic behavior. As ApoCyt-RIDC1 is a Zn^{2+}-mediated tetramer, we speculated that removal of the metal ion could alter the crystal's mechanical properties. Remarkably, chelation of the Zn^{2+} ions led to expanding protein crystals (**Fig. 1c**), while non-crosslinked protein crystals readily dissolved. Furthermore, the expansion was reversible in response to the presence of osmolytes in the solution. These promising preliminary results indicate how topology engineering can transform a brittle protein crystal into a strong and stimuli-responsive biomaterial. In our current quest to achieve complete covalent crosslinking across all "threads" within the ApoCyt-RIDC1 crystals, we have engineered cysteines in different positions (49 and 54) along the "arms" of ApoCyt-RIDC1 molecules. We are currently investigating whether these cysteines would directly form disulfide bonds or could be covalently crosslinked using bis-maleimide linkers within the ApoCyt-RIDC1 crystals to create fully woven assemblies. Alternatively, we engineered Tyr sidechains into positions 51 or 52 in order to explore the possibility of redox/radical-mediated coupling between these sidechains. Our structural characterization of the Tyr51- and Tyr52-ApoCyt-RIDC1variants shows that they form the desired lattice composed of D_2 symmetric tetramers and that the pairs of Tyr51 or Tyr52 sidechains are properly positioned for potential crosslinking (**Fig. 1d**).

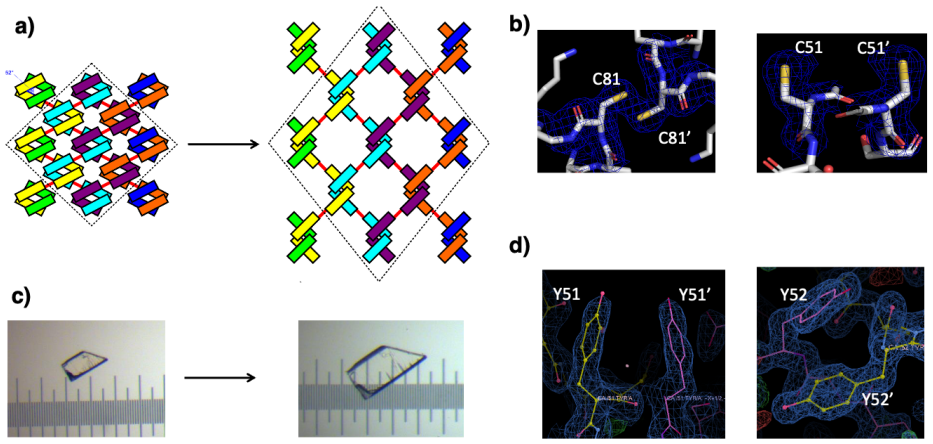

Figure 1. (a) Schematic illustration for the expansion of a "woven" protein crystal with a chain-link pattern. **(b)** Close-up views of Cys81 and Cys51 residues or *in crystallo* disulfide formation. **(c)** Light micrographs showing the expansion of a woven/crosslinked-ApoCyt-RIDC1 crystal upon removal of Zn ions and incubation in water. **(d)** Close-up views of Tyr51 and Tyr52 residues for radical-mediated crosslinking.

B.2. De novo design of proteins for autocatalytic isopeptide bond formation (unpublished): As summarized above, our efforts to construct interwoven protein materials highlights how extensive non-covalent/metal coordination interactions need to cooperate to orient protein building blocks in a proper arrangement such that they can form covalent linkages (disulfide bonds) with each

other in the correct positions. Interestingly, some natural proteins use the same principle to form isopeptide bonds (IPBs) between the side chains of lysine and asparagine or aspartate residues, thus providing exceptional structural stability due to the covalent nature of these bonds. Examples include surface proteins of Gram-positive bacteria (e.g., the pilus-associated adhesin RrgA from the pathogenic *Streptococcus pneumoniae*), in which autocatalytically formed IPBs crosslink the protein's inner core, as well as the capsid proteins of some bacteriophages (e.g., HK97), which consist of a chain mail structure locked into its topology by autocatalytic IPB formation. In fact, such natural IPB-forming proteins have been exploited successfully in covalent bioconjugation/tagging technologies (e.g., SpyTag-SpyCatcher). Clearly, the addition of IPBs into the protein design toolbox would greatly enhance our ability to design dynamic/functional protein-based materials. To this end, we set out to leverage recent advances in deep-learning-based tools (in particular, RFDiffusion and ProteinMPNN developed by the Baker Lab) to design *de novo* protein scaffolds with the ability to autocatalytically form IPB. Using the active site orientations of catalytically relevant residues (Lys/Asn for isopeptide bonds, Glu as acid/base catalyst, and few surrounding hydrophobic residues) from RrgA as a structural template, we designed a small set of 100-150-residue proteins which possessed less than 35% sequence identity to RrgA. Gratifyingly, three out of four designs were capable of forming the desired isopeptide bond, as characterized by mass spectrometry and X-ray crystallography (**Fig. 2**). These findings demonstrate that the three catalytic residues in these constructs were positioned in an atomically accurate fashion to enable IPB formation. Through alanine scanning studies, we also identified active site residues that were critical in providing the appropriate active site microenvironment, such that the pKa's of the catalytic Lys and Glu residues could be "inverted" for the IPB formation to occur. Our current goal is to incorporate such strategically placed IPBs into the design of supramolecular protein assemblies and extended 2- and 3D protein materials.

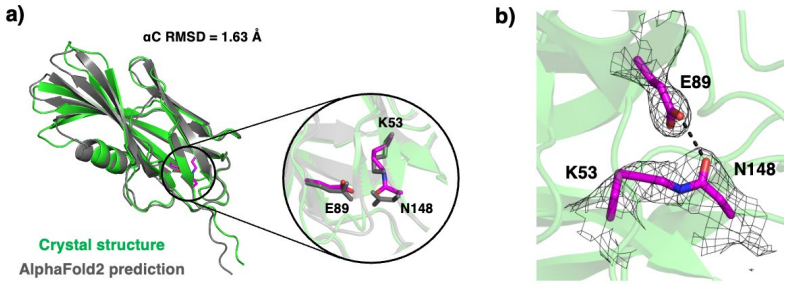

Figure 2. (a) Overlay of the experimental and predicted structures of a *de novo* designed protein construct for isopeptide bond formation. **(b)** Close-up view of the isopeptide bond between K53 and N48, and the catalytic E89 residue.

B.3. Design of dissipative protein assemblies (in review): There have been tremendous advances in the design of proteins/protein assemblies with arbitrary structural complexities and even obtaining dynamic, stimuli-responsive proteins. Yet, all such examples correspond to structures obtained or attained under equilibrium conditions. In contrast, active materials including biological cells use continuous energy consumption to drive unidirectional, non-equilibrium processes such as motility, generation of concentration gradients, and catalysis. At the cellular level, these processes are driven primarily by nucleoside triphosphate (NTP)-dependent protein-based nanomachines (e.g., enzymes, membrane pumps) and self-assembling, dynamic materials (e.g., cytoskeletal assemblies). These dissipative protein-based systems have inspired the development of diverse chemically-fueled molecular machines and active materials, but their structural and functional sophistication have yet to be matched by chemical or biomolecular design.

Given this challenge, we asked whether it is possible to transform a natural ATP-dependent protein nanomachine into a dissipative self-assembling material, thereby altering the structural/functional mode in which chemical energy is utilized. To this end, we focused on the family of AAA+ proteins which predominantly form ring-like hexameric assemblies that use ATP binding and hydrolysis to translocate and remodel various cellular substrates. We specifically targeted a ubiquitous AAA+ protease found in prokaryotes and eukaryotes, namely FtsH (Filamentation temperature-sensitive protein H) involved in the quality control/proteolysis of membrane-bound or cytosolic proteins. We found that upon removal of its membrane-anchoring domains, FtsH assembles into helical, nanotubular architectures (**Fig. 3a** and **b**). We carried out extensive biochemical and structural analyses which indicated that the FtsH nanotubes require constant energy input to maintain their integrity and degrade over time with the concomitant hydrolysis of ATP, in analogy to natural NTP-dependent cytoskeletal assemblies. Yet, in contrast to these natural dissipative systems, ATP hydrolysis is catalyzed exclusively by free FtsH protomers and the formation of FtsH nanotubes actually serves to conserve ATP. We have conducted extensive kinetics experiments and mathematical modeling to show that the dissipative dynamics of FtsH nanotube assembly is a nucleated process. Furthermore, we showed that the lifetimes of FtsH nanotubes could be tuned from days to minutes by controlling the rate of ATP consumption in the system through the inclusion of ATP-hydrolyzing enzymes in the solutions (**Fig. 3c**). These findings offer promise for designing other types of dissipative protein-based materials through the repurposing of existing NTP-dependent proteins. Once the assembly states of such dissipative materials are coupled to different functional outcomes through proper design (e.g., activation/deactivation of enzyme activity upon assembly/disassembly, cargo storage and release from the nanotube interior, interactions with cellular components), we can envision the engineering of artificial intracellular platforms whose functions can be spatiotemporally controlled through cellular ATP levels and flux.

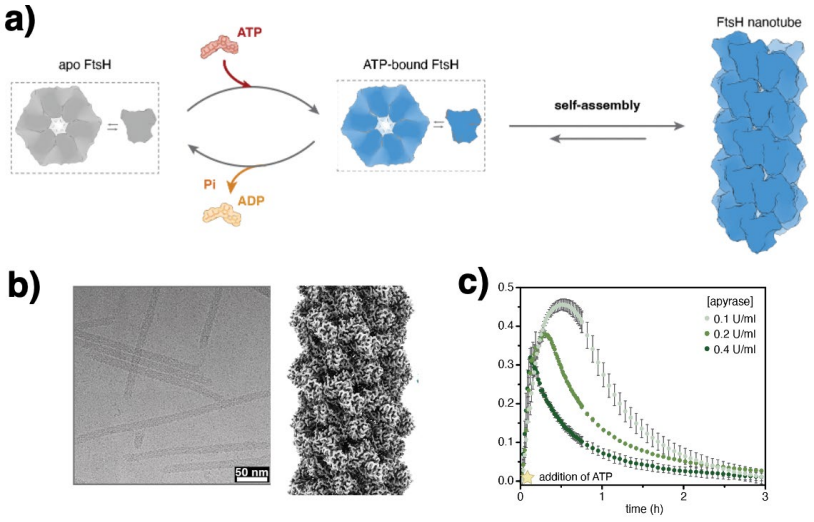

Figure 1. (a) Schematic illustration for the ATP-dependent, dissipative self-assembly of FtsH into helical nanotubes. **(b)** CryoEM images and helical reconstruction of FtsH nanotubes. **(c)** Controlling the lifetimes of FtsH nanotubes through external ATPases.

C. Future Plans. (1) generate multi-enzyme catalytic PIX systems that allow operation in non-aqueous solutions or allow O_2-sensitive enzymes to function under aerobic conditions, (2) use host-guest interactions to control protein/biomacromolecule uptake within PIX and control protein-polymer interaction dynamics, (4) finish characterization of first-generation "woven" protein crystals, (5) incorporate IPBs into the design of 2- and 3D protein materials, (6) use FtsH (and other AAA+ proteins) as a building block for dissipative 2- and 3D protein materials.

D. Publications (2022-2024)

1) J. Zhu, L. Samperisi, M. Kalaj, J. A. Chiong, J. B. Bailey, Z. Zhang, C-J. Yu, E. Sikma, X. Zou, S. M. Cohen, Z. Huang*, F. A. Tezcan*, *Metal-Hydrogen-Pi-Bonded Organic Frameworks*, Dalton Trans., **51**, 1927-1935 (2022).

2) K. Han, Y. Na, L. Zhang, F. A. Tezcan*, *Dynamic, Polymer-Integrated Crystals for Efficient, Reversible Protein Encapsulation*, J. Am. Chem. Soc., **144**, 10139-10144 (2022).

3) L. Spiegelman, A. Bahn, E. T. Montaño, L. Zhang, G. L. Hura, K. Patras, A. Kumar, F. A. Tezcan, V. Nizet, S. Tsutakawa, P. Ghosh*, *Strengthening of enterococcal biofilms by Esp*, PLoS Pathog. **18**, e1010829 (2022).

4) A. M. Hoffnagle, V. H. Eng, U. Markel, F. A. Tezcan*, *Computationally Guided Redesign of a Heme-Free Cytochrome with Native-like Structure and Stability*, Biochemistry, **61**, 2063-2072 (2022).

5) R. G. Alberstein, J. L. Prelesnik, E. Nakouzi, S. Zhang, J. J. De Yoreo, J. Pfaendtner, F. A. Tezcan, C. J. Mundy*, *Discrete Orientations of Interfacial Waters Direct Crystallization of Mica-Binding Proteins*, J. Phys. Chem. Lett., **14**, 80–87 (2023).

6) K. Han, Z. Zhang, F. A. Tezcan*, *Spatially Patterned, Porous Protein Crystals as Multifunctional Materials*, J. Am. Chem. Soc. **145**, 19932-19944 (2023).

7) S. Vijayakumar, R. G. Alberstein, Z. Zhang, Y. Lu, A. Chan, C. E. Wahl, J. S. Ha, D. E. Hunka, G. R. Boss, M. J. Sailor, F. A. Tezcan* "*Designed 2D Protein Crystals as Dynamic Molecular Gatekeepers for a Solid-State Device*", Nat. Commun., *accepted* (2024).

8) Y. Li, J. Zhu, Z. Zhang, J. Wei, F. Wang, G. Meisl, T. P. J. Knowles, E. H. Egelman, F. Akif Tezcan* "*Transforming an ATP-Dependent Enzyme into a Dissipative, Self-Assembling System*", *under review* (2024).

9) U. Markel, S. Sritantitham, A. L. Walker, F. A. Tezcan* "*De Novo Design of Proteins for Autocatalytic Isopeptide Bond Formation*", *to be submitted* (2024)

Patents:

1) Y. Suzuki, F. A. Tezcan, "Method for Fabricating Two-Dimensional Protein Crystals", US Patent 11,286,277, Issued March 2022.

2) L. Zhang, J. B. Bailey, F. A. Tezcan, "Self-healing macromolecular crystal materials", US Patent 11,975,307. Issued May 2024

3) K. Han, Y. Na, L. Zhang, F. A. Tezcan, "Controlled entrapment and release of molecular cargo", US Patent Application 18/253,766. Filed October 2023

Towards principles for bio-inspired and far-from-equilibrium adaptive, information storing materials

Suriyanarayanan **Vaikuntanathan**, University of Chicago

Keywords: non-equilibrium stat mech, actin, active nematic, associative memory

Research Scope

Biological materials, such as those composed of actin and driven by molecular motors, routinely sense molecular cues and initiate microscopic reorganization events in response. Understanding how force-generating arrays of actin, molecular motors, and associated proteins can be tuned, built, and sustained can lead to the discovery of general design principles for the construction of non-equilibrium bioinspired materials with similar exotic adaptive properties. Progress in uncovering these principles is however impeded by the lack of general frameworks for non-equilibrium materials that predict or constrain (1) force response relations far from equilibrium, (2) requirements for ensuring precise spatio-temporal modulation of material properties under external time-dependent conditions, and (3) requirements for adaptive behavior. Indeed, addressing these questions has been posed as a grand challenge in non-equilibrium statistical mechanics. Our work develops and combines novel powerful non-equilibrium statistical mechanics frameworks to address such questions. Additionally, we combine these with machine learning techniques to unravel design principles for the construction of adaptive force-generating bioinspired materials.

Recent Progress

In recent work we have made progress along multiple fronts, both towards advancing the state of the art in non-equilibrium statistical mechanics and combining such advances with AI inspired techniques.

a) *A physics inspired approach for control and learning in materials:* Standard approaches to controlling dynamical systems involve biologically implausible steps such as backpropagation of errors or intermediate model-based system representations. Recent advances in machine learning have shown that "imperfect" feedback of errors during training can yield test performance that is similar to using full backpropagated errors, provided that the two error signals are at least somewhat aligned. Inspired by such methods, we introduce an iterative, spatiotemporally local protocol to learn driving forces and control non-equilibrium dynamical systems using imperfect feedback signals. We present numerical experiments and theoretical justification for several examples. For systems in conservative force fields that are driven by external time-dependent protocols, our update rules resemble a dynamical version of contrastive divergence. We appeal to linear response theory to establish that our imperfect update rules are locally convergent for these conservative systems. For systems evolving under non-conservative dynamics, we derive a new theoretical result that makes possible the control of non-equilibrium steady-state

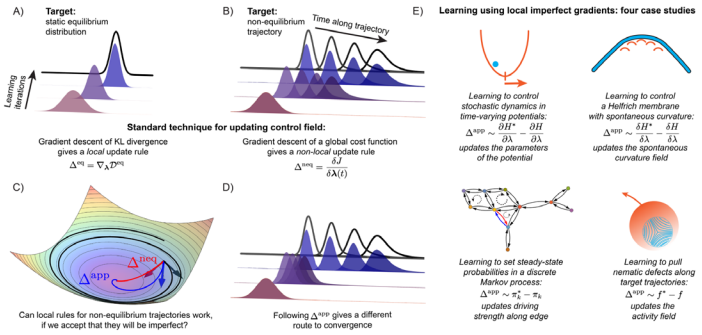

A new (bio-inspired) way to learn and control using imperfect gradients. (a) Standard approaches to learn and train are based on an equilibrium statistical mechanics framework. (b,c,d) Our new work provides a route to learn and control in dynamically changing environments using only local information. (e) We demonstrate our results on a wide variety of systems including active nematics. Our approach could potentially lead to a new class of physics inspired RL techniques.

probabilities through simple local update rules. Finally, we show that similar local update rules can also solve dynamical control problems for non-conservative systems, and we illustrate this in the non-trivial example of active nematics. Our updates allow learning spatiotemporal activity fields that pull topological defects along desired trajectories in the active nematic fluid. These imperfect feedback methods are information efficient and in principle biologically plausible, and they can help extend recent methods of decentralized training for physical materials into dynamical settings (Publication 6).

b) *A new route for templating pattern formation in bio-inspired non-equilibrium materials.* A striking feature of non-equilibrium systems is their tendency to undergo spatiotemporal pattern formation. Coherent structures such as convective, Turing patterns, and pulsatile contractions of active emerge spontaneously as the active driving in a system overcomes stabilizing dissipative forces. Pattern-forming instabilities are biologically important since, for example, they are utilized by growing organisms for morphogenesis. In many biological examples of soft active matter systems, patterns are driven by the interplay of an active contribution to the local stress, and a concentration field of chemical regulators. One can ask whether pattern formation in soft active matter systems can be reached through alternative routes which do not rely on active stresses and gradients of chemical regulators. In recent work we have discovered a new pattern formation mechanism in a viscoelastic fluid which

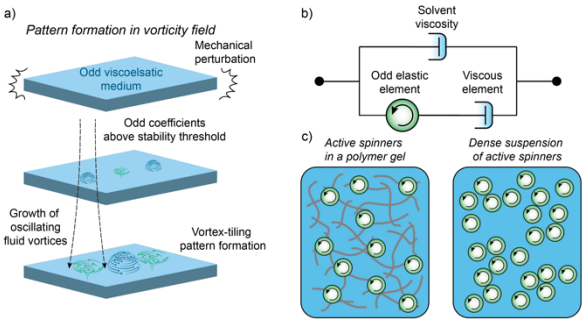

(a) Schematic illustration of the pattern formation instability observed in odd viscoelastic fluids. (b) A three-element mechanical circuit, comprising a viscous solvent in parallel with an odd Maxwell element, represents a minimal model for an odd viscoelastic fluid. (c) Two candidate systems which may display odd viscoelastic phenomenology.

can occur without either of these features, provided that the system displays *odd* non-equilibrium elastic responses to mechanical deformations. Using state of the art hydrodynamic simulations of a three-element active viscoelastic fluid using a recently developed extension of the hybrid lattice Boltzmann algorithm with analytical theory, we demonstrate that the interaction of passive viscosity and so called active odd elasticity allows for the emergence of an oscillating vortex array with a tunable characteristic wavelength and growth rate, a feature not observed in previous simplified models of odd viscoelasticity. We additionally show that the initial exponential growth of the vortices saturates if a shear-thickening non-linearity is included in the dynamics. Our results suggest that such dynamical signatures may be generic to broad classes of odd viscoelastic systems encompassing various microscopic dynamics. Further, these results can inform models of pattern formation in natural systems and guide engineering of odd dynamics in soft active matter.

c) *Using non-reciprocal forces to stabilize active matter:* Active matter with nonreciprocal interactions is known for its distinctive dynamics. To shed light on the stationary properties of such systems, we consider paradigmatic systems of nonreciprocally coupled active Ornstein-Uhlenbeck particles. For each system, we uniquely decompose the interparticle force into an energy gradient and a transverse nonconservative force. We show that the steady-state distribution of positions, which would only reflect the energy if the noise were thermal, features the transverse force as an effective potential that stabilizes the energy minima, due to the persistent noise that propels the particles. We exactly solve the distribution for nonreciprocal harmonic oscillators and numerically verify it for systems with more complex couplings. When the breaking of reciprocity in the interactions produces a transverse force without changing the energy gradient, we indeed find that the nonreciprocity plays a stabilizing role in the stationary state (Publication 5).

Future Plans

In future work, we will further develop the connections between the imperfect learning approach we have discovered and Reinforcement learning techniques. This could lead to design principles for the development of a class of bio-inspired materials that can minimally sense the environment and learn and adapt using imperfect measurements. We will also explore how non-reciprocal forces can help stabilize complex steady states (Publication 2,3), such as steady states that store memory. Our preliminary results already suggest this might be possible.

References

1. M. Du, A. Behera, S. Vaikuntanathan. *Active oscillatory memory.* JCP 2024
2. C. Floyd, A. Dinner, and S. Vaikuntanathan. *Pattern formation in odd viscoelastic fluids.* (in press) Physical Review Research (2023).
3. M. Du, S. Vaikuntanathan. *Hidden non-reciprocity as a stabilizing effective potential in active matter, (under review) PRL (2024)*

4. C. Floyd, A. Dinner, S. Vaikuntanathan. *Learning to control non-equilibrium dynamics using local imperfect gradient, (under review) PNAS (2024).*

Publications

1. A. Lamtyugina, Y. Qiu, E. Fodor, A. Dinner, S. Vaikuntanathan, *Thermodynamic control of activity patterns in cytoskeletal networks.* PRL, **129**, 128002 (2022).
2. A. Behera, M. Rao, S. Sastry, S. Vaikuntanathan. *Enhanced associative memory, classification, and learning with active dynamics.* Physical Review X **13,** 041043 (2023).
3. M. Du, A. Behera, S. Vaikuntanathan. *Active oscillatory memory.* Journal of Chemical Physics, **160,** 055103, 2024
4. C. Floyd, A. Dinner, and S. Vaikuntanathan. *Pattern formation in odd viscoelastic fluids.* (in press) Physical Review Research (2024).
5. M. Du, S. Vaikuntanathan. *Hidden non-reciprocity as a stabilizing effective potential in active matter, (under review at PRL)* arXiv:2401.14690 *(2024)*
6. C. Floyd, A. Dinner, S. Vaikuntanathan. *Learning to control non-equilibrium dynamics using local imperfect gradient, (under review at PNAS) arXiv:2404.03798 (2024).*

Steering the Pathways of Hierarchical Self-assembly at Solid Surfaces

Tao **Ye**,[1] Yonggang **Ke**,[2] and Gaurav **Arya** [3]

1. Chemistry & Biochemistry, University of California, Merced 2. Biomedical Engineering, Emory University and Georgia Institute of Technology 3. Mechanical Engineering and Materials Science, Duke University

Keywords: DNA origami, self-assembly, simulation, surface patterning

Research Scope

This project seeks to systematically elucidate the roles of surface/interfacial interactions on self-assembly of biomolecular nanostructures and tailor these interactions to steer the self-assembly pathways of complex hierarchical structures. We are studying the site-specific nucleation of surface-tethered DNA origami on dynamic surfaces and the interconnection of these mesoscale structures to form superstructures. By combining single molecule biophysical techniques and multi-scale simulations, we will develop a systematic understanding how the interactions of the solid surface influence self-assembly at three hierarchical levels: DNA origami folding itself, whose visualization will be facilitated by tethering, the interconnection of origamis, and creation of higher-order patterns of origamis.

Recent Progress

Mechanism of DNA origami folding. One of our goals was to use our surface seeding strategy for easy visualization of DNA origami folding intermediates, thereby helping us understand the folding mechanism of DNA origamis. We developed a novel *in situ* approach that successfully captured snapshots of the same structures as they grow, as the folding intermediates could be temporarily trapped for high resolution AFM imaging and released back into the solution to resume folding. Our results showed direct evidence of origami assembly proceeding through specific types of intermediates, and ultimately to complete structures. To better understand this mechanism, we developed a novel mesoscopic model that uses a switchable forcefield to capture the mechanical behavior and transitions between single- and

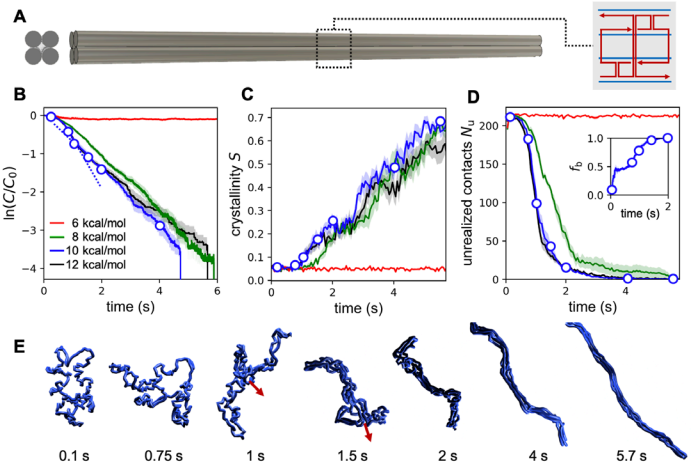

Figure 1 *Folding behavior of a 4HB structure. (A) Design. (B-D) Dependence of folding mechanism on strength of staple binding, as characterized by the time-evolution of staple concentration normalized by initial concentration (B), Landau-De Gennes crystallinity describing global order (C), number of unrealized contacts describing local order (D), and mean fraction of incorporated staples bound to the scaffold (D, inset). (E) Representative images of scaffold conformations from simulations during assembly. Arrows represent zipping direction.*

double-stranded DNA motifs at a coarseness level of 8 nucleotides per particle, allowing access to long origami folding timescales.[1] Brownian dynamics (BD) simulations showed that simple origamis with small cross-sections, such as the 4-helix bundle (4HB) (**Figure 1A**), undergo a hierarchical folding process involving zipping of structural domains into a partially folded precursor with local order followed by gradual crystallization into the final structure with global order (**Figure 1C-E**). This manifests as a two-phase behavior in the kinetics of staple incorporation, consistent with recent experiments (**Figure 1B, C**). In contrast, larger structures like the 32HB with interior geometry follow heterogeneous folding pathways, leading to global topological defects in the folded structure, consistent with experiments showing lower yields for complex or large structures. Our model thus opens an avenue to better understand and design DNA nanostructures for improved folding both in solution and close to surfaces.

Mechanistic study of adhesion of dsDNA to charged surfaces. Although surface mediated assembly of DNA structures typically relies on the multivalent cation mediated attraction to confine DNA to anionic or zwitterionic surfaces, the origin of cation-mediated attraction remains controversial. A major gap is the lack of quantitative measurements of the DNA-surface interactions. We used AFM-based single molecule force spectroscopy to measure the binding free energy of dsDNA, a model anionic polyelectrolyte, to an anionic self-assembled monolayer (SAM) surface **(Figure 2A)**.[2] The presence of divalent cations leads to constant-force plateaus, indicating attraction between DNA and surface. In the presence of Ni^{2+}, the binding energy is as high as 6-7 k_BT/bp, compared to 1-2 k_BT/bp in Mg^{2+} (**Figure 2B**). Additionally, the binding energy decreases as the concentration of monovalent cation increases (**Figure 2C**). Our observation that the adhesion force is independent of the type of monovalent cations calls into question the commonly held assumption that monovalent cations reduce adhesion by competing with the divalent cations for binding to the surface. Rather, it suggests that the attraction is electrostatic in nature and monovalent cations screen such attraction. We proposed a new mechanism that allows the correlated electrostatic interactions between counterions to be responsible for the attraction and at the same time allows the strength of metal-ligand binding to modulate the strength of the DNA-surface interactions. New insights derived from our model can guide precise tailoring of biomolecule-surface interactions in the self-assembly of complex structures at the solid-liquid interface.

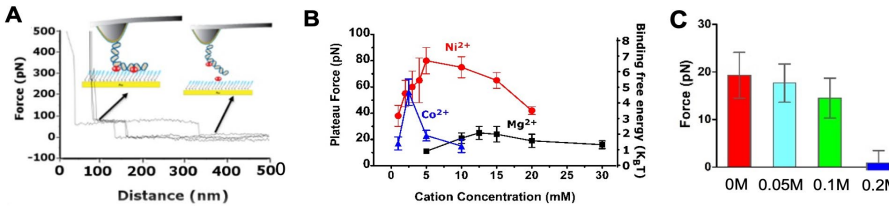

Figure 2 *(A) Single-molecule force spectra between DNA and MUDA SAM under an aqueous Ni^{2+} imaging buffer. By lowering and lifting the AFM tip, DNA molecules tethered to the tip repeatedly adhere and detach from the SAM. (B) Concentration dependence of the plateau force and binding free energy for divalent cations, Mg^{2+}, Ni^{2+}, and Co^{2+}. (C) Plateau force/binding energy as a function of $[Na^+]$. Concentrations of TrisAc and Mg^{2+} were held constant at 12.5 mM.*

DNA origami placement on nanografted self-assembled monolayers.

Using nanolithography techniques to print hydrophilic nanoscale binding sites onto an oxidized silicon or silica substrate, DNA origami placement (DOP) could site specifically place a single species of DNA origami onto these binding sites.[3] However, so far, DOP has only been practiced by only a few research groups as DOP typically requires expensive and time-consuming cleanroom nanofabrication, such as E-beam lithography (EBL) or nanoimprinting. Moreover, despite the critical role of DNA-surface interactions, surface functionality and surface topography of nanopatterns have not been systematically explored in DOP. Here we demonstrate that nanopatterned self-assembled monolayers (SAMs) produced by AFM nanografting is a powerful alternative platform for DNA origami placement (**Figure 3**). Our new platform (1) allows for DNA origami placement with high precision and yield; (2) can be performed in a standard wet lab in a few hours without need for expensive and time-consuming cleanroom access; (3) allows for the exploration of a broad range of surface chemistries to understand and control the interactions with DNA origamis.

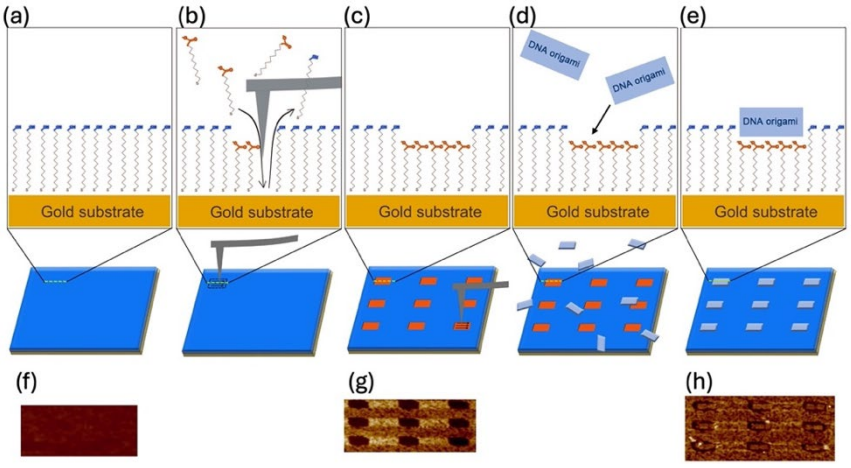

Figure 3. *Placement of DNA origamis on nanografted surface patterns. (a) Self-assembly of background SAM. (b, c) Nanopatterning of binding site SAM. (d, e) Placement of DNA origami. (f, g, h) corresponding AFM images of (a, c, e).*

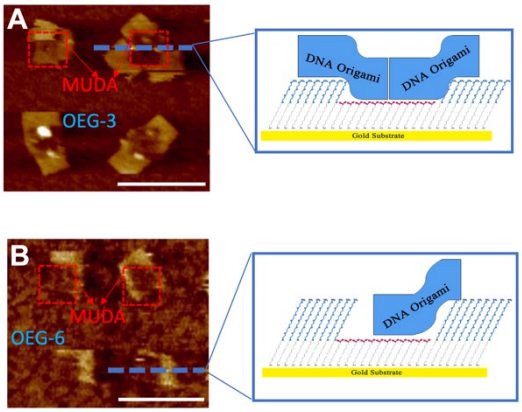

Figure 4. *AFM images of rectangular DNA origamis deposited onto MUDA binding sites in OEG-3 background (A) and OEG-6 background (B) under 12.5 mM Mg^{2+}. Scale bars: 200 nm. The callout boxes represent a schematic of the cross sectional view of the deposited DNA origami on the binding site.*

Our results have revealed that the yield and accuracy of binding of DNA origamis to the surface patterns in the presence of Mg^{2+} are highly sensitive to the surface chemistry, surface topography and addition of monovalent cations. In particular, we discovered that surface topography can be exploited to increase the energy penalty for deposition of mismatched shapes and improve deposition accuracy and yield. The nanografting technique allows the depth of the binding site to be easily adjusted by changing the SAM thickness. We found that indeed the surface topography plays an important role in DOP as the DNA origamis experiences energy penalty when a mismatched shape is adsorbed onto a deformed binding site. AFM imaging shows that the DNA

origami placed on a recessed binding site deforms to maximize interactions with the carboxylate groups (**Figure 4**). Multiple DNA origamis can be deposited onto a single 0.7nm deep MUDA binding site with OEG-3 background (**Figure 4A**). In contrast, if we used thicker OEG-6 SAM as the background to make the binding sites 1.4 nm deep, each site now captures only a single DNA origami (**Figure 4B**). The contrasting behaviors show that a deeper well incurs higher deformation energy penalty, which makes it unfavorable for multiple DNA origamis to bind to a single site. Therefore, the deeper well design can greatly improve accuracy of single-layer DNA origami binding to surface and was the key design feature that led to high-yield placement of rectangle DNA origamis shown in **Figure 5**.

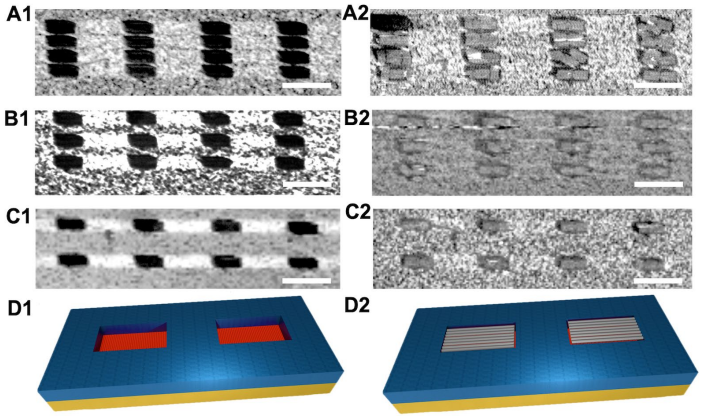

Figure 5. *AFM images of MUDA binding sites within OEG-6 background with different spacings (A1, B1, C1) before deposition and (A2, B2, C2) after deposition. The deposition of DNA origamis fills the ~1.6nm deep sites. Scale bar: 200 nm. (D1) and (D2) are the schematics of the nanopatterns before and after DNA origami deposition.*

Future Plans

We will quantitatively understand the forces and dynamics of mesoscale self-assembly of DNA origami on nanopatterned solid supports and rationally engineer interfacial interactions to allow top-down techniques to program the formation of 2D and 3D DNA origami superstructures.
Elucidate how interfacial interactions drive the binding of DNA origami on nanopatterned solid supports. We will use novel single molecule force spectroscopy techniques to quantify the adhesion and lateral forces between DNA origami and the patterned surface and understand how these interfacial forces impact DOP. Quantitative measurements coupled with mesoscopic modeling will help us understand how the interfacial forces determine the dynamics of DOP.
Design interfacial interactions for constructing 3D hierarchical networks.
We hypothesize that the bottleneck of interconnection between DNA origamis bound to surface patterns lies in the paradoxical demands for conformational freedom needed for facile interconnection and confinement imposed by binding to lithographic patterns. We will explore how a new strategy based on DNA origami multilayers can meet these paradoxical needs.

References

1. DeLuca, M.; Duke, D.; Ye, T.; Poirier, M.; Ke, Y.; Castro, C.; Arya, G., Mechanism of DNA origami folding elucidated by mesoscopic simulations. *Nat Commun* **2024,** *15* (1), 3015.
2. Hao, X.; Gu, Q.; Isborn, C.; Long, M.; Ye, T., Quantitative Measurement of Cation-Mediated Adhesion of DNA to Anionic Surfaces. *Under review* **2024**.

3. Gopinath, A.; Miyazono, E.; Faraon, A.; Rothemund, P. W. K., Engineering and Mapping Nanocavity Emission Via Precision Placement of DNA Origami. *Nature* **2016,** *535* (7612), 401-405.

Publications

1. Zhou, C. Y.; Yang, D. L.; Sensale, S.; Sharma, P.; Wang, D. F.; Yu, L.; Arya, G.; Ke, Y. G.; Wang, P. F., A bistable and reconfigurable molecular system with encodable bonds. *Sci Adv***, *8***, eade3003 (2022)
2. Shao, J. R.; Breuer, R.; Schmittel, M.; Ye, T., Potential-Dependent Adhesion Forces between dsDNA and Electroactive Surfaces. *Langmuir*,**38**, 11899–11908 (2022)
3. DeLuca, M.; Sensale, S.; Lin, P. A.; Arya, G., Prediction and Control in DNA Nanotechnology. *ACS Appl Bio Mater* **2023**.
4. Zhang, Y. L.; Yang, D. L.; Wang, P. F.; Ke, Y. G., Building Large DNA Bundles via Controlled Hierarchical Assembly of DNA Tubes. *ACS Nano 17* (11), 10486-10495 (2023)
5. Gu, Q. F.; Petrek, Z.; Rezayan, R.; Ye, T., Single molecule insights into interfacial molecular recognition for model electrochemical DNA biosensors. *Curr Opin Electroche* **2023,** *40*, 101348.
6. Wang, S.; Lin, P. A.; Deluca, M.; Zauscher, S.; Arya, G.; Ke, Y. G., Controlling Silicification on DNA Origami with Polynucleotide Brushes. *J Am Chem Soc* **2023,** *146* (1), 358-367.
7. Rahmani, P.; Goodlad, M.; Zhang, Y. H.; Li, Y. C.; Ye, T., One-Step Ligand-Exchange Method to Produce Quantum Dot-DNA Conjugates for DNA-Directed Self-Assembly. *ACS Appl Mater Inter* **2022,** *14* (42), 47359-47368.
8. Gu, Q.; Hao, X.; Isborn, C. M.; Long, M. P.; Ye, T., Quantitative Measurement of Cation-Mediated Adhesion of DNA to Anionic Surfaces. *Under review*.
9. DeLuca, M.; Duke, D.; Ye, T.; Poirier, M.; Ke, Y.; Castro, C.; Arya, G., Mechanism of DNA origami folding elucidated by mesoscopic simulations. *Nat Commun* **2024,** *15* (1), 3015.
10. Zhang, Y.; Allen, A. C.; Petrek, Z. J.; Huan, C. H.; Kumar, D.; Goodlad, M. C.; Martinez, V. G.; Singh, J.; Zhang, J. Z.; Ye, T., Formation of Linear Plasmonic Heterotrimers Using Nanoparticle Docking to DNA Origami Cages. *J Phys Chem C* **2024**, https://doi.org/10.1021/acs.jpcc.4c02229.

Author Index

Participant List

Name	Organization
Abbott, Nicholas	Cornell University
Aizenberg, Joanna	Harvard University
Aizenberg, Michael	Harvard University
Ashby, Paul	Lawrence Berkeley National Laboratory
Baer, Marcel	Pacific Northwest National Laboratory
Brady, John	California Institute of Technology
Chaikin, Paul	New York University
Chen, Chun-Long	Pacific Northwest National Laboratory
Chen, Qian	University of Illinois, Urbana-Champaign
Chen, Wei	Argonne National Laboratory
Choi, Jong Hyun	Purdue University
de Pablo, Juan	University of Chicago
De Yoreo, James	Pacific Northwest National Laboratory
Delhommelle, Jerome	University of Massachusetts, Lowell
Dishari, Shudipto	University of Nebraska, Lincoln
Dogic, Zvonimir	University of California, Santa Barbara
Dorman, James	US Department of Energy, Office of Basic Energy Sciences
Duclos, Guillaume	Brandeis University
Emrick, Todd	University of Massachusetts, Amherst
Estroff, Lara	Cornell University
Gang, Oleg	Columbia University
Gimm, Aura	US Department of Energy, Office of Basic Energy Sciences
Green, Jason	University of Massachusetts, Boston
Grover, Piyush	University of Nebraska, Lincoln
Guan, Zhibin	University of California, Irvine
Hagan, Michael	Brandeis University
Hartley, Christopher	Miami University
Ke, Yonggang	Emory University
Kim, Jimin	Massachusetts Institute of Technology
Kloxin, Christopher	University of Delaware
Kumar, Manish	University of Texas, Austin
Liu, Andrea	University of Pennsylvania
Luijten, Erik	Northwestern University
Mallapragada, Surya	Ames National Laboratory
Monroe, Jacob	University of Arkansas
Nagel, Sidney	University of Chicago
Noy, Aleksandr	Lawrence Livermore National Laboratory
Olvera de la Cruz, Monica	Northwestern University
Omar, Ahmad	University of California, Berkeley
Osmanovic, Dino	University of California, Los Angeles

Palmer, Liam	Northwestern University
Pochan, Darrin	University of Delaware
Roizen, Jennifer	US Department of Energy, Office of Basic Energy Sciences
Rotskoff, Grant	Stanford University
Russell, Thomas	University of Massachusetts, Amherst
Sacanna, Stefano	New York University
Santore, Maria	University of Massachusetts, Amherst
Saven, Jeffery	University of Pennsylvania
Schlau-Cohen, Gabriela	Massachusetts Institute of Technology
Schulman, Rebecca	Johns Hopkins University
Shih, William	Dana-Farber Cancer Institute
Silberstein, Meredith	Cornell University
Snezhko, Alexey	Argonne National Laboratory
Sokolov, Andrey	Argonne National Laboratory
Solomon, Michael	University of Michigan
Stebe, Kathleen	University of Pennsylvania
Strano, Michael	Massachusetts Institute of Technology
Stupp, Samuel	Northwestern University
Tezcan, Faik	University of California, San Diego
Vaikuntanathan, Suriyanarayanan	University of Chicago
Valiev, Marat	US Department of Energy
Willard, Adam	Massachusetts Institute of Technology
Ye, Tao	University of California, Merced